Novel Degradable Bioactive Silicate/Phosphate Glass Mixtures for Clinical Periodontal Treatment

By

Nuha Agab Hamed

BDS, MSc Periodontics

2018

A thesis submitted in fulfilment of the requirements for the Degree of Doctor of Philosophy in Institute of Dentistry, Barts and the London School of Medicine and Dentistry, Queen Mary University of London

Statement of Originality:

I, Nuha Agab Hamed, confirm that the research included within this thesis is my own work or that where it has been carried out in collaboration with, or supported by others, that this is duly acknowledged below and my contribution indicated. Previously published material is also acknowledged below.

I attest that I have exercised reasonable care to ensure that the work is original, and does not to the best of my knowledge break any UK law, infringe any third party's copyright or other Intellectual Property Right, or contain any confidential material.

I accept that the College has the right to use plagiarism detection software to check the electronic version of the thesis.

I confirm that this thesis has not been previously submitted for the award of a degree by this or any other university.

The copyright of this thesis rests with the author and no quotation from it or information derived from it may be published without the prior written consent of the author.

Signature: **Nuha Agab Hamed**

Date: 17/09/2018

Abstract:

Objective: Bioactive silicate glass-based Perioglas® has been used to treat periodontal-bony-defects. During glass degradation in body fluids, this glass generates a high pH>8. This high pH may enhance the growth of periodontopathic bacteria such as *P.gingivalis* which grows optimally at a pH ≈ 8.3. Furthermore, the high pH is likely to inhibit osteoblast activity, resulting in suppression of osteogenic differentiation/proliferation in the local biological environment. Therefore, this work aims to develop novel strontium-containing silicate/phosphate glass-mixtures where the phosphate glass generates an acidic pH to offset the alkaline pH arising from the silicate bioactive glass. The objective is being to (i) inhibit the alkaline periodontal bacterial growth of virulent *P.gingivalis* and (ii) create a neutral periodontal environment for osteoconductive bone regeneration. Strontium is known to stimulate osteoblasts and has a bactericidal action against *P.gingivalis*, it also provides radio-opacity enabling the dissolution process to be potentially followed clinically by X-rays.

Methods: Nine compositions of bioactive silicate/phosphate glass-mixtures were prepared. The glasses synthesised were ground and sieved to obtain a specific selection of particle size fractions for glass-mixtures preparation. The glass-bioactivity was performed by immersing the prepared glass mixtures in Tris, SBF and ALP containing Tris buffer solution. The pH change in solutions was measured and the ions release was quantified by ICP-OES as a function of time. The glass-mixtures degradation and apatite formation were investigated by Infrared-Spectroscopy-FTIR, MAS-NMR Spectroscopy and Solution-NMR Spectroscopy.

Results: The pH behaviour was modulated by immersing the nine compositions of glass-mixtures in buffers solution. The degradation of glass mixtures in Tris buffer was evaluated by MAS-NMR and revealed the transformation of the Q^2 metaphosphate species into large amounts of Q^1 species with a small amount of Q^0 orthophosphate species. The rate of these transformations of glass mixtures depends on the mixture composition (the ratio of silicate glass to phosphate glass). ALP which is elevated in periodontal bony defects hydrolysed the terminal phosphate Q^1 species of the Q^2-metaphosphate chain of phosphate glass and converted it into Q^0-orthophosphate species as demonstrated efficiently by Solid and Solution NMR spectroscopies.

Conclusion: Smart modulation of pH profile was essential to inhibit the alkaline bacterial growth of *P.gingivalis*. The transformation of $Q^{\mathbf{2}}$-metaphosphate species into $Q^{\mathbf{1}}$-species demonstrated by spectroscopy was significant finding as the emerging $Q^{\mathbf{1}}$-species was hydrolysed by ALP enabling hydroxyapatite precipitation for new bone formation. This extremely pioneering technology of mixing phosphate and silicate glasses and using them with ALP has potential for the development of new biomedical materials for different applications.

Table of Contents:

List of Figures:

List of Tables:

List of Abbreviations:

ALP	Alkaline Phosphatase Enzyme
BO	Bridging Oxygen Bond
DSC	Differential Scanning Calorimetry
FTIR	Fourier Transform Infra-Red Spectroscopy
GCF	Gingival Crevicular Fluid
HCA	Hydroxycarbonate Apatite
ICP-OES	Inductively Coupled Plasma-Optical Emission Spectroscopy
MAS-NMR	Magic Angle Spinning-Nuclear Magnetic Resonance
NBO	Non-Bridging Oxygen Bond
NC	Network Connectivity
P-glass	Phosphate Glass
PS	Particle Size
SBF	Simulated Body Fluid
S-glass	Silicate Glass
TB	Tris Buffer Solution
Tc	Crystallisation Temperature
Tg	Glass Transition Temperature
XRD	X-Ray Diffraction

Acknowledgements:

My deepest gratitude and appreciation to my supervisors Prof. Robert Hill, Dr. David Gillam and Dr. Natalia Karpukhina, without their generous assistance, invaluable guidance and massive knowledge, this accomplished work would not be achieved.

I would like to thank my sponsor the Iraqi Ministry of Higher Education and Scientific Research (MOHER) for funding my PhD study.

My acknowledgements are also extended to all staff and colleagues in the Institute of Dentistry, Queen Mary University of London for their kind help and support during the period of this research work.

A special thanks to my friends Jamila Al-Mohammadi, Alexander Cresswell-Boyes, Saja Mannaa, Alessia D'Onofrio, Sherif Elsharkawy, Tomas Duminis and Bajram Ferizolli.

I would never forget to thank my family, particularly my father for their prayers, endless care, encouragement and financial support to carry on and complete my PhD.

1 Literature Review:

1.1 Periodontitis:

Generally, periodontal diseases are classified according to the severity of the disease. The two major stages are gingivitis and periodontitis. Gingivitis is a milder and reversible form of periodontal disease that only affects the gingiva. Gingivitis may however, lead to more serious, destructive forms of periodontal disease called periodontitis.

Periodontitis has been defined as *"an infectious disease resulting in inflammation within the supporting tissues of the teeth, progressive attachment loss and bone loss"* (Newman et al., 2011). As a consequence, it can be suggested that the main clinical and aetiological characteristic features of periodontitis are:

1. supragingival and subgingival bacterial plaque accumulation which in turn may lead to calculus formation;
2. gingival inflammation and pocket formation;
3. attachment loss and alveolar bone resorption;
4. in severe cases, spontaneous gingival bleeding, tooth mobility and loss of the teeth (Newman et al., 2011).

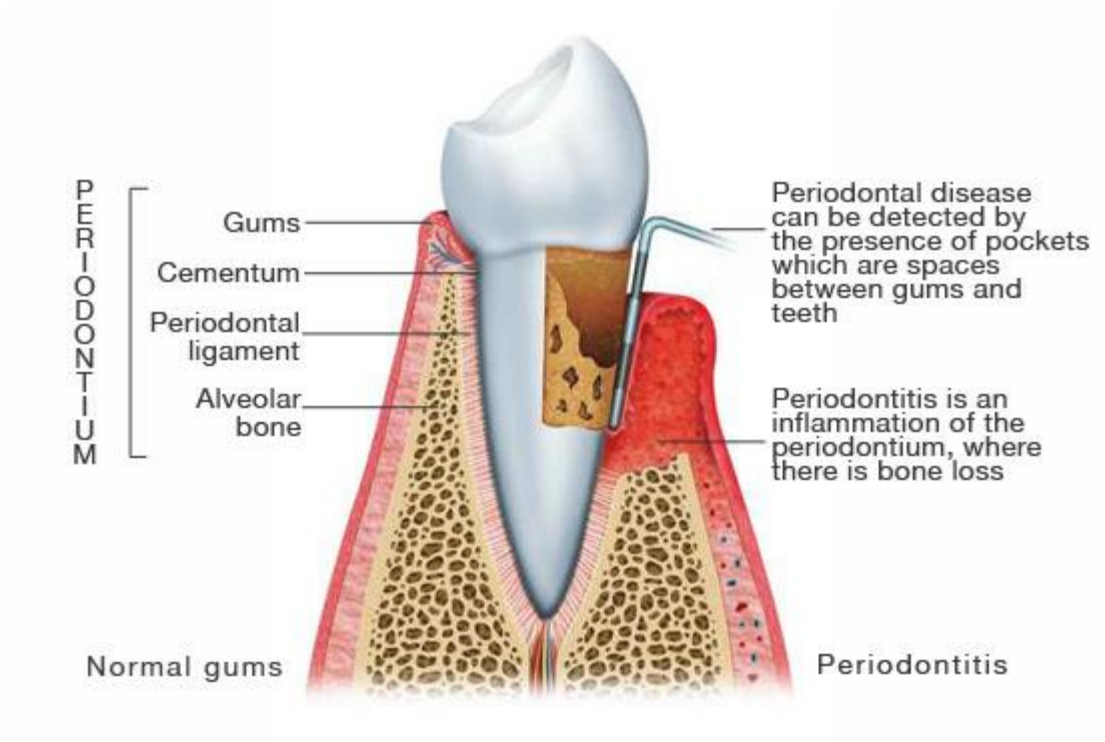

Figure 1.1 Showing periodontitis with deep pocketing, loss of attachment and alveolar bone resorption (Whitney, 2018).

Carranza and Newman (Newman et al., 2011) cited some of the potential risk factors which have been associated with the risk of developing periodontal diseases, which can also be classified as systemic and local factors as listed below:

- Tobacco smoking (environmental factor);
- Systemic diseases such as diabetes;
- Some types of medications such as steroids, some types of anti-epilepsy drugs, cancer therapy drugs, some calcium channel blockers;
- Pathogenic bacteria such as *Actinobacillus actinomycetemcomitans (Aa)* and *Porphyromonas gingivalis (Pg)*;
- Psychological factors e.g. stress;
- Bridges that no longer fit properly (local factor);
- Anatomical factor e.g. crooked teeth (local factor);

- Defective restorations (with overhangs affecting the gingival crevice) (local factor);
- Hormonal changes associated with pregnancy or use of oral contraceptives.

1.1.1 Periodontal Pocket:

A periodontal pocket may be classified as follows**:**

1) *Gingival pocket*: known as pseudo-pocket or false pocket which is formed by gingival overgrowth without any associated destruction of the alveolar bone tissues.

2) *Periodontal pocket*: this type of pocket occurs with the destruction of the underlying alveolar bone tissues. Mobility of the teeth may also occur as a result of extensive periodontal ligament disruption and bone loss (Figure 1.2) (Newman et al., 2011).

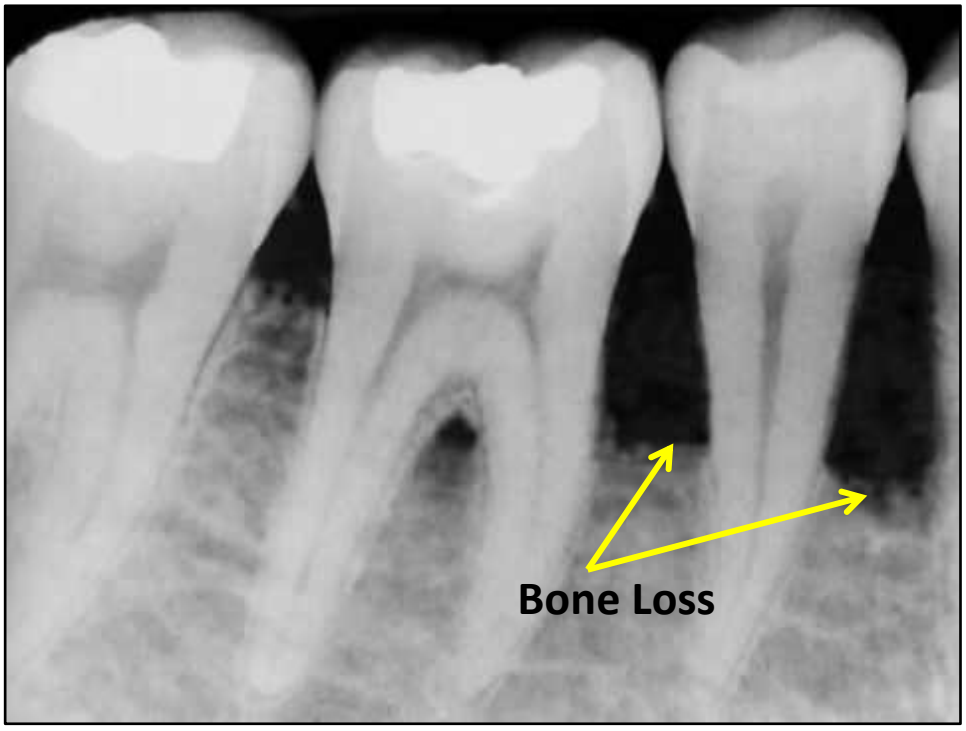

Figure 1.2 X-ray photograph showing bone resorption associated with chronic periodontitis. Taken from (https://areteethbones.com).

Furthermore, a periodontal pocket can be classified according to its distinguishable features into two types (Newman et al., 2011)**:**

1) A supra-bony pocket in which, the base of the pocket is coronal to the level of the underlying alveolar bone and the pattern of bone loss is horizontal.

2) An infra-bony pocket, where the base of the pocket is apical to the adjacent bone so that the bone is juxtaposed to the soft tissue wall and the model of bone destruction is vertical (angular). This is depicted in Figure (1.3).

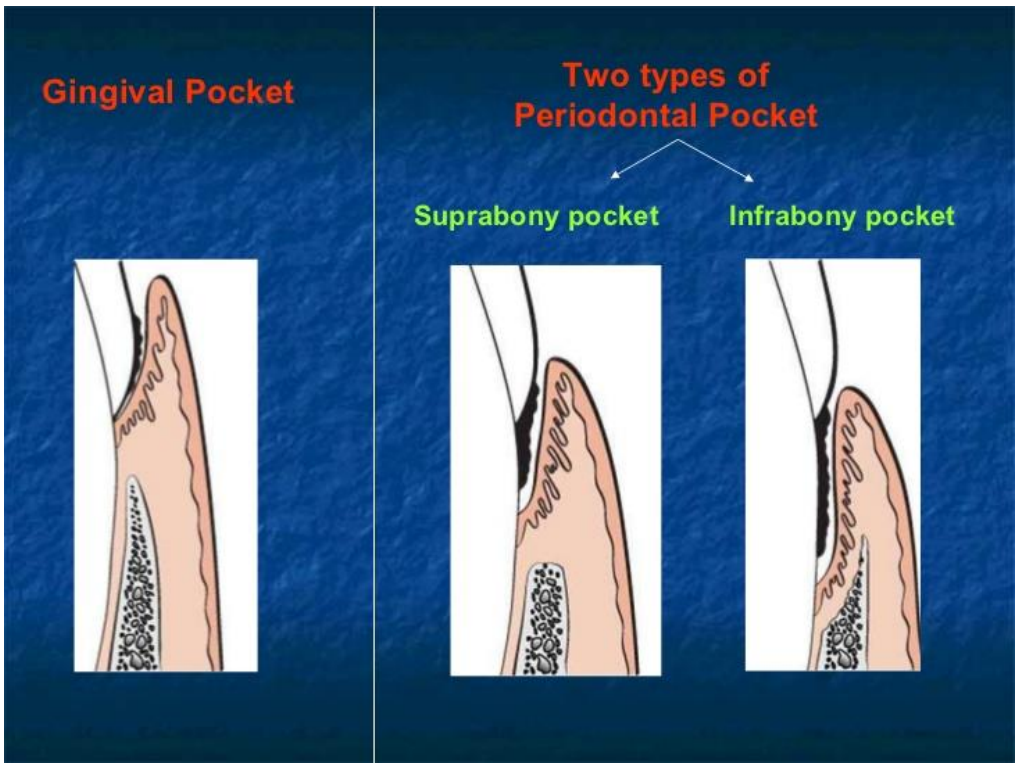

Figure 1.3 Demonstrating the different types of periodontal pockets (Newman et al., 2011).

In addition, an infra-bony pocket can be classified according to the number of residual bony walls into one-wall, two-wall and three-wall defects as illustrated in Figure 1.4.

The morphology of infra-bony defects has a significant influence on the periodontal regenerative process. Some studies have demonstrated the intimate relationship between the depth and width of the infra-bony defects and the outcome of both the clinical attachment and bone repair following one year of periodontal treatment. In other words, the greater outcome of the improved clinical attachment was strongly related to the deeper defect, whereas the lower clinical attachment and bone repair were attributed to the wider defect (Garrett et al., 1988, Tonetti et al., 1993, Tonetti et al., 1996).

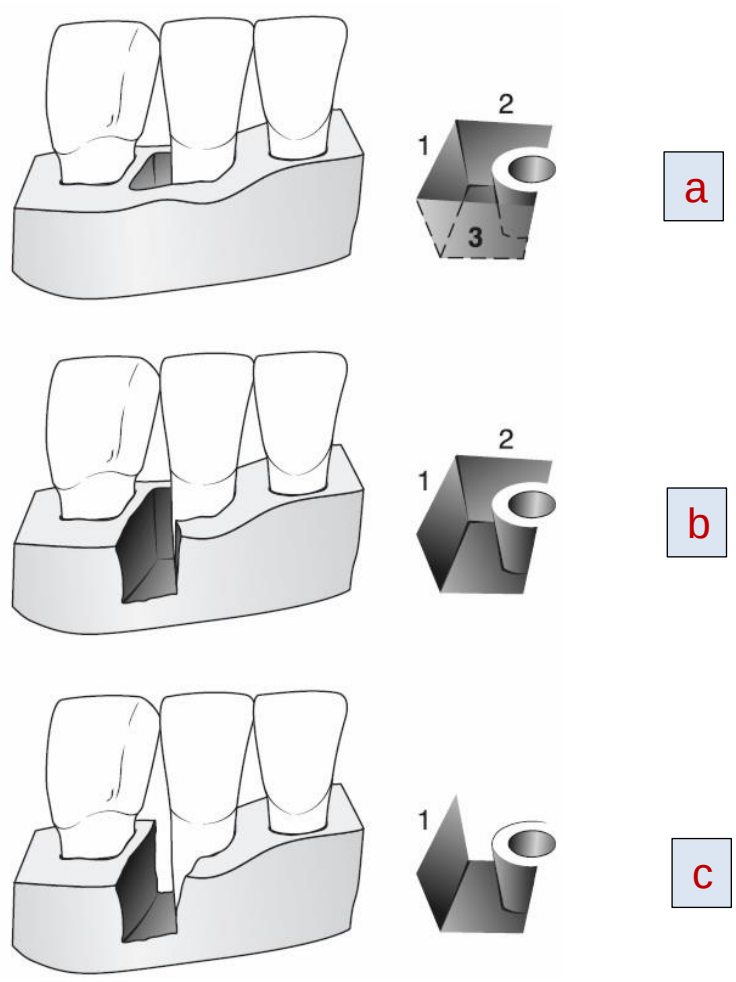

Figure 1.4 Infra-bony defects. (a) Three-wall infra-bony defect. (b) Two-wall infra-bony defect. (c) One-wall infra-bony defect (Newman et al., 2011).

1.1.2 Pathogenic Bacteria of Periodontal Diseases:

The term ‘keystone pathogen’ can be described and defined in the field of microbial ecology as an architecture of microbial communities and their interaction with the living host tissues. Keystone pathogens refer to crucial keystone microorganisms that initiate and enhance microbiota associated with disease status. In periodontitis, periodontal pathogens such as *Porphyromonas gingivalis* (*P. gingivalis*) impair the normal homeostatic host-microbial interplay causing subversion of the host immune system strategies (Hajishengallis et al., 2012).

In the field of molecular biology, most pathogenic microorganisms have the ability to adhere either to the soft tissue surfaces such as mucosa and epithelium or the hard tissue surfaces such as teeth/bone, as well as artificial surfaces in the form of dentures and implants. This bacterial adhesion to its host cells can be regarded as a crucial trigger for the induction of periodontal infections, such as gingivitis or periodontitis. One of the periodontopathogens namely *P. gingivalis* has an extensive battery of virulence factors for the progression of periodontal diseases (Newman et al., 2011). According to Newman *et al*. 2011, the proposed strategy upon which these virulence factors contribute to develop periodontal diseases is as following:

(1) By promoting bacterial growth and colonization (adhesins) to host cells such as in the pocket epithelium.
(2) Destruction of the host tissues by bacterial proteinases and toxins.
(3) Protection of pathogenic bacteria against the defence response of the host tissues.

It has been reported that the pH of the normal gingival crevice is below neutrality in healthy periodontal tissues (McDermid et al., 1988). During the development of the periodontal pocket via the process of pathogenesis of periodontal diseases (which

includes the apical migration of the junctional epithelium, subsequent attachment loss of fibres, destruction of connective tissues and alveolar bone resorption). The normal gingival crevice transforms into a pocket and the pH increases to above pH 8 which favours the conditions that promote the progression of the disease process (McDermid et al., 1988). Therefore, in a deeper periodontal pocket, the pH may be as high as 9 as reported by the Bickel & Cimasoni study (Bickel and Cimasoni, 1985). This change in the local pH of the developing pocket has a significant effect on the growth and enzyme activity of the bacteria present in periodontal pockets such as *P. gingivalis*.

P. gingivalis is a gram-negative, non-motile, acid-sensitive and anaerobic bacterium, it plays an active and key role in the development and progression of periodontal diseases. It has been reported that *P. gingivalis* inhabits the alkaline environment of subgingival sites (periodontal pockets) where the “optimum pH for *P. gingivalis* growth is approximately 8” (Nakayama, 2015).

1.1.3 ALP in Periodontal Degeneration and Regeneration:

Typically, a correct diagnosis of periodontal disease depends on the collection of data from the periodontal patients' examination and subsequent charting of the information as indicated below. The clinical examination is supplemented by taking a thorough medical and dental history to determine whether genetic, environmental (such as smoking), systemic conditions (such as diabetes), concomitant medication, stress, obesity may affect the extent and severity of periodontal disease (so-called risk factors and indicators). Traditionally, the severity of the individual patient's periodontal status can be identified and quantified by conventional periodontal diagnostic clinical parameters such as measurement of pocket depth, gingival index, plaque index, loss of attachment apparatus and radiographic analysis of alveolar bone resorption (Armitage, 2004). However, these classic diagnostic tools have limitations since they can only provide the clinicians with a previous history of the periodontal status e.g. radiographic bone loss, but not the current periodontal status to be evaluated. Recently, advanced diagnostic procedures based on biochemical markers have been developed for the early detection of an individual's periodontal risk assessment.

Through the area of both the periodontium and gingival crevice, the inflammatory process of periodontal pathogenesis occurs as a host response to plaque bacteria biofilms. This process leads to the release of some enzymes from the injured periodontal tissues into the gingival crevicular fluid (GCF) and saliva. Among these released enzymes are "alanine aminotransferases, lactate dehydrogenase, gamma-glutamyl transferase, creatine kinase, alkaline phosphatase, and acid phosphatase" (Sanikop et al., 2012).

The biochemical marker ALP was detected in dental plaque biofilm, gingival crevicular fluid (GCF), and collected saliva (Sanikop et al., 2012). ALP has gained attention in periodontal research as a potential novel biotechnology for diagnosis, prognosis periodontal therapy, and drug innovations as elucidated in Figure 1.5.

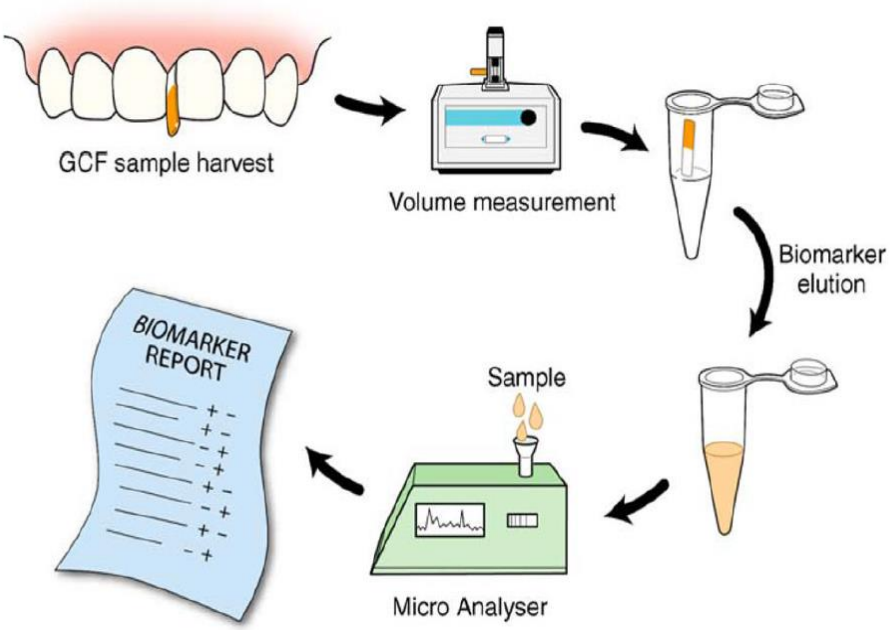

Figure 1.5 Futuristic chairside diagnostic test based on GCF sampling. Considering the GCF fluid as a potential analyte for the screening of multiple biomarkers, a rapid, chairside diagnostic tool (represented in the Figure as a Micro Analyser) or a "mini-lab" could be used by clinicians for risk assessment and decision making on treatment planning. The advantages of such a tool would be enhanced predictability of clinical outcomes and well-informed patients regarding personalized treatment needs. As shown, a simple clinical procedure for GCF collection could be used, followed by extraction of analytes from the test strip. The fluid present on the test strip would be subjected to volumetric quantification. After an elution procedure to "wash" and retrieve the compounds from the fluid, the sample would be analyzed. An immediate comprehensive risk report profile and biomarkers screening would enable evidence-based decision making (Taba et al., 2005).

Alkaline phosphatase (ALP) refers to a “calcium- and phosphate-binding protein and a phospho-hydrolytic enzyme” (Sanikop et al., 2012). It can also be defined as a “membrane-bound glycoprotein produced by cells such as polymorphonuclear leukocytes (PMNLs), osteoblasts, macrophages, and fibroblasts within the area of the periodontium and gingival crevice”(Daltaban et al., 2006).

ALP has the unique feature of being involved both in pathogenic processes as well as in bone regenerative processes (Groeneveld et al., 1996). It has been identified in gingival crevicular fluid (GCF), saliva and dental plaque bacteria. Increased levels of ALP is associated with the progression of periodontal disease from the healthy periodontium to a chronic periodontitis status indicate that this enzyme may be of diagnostic value in the diagnosis of periodontal diseases or at the very least a monitor of decreased/increased activity during periodontal treatment. The direct relationship between the elevated level of ALP and the severity of the periodontal disease can be observed in Table 1.1. This table demonstrates how high the actual value of ALP levels can be when comparing to healthy periodontal condition, gingivitis and chronic periodontitis with other traditional clinical parameters, including probing depth and attachment level. These clinical conditions correlate strongly with the recorded ALP concentrations. Figure 1.6 also records the relationship between the ALP levels in GCF and the three periodontal groups (healthy periodontium, gingivitis and chronic periodontitis).

Table 1.1 Showing the correlation of the mean ALP levels with the various clinical parameters in the three groups of periodontal status: (healthy, gingivitis and chronic periodontitis) (Sanikop et al., 2012).

Groups	ALP Levels (in IU/L) Mean ± SD	Gingival index Mean ± SD	Plaque index Mean ± SD	Probing depth (in mm) Mean ± SD	Clinical attachment Level (in mm) Mean ± SD
Healthy	170 ± 70	0.00	0.46 ± 0.6	1.26 ± 0.5	1.40 ± 0.5
Gingivitis	271 ± 11	2.13 ± 0.6	2.73 ± 0.5	2.20 ± 0.7	1.93 ± 0.7
Chronic Periodontitis	732 ± 42	2.40 ± 0.7	2.46 ± 0.5	6.13 ± 1.5	7.07 ± 1.4
ALP-Alkaline Phosphatase, SD-Standard Deviation					

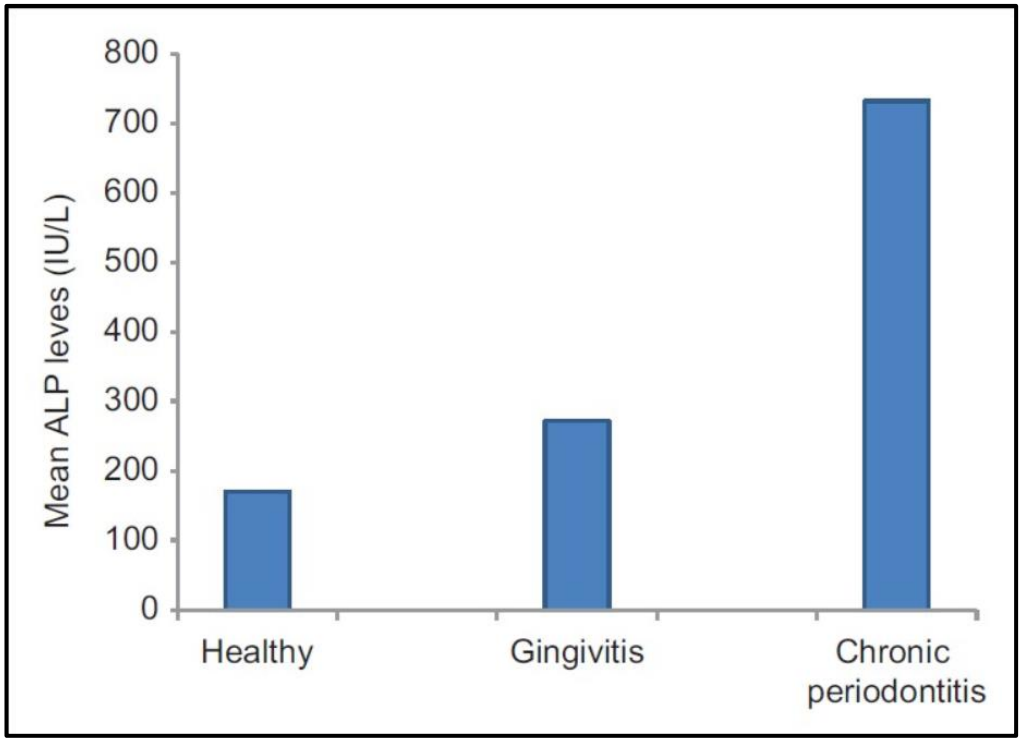

Figure 1.6 Comparison of mean GCF ALP levels (IU/L) in the three groups (Sanikop et al., 2012).

Interestingly, ALP stimulates new bone remineralisation due to its activity to hydrolyse the Q^1-pyrophosphate species (inhibitor of bone mineralisation) into Q^0-orthophosphate species (Grover et al., 2013), providing local supersaturation of the biological environment with high levels of phosphate and calcium ions. This activity results in hydroxyapatite precipitation which is essential for new bone formation as indicated in Figure 1.7 below:

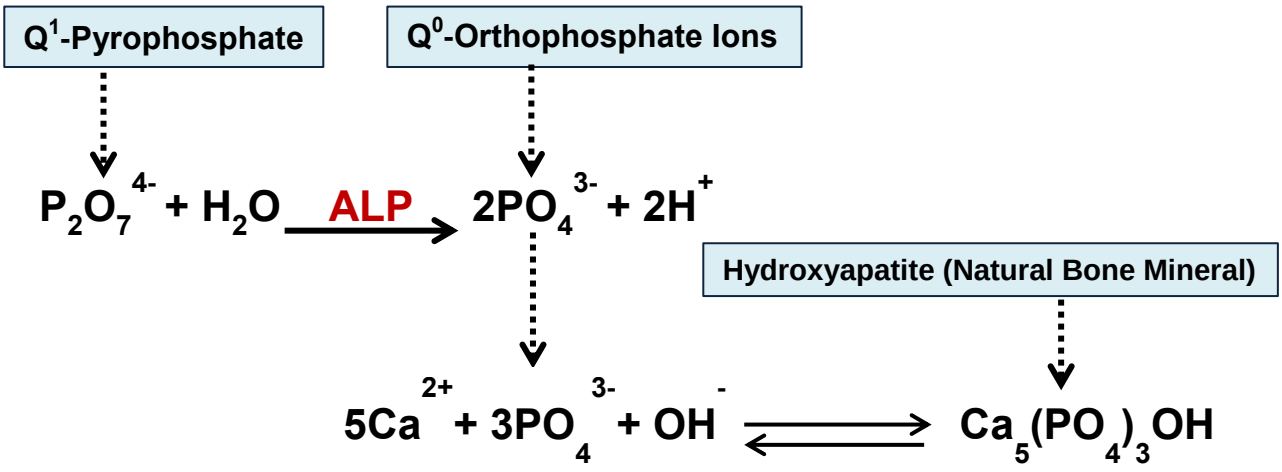

Figure 1.7 Schematic diagram demonstrating the ability of ALP enzyme to extract the orthophosphate species from the pyrophosphate species.

However, the enzyme kinetics may be influenced by pH changes (Bisswanger, 2017). For example, the bell-shaped pH curve can elucidate the dependence of the tested enzyme activity on the pH value as demonstrated in Figure 1.8 (Bisswanger, 2014). This activity is ascending from zero (area of strong acidity) up to an optimum pH, then the reading is descending to zero again (area of strong alkalinity).

The maximum value of pH in the bell-shaped pH curve is the pH optimum; this value represents the maximum enzyme activity (V_{max}) which can be employed as a criterion of pH standardisation through enzymatic kinetics studies. Predominately, the physiological range of almost pH 7.5 is the pH optimum for most enzymes;

however, each enzyme has an optimum pH, at which it shows different maximum activity. For instance, the pH optimum of protease stomach enzyme is 2, acid phosphatase with pH 5.7 and with the alkaline phosphatase pH 10.5 (Bisswanger, 2014). Therefore, the enzymatic sensitivity must be investigated under the individual enzyme special pH maximum.

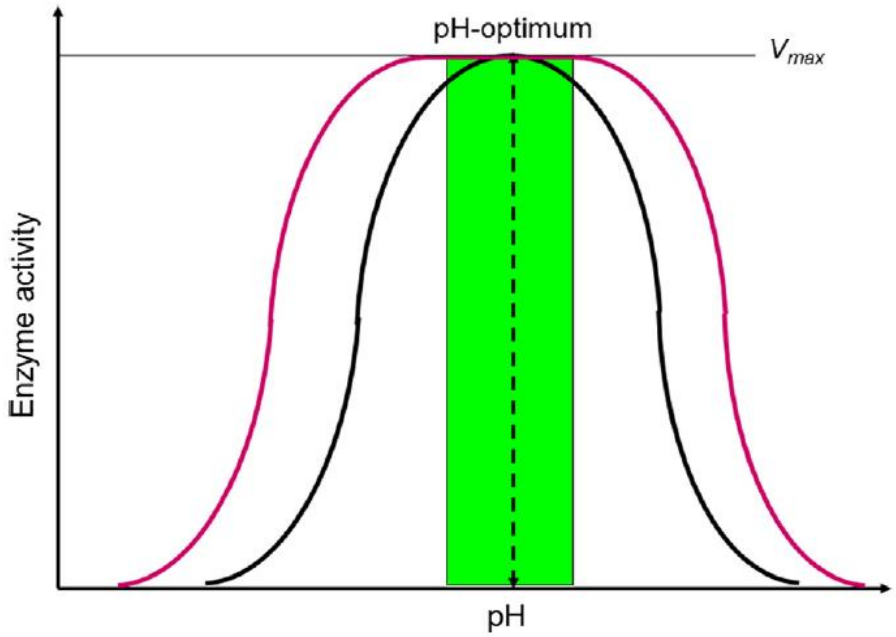

Figure 1.8 pH optimum curve for the activity of an enzyme (black). The pH of the maximum is the pH optimum. The green area shows the physiological range. The red line shows the broader pH stability curve of the enzyme (Bisswanger, 2014).

A study was undertaken by Flynn *et al.* (Flynn et al., 2002), where the investigators studied the influence of pH levels on the intestinal mucosa alkaline phosphatase (ALP) activity. The investigators reported a positive correlation between pH values and the ALP activity. This effect has been attributed to the presence of ionisable groups within the active site of the enzyme. Flynn and his co-authors reported that optimum ALP enzyme activity (V_{max}) was elevated with both increased ALP concentrations (K_m) and increased pH levels as indicated in Table 1.2:

Table 1.2 Displaying both V_{max} and K_m of Alkaline phosphatase at different pH measurements (Flynn et al., 2002).

pH level	V_{max} (unit/ml)	K_m (μg/ml)
7.0	1.31	9.3
7.5	2.25	34.3
8.0	2.55	40.8
8.5	2.94	58.9
9.0	4.52	93.1

Moreover, Flynn and his colleagues studied the behaviour of the ALP catalytic activity with various artificial substrate concentrations of p-nitrophenol phosphate (pNPP) at different pH values. They reported that the enzyme catalysis increased up to a three-fold value with increasing concentrations of the substrate (pNPP) within a pH range from 7 to 9 as expressed in Figure 1.9 (Flynn et al., 2002). However, a dramatic increase in the enzymatic activity was distinct from shifting pH 7.0 to 7.5 and from 8.5 to 9.0, whereas the pH readings between the two values were slightly deviated.

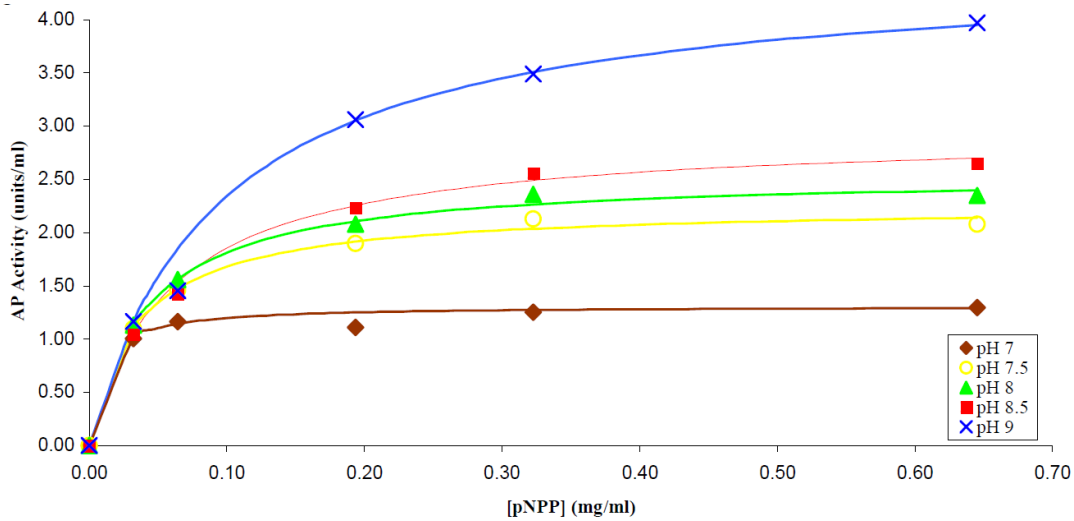

Figure 1.9 The effect of pH on the enzymatic activity of alkaline phosphatase under different concentrations of substrate pNPP (Flynn et al., 2002).

1.2 Biomaterials used in Periodontology:

According to Williams (1999), bioactive materials can be defined as “materials that have the ability to dissolve in physiological body fluids, forming a chemical bond between the glass and host tissues”.

Over the last two to three decades, the main goal in periodontal treatment was to regenerate the damaged periodontium with therapeutic approaches based on a scientific rationale to initiate, replace and encourage cells that were regenerating the lost tissue structure such as periodontal ligament cells. A variety of biomaterials have been developed for the application of both periodontal tissue regeneration and osseo-integration procedures in the defect site. These include materials such as barrier membrane, growth factors, bone graft material and combined procedures as indicated in the Tables below 1.3, 1.4 and 1.5:

Table 1.3 Types of barrier membrane used in periodontal treatment (Cho et al., 2017).

Type	Material	Brand
Resorbable	*Natural membrane*	
	A cellular dermal allograft	Alloderm
	Oxidized cellulose mesh	Surgicel
	Type I collagen membrane	Biogide, Biomend, Ossix plus, Biosorb
	Synthetic membrane	
	Polylactic acid derivatives	Epiguide, Atrisorb, Osmed, Guidor
	Combination of polylactic and polyglycolic acid derivatives	Ethisorb, Resolute, Vicryl mesh
Nonresorbable	Cellulose acetate filter	Millipore paper filter
	Rubber dam	Rubber filter
	Expanded polytetrafluoroethylene (e-PTFE)	Gore Tex
	Dense polytetrafluoroethylene (d-PTFE)	Cytoplast
	Titanium mesh	Cytoflex
	Ethylene cellulose	BenaCel

Table 1.4 Types of bone graft materials used in periodontal regeneration procedures (Cho et al., 2017).

Type	Material
Autograft	*Extraoral* Iliac Crest, Tibia, Fibula, Ribs *Intraoral* Chin, Exostosis, Ramus, Tuberosity
Allograft	Mineralized (FDBA) and demineralized freeze-dried bone allografts (DFDBA)
Xenograft	Bovine derived, porcine derived, equine derived
Alloplast	Hydroxyapatite, calcium phosphate, β-TCP, bioactive glass, synthetic glass

Table 1.5 Showing a summary of growth factors used in periodontal regeneration procedures (Suárez-López del Amo et al., 2015).

(a)

Agent	rhPDGF-BB	EMD	PRP/PRF	FGF-2
Origin	Blood platelets	Hertwig's epithelial root sheath	Platelet alpha granules	Fibroblast growth factors family
Composition	Protein	90% Amelogenin	PDGF, I-LGF, VEGF, TGF-β	Protein
MOA	Mainly chemotaxis and mitogenesis	Precise MOA still unknown	Combination of different MOA of different growth factors contained with the platelet concentrates	Proliferation PDL cells Migration PDL cells Differentiation PDL cells ECM production
Indications/common uses	(i) Intrabony defects (ii) Furcations (iii) Gingival recession defects (iv) Often used in combination with allograft or xenograft	(i) Intrabony defect (ii) Class II furcation defects (iii) Recession coverage procedures	(i) Recession coverage procedures (ii) Barrier membrane	(i) Peri-implant defects (ii) Intrabony defects
FDA approval	(i) Intrabony defects (ii) Furcations (iii) Gingival recession	(i) Intrabony defects (ii) Optimize tissue height in esthetic zone	Not regulated	Not yet approved
Manufacturer	GEM 21S (Osteohealth)	Emdogain (Straumann)	Multiple machines for platelet concentrates fabrications are available	Not yet commercially available

(b)

Agent	BMP-2	BMP-7	GDF-5	Teriparatide
Origin	Recombinant DNA biotechnology using mammalian cells	Recombinant DNA biotechnology using mammalian cells	Recombinant DNA process using bacterial expression followed by *in vitro* refolding	Recombinant DNA
Composition	Bone Morphogenic Protein-2	Bone Morphogenic Protein-7	Growth Differential Factor-5	Parathyroid hormone's (PTH) first 34 amino acids
MOA	Increased proliferation, mineralization, and expression of alkaline phosphatase and osteocalcin	Increased proliferation, mineralization, and expression of alkaline phosphatase and osteocalcin	Increased early differentiation and matrix production	Modify proliferation of mineralized markers
Indications/common uses	(i) Systemic or anatomic condition where successful bone regeneration cannot be achieved with conventional grafts (ii) No with demineralized bovine bone	(i) Systemic or anatomic condition where successful bone regeneration cannot be achieved with conventional grafts (ii) No with demineralized bovine bone	Systemic or anatomic condition where successful bone regeneration cannot be achieved with conventional grafts	Bone metabolism disease that can jeopardize implant stability and osseointegration process
FDA approval	Sinus augmentation Socket preservation	Sinus augmentation Socket preservation	Sinus augmentation Socket preservation	—
Manufacturer	Infuse Bone Graft (Medtronic Inc.)	Osigraft (Stryker Biotech Inc.)	Scil Technology Inc.	Forteo (Eli Lilly Inc.)

MOA: mechanism of action; FDA: Food and Drug Administration.

1.2.1 Properties of an Ideal Bone Graft Material:

Currently in dentistry there are significant clinical challenges associated with the replacement of severe localized bone loss from periodontal disease. For this reason, a variety of materials and techniques have been developed to enable surgeons to address this problem, each of these materials having both advantages and disadvantages. However, four characteristic features are desirable when developing a valuable mainstream bone graft material and these include:

(i) *Osseointegration*: is the ability to form a chemical bond with the surface of the bone without any interference of fibrous tissue encapsulation (Costantino and Friedman, 1994);

(ii) *Osteogenesis*: is the process by which osteoblasts that exist in the grafting material are able to form bone into the surgical site (Cypher and Grossman, 1996). Autogenous iliac bone and marrow grafts are optimal examples of these materials;

(iii) *Osteoconduction*: is the characteristic of a grafting material to enhance bone apposition from existing living bone and this process necessitates the availability of differentiated mesenchymal cells. A grafting material is osteoconductive when it provides a scaffold suitable for the apposition of new bone. Hydroxyapatite is an example of osteoconductive graft;

(iv) *Osteoinduction*: is the ability of a grafting material to stimulate the transformation of the undifferentiated pre-osteoblast into a viable osteoblast; thereby enabling the newly osteoid tissue to be deposited and mineralised. This mechanism is mediated by a specific type of protein, such as bone morphogenic proteins (BMPs) (Ogunsalu, 2011).

1.2.2 Classification of Current Bone Graft Materials:

(i) *Autografts*: these materials exhibit osteogenic, osteoconductive and osteoinductive properties. Limitations have been attributed to the longer operative time, lack of availability, serious morbidity related to blood loss, localized loss of sensation, wound complications and donor site chronic pain (Kurz et al., 1989);

(ii) *Allografts*: these are non-vital grafting material (tissue) transferable from one individual to another of the same species. They possess osteoconductive but poor osteoinductive properties, their main beneficial advantages include greater availability in hospital bone banks as well as removing the requirement for surgical intervention from the donor site. However, their disadvantages are associated with a potential risk of disease transmission, exclusion of osteogenic features, variable clinical outcomes and high cost;

(iii) *Xenografts*: which are materials (tissues) shared between different species. Xenografts exhibit osteoconductive, good availability and have no risk of disease transmission (Dumitrescu, 2011). In dentistry, xenografts applied as a bone graft are currently obtainable in three sources: bovine bone, equine bone and natural coral or algae.

(iv) *Synthetic Bone Graft*: a miscellaneous artificial bone graft material has been engineered during the past 30 years with the aim to restore bone voids. Mostly these materials provide only two out of four properties for an ideal bone graft material. These are osteointegration and osteoconduction properties respectively. Optimally, synthetic bone graft substitutes should mimic the native bone in both mechanical and osteogenic properties.

In terms of mechanical properties, the compressive strength of a synthetic bone graft substitute should be identical to the cortical/cancellous bone that is being

replaced. To approach this requirement, a similar modulus of elasticity to that of natural bone should be acknowledged to avoid any stress shielding in addition to keeping sufficient toughness against fatigue fracture under overloading.

Based on Ashman (1992) an “ideal artificial bone graft material should demonstrate the following properties indicated below:

1) Biocompatible (no inflammatory tissue reactions);
2) Able to serve as a framework for new bone formation;
3) Resorbable in the long term and have potential for replacement by the host bone;
4) Osteogenic, or at least facilitate new bone formation;
5) Radiopaque;
6) Easy to manipulate clinically;
7) Not support the growth of oral pathogens;
8) Hydrophilic;
9) Available in particulate and moulded forms;
10) Have surface electrical charge (i.e., be charged negatively);
11) Microporous and provide added strength to the regenerating host bone matrix, and permit biological fixation;
12) Readily available;
13) Non allergenic;
14) Adapt to be effective in a broad range of medical situations (e.g., cancer, trauma and infective bone destroying diseases)”(Ashman, 1992);
15) Have a surface that is amenable to grafting;

16) Act as a matrix or vehicle for other materials (e.g., bone protein inducers, antibiotics and steroids);
17) Have a compressive strength comparable to cancellous bone (Ashman, 1992).

A variety of alloplastic synthetic grafts materials have been used to replace bone defects such as bioactive glass (Bioglass®45S5), β-tricalcium phosphate, synthetic hydroxyapatite and calcium phosphate cements (Moore et al., 2001).

Finally, the optimal bone grafting material should be substituted by new bone deposition during the physiological stages of bone remodelling. However, the key determinant factors such as material type, structural features, pH and processing of the material play a significant role in determination the speed of biomaterial resorption and also the type of cells involved in this process (Legeros, 1993). Ideally, the graft resorption rate should be identical with the rate of bone formation; otherwise, faster resorption of graft material may produce gaps in the bony defects having an imbalance with bone apposition. Meanwhile, a slower resorption rate of the implanted material might suppress bone formation and increase fibrous tissue encapsulation.

1.2.3 Periodontal Guided Tissue Regeneration (GTR):

Guided tissue regeneration (GTR) is one of the procedures used for the treatment periodontal bony defects. Through this procedure, different types of barriers (membranes) have been placed in the surgical site of periodontal bony defect to separate the alveolar bone and periodontal ligament from the gingival epithelium and connective tissues (Sheikh et al., 2014). The advantage of GTR is to prevent the migration of the epithelium and the gingival connective tissue to the root surface during periodontal healing process. Thereby, the repopulation of the attachment

loss in periodontal bony defect is regenerated only by the cells from the periodontal ligament and bone tissue cells. The GTR technique is demonstrated in Figure 1.10.

PerioGlas® has been used in combination with different types of barrier membranes in guided tissue periodontal regeneration as reported by (Mengel et al., 2003, Wadhawan et al., 2012). The clinical outcomes of these studies have reported significant improvement in periodontal parameters.

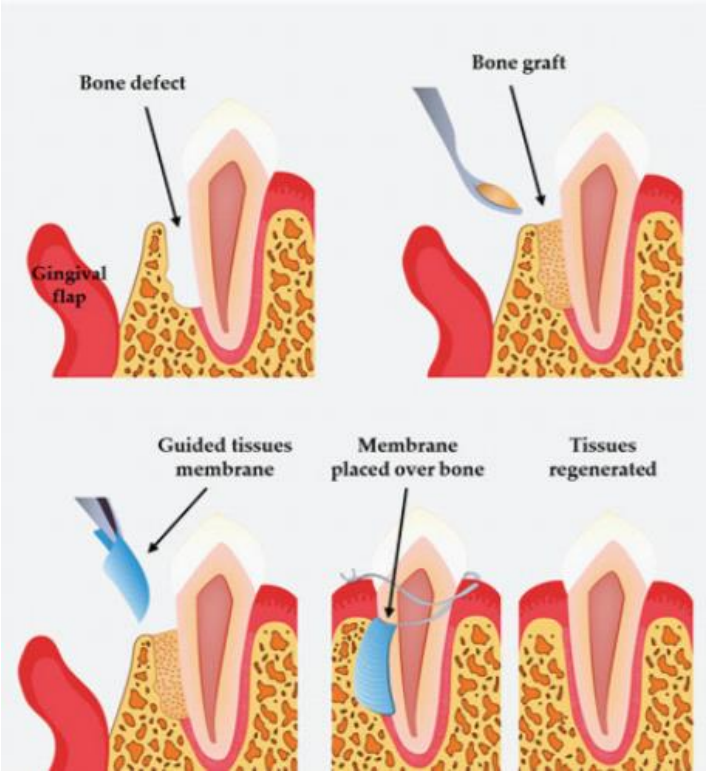

Figure 1.10 Demonstrating the GTR procedure with and without bone grafting (Sheikh et al., 2014).

1.2.4 Bioactive Glass PerioGlas® (Bioglass®45S5) as a Synthetic Bone Graft Substitute in Dentistry:

Periodontal disease(s) can initiate irreversible damage to the underlying periodontal tissues as manifested by a loss of the attachment apparatus and alveolar bone resorption (Socransky and Haffajee, 1997). Bone loss is regarded as a serious clinical problem in dentistry (periodontology), and the repair of damaged osseous tissues initiated by periodontal disease via the use of bioactive glass material as an alternative synthetic bone graft substance was a significant shift in perspective towards developing novel products for dental use (AboElsaad et al., 2009). Historically, bioactive glasses have been used for the treatment of human conductive deafness, resorption of the alveolar ridge and to restore bone loss in periodontal diseases (Wilson et al., 1994).

Bioglass® 45S5 (PerioGlas)® has been previously used in the surgical treatment of periodontal bony defects for the purpose of bone regeneration due to its ability to dissolve in physiological body solutions and releasing ions such as Na^{+}, Ca^{2+}, PO_4^{3-} forming an apatite layer on the glass surface. The particles of this material when used in dentistry have the ability to form a cohesive cluster upon mixing with blood, with easy manipulation and packing into the surgical extracted sockets or periodontal defects (Schepers et al., 1998). This material is haemostatic and upon contact with body fluid, it can bond physio-chemically with the living bone and fibrous connective tissue without an intervening interfacial encapsulation (Wilson and Low, 1992). The outcome of the biological activity is the formation of a biological apatite identical to that of the mineral phase existing in natural bone, which in turn enhances bone damage repair and regeneration. However, the main rationale for periodontal therapy was to construct a healthy periodontium including

architecture, function and mechanical properties in order to restore both the lost periodontal and osseous tissues.

PerioGlas® is a particulate form of bioactive glass (Bioglass®45S5), which has been used in dental applications since 1990 as a synthetic bone graft substitute (Chacko et al., 2014). PerioGlas® was approved by the US Food and Drug Administration (FDA) in 1984 for clinical applications of osteostimulation (Ali et al., 2014). Thermal incorporation of inorganic components of PerioGlas® such as calcium and phosphorous create a sodium silicate network which can be employed specifically for both absorbability and osteoconductivity.

PerioGlas® has also been identified as a biocompatible and non-cytotoxic material (Wilson et al., 1981). Biocompatibility can be defined as "one that allows close contact of living cells at its surface, which does not contain leachables which produce inflammation and which does not prevent growth and division of cells in culture" (Shimizu et al., 1997). Furthermore, it has been stated that Bioactive glasses (PerioGlas®) may act primarily as an osteointegrative and osteoconductive material when exposed to body fluid (Wilson and Low, 1992). In comparison with the other synthetic materials such as hydroxyapatite ceramics, PerioGlas® develops a chemical interfacial bond with both hard and soft tissues through the development of the apatite gel layer on the surface of the glass. This in turn enhances the attraction and concentration of osteoblast cells, thus stimulating new bone deposition and osteoid mineralization (Hench and Ethridge, 1982, Wilson and Nolletti, 1990, Pazzaglia et al., 1989).

The first animal studies on bioactive glass in the treatment of infra-bony defects as a bone filling material was undertaken by Wilson in 1987 (Wilson et al., 1987). It has been determined that the granules of bioactive glass act simultaneously as a bone filler in the periodontal defects enhancing bone proliferation within the defect.

A case study of two-walled defects was performed in the Patas monkey model to compare clinical and histological findings from the following materials and procedures: PerioGlas®, dense hydroxyapatite, tricalcium phosphate and an open surgical debridement technique to study their therapeutic effects on the host tissue response. Subsequently a significant reduction of the junctional epithelium migration was observed in the surgical sites grafted with PerioGlas®, where the migration stopped at the level of the material and bone was formed around the particles within four months. In contrast to the other implanted materials such as hydroxyapatite which exhibited much more junctional epithelium migration (Fetner et al., 1994). This report also showed the ease in handling and manipulation of the bioactive glass material compared to the other graft materials.

A subsequent animal study was performed to evaluate the effect of Bioglass® 45S5 as a bone tissue substitute on the distal femur in the rabbit model (Chou et al., 1998). This study demonstrated a positive response of Bioglass® 45S5 to stimulate new bone growth.

In a clinical study undertaken by Satyanarayana (Satyanarayana et al., 2012), the efficiency of PerioGlas® was evaluated in the treatment of intra-bony defects with localized aggressive periodontitis. Twelve patients with age ranges between 18 and 25 years old have been treated with and without PerioGlas®. Through clinical and radiological investigations, the outcome was improved significantly with PerioGlas® test group than in the control group. This significant improvement was recorded by gaining clinical attachment level and reducing probing depth (P= 0.001).

The evaluation of Bioglass® 45S5 (PerioGlas®) as a therapeutic treatment of periodontal bony defects was reported by Sohrabi (Sohrabi et al., 2012). A meta-analysis study of the data from clinical studies was used as shown in Table 1.6. This

meta-analysis study concluded that PerioGlas® was an efficient treatment for infra bony defects both in probing depth and clinical attachment level over both the control treatment and open flap debridement groups.

Table 1.6 Showing some characteristics meta-analysis data and participants to evaluate the bioactive glass as a therapeutic treatment of periodontal bony defects (Sohrabi et al., 2012):

Citation	Country	Treatment	Control	Study Design	Sample Size	Defect Type	Age (Years)	% Male	Trial Duration	Measured Outcomes*
Subbaiah and Thomas (2011)[37]	India	BG	OFD	Randomized split mouth	8 Participants 16 Teeth	Intrabony defects	NR	NR	9 months	PD and CAL
Leknes et al. (2009)[38]	Norway	BG	EMD	Randomized split mouth	13 Participants 26 Teeth	Intrabony defects	Mean, 52.5	NR	12 months	PD and CAL
Dybvik et al. (2007)[39]	Norway	BG	OFD	Randomized parallel trial	19 Participants 19 Teeth	Intrabony defects	Mean, 54.4	68	12 months	PD and CAL
Keles et al. (2006)[40]	Turkey	BG + GTR	PP + GTR	Randomized split mouth	15 Participants 30 Teeth	intrabony defects	Mean ± SD, 39.1 ± 7.4	53	6 months	CAL
Kuru et al. (2006)[41]	Turkey	BG + EMD	EMD	Randomized parallel trial	23 Participants 30 Teeth	Intrabony defects	Mean, 44.7	NR	8 months	PD and CAL
Sculean et al. (2005)[42]	Netherlands	BG + EMD	EMD	Randomized parallel multicenter	30 Participants 30 Teeth	Intrabony defects	NR	47	1 year	PD and CAL
Mengel et al. (2003)[43]	Germany	BG	GTR	Randomized split mouth	12 Participants 30 Teeth	Intrabony defects	Range, 34 to 59	25	12 months	PD and CAL
Park et al. (2001)[35]	Korea	BG	OFD	Randomized parallel trial	38 Participants 38 Teeth	Intrabony defects	Mean ± SD, 43.9 ± 9.0	62	6 months	PD and CAL
Yukna et al. (2001)[44]	United States	BG	GTR	Randomized split mouth	27 Participants 54 Teeth	Furcation defects	Mean, 54; range, 39 to 72	41	6 months	PD and CAL
Rosenberg et al. (2000)[45]	United States	BG	OFD	Randomized split mouth	12 Participants 12Teeth	Intrabony defects	Mean, 41	50	6 months	CAL
Anderegg et al. (1999)[46]	United States	BG	OFD	Randomized split mouth	15 Participants 30 Teeth	Furcation defects	Mean, 55; range, 42 to 67	40	6 months	PD
Froum et al. (1998)[47]	United States	BG	OFD	Randomized split mouth	16 Participants 59 Teeth	Intrabony or furcation defects	Mean, 43	50	12 months	PD and CAL
Lovelace et al. (1998)[48]	United States	BG	DFDBA	Randomized split mouth	15 Participants 30 Teeth	Intrabony defects	Mean, 45; range, 30 to 63	40	6 months	PD and CAL

Citation	Country	Treatment	Control	Study Design	Sample Size	Defect Type	Age (Years)	% Male	Trial Duration	Measured Outcomes*
Ong et al. (1998)[34]	United States	BG	OFD	Randomized split mouth	14 Participants 27 Teeth	Intrabony defects	Mean, 49.1; range, 35 to 67	78.5	9 to 13 months	PD and CAL
Zamet et al. (1997)[36]	United Kingdom	BG	OFD	Randomized split mouth	22 Participants 44 Teeth	Intrabony defects	Mean ± SD, 39.6 ± 9.6	45.5	12 months	PD and CAL

NR = not reported.
* Measured outcomes includes those outcomes relevant for this meta-analysis (PD and CAL).

The biomedical device PerioGlas® (Block Drug Co., NJ, USA) is composed of a calcium phosphosilicate bioactive glass having a range of particle size from 90 to 710 µm in diameter, as identified by optical microscopy (Dumitrescu, 2011). Furthermore, there are spaces between the large particles which play a role in accelerating the rate of osseo-integration and hard tissue ingrowth (Jones, 2015). However, the smaller particle size(s) of the bioactive glass may provide larger surface areas of glass with more sites for osteoblast adhesion, aggregation and new bone deposition.

When PerioGlas® was implanted *in vivo*, an immediate exchange of ions occurs between the implanted glass and the surrounding environment. This results in releasing ions such as Ca^{2+} and PO_4^{3-} which are then precipitated into the bone-like apatite on the glass surface forming an adherent-interface with biological tissues. This promotes the adhesion of osteoblast cells, which then enhances new bone growth. However, the release of cations, such as Na^{+} and Ca^{2+} generates a rapid pH rise, which is suspected to be too high in the extracellular environment particularly within the confines of the periodontal pocket, which is not considered in the previous studies. It should also be noted that this higher pH has two deleterious biological effects: (i) the alkaline pH inhibited osteoblast activity (specifically the alkaline phosphatase [ALP] activity), osteogenic differentiation and proliferation of the local biological environment as reported by Monfoulet *et al.* (Monfoulet et al., 2014). This is an interesting bone tissue-engineering study investigating the drawbacks of Bioglass® 45S5 and demonstrated the negative influence of a higher pH in the local biological environment on osteogenic proliferation; (ii) the higher pH can actually provide an optimal environment for the growth of one of the most virulent periodontopathic bacteria associated with the development of periodontitis, e.g. *P. gingivalis*. This bacteria has a huge battery of virulence factors for the

progression of periodontal diseases (Haffajee and Socransky, 1994). It has also been reported that “the optimum pH of activity in *P. gingivalis* was 8.3” (Takahashi and Schachtele, 1990). Therefore, the high pH generated by the silicate bioactive glasses dissolution in body fluid may result in an increased growth of *P. gingivalis* which may be detrimental for the initial wound healing stage within the bony defect.

1.3 Silicate Glass:

1.3.1 Glass Definition:

The glass can be defined as *"A non-crystalline solid exhibiting the phenomenon of a glass transition"* (Zarzycki, 1991). The identical physical state is known as the vitreous state. According to McMillan (1979), a glass may also be defined as *"an inorganic product of fusion that has been cooled into a rigid condition without crystallization"*.

Paul (1989) remarked that there was no significant difference between a glass and the equivalent liquid in terms of the irregular atomic arrangement of the glass; which was opposite to the regular atomic structure of a crystalline material (Paul, 1989). However, it should be noted that the glassy state has a short-range order between the atoms and lacks any long-range order. Accordingly, the X-ray diffraction pattern of glass should exhibit only diffuse haloes in contrast to the sharp peaks or lines obtained from a crystalline substance (McMillan, 1979). Glass can be manufactured by two main methods: the first is called the melt-derived route. This process requires less time and expenditure in order to prepare the glass which should be cooled rapidly in this process in order to avoid crystallisation, although it should be noted that this method necessitates the use of higher temperatures to melt the glass (1350°C – 1450°C). Glass crystallisation is prevented by cooling the glass as quickly as possible in order to restrict the opportunity of the atomic symmetrical long-range rearrangement to occur that exists within the crystalline lattice. Turnbull has advocated the rapid quenching method to prevent glass crystallisation (Turnbull, 1969). The second process known as the sol-gel method can produce bioactive glass at a lower temperature (600°C - 700°C) via the hydrolysis and condensation of tetraethylorthosilicate (TEOS) (Li et al., 1991).

The first silicate bioactive glass (Bioglass®45S5) was invented and developed by Professor Larry Hench and co-workers at the University of Florida in 1969. The original Bioglass® 45S5 composition was: 46.1% SiO_2, 24.4% Na_2O, 26.9% CaO and 2.6% P_2O_5 (mol%) (Hench et al., 1971). The bioactivity of bioactive glass was relevant to the formation of a surface layer of hydroxycarbonate apatite like deposit on the surface of the glass which resulted in the development of an adherent interface with the living bone tissues (Elgayar et al., 2005). Currently, bioactive glass 45S5 is available commercially in a range of clinical use such as NovaBone® for orthopaedic application, PerioGlas® for periodontal regeneration and anti-hypersensitivity toothpastes NovaMin™ as well as for the remineralisation of teeth. However, more recently attention has focussed on developing new versions of bioactive glass compositions with improved physical and chemical properties for different dental and medical applications.

1.3.2 Structure of Bioactive Silicate Glass:

Glass structure can be described as the geometrical arrangement of the glass constituents, connecting with each other in a network. This arrangement is irregular and random, unlike the uniform organization of crystalline lattice. Physical and mechanical properties of the glass are determined significantly by its structure; therefore, a fundamental understanding of glass structure is essential in order to optimize the design of glass compositions for new technological applications as described by Tilocca (Tilocca, 2009).

1.3.3 Zachariazen's Model of the Silicate Glass Oxides:

The silica network in the vitreous state is composed of oxygen tetrahedra which encircle the silicon atoms (Figure 1.11). The oxygen tetrahedra share corners with each other in such a pattern that an oxygen atom is connected to two silicon atoms through partially covalent bonds (Zachariasen, 1932). Similarity in the principal structure of a polyhedral network between the glassy state and the crystalline structure has been described and illustrated in the published literature.

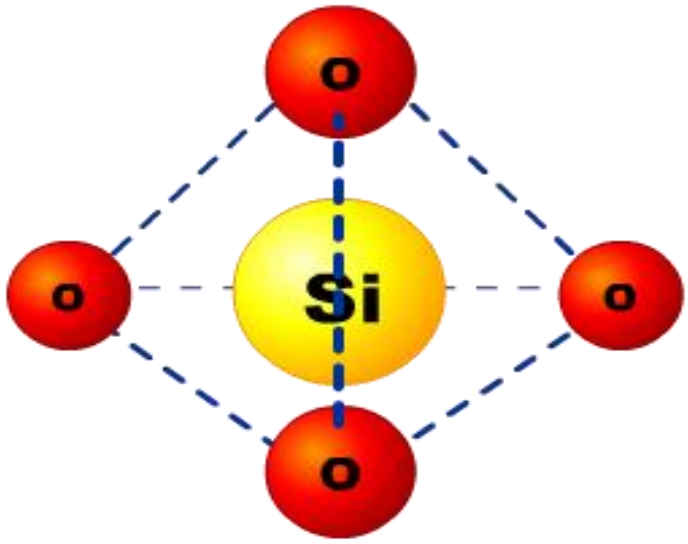

Figure 1.11 The structure of SiO_4 tetrahedra (Pudidotdk, 2009).

Both random atomic distribution in the glass network and the absence of molecular periodicity and symmetry (Figure 1.12), differentiates the glass structure from the crystalline structure and provides its amorphous XRD halo. However, the structural difference between the glass and the equivalent crystal is attributed to the variation in the bond angles and distances between the neighbouring tetrahedra.

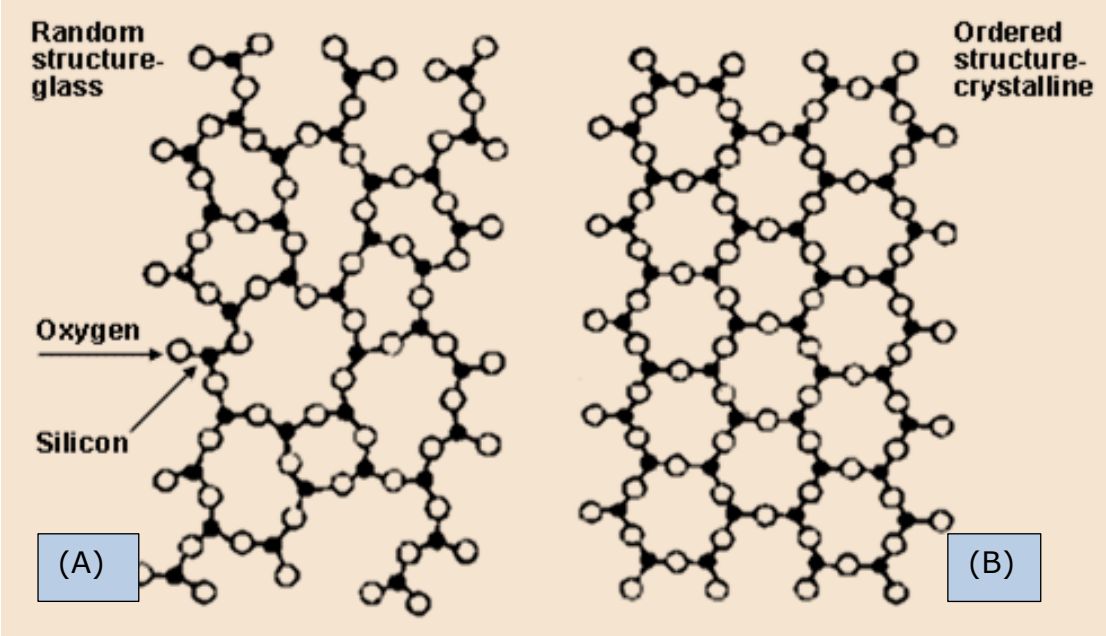

Figure 1.12 Molecular difference between: (A)-glass structure and (B)- crystalline (Zarzycki, 1991).

Additionally, Zachariazen hypothesized that “the Si-O-Si bridge rupture mechanism leads to a loosened network structure with two types of oxygens: an oxygen bonded to two Si is called a bridging oxygen and an oxygen bonded to one Si is called a non-bridging oxygen” (Zarzycki, 1991). Accordingly, Zachariazen classified the oxides into three different categories as the following**:**

1) *Network formers*: these oxides are considered as the essential components of glass structure, they are able on their own to form a glass upon rapid cooling. For example, Silicon dioxide (SiO_2), Boric oxide (B_2O_3) and Phosphorus pentoxide

(P_2O_5). The most important glass former is the SiO_4 tetrahedron where the silicon atom is bonded with an oxygen atom via the bridging oxygens.

2) *Network modifiers*: these cations have the ability to disrupt Si-O-Si bonds and weaken the glass framework by forming non-bridging oxygens with highly ionic-bonds between the non-bridging oxygen and these cations. Sodium oxide and calcium oxide are good examples of network modifiers. One non-bridging oxygen is formed by incorporating a monovalent cation (Na^+) into the glass structure; whereas two non-bridging oxygens are created with a divalent cation (Ca^{2+}) as shown in Figure 1.13.

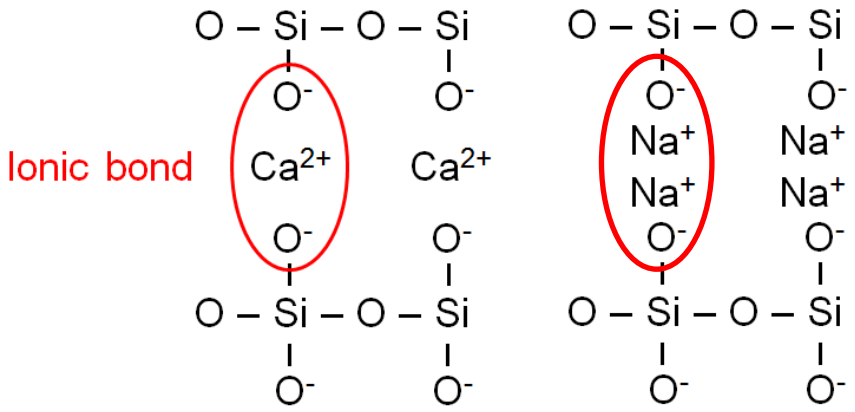

Figure 1.13 Network modifiers in the glass structure (Wallace et al., 1999).

3) *Intermediate oxides*: these oxides are not usually able to form a glass on their own, but they can take part in the establishment of the glass network. Aluminium oxide is a typical example of an intermediate oxide.

1.3.4 Hench's Mechanism of Silicate Glass Dissolution:

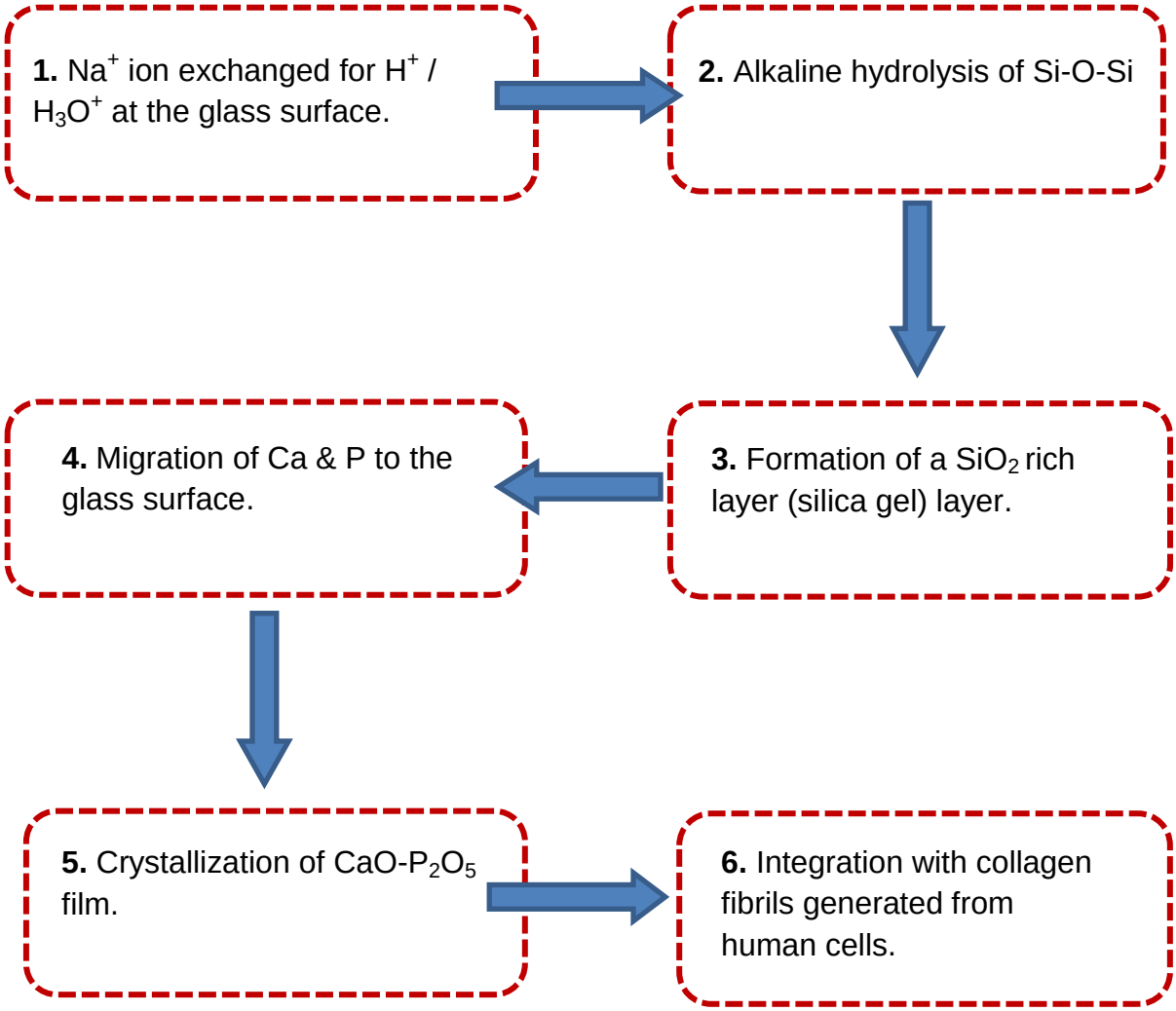

Figure 1.14 Schematic diagram of the Hench mechanism for bioactive silicate glasses degradation (Mneimne, 2014).

The mechanism of bioactive glasses degradation was initially proposed by Larry Hench (Hench, 1991) as shown in Figure 1.14. This glass degradation starts with the process of ion exchange, which includes the exchange of sodium ions from the glass with hydrated protons from the interstitial fluid resulting in a lack of protons from the surrounding body fluids with a simultaneous increase in the concentration of hydroxyl ions, and a subsequent local pH rise. Thereafter, the Si-O-Si bonds in

the glass network would be disrupted by the hydroxyl ions and alkaline hydrolysis, forming the Si-OH silanol group at the glass-solution interface. Due to the silanol concentration, a silica rich layer (known as a silica gel) is formed due to condensation repolymerisation of the silanol groups. Afterward, the migration of calcium and phosphate ions to the glass surface occurs producing an amorphous calcium phosphate rich film on the glass surface. Crystallization of the amorphous calcium phosphate rich layer occurs gradually due to further incorporation of ions from the solution such as hydroxyl and carbonate (Hill, 1996), which creates a mixed hydroxy-carbonate apatite layer (HCA). Osteoblasts attach to the apatite formed and produce Type I collagen on which further apatite forms resulting in new bone formation.

However, Hench's mechanism ignored the release of other network modifiers during the ion exchange step, such as calcium cations, which are likely to generate a high pH in the surrounding solution, leading to the suppression of the ion exchange process of the glass dissolution. This leads to a potential retardation of the apatite formation as demonstrated by Bingel *et al.* (Bingel et al., 2015), who stated that an alkaline buffer solution at pH 9 inhibited the apatite formation, whereas an acidic pH of 5 resulted in significantly faster apatite formation.

1.3.5 Theoretical Network Connectivity (NC) and Silicate Glass Bioactivity:

According to the theory by Hill (Hill, 1996), network connectivity can be defined as "the average number of bridging oxygens per network forming element". The value of network connectivity can be regarded as a good indicator to predict the glass bioactivity (defined as the speed at which apatite forms). It can also predict the glass dissolution behaviour and the susceptibility to glass-in-glass phase separation (Hill, 1996, Elgayar et al., 2005). The network connectivity is related to the average silicon Q distribution. The Q structure is defined as the number of bridging oxygens atoms connected to a silicon atom. The structure of the silicate glass is governed significantly by the proportion of bridging oxygens as shown in Figure 1.15. A silicate glass with four bridging oxygens/silicon has a Q^4 structure and this would correspond to a network connectivity of 4, and a glass with two bridging oxygens/silicon would consist entirely of Q^2 species. This would have a network connectivity of two. As a consequence, it is inevitable to conclude that there was a strong relationship between the network connectivity and the Q distribution model of the glass, this relationship may be categorized in the following manner**:**

- In a pure silica glass where the network connectivity of 4 correlated with the Q^4 species;
- A network connectivity of three is correlated with Q^3 glass structure such as three dimensional glass network;
- A network connectivity of two is correlated with Q^2 distribution which contains linear or two dimensional silicate chains;
- A network connectivity of < two corresponds to Q structure < 2 as present in the case of an invert glasses.

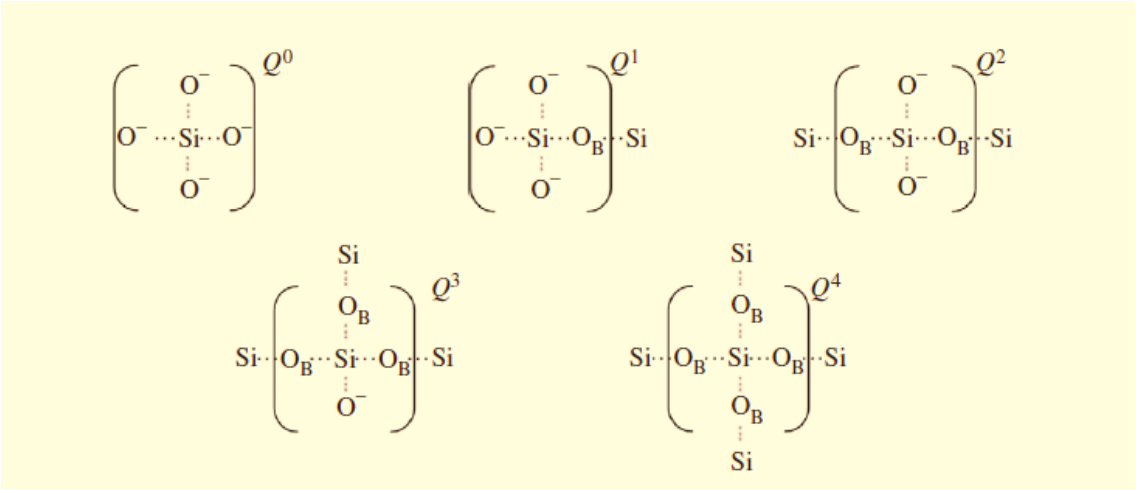

Figure 1.15 Schematic of the different Q structures that can describe Si network connectivity in silicate glasses. OB represents a network-forming bridging oxygen bond (Si–O–Si) (Martin et al., 2012).

The network connectivity (NC) for the present study was calculated using the modified NC equation developed by Hill and Brauer (Hill and Brauer, 2011). It should be taken into account that the phosphate is present as negatively charged orthophosphate species (PO_4^{3-}) where M^{I}_2O and $M^{II}O$ are the mono and divalent modifier oxides in the bioactive glass as in equation 1.1 below:

$$NC = \frac{4[SiO_2] - 2[M^{I}_2O + M^{II}O] + 6[P_2O_5]}{[SiO_2]} \qquad \text{(eq. 1.1)}$$

In order to satisfy the above model and achieve a bioactivity in the designed glass compositions, a glass network connectivity of two is usually preferred for optimal glass bioactivity as recommended by Hill (Hill, 1996) where the glass structure would have a linear or two dimensional chains of infinite molar mass. Glasses with a network connectivity higher than two, tend to be cross-linked or three dimensional structures; whereas below a network connectivity of two the glasses are very prone to an amorphous phase separation and crystallisation. These are referred to as

invert glasses, where the glass modifiers are present at higher molar concentrations than the network formers in the silicate network.

1.3.6 Assessment of Silicate Glass Bioactivity:

Hench (1980) used Tris buffer solution to test the surface bioactivity of the bioactive glass and reported that the bioactive glass had the ability to produce a silica gel film and calcium phosphate layer on its surface upon glass immersion in Tris buffer solution at pH 7.4 (Li et al., 1991).

In order to investigate the bioactivity of the bioactive glass, Kokubo developed a highly supersaturated solution, known as simulated body fluid (SBF), which contained electrolytes in concentrations nearly identical to those ions present in human blood plasma (Kokubo and Takadama, 2006). SBF with its definitive recipe was approved in 2003 by the Technical Committee ISO of International Organisation for Standardisation as a recommended solution for the purpose of assessing and predicting bioactivity for *in vitro* studies measurement as well as for *in vivo* systems**.**

The ISO standard test has been largely accepted by the scientific community and particularly those studying bioactive glasses, as a good indicator for evaluating the glass bioactivity (e.g., apatite formation). In the ISO test, a typical fixed surface area per solution volume ratio is usually used. It is however difficult to apply the ISO test for the glass powders that possess irregular particle shapes (Maçon et al., 2015), while it was considered reliable for testing the bioactivity of solid glasses with uniform geometric shapes only. This can include discs/monolithic and/or tiles shaped samples.

It is acknowledged that the formation of *in vivo* bone-like hydroxyapatite (HAP) is a fundamental requirement for a bioactive material to be able to bond with the host living tissue, when implanted in the human body. Similarly, this apatite formation can be reproduced in an *in vitro* environment when the material is immersed in the simulated body fluid (SBF) having ion concentrations consistent with concentrations found in human blood plasma.

It is worth mentioning however that human blood serum is normally in equilibrium at CO_2 partial pressure of 0.05 atm (5%) which is known to play a key role in buffering the blood serum pH. This condition however cannot be achieved in an *in vitro* serum-like solution (SBF) as proposed by Kokubo, since the controllability of carbonate content at such pressure can be problematic, and this may significantly alter the pH solution (Bohner and Lemaitre, 2009). Using the thermochemical calculations, Bohner and Lemaitre (Bohner and Lemaitre, 2009) reported that simulated body fluid (SBF) was a supersaturated solution with regards to apatite nucleation. This means that the SBF was initially a metastable solution and becomes thermodynamically stable thereafter once the apatite crystals are precipitated. However, the apatite crystallisation might simply be induced by the presence of external bodies such as the surface of a glass container or the edge of scratches. Thus, in order to ensure that apatite was formed from the inner surface of the glass during the time of immersion in the SBF solution, it was recommended to use plastic containers with smooth surfaces with the absence of any edge scratches (Bohner and Lemaitre, 2009). Evaluation of the glass bioactivity in two different physiological solutions; SBF and blood serum can, however, give false positive or false negative results, due to the fact that SBF composition was somewhat different from human blood serum, where proteins which are known to act as apatite nucleation inhibitors are absent (Bohner and Lemaitre, 2009). In addition, other materials for example, calcium sulphate hemihydrates can easily form apatite-like

phase in SBF solution, although it may not be possible to exhibit the similar behaviour *in vivo* (Walsh et al., 2003). Similarly, bone substitute materials such as beta-tricalcium phosphate (β-TCP) was considered insoluble (inert) in SBF, but it has the ability of forming apatite and producing bone bonding in *in vivo* studies (Bohner and Lemaitre, 2009). If the above mentioned facts are taken into consideration, it would appear reasonable to suggest that SBF must not be considered as the ideal test for investigation the glass bioactivity behaviour and should be used with care.

1.3.7 Essential Constituents of the Bioactive Silicate Glasses:

1.3.7.1 The Role of the Phosphate Content on Silicate Glass Structure and Bioactivity:

Although there have been published studies on the effect of the phosphate content on the bioactive glass structure, this area is somewhat controversial. The key point however, is to understand the phosphate structure and speciation in the glass. Previously, it was hypothesized that phosphorus was incorporated into the bioactive silicate glass structure as a pyrophosphate complex by forming Si-O-P bonds (Ahsan et al., 2005, Mysen et al., 1981). On the other hand, other studies have reported that the phosphorus resides in the glass network as an orthophosphate species (Lockyer et al., 1995, O'Donnell et al., 2008b, Elgayar et al., 2005). Therefore, in order to investigate the effect of phosphate on the structure of bioactive glasses, O'Donnell *et al*. (O'Donnell et al., 2008b) studied two series of silicate glasses containing varying phosphate contents (0—9.25 mol%). The first and second series were designed based on the hypothesis that the phosphate existed either as a pyrophosphate phase Q^1 or an orthophosphate species Q^0 respectively. As a result, the first series was designed by adding phosphate to the glass composition and substituting it for silica, while keeping the ratio of sodium oxide to calcium oxide fixed. In contrast, the second series was designed by increasing the phosphate content and simultaneously adjusting the amount of alkali metals (CaO and Na_2O) to ensure charge balance for the suspected orthophosphate phase.

In the first series, termed the non-charge balanced phosphate series, the network connectivity of the glasses increased as the phosphate content increased (O'Donnell et al., 2008b). This could be attributed to the polymerisation of the glass network upon the addition of phosphate to the glass structure, forming a less degradable glass with a negative effect on the glass bioactivity.

However, in the charge balanced series (O'Donnell et al., 2008b) the silicon Q speciation and glass network connectivity did not exhibit any change due to the addition of adequate modifier (Ca^{2+} and Na^{+}) to neutralize the extra negative charge of orthophosphate species. The presence of separate orthophosphate species in the 45S5 glass composition and the absence of Si-O-P bonds however, has been confirmed by Pedone *et al*. studies (Pedone et al., 2010).

Edén (Edén, 2011) stated that the phosphate content in the bioactive glass may be considered as an overriding factor. Increasing the phosphate content enhances the glass bioactivity, assuming the phosphorus is incorporated into the glass network as predominantly an orthophosphate (PO_4^{3-}) species and the network connectivity is less than 2.6. Moreover, according to Edén's suggestion (Edén, 2011), the range of network connectivity for bioactivity was between 2.0 and 2.6. However, the favourable network connectivity for the optimal bioactivity should be close to 2.0 based on Hill's suggestion (Hill and Brauer, 2011) and below 2.4 according to Philips's percolation theory (Phillips and Thorpe, 1985, Thorpe, 1983).

Significantly, the relationship between the glass bioactivity and the phosphate content has been evaluated and it has been suggested that the phosphate content was a more influential factor for glass bioactivity than the network connectivity. This approach has been investigated through an *in vitro* bioactivity study by (O'Donnell et al., 2009). Two series of soda-lime-phospho-silicate glasses (as discussed earlier) were immersed in simulated body fluid (SBF) at different time points up to 21 days. In both series, the treated samples in (SBF) were then characterised by Fourier Transform Infrared Spectroscopy (FTIR) and X-ray diffraction (XRD) in order to reveal the presence of crystalline apatite formation.

Based on the FTIR spectra and the Bragg peaks of XRD, both series glasses with a higher phosphate content (> 3.0 mol%) clearly exhibited a faster apatite deposition

in SBF in contrast to the equivalent glasses with a low phosphate content (< 3.0 mol%). Furthermore, (O'Donnell et al., 2009) investigated the differential impact between the glass containing higher phosphate (6.33 mol% phosphate) versus 45S5 Bioglass® (2.6 mol% phosphate) under identical experimental circumstances upon immersion in SBF up to 24 hours. The FTIR spectra demonstrated that the glass with a higher phosphate content formed more crystalline apatite after 1 day in SBF than 45S5 Bioglass® which showed less intense phosphate bands for apatite in the FTIR spectra. This observation would suggest that the optimal bioactivity may be achieved by increasing the phosphate content.

However, it must be considered that the higher phosphate content could have a negative impact on the glass bioactivity depending on the structural design of the glass as suggested by (Tilocca and Cormack, 2007). In other words, there are limitations to increasing the amount of phosphorus content in the silicate glass composition. For example, if the phosphate enters the glass network as a pyrophosphate species which subsequently increases the network connectivity. This could generate a less resorbable glass and inhibit the apatite precipitation upon the glass's exposure to physiological solutions, thereby reduces the glass bioactivity.

1.3.7.2 Strontium (Sr^{2+}) and its role on the Silicate Glass Structure and Bioactivity:

It has been previously stated that strontium-substituted bioactive glasses may be a promising candidate as a therapeutic treatment in bone substitution (Fredholm et al., 2012). Therefore, strontium (Sr^{2+}) releasing biomaterials have received significant attention for their medical applications due to their potential effect to support bone regeneration. Several investigators have reported that Sr^{2+} was well documented to have a dual simultaneous activity through its action to enhance

osteoblasts (bone forming cells) differentiation and inhibiting osteoclasts (bone resorbing cells) (Bonnelye et al., 2008, Gentleman et al., 2010). Sr^{2+} was also reported to induce osteoblast proliferation and increase alkaline phosphatase activity (ALP) without any deleterious effect on bone mineralization as assessed by the mineral deposition rate and osteoid thickness in alveolar bone (Marie et al., 2001). Furthermore, the available studies report that Sr^{2+} disrupts osteoclast activity by breaking down the actin-containing sealing zone and increasing osteoclast apoptosis (Zhang et al., 2014).

Previous evidence has also demonstrated that the Sr^{2+} can act as an antimicrobial agent at the same concentration at which it up-regulated osteoblast activity. The reason behind this is due to its ability to retard bacterial growth colonization and proliferation throughout *"impeding permeability of cytoplasmic membrane, cell wall synthesis, replication of bacterial chromosomes and cell metabolism"* (Brauer et al., 2012). In addition, strontium was reported to have a bactericidal action against *P. gingivalis* (Liu et al., 2016) and therefore may be used as a therapeutic agent. Strontium resembles calcium (Ca^{2+}) in terms of its charge to size ratio, and thereby can readily be substituted with Ca^{2+} in the lattice of hydroxyapatite (O'Donnell et al., 2008a). Strontium accelerates both the glass dissolution rate and the ion release since it expands the glass network leading to weakening of the surrounding silicate network (Fredholm et al., 2012).

On the other hand, a rapid dissolution rate of bioactive glasses containing strontium and faster ion release generates a higher pH rise, which in turn may suppress the first step of Hench's theory of ion exchange (Na^+ ion exchanged for H^+ / H_3O^+ at the glass surface) of bioactive glass dissolution and may subsequently retard the apatite formation. In terms of the inhibition of apatite formation by a higher pH rise, this was in good agreement with Brauer's experimental data (Bingel et al., 2015).

Therefore, to address the problem of a rapid pH rise and to decelerate a faster dissolution process of bioactive glass, coarse particle size (100-400 μm) and higher P_2O_5 content have been deployed with a synthetic bioactive silicate glass in the current project.

1.4 Phosphate Glass:

1.4.1 Structure of Bioactive Phosphate Glass:

Phosphate glasses can be defined as inorganic polymers. They have been in use over the last 50 years for a variety of different applications due to the biocompatibility between their chemistry and the inorganic matrix of natural bone material. The biocompatibility of the phosphate glasses is attributed to their high solubility and release of ions into the biological environment. They have been used as agricultural fertilisers (Lee et al., 2005) as well as medical devices to release therapeutic ions from their oxides into the cellular media to function cell response stimulation (Neel et al., 2009). However, phosphate glasses are very reactive, highly soluble glasses with no precipitate formed in solution and extremely hygroscopic. They are connected together by non-bridging oxygen and metal cations forming three dimensional structures. Phosphorus pentoxide (P_2O_5) is the basic network former of the geometrical structure of phosphate glasses. The tetrahedron of phosphate glass is classified into four types of Q-speciation (Q^3, Q^2, Q^1 and Q^0) based on the number of bridging oxygens sharing the corner of neighbouring phosphate tetrahedra as demonstrated in the diagram below (Figure 1.16):

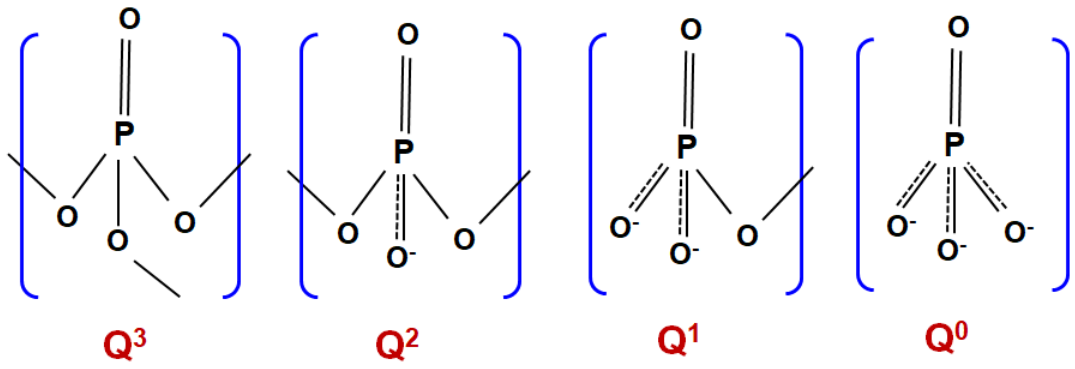

Figure 1.16 Phosphate tetrahedra structure existing in phosphate glasses (Brow, 2000).

In a phosphate glass the Q^n terminology describes the number of bridging oxygens attached to the phosphorus atom to tailor the phosphate tetrahedron. In Figure 1.16 the phosphate atom associated with four oxygen atoms is indicated by “Q” and “n” represents the number of bridging oxygen in the tetrahedral linkage varying from zero to three. However, phosphate glasses can be classified according to their chemical structure into five categories (Carta et al., 2007) namely: 1) ultraphosphates, 2) metaphosphates, 3) polyphosphates, 4) pyrophosphates and 5) orthophosphates as demonstrated in the Table 1.7.

Table 1.7 Elucidating the Q structure of a phosphate glass with respect to its oxygen/phosphorus ratio (Carta et al., 2007).

Q species of phosphate glasses versus oxygen/phosphorus ratio		
O/P	**Classification**	**Q^n geometry**
2.5-3	**Ultraphosphate**	**Q^2+Q^3**
3	**Metaphosphate**	**Q^2**
>3	**Polyphosphate**	**Q^2+Q^1**
3.5	**Pyrophosphate**	**Q^1**
4	**Orthophosphate**	**Q^0**

Similar to the silicate glass, the incorporation of modifier oxides into the phosphate network results in depolymerisation of the network via increasing the number of non-bridging oxygen bonds at the expense of reducing the number of bridging oxygen bonds. Thereby, negative charged non-bridging oxygens would be constituted which are neutralised by the positive charged metal cations. Typically, phosphate glasses require very low temperatures to be prepared and processed, thereby facilitating their incorporation with proteins, antibiotics and cancer therapies for use in medical treatment.

Some studies (Bitar et al., 2004, Bitar et al., 2005, Salih et al., 2007, Lakhkar et al., 2012) have investigated the chemistry of phosphate glass and developed several formulations with different modifiers in order to create an improved phosphate biomaterial potential for both soft and hard tissue regeneration. The incorporation of ions such as strontium into the system of phosphate glasses has been previously reported (Yang et al., 2010, Lakhkar et al., 2011) to up-regulate osteoblasts and down-regulate osteoclasts thereby providing a scaffold upon which new bone growth can occur.

1.4.2 Dissolution Mechanism of Phosphate Glass in Aqueous Medium:

As with Hench's mechanism of the silicate glass dissolution which is outlined in (section 1.3.4), Gao *et al*. (Gao et al., 2004) proposed the mechanism of phosphate glass dissolution by two interdependent steps as in Figure 1.17 below:

(1) Step of ion exchange of Na^+ cations with proton H^+ or H_3O^+

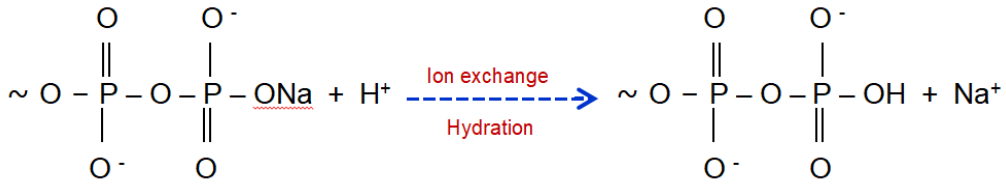

(2) Step of hydrolysis of P—O—P bond

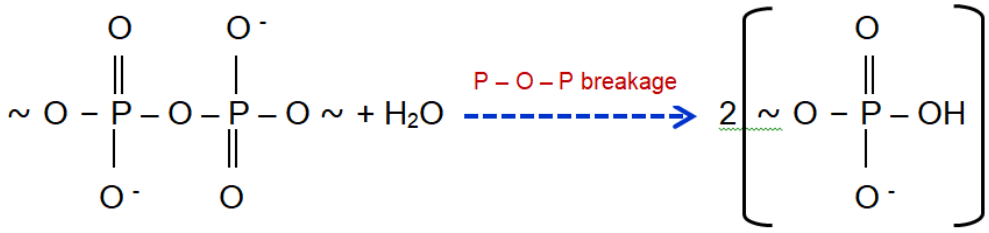

Figure 1.17 Mechanism of phosphate glass dissolution as proposed by Gao et al. (Gao et al., 2004).

(1) *Hydration process*: the ion exchange reaction which involves the replacement of sodium ions from the phosphate glass with hydrated protons from the solution in order to perform Na–H ion exchange reaction, generating a hydrated layer on the glass surface.

(2) *Network cleavage*: resorption of the hydrated layer, causing hydrolysis of P—O—P bonds by the attack of protons ions, resulting in the dissociation of the phosphate glass network and release different chains of polymerization of phosphate glass into the solution.

Based on Bunker *et al*. (Bunker et al., 1984), the kinetics of phosphate glass dissolution is determined by the Na–H ion exchange reaction in which the phosphate glass dissolves uniformly, where the composition of dissolution products in solution is identical with the bulk glass. Conversely, Liu *et al*. (Liu et al., 1996) suggested that the phosphate glass dissolution is dominated by disruption of phosphate glass network, whereas the role of Na–H ion exchange process is limited to hydrate the glass surface and establish the process of phosphate network breakage.

Finally and to conclude, the limitations of silicate PerioGlas® are high pH, low phosphate content and free content of strontium. Stimulation of periodontal tissue regeneration and osteogenesis can be achieved by pH regulation, higher phosphate incorporation and strontium ions release. Therefore, to address these drawbacks, a novel silicate/phosphate glass mixture containing strontium with different fractions of particle size(s) will be created and investigated in this study. ALP will also be included due to its ability to hydrolyse the bonds of phosphate glass in glass mixture and deliver the orthophosphate ions for new bone formation.

1.5 Aim and Objectives of the Study:

Aim:

The main purpose of this project was to design novel degradable bioactive Silicate/Phosphate glass mixtures containing strontium for the therapeutic treatment of periodontal disease to be capable of: (i) the inhibition of the high alkaline bacterial growth of virulent *P.gingivalis* and (ii) the stimulation new bone mineralisation.

Objectives:

- To synthesize and characterize the new developed glasses using X-ray Diffraction (XRD), Differential scanning calorimetry (DSC), Fourier transform infrared spectroscopy (FTIR) and NMR spectroscopy.
- To modulate and regulate the high alkaline pH generated by bioactive silicate glass dissolution in body fluids through the mixing of the silicate glass with a phosphate glass.
- To investigate the ability of the novel synthetic glass mixtures to dissolve and form apatite upon immersion in both Tris-buffer (TB) and simulated body fluid (SBF) depending on the glass particle size.
- To optimize a final novel bioactive glass composition which can be used as a promising bone graft material for therapeutic periodontal application.

2 Materials and Methods:

2.1 Silicate Glass Design and Synthesis:

The novel design strategy based on bioactive silicate glass 45S5 was to increase the phosphorus pentoxide (P_2O_5) content varying from 2.6 mol% in 45S5 to 5.61 mol% in G10 (Table 2.1). it has been previously reported in published studies (Edén, 2011, O'Donnell et al., 2008b, O'Donnell et al., 2008c, O'Donnell et al., 2009, Mneimne et al., 2011) that the higher phosphate content has an influence on enhancing the silicate glass bioactivity and accelerating apatite formation. Therefore, this phosphosilicate series was designed by increasing the phosphate content and simultaneously adjusting the amount of calcium oxide (CaO) to ensure charge balance for the suspected negatively charged orthophosphate species. This also helped to avoid polymerising the silicate glass network upon the phosphate addition, thus forming a degradable silicate glass with optimal bioactivity. Thus, the ratio of [CaO***/(***CaO+Na_2O**)**] increased with an increased phosphate content. Although in the second series of O'Donnell *et al*. study (O'Donnell et al., 2008b), the negative charge of orthophosphate (PO_4^{3-}) species has been neutralised by adjusting the amount of network modifiers sodium oxide and calcium oxide (CaO and Na_2O) together to ensure charge neutrality. In the compositions developed here, only CaO was used to adjust the increasing phosphate content as higher sodium content is likely to cause spontaneous glass crystallisation. In addition, 10% of strontium oxide in molar percent was substituted for calcium oxide in the composition developed here.

Table 2.1 Silicate glass composition in Mol% with a fixed NC of 2.1 of the glass series.

Glass (mole %)	SiO_2	P_2O_5	CaO	Na_2O	SrO	NC
45S5	46.2	2.6	26.9	24.4	0.0	2.1
G2	46.2	2.6	24.2	24.4	2.7	2.1
G4	42.7	4.2	28.0	22.6	2.5	2.1
G5	41.2	4.9	29.7	21.8	2.4	2.1
G10	39.8	5.6	31.2	21.0	2.3	2.1

A 200 g batch of analytical grade glass components, Silicon dioxide (Prince Minerals Ltd., Stoke-on-Trent, UK), Sodium Carbonate, Calcium Carbonate, Phosphorus Pentoxide and Strontium Carbonate (all from Sigma-Aldrich, Gillingham, UK) were mixed and placed in a platinum-rhodium (80/20) crucible and melted for 1 hour at temperature (1390°C - 1400°C) in an electric furnace (EHF 17/3, Lenton, Hope Valley, UK). Subsequently, the glass melt was rapidly quenched in deionised water to prevent crystallisation. Glass frit was dried at 80 °C overnight in an electric dryer (Harvard LTE, UK). After drying, 100 g of glass frit was ground using a vibratory mill (Gyro mill, Glen Creston, London, UK) for 15 seconds to form glass powders, which were then sieved for 30 minutes by using mesh analytical sieves (Endecotts Ltd., London, UK), to obtain three fractions of glass particle sizes (fine < 38 µm, medium 38-100 µm and course 100-400 µm). Ultimately, all the glass powders were stored in dry plastic bags and saved in a dry desiccator for further use.

2.2 Phosphate Glass Design and Synthesis:

Three phosphate glasses P1, P2 and P3 were prepared by using $NH_4H_2PO_4$, $SrCO_3$, K_2CO_3 and $CaCO_3$ as starting materials. The investigated compositions of phosphate glasses are listed in Table 2.2. The precursors were weighed and placed in Platinum/Rhodium crucible with glass batch of 50 gram. Then, the crucible was placed in an electric furnace (EHF 17/3, Lenton, Hope Valley, UK) in order to melt the phosphate glass. The 22 hours temperature programme starting from 25°C (room temperature) and ending at 1150 °C, was used to slowly eliminate the gases produced by the decomposition of the batch materials such as H_2O, NH_3, and CO_2, in addition to reduced evaporation of P_2O_5.

Table 2.2 Phosphate glasses (P-glass) compositions in Mol%

P-glass (Mol%)	P_2O_5	SrO	K_2O	CaO
P1	55	30	15	0
P2	55	0	15	30
P3	55	10	15	20

The procedure of making phosphate glass is described in Figure 2.1. Following placement the crucible with its content of phosphate glass composition in the furnace at approximately 25°C, the temperature was set up to be ramped to 100°C with heating rate [@5°C/min] and stayed for 1 hour. Then the temperature was ramped to 150°C [@5°C/min] and left for 30 min; afterwards the temperature was raised to 200°C [@2°C/min] and left for 2 hours. It was then further heated up to 250°C [@5°C/min] and left for 1 hour. Then, the temperature was increased to 300°C [@5°C/min] and kept for 2 hours. Thereafter it was raised to 600°C

[@2°C/min] and left for 5 hours. Then, it was further ramped to 900°C [@2°C/min] and kept for 2 hours. Finally, the temperature was ramped to 1150°C [@2°C/min] and left for one hour, and then the glass was poured.

The molten phosphate glass was poured into a metal plate and covered by another metal plate. It was left for 10 minutes to be cool and then the glass was crushed and ground manually by the help of mortar and pestle. Then the glass frit was placed in sample plastic bags and labelled. Some samples of each composition were sent to the XRD lab to detect whether the glass is amorphous or crystalline, other samples were investigated in DSC for thermal analysis studies. By using a vibratory mill (Gy-Ro mill, Glen Creston, London, UK), 50 g of phosphate glass frit was ground for 7 minutes to form glass powders, which were then sieved for 30 minutes by using mesh analytical sieves (Endecotts, Ltd., London, UK) to obtain fine particle size < 38 µm. Ultimately, all the glass powders were stored in dry plastic bags and saved in a dry desiccator for further use.

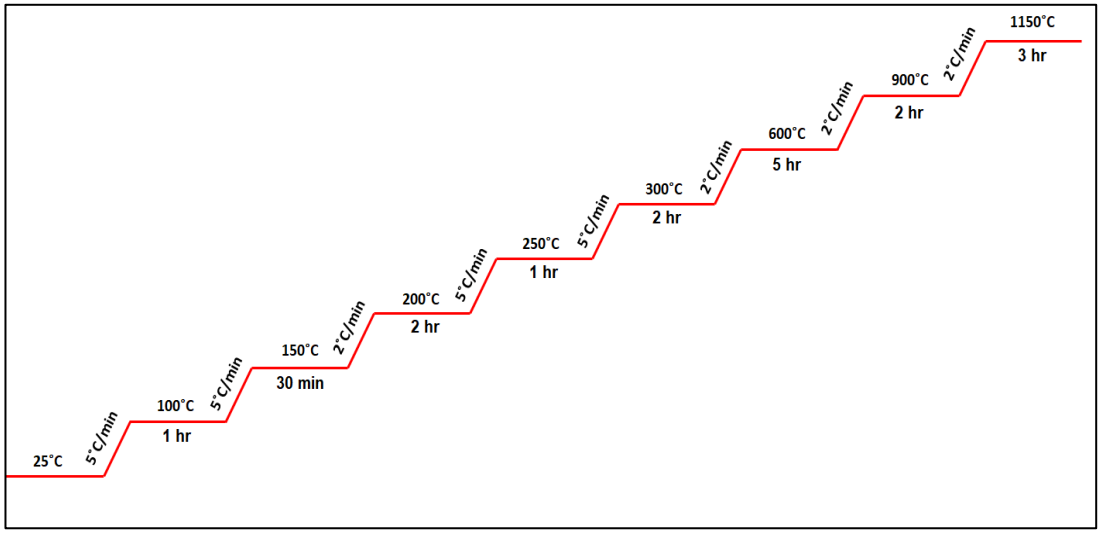

Figure 2.1 Schematic diagram showing the range in temperature and ramping rate used to synthesize the experimental phosphate glasses.

2.3 Glass Characterisation (Solid and Solution State):

2.3.1 Differential Scanning Calorimetry (DSC):

A Stanton Redcroft DSC 1500 (Rheometric Scientific, Epsom, UK) was used for DSC measurements on all glass powders. DSC is a thermal analytical technique, which can be used to determine the glass transition temperature (Tg), crystallisation temperature peak (Tc) and melting temperature (Tm) as shown in Figure 2.3.

A 50mg glass frit was placed in a Pt-Rh crucible and heated under Nitrogen (60ml/min^{-1}) from room temperature (25°C) to (1000°C) at a heating rate of 20°C/min using analytical grade alpha-alumina as a reference. The glass transition temperature (Tg) corresponding to the onset of the glass transition interval was extracted from the DSC plots with an accuracy of ± 5°C.

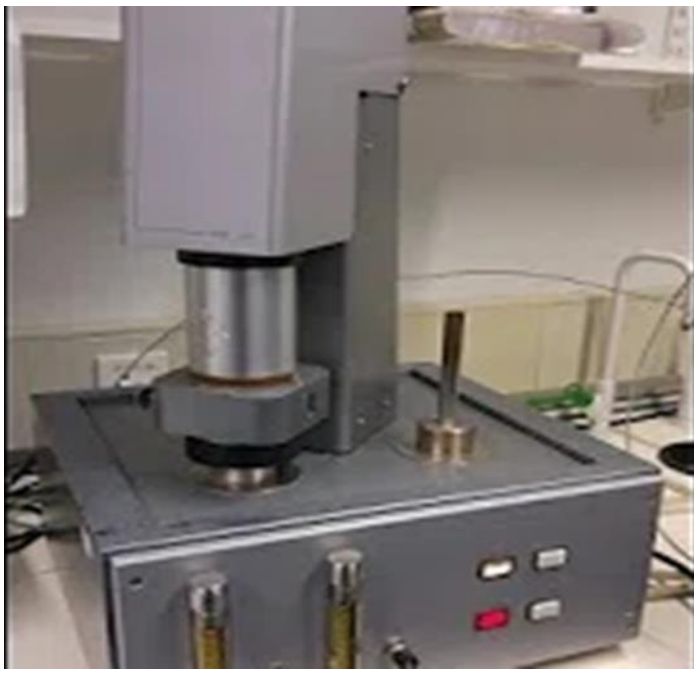

Figure 2.2 A Stanton Redcroft DSC 1500.

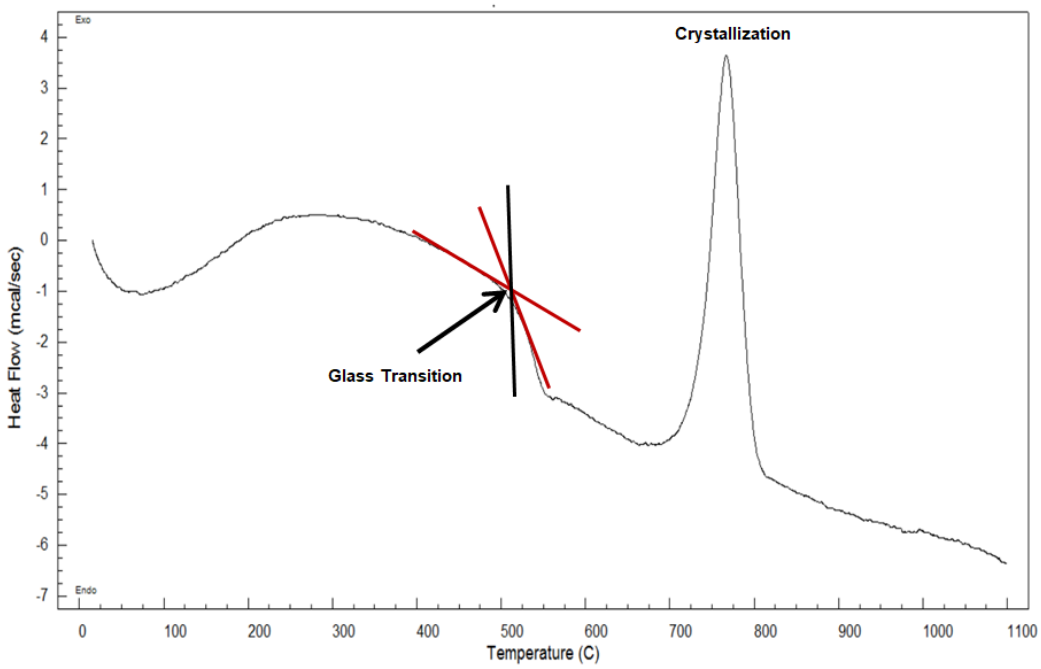

Figure 2.3 Schematic model of DSC trace features demonstrating glass transition and crystallization temperatures.

2.3.2 X-ray diffraction (XRD):

In this project, an X'Pert Pro X-ray diffractometer (PANalytical, Eindhoven, The Netherlands) was employed to determine whether the prepared bioactive glasses were amorphous or crystalline. The amorphous phase of the glassy state displays only diffuse halos compared to the intense sharp peaks given by a crystal phase. XRD was also used to detect the crystalline phase of the apatite formed after immersing the bioactive glass in Tris and SBF solutions at specific time points for the purpose of investigating the glass bioactivity. A small amount of sample was used in this technique. A Bragg-Brentano flat plate geometry was used along with Cu Kα radiation (λ_1=1.54059 Å and λ_2=1.54442 Å). The patterns were collected from 5 to 70° 2θ with a step interval of 0.0334° and a step time of 200.03 sec. The X-ray diffraction pattern was obtained by plotting 2-θ intensity as a function of 2-θ angle.

2.3.3 Fourier Transform Infrared Spectroscopy (FTIR):

FTIR spectroscopy (Spectrum GX, Perkin-Elmer, Cambridge, UK) is a sensitive quantitative and qualitative technique, used to detect the amorphous nature of the untreated glass, the glass dissolution behaviour and possible formation of apatite crystals after studying the glass bioactivity in physiological solutions such as Tris buffer and simulated body fluid. FTIR (Figure 2.4) was employed to reveal the vibrations of the chemical atoms constructing the material. The infra-red spectrum is typically in the range between 4000-400 cm^{-1} since the infra-red frequencies within this range are identical to the essential vibrations of the active group of molecules (Doyle, 1992). The mode of FTIR used in the current project is called Attenuated Total Reflectance (ATR) and has been classified as a sampling technique which can be used together with the infrared spectroscopy to test a solid specimen. During the measurements the infrared beam initially passes through the ATR crystal and then reflects back from the internal surface that is in direct contact with the sample. This reflection produces evanescent waves which later continue to reach the sample with a typical penetration depth varies between 0.5-2 μm. The penetration depth value is highly dependent on the wavelength of light, the angle of incidence; as well as the incidence of refraction for the ATR crystal. Once the beam departed the crystal, it was collected by a detector and interpreted by Fourier transformation technique as interferogram signals. In this study, the data were collected from 500 to 1800 cm^{-1} (wavenumbers).

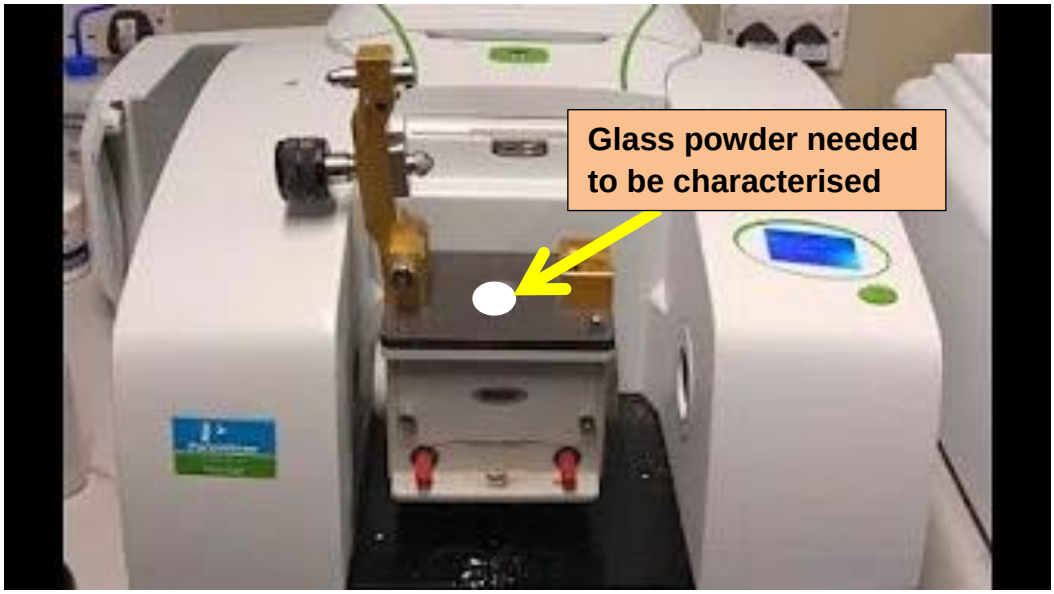

Figure 2.4 The ATR-FTIR Spectrometer (Spectrum GX, Perkin-Elmer, Cambridge, UK).

2.3.4 Particle Size Analyser:

Particle size analysis was undertaken by using the Beckman Coulter LS 13 320 Laser Diffraction (Figure 2.5). This particle size analyser was used to measure the size distribution of the glass particles. It works by measuring the intensity of the light scattering from the glass particles which are suspended in the distilled water through an exposure to the laser beam. The large angle of the scattered laser results in a small particle size and vice versa. The amount of sample required was related to the particle size range of the sample; the lower particle size the less sample required. The minimum amounts for selected ranges are: 0.5 g for <40 µm, 1.5 g for 40-100 µm and 5 g for 100-500 µm.

Figure 2.5 The Beckman Coulter LS 13 320 Laser Diffraction.

2.3.5 Magic Angle Spinning-Nuclear Magnetic Resonance (MAS-NMR):

Magic Angle Spinning-Nuclear Magnetic Resonance (MAS-NMR) is a powerful technique used to study the physical and chemical properties of atoms and molecules of materials by providing full details and information of their dynamics, chemical structure and reaction state. A wide range of solids and solutions samples can be studied by using this technique. In this project, the ^{31}P MAS-NMR was carried out using the Bruker probe and 600MHz Bruker spectrometer with permanent magnetic field of 14.1 Tesla at the resonance frequency of 242.9 MHz. Two different spinning speeds were set up for the solid sample depending of the rotor used 22 kHz for 2.5 mm rotor and 12 kHz with 4 mm rotor. The solid sample was run for 32 minutes using a rotor 2.5 mm and 16 minutes in case of rotor 4 mm. The recycle delay of 60 s was used. The reference of the chemical shift was 85% H_3PO_4. The chemical species of ^{31}P nucleus and glass structure were interpreted by the chemical shift and the intensity of the peaks. Both untreated and treated glass samples were investigated in this technique.

2.3.6 ^{31}P Solution State NMR spectroscopy:

The ^{31}P solution NMR was run on a Bruker Avance III 400 MHz spectrometer. The frequency for ^{31}P was 162.0 MHz. 32 scans were acquired with a spectral width of 395.7 ppm (64102 Hz) were used prior to acquisition. The important NMR point being that ~10% Heavy Water D_2O was added to them for the field/frequency lock. This analysis was performed by transferring 500 microliter of the aqueous samples required to be run into the NMR tubes (Wilmad® NMR tubes 5 mm diameter) together with 50 microliter of D_2O using a Gilson pipette. The D_2O was required for two purposes: (i) as a reference to compensate for magnetic field fluctuations which are significant for solution spectra where the line width is of the order of 1 Hz, and (ii) as the means of adjusting magnetic field homogeneity to obtain sharp lines.

2.3.7 Inductively Coupled Plasma–Optical Emission Spectroscopy (ICP-OES):

ICP-OES (Varian Vista-PRO, Varian Ltd., Oxford, UK) is a sensitive technique used to measure ions in the filtered solution such as Ca^{2+}, Si^{4+}, P^{5+}, Na^{+}, K^{+} and Sr^{2+} concentrations up to a very low concentration (as low as 0.1 ppm). The advantages of ICP-OES are related to the qualitative and quantitative measurement of the investigated samples. In addition, through ICP-OES many different elements can be measured at the same time to provide profile of ions released from the tested solution.

In this study all samples were acidified by using 69% nitric acid (VWR International Ltd) before analysis in order to prevent precipitation of ions during solution analysis. In silicate glass, the dilution of the samples with deionised water was (1:4), whilst

the dilution in glass mixtures was (1:33.3). Different dilution was accounted to the difference in the ions concentration released from different original glasses.

2.4 Bioactivity Test (Immersion Test):

2.4.1 Tris Buffer Solution (TB):

This solution is free of calcium and phosphate ions and it can be used to investigate the bioactivity of the glass to dissolve and form apatite. Tris buffer was prepared by adding 15.09 g of Tris (hydroxymethyl aminomethane) (Sigma-Aldrich, Gillingham, UK) into 800 ml of deionised water. Afterwards, 44.2 ml of 1M HCl (Sigma-Aldrich, Gillingham, UK) was slowly added to the solution under stirring, the resulting solution was then put in a plastic bottle and kept in a shaking incubator overnight at 37°C. The next step involved the adjustment the pH of the solution by slowly adding 1 M HCl using pH meter (Oakton Instruments, Nijkerk, the Netherlands). Once the pH value of the solution has reached 7.35, the solution was transferred into 2 litres flask and diluted by adding deionised water to fill up to a volume of 2 litres.

2.4.2 Simulated Body Fluid (SBF):

SBF is a highly supersaturated solution, which contains electrolytes in concentrations roughly similar to those ions existing in human blood plasma; therefore, it is useful to assess the bioactivity of the glass. SBF was prepared as described by Kokubo *et al.* (Kokubo et al., 1990) in two steps. In the first step, the following chemical reagents were added slowly and sequentially into 1500 ml of deionised water: 15.992g of NaCl, followed by 0.70g of $NaHCO_3$, 0.448g of KCl, then 0.456g of $K_2HPO_4.3H_2O$, 0.610g of $MgCl_2.6H_2O$, 70ml of 1.0M HCl, 0.736g of $CaCl_2.2H_2O$, 0.142g of Na_2SO_4 and finally 12.114g of Tris hydroxymethyl aminomethane (all Sigma-Aldrich, UK). The resulting solution was kept in two litres

polyethylene bottle in an incubator overnight at 37ºC. The second step was the pH adjustment to 7.35 at 37ºC by slowly adding 1 M HCl to the solution. The pH change was measured by using pH meter (Oakton Instruments), and then the solution was transferred into two litres of deionised water. The completed SBF solution was kept in an incubator at 37ºC prior to use for dissolution studies.

2.4.3 ALP Enzyme Containing Tris Buffer Solution:

This solution was made by adding 1.53 microliter of bovine ALP (Sigma-Aldrich) into 100 ml Tris buffer solution. This addition was performed based on the calculated concentration of ALP enzyme in GCF of periodontal bony defects (Sanikop et al., 2012). Then, the resulting solution was kept in an incubator shaker (KS 4000 ic Control, IKA, Germany) at temperature 37ºC and pH 7.35 to be used for immersion test.

2.5 The Procedure of Glass Dissolution:

2.5.1 The Immersion Test of the ISO-Standard and Non-ISO-Standard Bioactivity Tests in Tris Buffer:

In order to assess the glass bioactivity (the apatite formation rate), the ISO-Standard and Non-ISO-Standard methods were used in the present study (Figure 2.6). The ISO-Standard test was performed for a fixed surface area per solution volume ratio where 0.5 g of glass powder was immersed in 10ml Tris buffer solution, whereas the Non-ISO-Standard bioactivity test was used for a Non-Fixed ratio where 0.075 g of glass powder was immersed in 50ml Tris buffer.

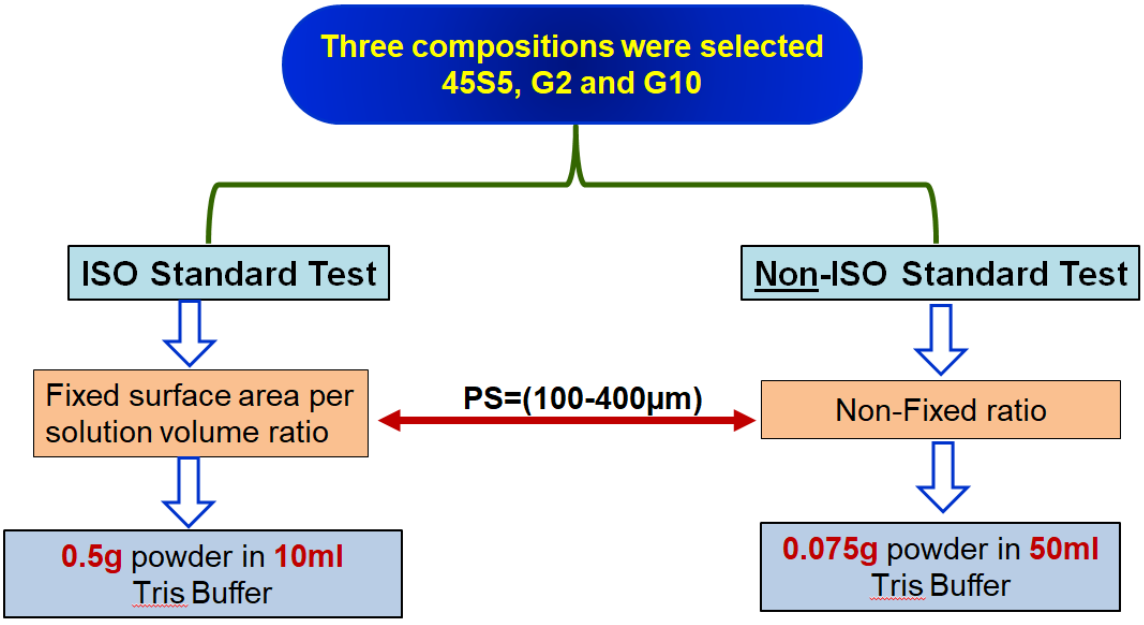

Figure 2.6 Schematic diagram illustrating the ISO-Standard and Non-ISO-Standard bioactivity tests in TB.

2.5.2 The Immersion Test of the Influence of Bioactive Glass Particle Size on Glass Dissolution Rate, pH and apatite Formation in SBF:

In this process, 0.075 g of glass powders were immersed in 50 ml of SBF using three fractions of glass particle size (<38 µm, 38-100 µm and 100-400 µm) (Figure 2.7).

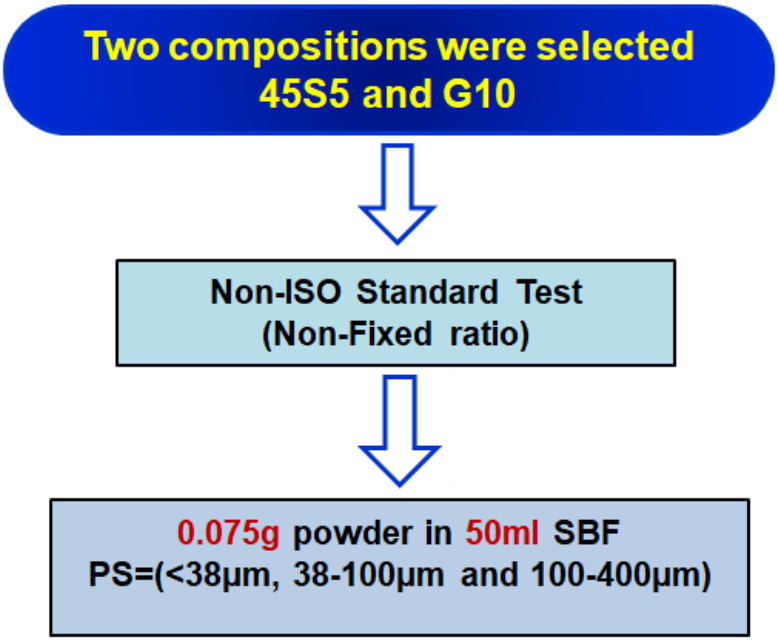

Figure 2.7 Schematic diagram illustrating the immersion test of the influence of the glass particle size on the glass bioactivity.

2.5.3 The Immersion Test of the Silicate/Phosphate Glass Mixtures Dissolution Process in Tris Buffer and ALP Enzyme Containing Tris Buffer Solution:

In these experimental works, 0.15 g of the silicate/phosphate glass mixtures was immersed in 10 ml for both Tris Buffer and ALP Containing Tris Buffer Solution (Figure 2.8).

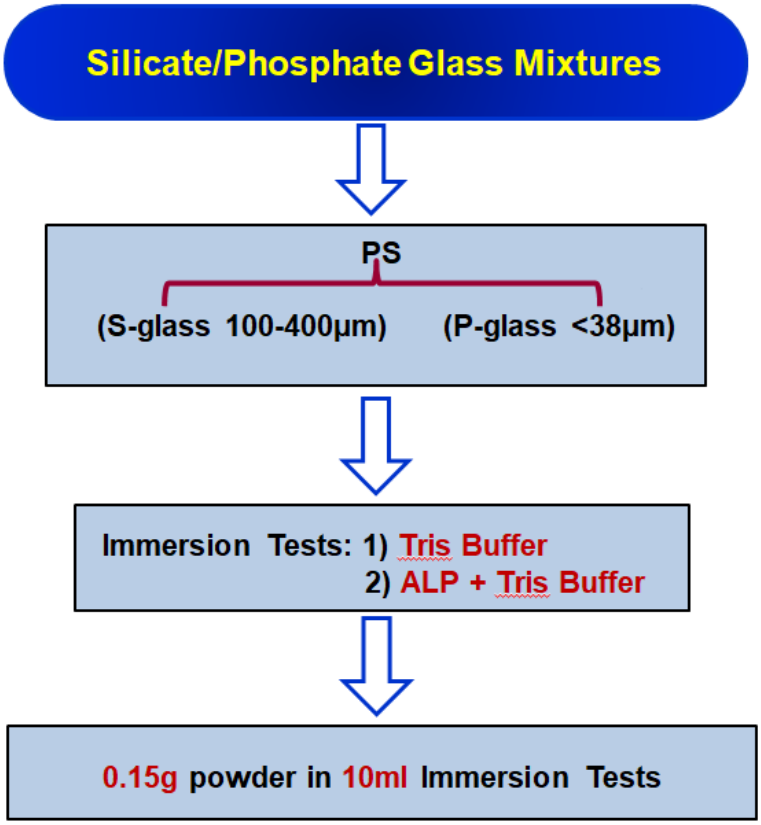

Figure 2.8 Schematic diagram illustrating the immersion test of the Silicate/Phosphate glass mixtures in TB and ALP containing TB Solution.

2.6 General Immersion Protocol:

Overall, after immersion the glass powders in all of the three processes mentioned above, the suspended solutions were placed in plastic containers and these containers were kept in a shaking incubator at 37ºC for a specific period based on the range of immersion time points of the experiment. At the end of each immersion time point, the samples were taken out from the incubator and the pH change was measured by a pH meter (Oakton Instruments, Nijkerk, Netherlands). Then, the suspended solution was filtered using filter paper (Fisher Scientific with a diameter of 150mm) and the collected solid powders were placed in Petri dishes and kept in drying cabinet at 37ºC overnight. While, the filtered solutions were kept in falcon tubes (Fisher Scientific) and stored in a fridge at 4ºC. The dried collected solid powders were characterised by using FTIR, XRD and ^{31}P MAS-NMR techniques to investigate the apatite forming ability of the glass, whilst the filtered solutions were characterised by ICP-OES analysis to study the ion release trend. Two measurements were used for the individual glass compositions at each time point; the standard deviations were estimated to be ± 0.2 for the ions released and ± 0.1 for the pH data.

3 Development and Characterisation of Bioactive Silicate Glass:

3.1 Introduction:

Bioactive silicate glasses dissolve in body fluids releasing Ca^{2+}, PO_4^{3-} ions and form a hydroxycarbonate apatite-like layer. The 45S5 glass known as Bioglass® is sold under the trade names NovaBone and PerioGlas® and was used as a bone grafting material and for treating periodontal disease.

Hench first developed Bioglass® in the late 1960s. He identified the mechanism of bioactive glasses degradation (Hench, 1991). Whilst this mechanism is widely accepted, it does not explain the high dependence of glass dissolution and bioactivity on the silica content and on the network connectivity of the glass (Elgayar, 2004).

The first step in the mechanism involves the ion exchange of Ca^{2+} and Na^{+} ions for protons in the external medium. This ion exchange process results in an increase in the local pH. Brauer and co-workers have shown that glass dissolution is inhibited by pHs > 8 (Bingel et al., 2015). The pH rise that results from the initial dissolution of the bioactive silicate glasses can inhibit further dissolution and apatite-like phase formation. The high pH can result in cytotoxicity (Monfoulet et al., 2014), but may also favour hydroxyapatite formation since hydroxyl ions are needed for the formation of hydroxyapatite. In some cases the high pH along with the relatively high ion concentrations can be beneficial, since many of the bacteria involved in wound infections grow optimally under acidic conditions e.g. osteomyelitis (Alomar et al., 2008). This is particularly the case with osteomyelitis and the 53P4 glass composition, which is sold under the trade name BoneAlive®, which has a well-documented clinical efficacy in treating osteomyelitis (Drago et al., 2014, Drago et al., 2015). Cariogenic bacteria involved in tooth decay also have optimum growth at acidic pHs. However, many of the bacteria involved in periodontal disease in

contrast have optimum growth at pHs > 8. For example *P. gingivalis* the organism widely regarded as playing a key orchestrating role in periodontitis (Haffajee and Socransky, 1994) has an optimum growth at a pH of about 8.3 (Takahashi and Schachtele, 1990). Whilst the high pH generated by bioactive silicate glasses may be attractive for many applications it could be detrimental for treating periodontal disease, particularly if pocket debridement/cleaning is incomplete leaving behind viable bacteria. Under these circumstances the high pH generated by a bioactive silicate glass could stimulate the bacteria involved in periodontal disease. The use of 45S5 in the form of PerioGlas® has received a mixed reception from clinicians either good (Lovelace et al., 1998) or bad (Singh et al.). The potential high pH generated by NovaBone (PerioGlas®) could also be detrimental, particularly where:

i) there is a relatively low turnover of body fluids at the implant site

ii) the defect size to be grafted is large

iii) The glass particles are densely packed and the fluid flow through the construct is low.

The bioactivity of bioactive glasses is often performed by following their dissolution and apatite-like phase forming ability in simulated body fluid that mimics the ionic concentration of ions found in body fluids (Kokubo and Takadama, 2006). However, the clinical relevance of this test has been questioned (Bohner and Lemaitre, 2009). This test specifies a glass surface to volume ratio. However, the clinical use of bioactive glass will not involve a fixed ratio of glass to body fluid and furthermore this body fluid will have a continuous turnover. However there is virtually no data on the turnover of fluids in different bone sites.

3.2 Silicate Glass Characterisation (Results and Discussion):

3.2.1 X-ray Diffraction (XRD) Results:

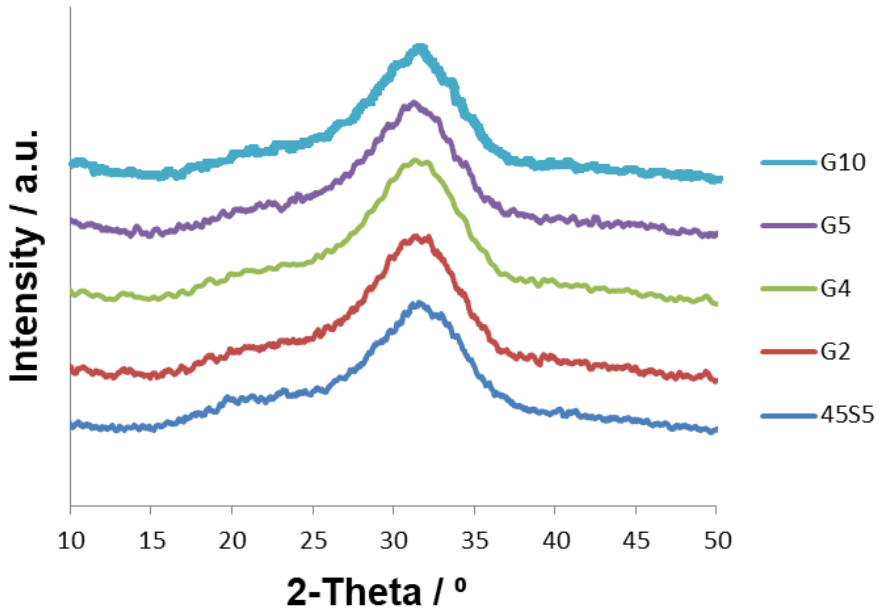

Figure 3.1 XRD patterns demonstrate that all the unreacted phosphosilicate glasses were amorphous.

The XRD patterns in Figure 3.1 demonstrate that all glasses in this phosphosilicate series including 45S5 reveal broad halos localised around 32° 2-Theta, which is a characteristic feature of an amorphous structure. It is essential to evidence the amorphous state of these unreacted glasses before performing the bioactivity tests because the presence of crystalline species results in suppression of the ion exchange reaction of glass dissolution in physiological buffer solutions, subsequently inhibiting the apatite forming ability.

3.2.2 Fourier Transform Infrared Spectroscopy (FTIR) Results:

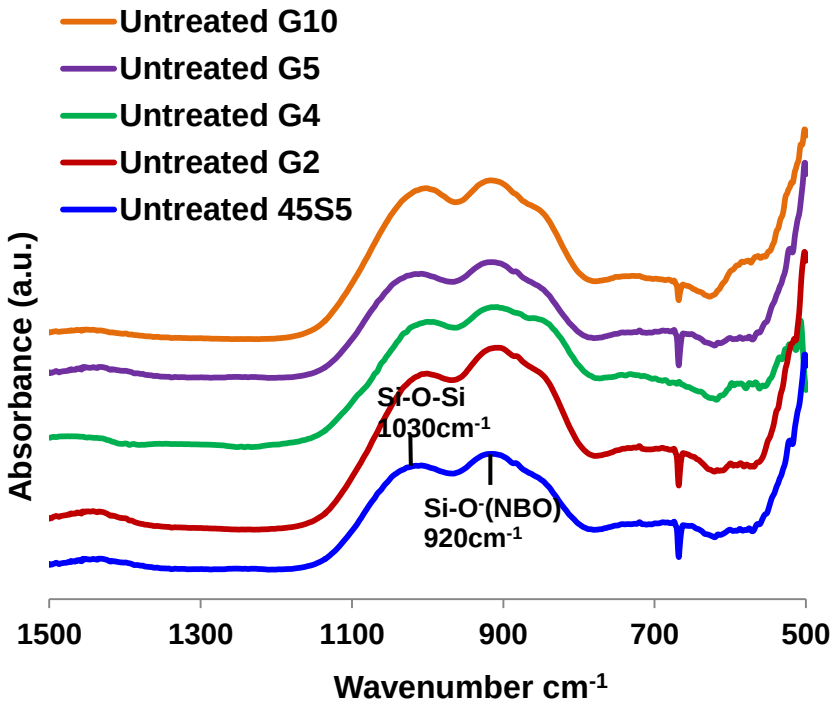

Figure 3.2 FTIR spectra demonstrate that all unreacted glasses in phosphate series were amorphous.

The FTIR spectra in Figure 3.2 reveal that all the glasses including the 45S5 are amorphous as indicated by the presence of: (i) only broad bands as expected for an amorphous solid as opposed to the sharp features that would indicate the presence of crystalline species; (ii) well-defined bands at 920 cm^{-1}, which is assigned to non-bridging oxygens ($Si\text{-}O^{-}\text{-}M^{+}$, where M^{+} is an alkali metal modifier cation) and also (iii) vibrational stretches at 1030 cm^{-1} of Si-O-Si in the silicate glass network (Jones et al., 2001); (Brauer et al., 2010). The major difference in the spectra of the glasses is the vibrational P-O band at 580 cm^{-1} which is more pronounced with higher phosphate content and is particularly strong in G10 (the highest phosphate content). Whereas, this band is weak in the low phosphate glass (45S5). This phenomenon

has been observed previously by a number of authors (O'Donnell et al., 2008c, Mathew et al., 2013, Mneimne, 2014).

3.2.3 Particle Size Analysis Results:

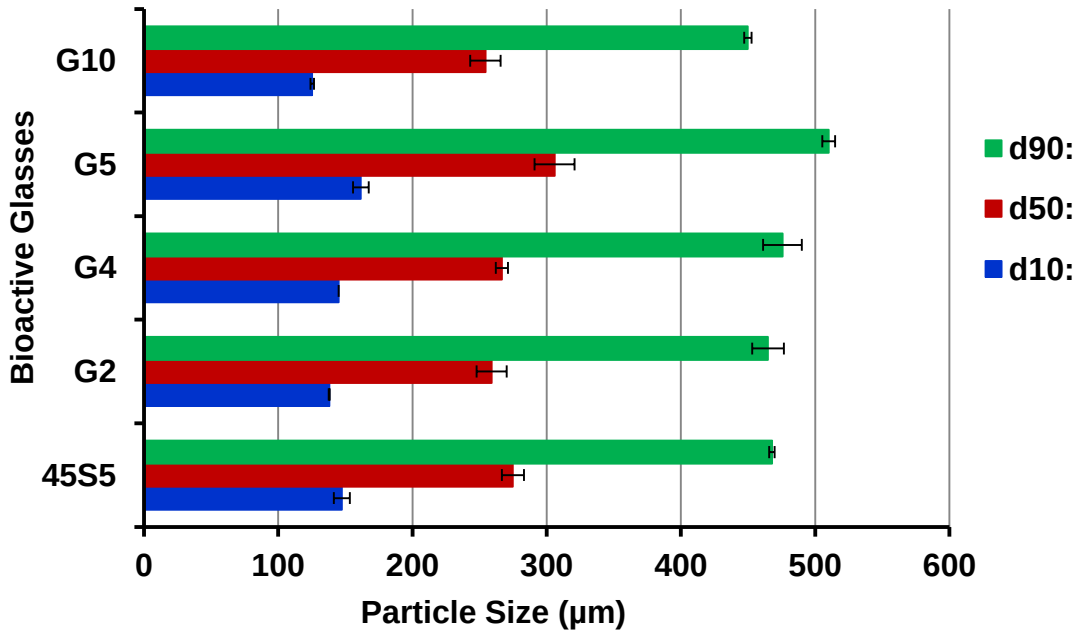

Figure 3.3 The particle size analysis of all silicate bioactive glasses.

The results of the particle size measurement (in micrometres; µm) of 45S5 and all the experimental glasses G2, G4, G5 and G10 are shown in Figure 3.3, expressed by d10, d50 and d90. The d10 gives the size for which 10% of the glass particles by volume within distribution are smaller than the given value. The d50 value represents 50% of the glass particles by volume are larger and 50% are smaller, d90 gives the value above, which 90% are coarser than the given value.

Table 3.1 The particle size distribution of 45S5 and experimental glasses.

Bioactive glasses	Particle size (100-400 µm)		
	d10	d50	d90
45S5	147.5 ± 5.9	274.8 ± 8.2	467.8 ± 1.9
G2	138.1 ± 0.4	259.1 ± 11.3	464.9 ± 11.8
G4	145.0 ± 0.0	266.6 ± 4.6	475.7 ± 14.4
G5	161.6 ± 5.8	305.9 ± 14.8	510.1 ± 4.8
G10	125.3 ± 1.3	254.4 ± 11.3	449.9 ± 2.7

Furthermore, Table 3.1 demonstrates that d90 of all experimental glasses including 45S5 have coarse particle size greater than 400 µm, whereas d10 and d50 of these glasses have particle size distribution within the range (100-400 µm), which has been used in this research to evaluate the apatite forming ability upon silicate glass dissolution in physiological buffer solutions.

3.2.4 Differential Scanning Calorimetry (DSC) Results:

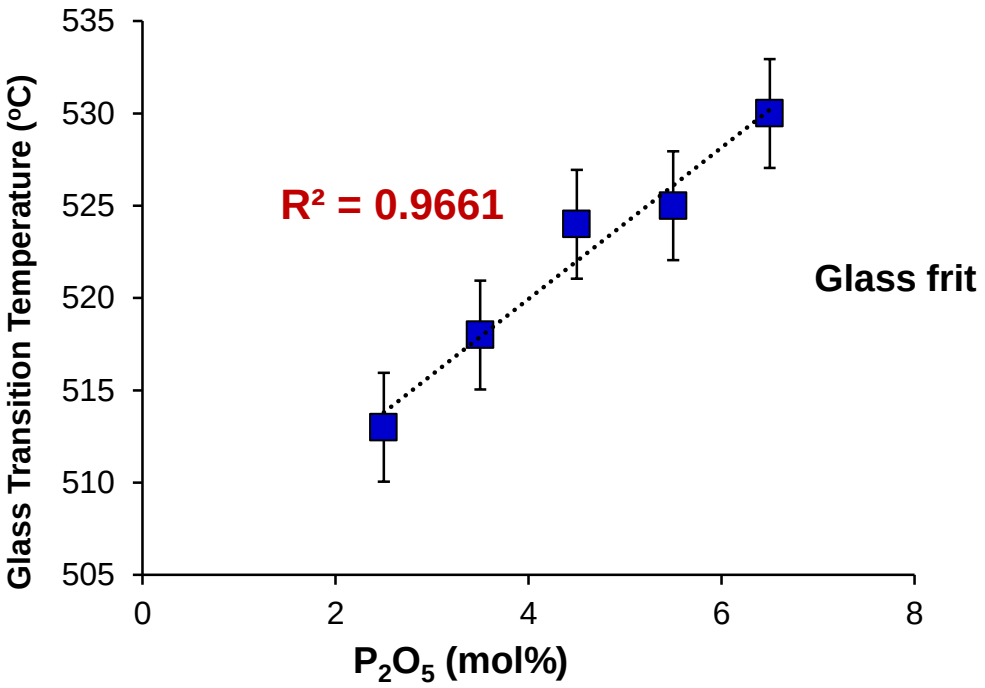

Figure 3.4 Graph demonstrating glass transition temperature (Tg) vs P_2O_5 content (mol%), where $R^2 = 0.9661$ and the equation for the trend line is y = 4.1x + 503.55.

Figure 3.4 shows that there is a linear relationship between the glass transition temperature (Tg) and the phosphate content of the glass series. An increase in Tg can be observed with increased phosphate content and increased Ca^{2+} concentration in the glass series, this trend in Tg can be related to the increase in the divalent cation (Ca^{2+}) concentration, which increases the ionic cross-linking between two $Si\text{-}O^-$ species (two non-bridging oxygens) in adjacent silicate chains of the silicate glass network. Therefore, the electrostatic forces between non-bridging oxygen atoms become considerably more intense, resulting in an increase in Tg. However, it has been observed in the O'Donnell *et al*. study (O'Donnell et al., 2008c) that the Tg lowers with increasing phosphate content due to the silica content reduction in the bioactive glass compositions, upon phosphate addition with both calcium oxide and sodium oxide charge adjustment.

3.3 Bioactivity Dissolution Tests:

3.3.1 The ISO-Standard and Non-ISO-Standard Bioactivity Test:

3.3.1.1 pH Measurement Results:

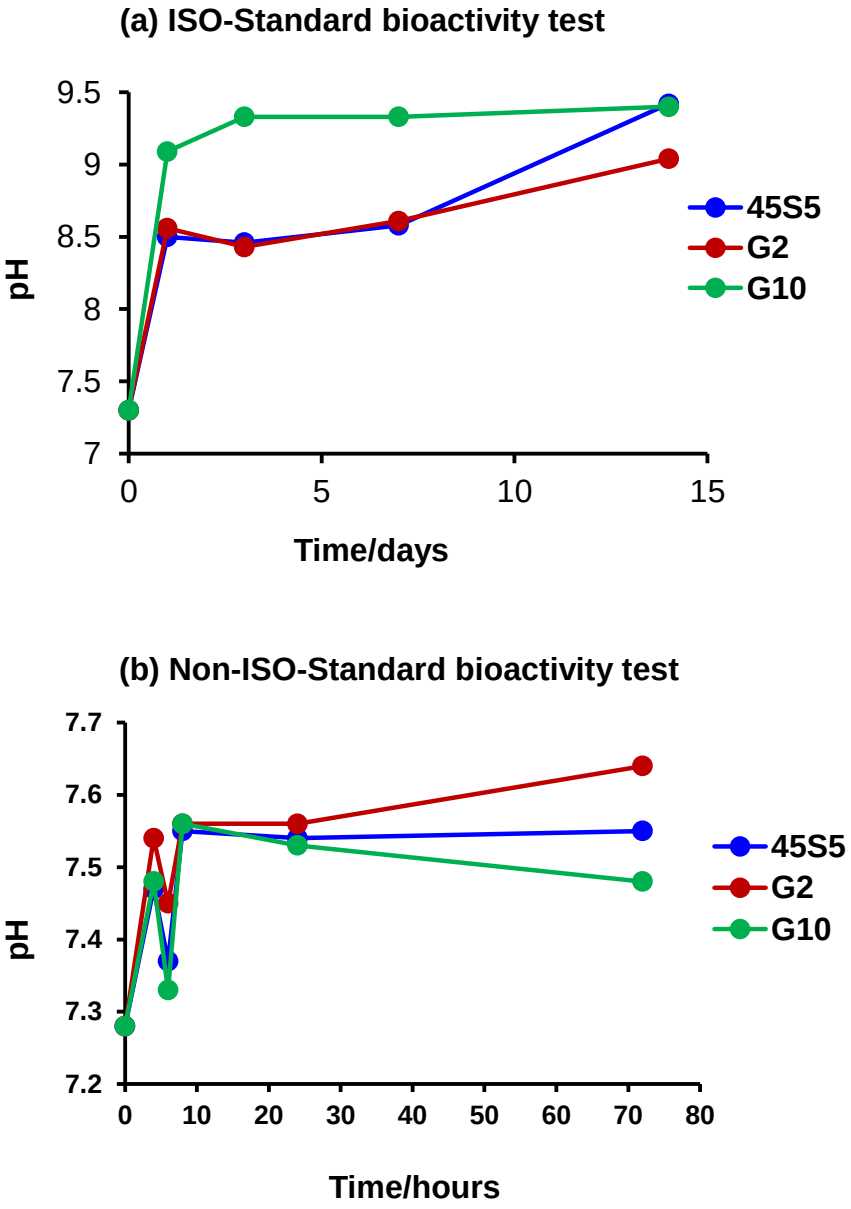

Figure 3.5 The pH behaviour of three glass compositions on immersion in Tris buffer solution during the (a) ISO-Standard and (b) Non-ISO-Standard bioactivity tests. The time scale is in days for (a) and in hours for (b). Three compositions studied are 45S5, G2 with 10% of Sr substituting for Ca in 45S5 composition, G10 with additional higher phosphate content for increasing the apatite formation rate.

As a general trend, a high alkaline pH up to 9 is generated in buffers during the ISO-Standard bioactivity test of the glass powder as indicated in (Figure 3.5 (a)). Whereas, the pH does not rise much compared to the initial value of 7.3 during the Non-ISO-Standard test as described in (Figure 3.5 (b)). The dramatic pH rise seen in the ISO-Standard bioactivity test is associated with an instant high release of calcium and sodium cations into a small volume of the buffer solution, which rapidly exceeds its buffering capacity. Therefore, the pH increases due to the higher glass concentration immersed in solution resulting from excessive amount of cations replacing the hydrated proton (H^+) ion for ion exchange reaction in the solution, causing a pH rise.

Moreover, the pH of G10 glass solution in the ISO Standard test (Figure 3.5 (a)) at different time points of the experiment is higher than for the solution containing 45S5. Whilst, the higher phosphate containing bioactive glass exhibits reduced pH rise due to the increased release of phosphate ions from the glass into the solution as reported by O'Donnell *et al*. study (O'Donnell et al., 2009). Therefore, the increase in the pH of G10 glass in the ISO Standard test could be attributed to the particles size distribution. The d10, d50 and d90 values for G10 glass as given in Table 3.1 appear to be less than that of 45S5 and the other glasses. The G10 glass therefore has a smaller particle size and consequently a larger surface area which gives rise to a faster ion exchange and a higher dissolution rate. Thus, greater quantities of cations such as calcium and sodium are released from the surface of G10 glass into the solution through ion exchange process with the protons from the solution into the glass causing a reduction in the H^+ concentration and a higher pH rise in solution.

The experimental pH data of the whole glass series (45S5, G2 and G10) in the ISO Standard test are in good agreement with the previous findings reported by the Jones *et al.* study (Jones et al., 2001). Jones and co-workers suggested that the

higher glass amount in solution, the higher the pH rise. Therefore, the amount of the bioactive glasses influences significantly on the glass dissolution and pH profile. This phenomenon appears to be of some significance in periodontology, since the high concentration of Perioglas® in periodontal pocket causes high release of cations such as Na^+ and Ca^{2+} into the extracellular environment. This in turn generates a pH rise which is suspected to be too high regarding the small volume of a periodontal pocket as discussed previously in section 1.2.4.

On the other hand, the pH of the G10 glass solution in the Non-ISO-Standard test (Figure 3.5 (b)) is slightly lower than that of the 45S5 solution. To some extent, this pH behaviour could be reasonable since the pH reduction could be attributed to the high phosphate concentration in the composition of G10 glass as supported by O'Donnell *et al*. findings (O'Donnell et al., 2009).

3.3.1.2 Fourier Transform Infrared Spectroscopy (FTIR) Results:

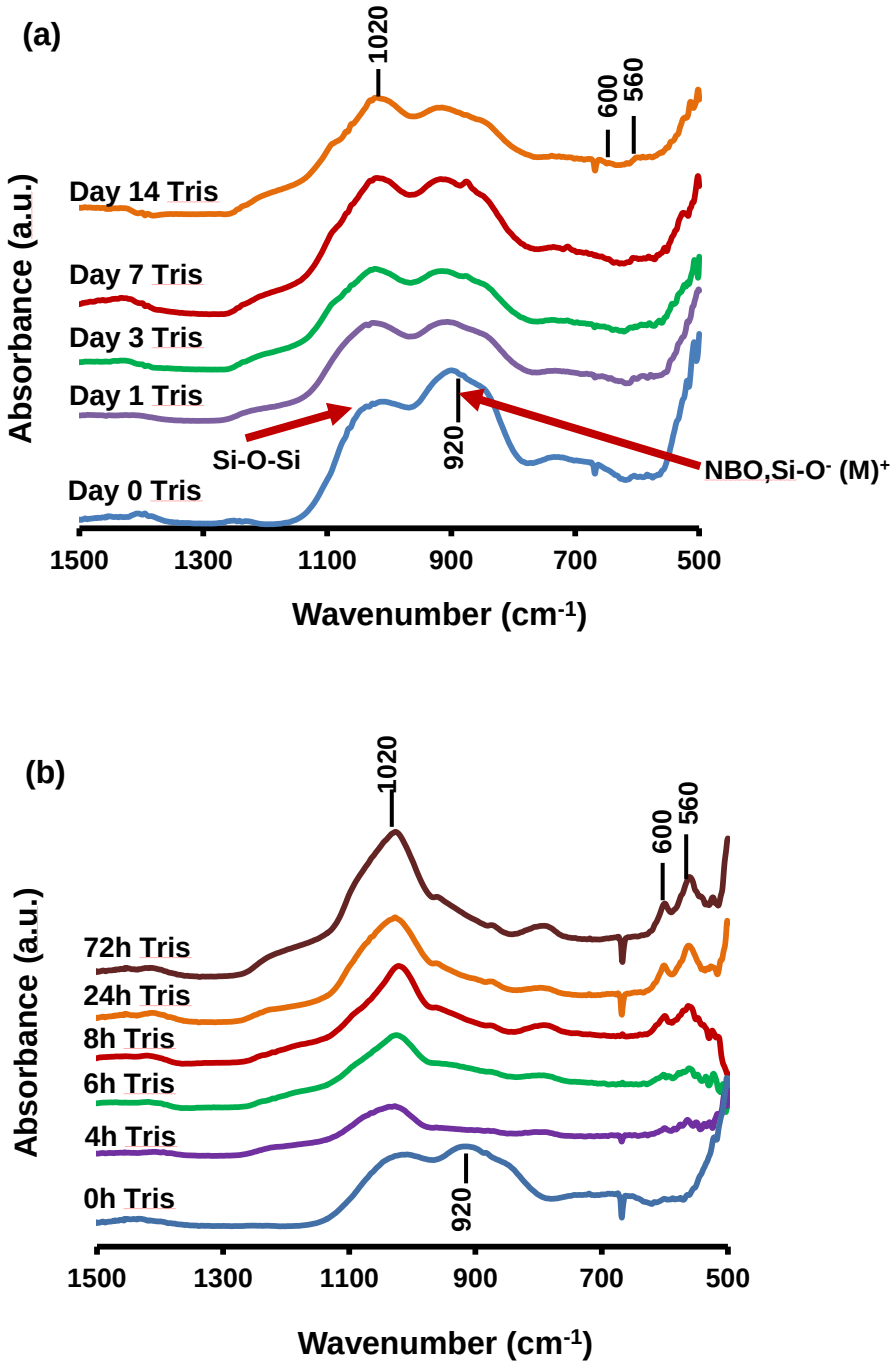

Figure 3.6 FTIR spectra of 45S5 glass (PS 100-400 µm) before and after immersion in Tris during the (a) ISO-Standard test and (b) Non-ISO-Standard test bioactivity test. The different immersion periods are colour coded as indicated in the Figure.

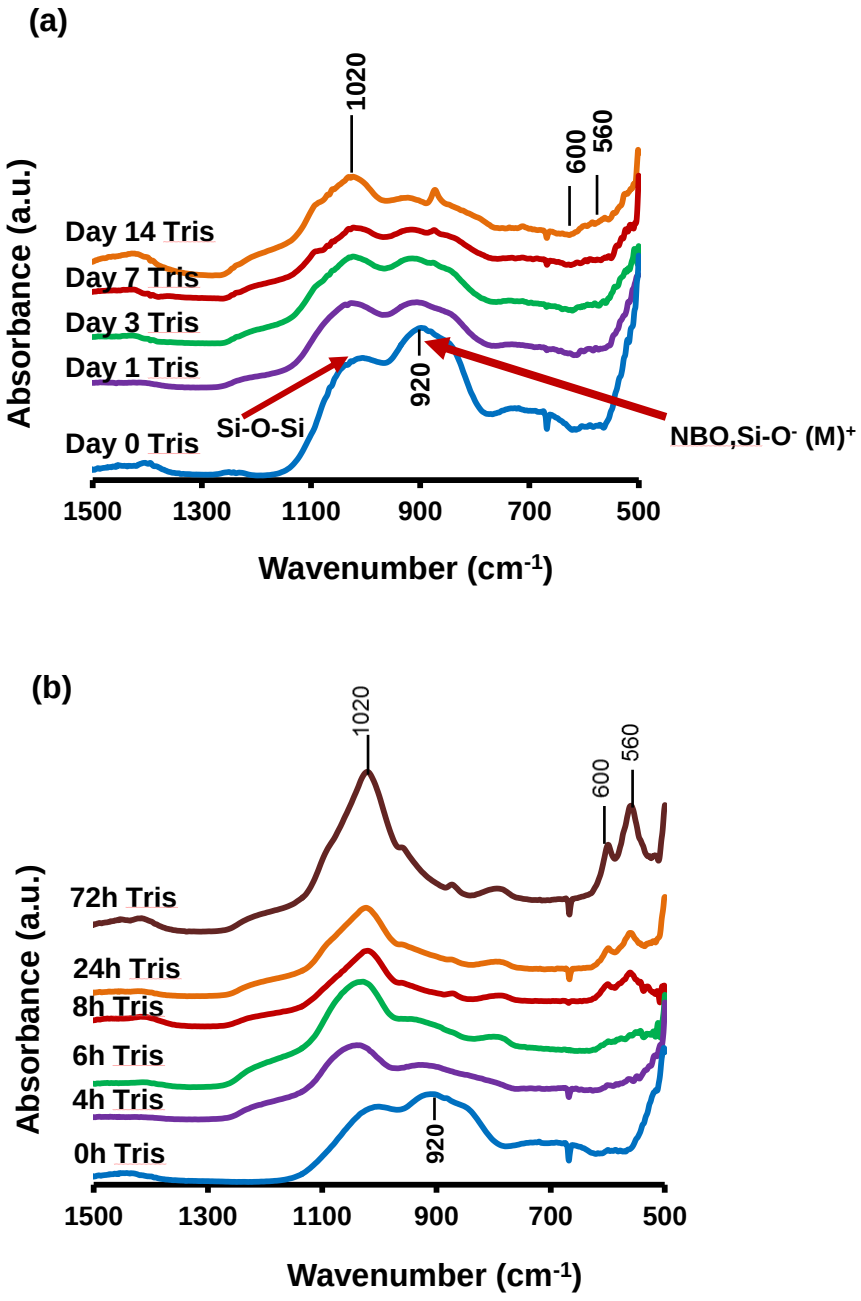

Figure 3.7 FTIR spectra of G2 glass (PS 100-400 µm) before and after immersion in Tris during the (a) ISO-Standard test and (b) Non-ISO-Standard test bioactivity test. The different immersion periods are colour coded as indicated in the Figure.

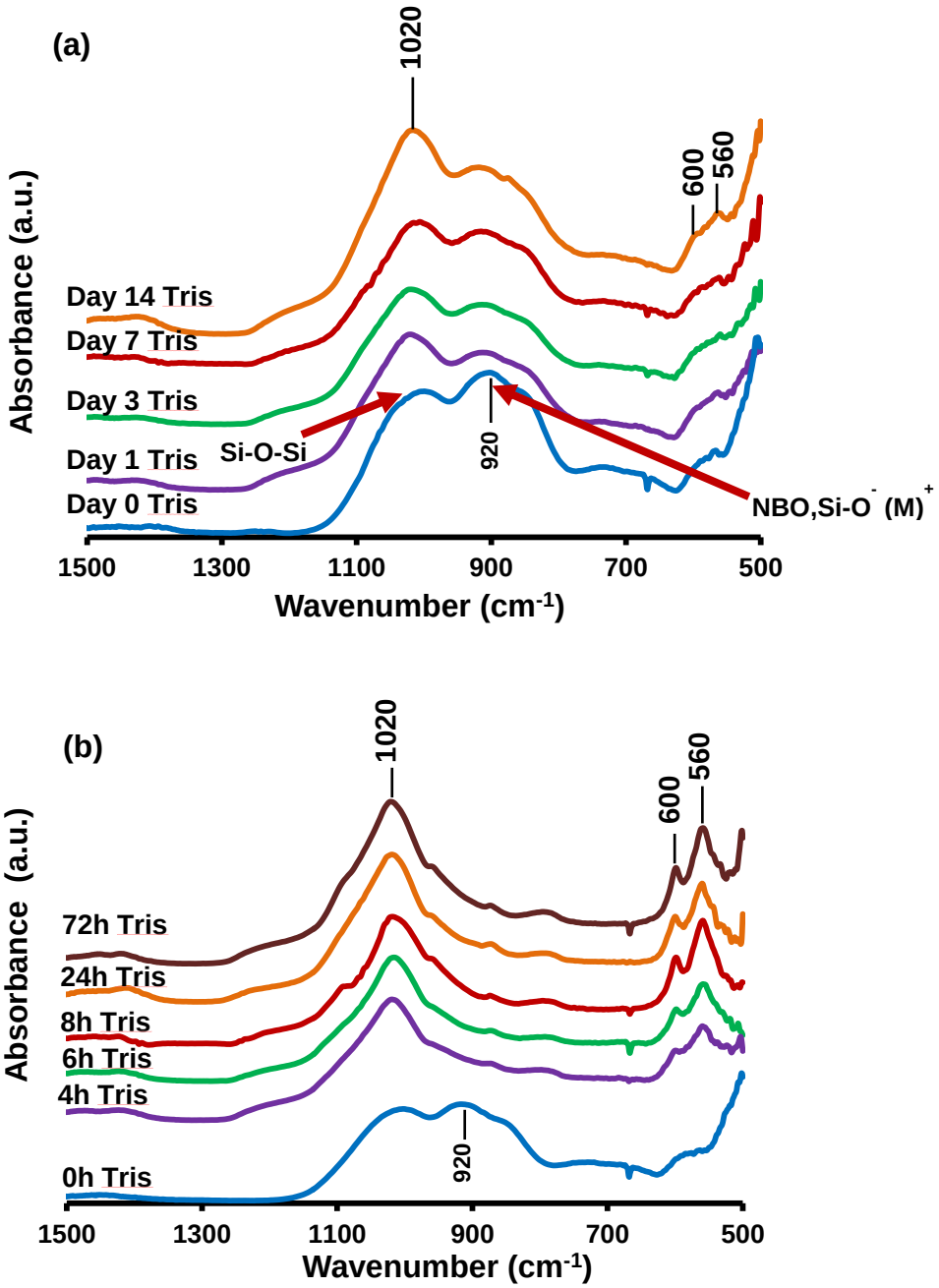

Figure 3.8 FTIR spectra of G10 glass (PS 100-400 µm) before and after immersion in Tris buffer during the (a) ISO-Standard test and (b) Non-ISO-Standard test bioactivity test. The different immersion periods are colour coded as indicated in the Figure.

The FTIR results of the compositions 45S5, G2 and G10 obtained via the ISO-Standard method are presented in Figure 3.6 (a), Figure 3.7 (a) and Figure 3.8 (a) respectively. No apatite formation was present in 45S5 and G2 glasses over the entire time of experiment up to 14 days despite partial glass dissolution indicated by the partial disappearance of silicon-non-bridging oxygen bond (Si^{+}-O^{-}- $alkali^{+}$) at 920 cm^{-1} of unreacted glass. However, there was a small amount of apatite in G10 after 14 days immersion in Tris buffer ISO-Standard. Apatite formation in G10 through the ISO-Standard test is favoured by the high phosphate content.

The inhibition of apatite precipitation in the ISO-Standard test is, therefore likely to be associated with the following reasons:

(i) The high pH rise, which could probably inhibit the glass dissolution by suppressing the ion exchange process. This process involves the exchange of sodium and calcium ions from the glass with hydrated protons from the solution. Therefore, the suppression of ion exchange causes retardation of apatite formation.

(ii) The ratio of calcium to phosphate ions could probably increase because of the excessive amounts of bioactive glass which are immersed in solution. Consequently, calcium carbonate (calcite) may therefore be precipitated on the surface of the glass particles at the expense of hydroxyapatite formation.

The FTIR spectra of selected glasses 45S5 and G2 that reacted in Tris buffer indicated that there was no apatite precipitation over the immersion periods of up to 14 days through the ISO-Standard experiments. Whereas, the apatite formation was observed earlier at eight hours of immersion in the Non-ISO-Standard test. The FTIR results revealed that the developed glass G10 with high phosphate content reduced the rapid pH rise and accelerated apatite formation in Tris buffer.

The inhibition of apatite formation due to the high pH rise in the ISO-Standard test was largely in agreement with the findings of Bingel (Bingel et al., 2015), who indicated that the alkaline buffer solution at pH 9 inhibited the apatite formation. While, the inhibition of apatite formation due to the precipitation of calcium carbonate on the surface of the glass was consistent with the Jones *et al.* observations (Jones et al., 2001).

However, the ISO-Standard method was employed to investigate the influence of pH on the glass degradation rate and apatite forming ability. This pH was suggested to be too high within the small volume of the periodontal bony defect. Therefore, this needed to be taken into consideration when the bioactive glass is being designed for future periodontal grafting materials.

The FTIR spectra of the Non-ISO Standard samples are shown in Figure 3.6 (b), Figure 3.7 (b) and Figure 3.8 (b). As a general trend, the FTIR spectra in the Non-ISO Standard test exhibited the prominent features of the glass dissolution in Tris buffer, which are indicated by the disappearance of silicon non-bridging oxygen at 920 cm^{-1}. As the immersion time progresses, the intensifying of the Si-O-Si vibrational peak at approximately 1020 cm^{-1} (stretch) appeared well-defined in the FTIR spectra, which represented the formation of silica gel layer. At longer immersion times, the well-developed split bands at about 560 cm^{-1} and 600 cm^{-1} appeared; indicating the presence of crystalline apatite formation. The faster apatite formation was evident with G10 glass at approximately 4 hours (Figure 3.8 (b)) due to the significant effect of the higher phosphate content on the rate of apatite formation. It was reported that the high phosphate content enhanced the glass bioactivity and accelerated the apatite formation rate (O'Donnell et al., 2009, Mneimne et al., 2011).

3.4 The Influence of Bioactive Glass Particles Size on Glass Dissolution Rate, pH and apatite Formation:

In order to investigate the influence of the bioactive glass particle size (PS) on the glass dissolution rate, pH behaviour and apatite forming ability, three fractions of particles size (<38 µm, 38-100 µm and 100-400 µm) have been used in this investigation.

3.4.1 Particle Size Analysis Results:

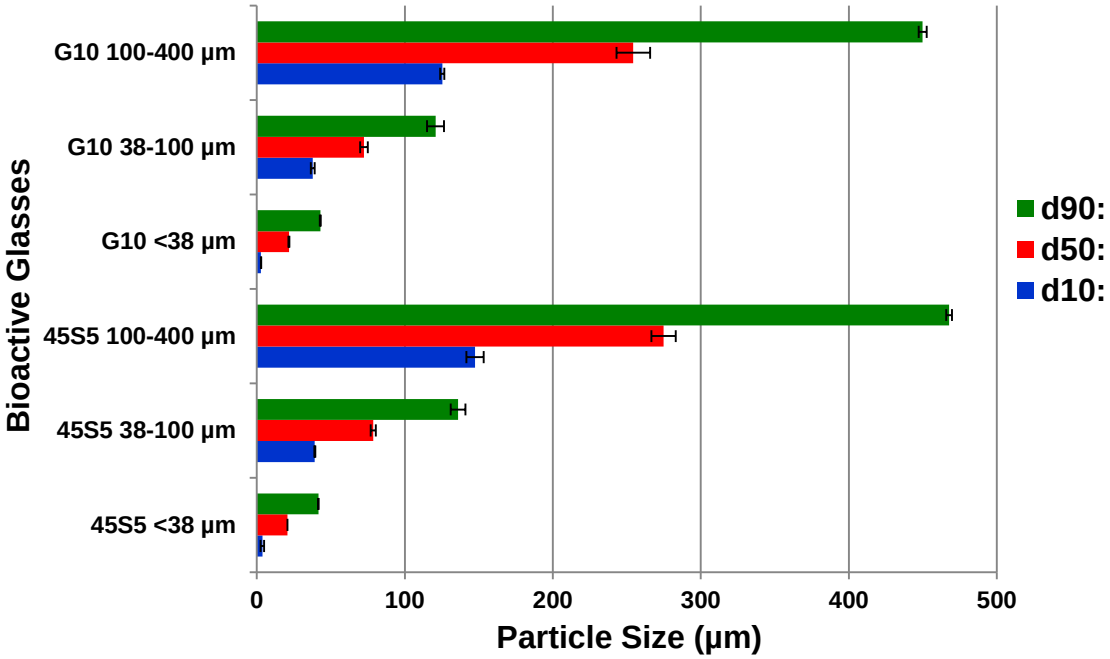

Figure 3.9 Graph showing particle size analysis for three fractions (<38 µm, 38-100 µm and 100-400 µm) of the selected silicate bioactive glasses 45S5 and G10.

Figure 3.9 illustrates the particle sizes measurement (in micrometres; µm) of the 45S5 and the G10. The particle size distribution is expressed by the d10, d50 and d90 values for three fractions of both glasses (<38 µm, 38-100 µm and 100-400 µm).

Table 3.2 Particle size distribution of 45S5 and G10 glasses for three fractions (<38 µm, 38-100 µm and 100-400 µm).

Bioactive glasses	Particle size (µm)		
	d10	d50	d90
45S5 <38 µm	**3.8 ± 1.2**	**20.7 ± 0.0**	**41.6 ± 0.2**
45S5 38-100 µm	**39.2 ± 0.4**	**78.7 ± 1.8**	**136.0 ± 5.0**
45S5 100-400 µm	**147.5 ± 5.9**	**274.8 ± 8.2**	**467.8 ± 1.9**
G10 <38 µm	**2.8 ± 0.1**	**21.7 ± 0.3**	**42.9 ± 0.3**
G10 38-100 µm	**37.8 ± 1.3**	**72.5 ± 2.6**	**120.8 ± 5.7**
G10 100-400 µm	**125.3 ± 1.3**	**254.4 ± 11.3**	**449.9 ± 2.7**

Table 3.2 illustrates the particles size distribution of the 45S5 and G10 glasses, giving three fractions (small, medium and large) for each glass. As observed in Table 3.2, the d90 particle size was greater than the sieve size of each glass. Whereas 10% and 50% of these glasses have particle size distribution within the designed range. It should be noted that the particle size analysis software interprets the glass particles as spherical particles whereas angular particles with an equivalent spherical radius larger than the mesh size would pass through the mesh. Therefore, the particle size analyser may record higher values than the sieve size.

3.4.2 Fourier Transform Infrared Spectroscopy (FTIR) Results:

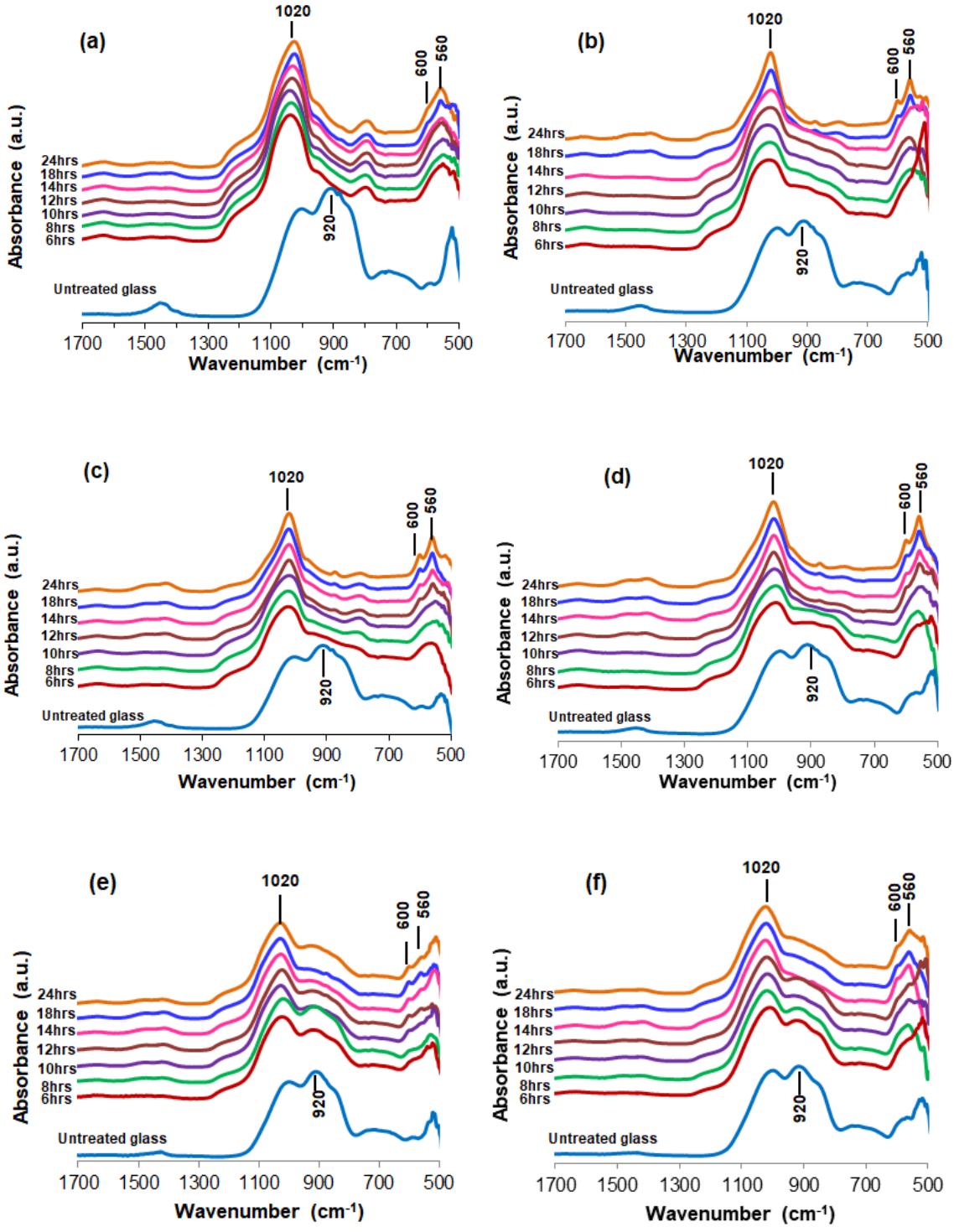

Figure 3.10 FTIR spectra before and after immersion in SBF were plotted as a function of time for (a) 45S5 PS <38 µm, (b) G10 PS <38 µm, (c) 45S5 PS 38-100 µm, (d) G10 PS 38-100 µm, (e) 45S5 PS 100-400 µm and (f) G10 PS 100-400 µm.

The significant relationship between the glass bioactivity (glass dissolution and apatite formation) and glass particles size in SBF can be observed in Figure 3.10. As a comparison between the FTIR spectra of 45S5 <38 µm and the FTIR spectra of 45S5 100-400 µm, the glass dissolution rate in SBF was faster with small particles (Figure 3.10 (a)) than the large particles (Figure 3.10 (e)). This difference was indicated by: (i) faster disappearance of a silicon non-bridging oxygen at 920 cm^{-1} of unreacted glass over the entire time of the experiment (i.e. the glass dissolved completely) compared to the glass dissolution behaviour of the same glass. The disappearance of silicon non-bridging oxygen in (Figure 3.10 (e)) was slower and i.e. there were still unreacted glass particles. And (ii) the sharpening (stretch) of the Si-O-Si located at approximately 1020 cm^{-1} as a function of time (Figure 3.10 (a)) was clearly more pronounced than that in (Figure 3.10 (e)). Therefore, the small particle size accelerated the dissolution rate of the glass in solution. Similarly, the FTIR results of the G10 glass with a fine particle size <38 µm (Figure 3.10 (b)) revealed a rapid G10 glass dissolution in SBF compared to the G10 glass with a coarse particle size 100-400 µm (Figure 3.10 (f)).

With respect to the effect of the glass particle size on the apatite formation, it can be observed that the coarse particle size of 45S5 100-400 µm accelerated the apatite formation. The apatite formed within the earliest time point of immersing 45S5 in SBF as demonstrated in (Figure 3.10 (e)). In contrast, the fine particle size <38 µm of 45S5 did not speed up the rate of apatite formation (Figures 3.10 (a)). The apatite precipitated after 18 hours of 45S5 treatment in SBF in spite of emerging single peak at 570 cm^{-1} during earliest immersion time point. This peak can be attributed to the P-O vibration bond indicating the emergence of apatite precursors; i.e. the development of amorphous calcium phosphate layer (Brauer et al., 2008). However, with longer immersion times, this single peak then splits approximately at 18 hours (Figure 3.10 (a)) into two distinct bands at 560 and 600 cm^{-1} forming the apatite

crystal phase. Similar comparisons were observed between the FTIR spectra of the G10 fine particle size <38 µm and the G10 coarse particle size 100-400 µm as in (Figure 3.10 (b) and (f)). The apatite formation with the G10 100-400 µm in SBF (Figure 3.10 (f)) was faster than with the G10 <38 µm (Figure 3.10 (b)).

Regarding the influence of the glass particle size on the apatite formation in Tris buffer, the 45S5 has the same trend as in SBF, where the apatite formation is faster with 45S5 100-400 µm than with <38 µm. The 45S5 100-400 µm forms apatite at approximately 8 hours immersion in Tris buffer (Figure 3.6 (b)). Whereas, the 45S5 <38 µm forms apatite after 72 hours immersion in Tris buffer as investigated by the Mneimne *et al.* study (Mneimne, 2014).

Moreover, both 45S5 and G10 glasses with large particles 100-400 µm seem to have the same rate of apatite formation. Despite the fact that the G10 glass should accelerate the apatite formation rate due to its higher phosphate concentration as reported in other studies (O'Donnell et al., 2009, Mneimne et al., 2011). Hence, the particle size of bioactive glass has bigger effect on the rate of apatite formation on glass dissolution than the glass composition in this case.

3.4.3 X-ray Diffraction (XRD) Results:

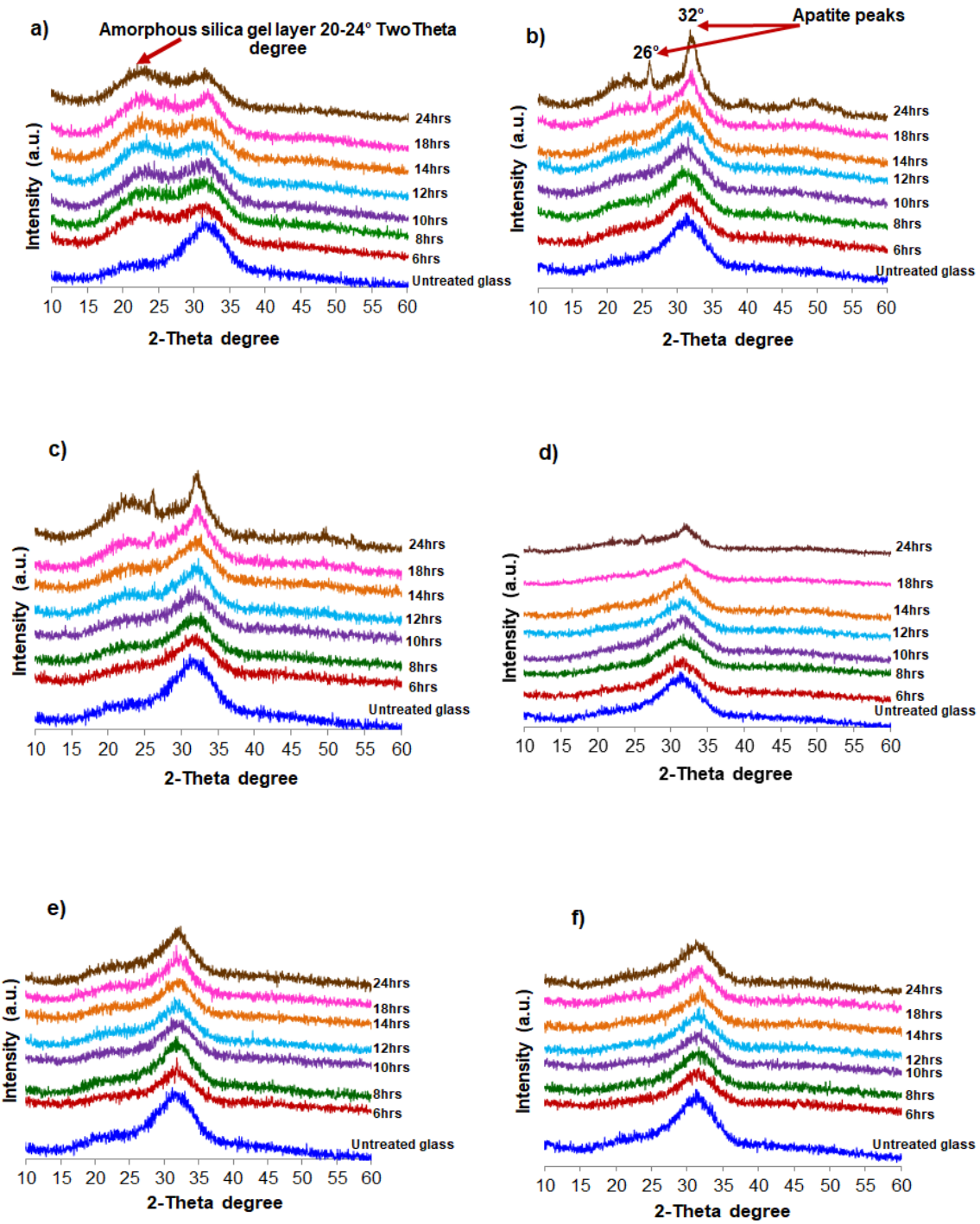

Figure 3.11 XRD patterns before and after immersion in SBF were plotted as a function of time for a) 45S5 PS <38 µm, b) G10 PS <38 µm, c) 45S5 PS 38-100 µm, d) G10 PS 38-100 µm, e) 45S5 PS 100-400 µm and f) G10 PS 100-400 µm.

Figure 3.11 illustrates the specific feature of apatite crystal phase in XRD traces as identified by Bragg peaks labelled at approximately 26° and 32° 2 θ, which overlap the amorphous broad halo of unreacted glass. These peaks 26° and 32° Two-Theta which reference the apatite formation are initially developed as nanocrystals. Therefore, these peaks cannot be easily distinguished at earlier reaction time due to their broad and weak XRD intensities. However, with progressing immersion time, these nanocrystals grow in size as more apatite precipitation occurs, resulting in sharper and more intense diffraction peaks as expected based on the Scherrer equation for crystal size analysis (Cullity and Weymouth, 1957).

The G10 glass with <38 µm shows more intense diffraction peaks labelled approximately at 26° and 32° Two-Theta. Whereas 45S5 does not show such sharp apatite diffraction lines as in (Figure 3.11 (a)) in spite of the emergence of amorphous silica gel layer 20-24° Two Theta degrees. The appearance of silica gel layer confirmed the glass degradation in SBF. The faster rate of apatite formation which can be observed clearly with G10 glass (Figure 3.11 (b)) is attributed to the high phosphate content of G10 glass (O'Donnell et al., 2009, Mneimne et al., 2011).

Figure 3.11 (e) and (f) of 45S5 and G10 respectively do not reveal intense diffraction peaks of apatite. The reason behind this weakness in XRD intensity can be attributed to the significant effect of coarse particles size (100-400µm) to decelerate the glass dissolution rate in SBF. The 45S5 and the G10 glasses might not dissolve completely. Therefore, the XRD patterns cannot detect the apatite peaks easily, exhibiting this weak intensity due to the presence of residual amorphous halo of the unreacted glass. Conversely, the 45S5 and the G10 were dissolved completely due to their fine particles size <38 µm as shown in Figure 3.11 (a) and (b) and the apatite crystal phase was well-defined. The FTIR spectra in

Figure 3.10 are supported by the XRD patterns in Figure 3.11 with respect to the significant influence of particles size on the glass bioactivity.

3.4.4 pH Measurement Results:

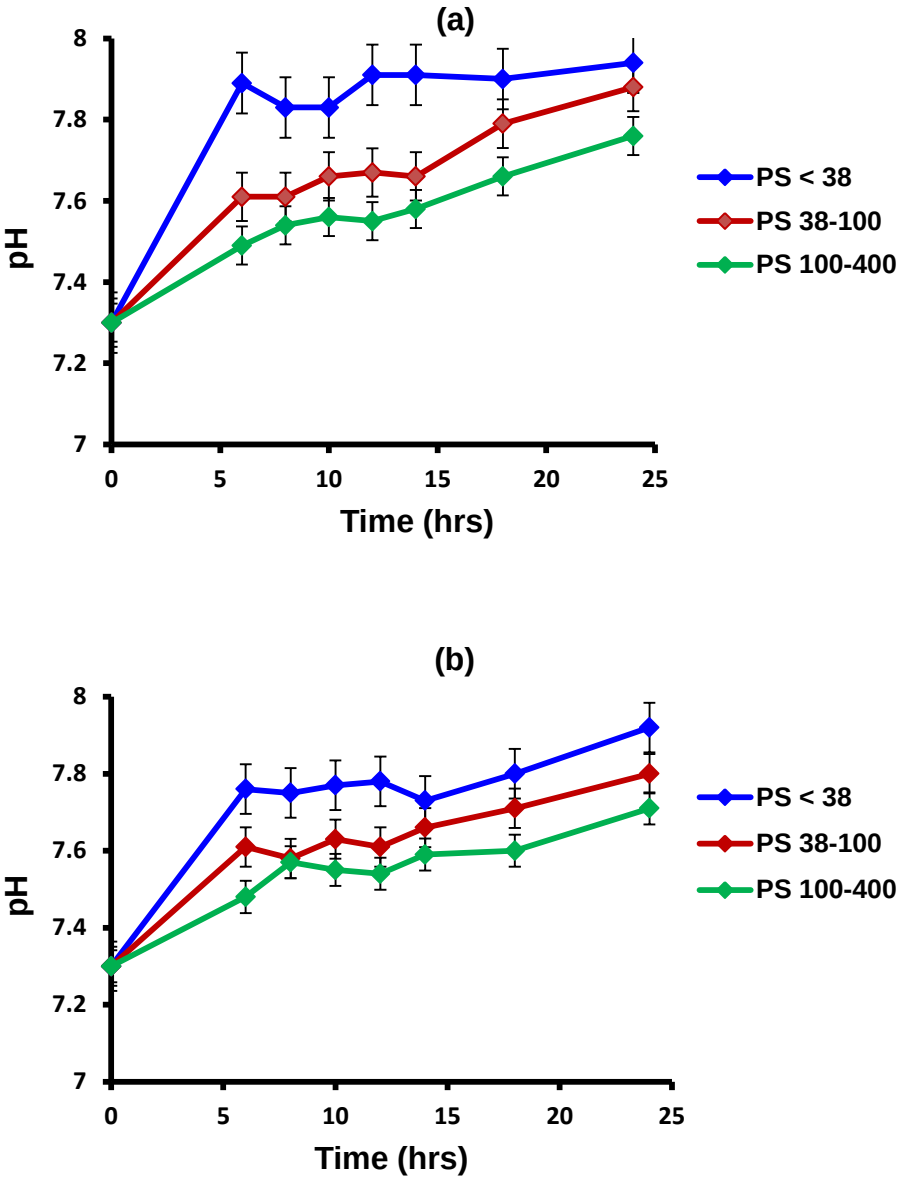

Figure 3.12 The pH profile in SBF for the three fractions of particles size (<38 µm, 38-100 µm and 100-400 µm) of (a) 45S5 and (b) G10.

Figure 3.12 (a) and (b) demonstrates the pH behaviour versus time after immersion in SBF including three fractions of particle size (<38 µm, 38-100 µm and 100-400 µm) for (a) 45S5 and (b) G10. For both 45S5 and G10, the highest pH rise seems clearly to be associated with fine particles size (<38 µm), followed by the pH of medium particle size (38-100 µm). However, the lowest pH rise is associated with large particle size (100-400 µm).

As a general trend, the pH rise of the G10 glass was less than the pH rise of 45S5 with all fractions, and this property can be attributed to the effect of the higher phosphate content on reduction pH rise (O'Donnell et al., 2009).

3.4.5 Ion Release Results:

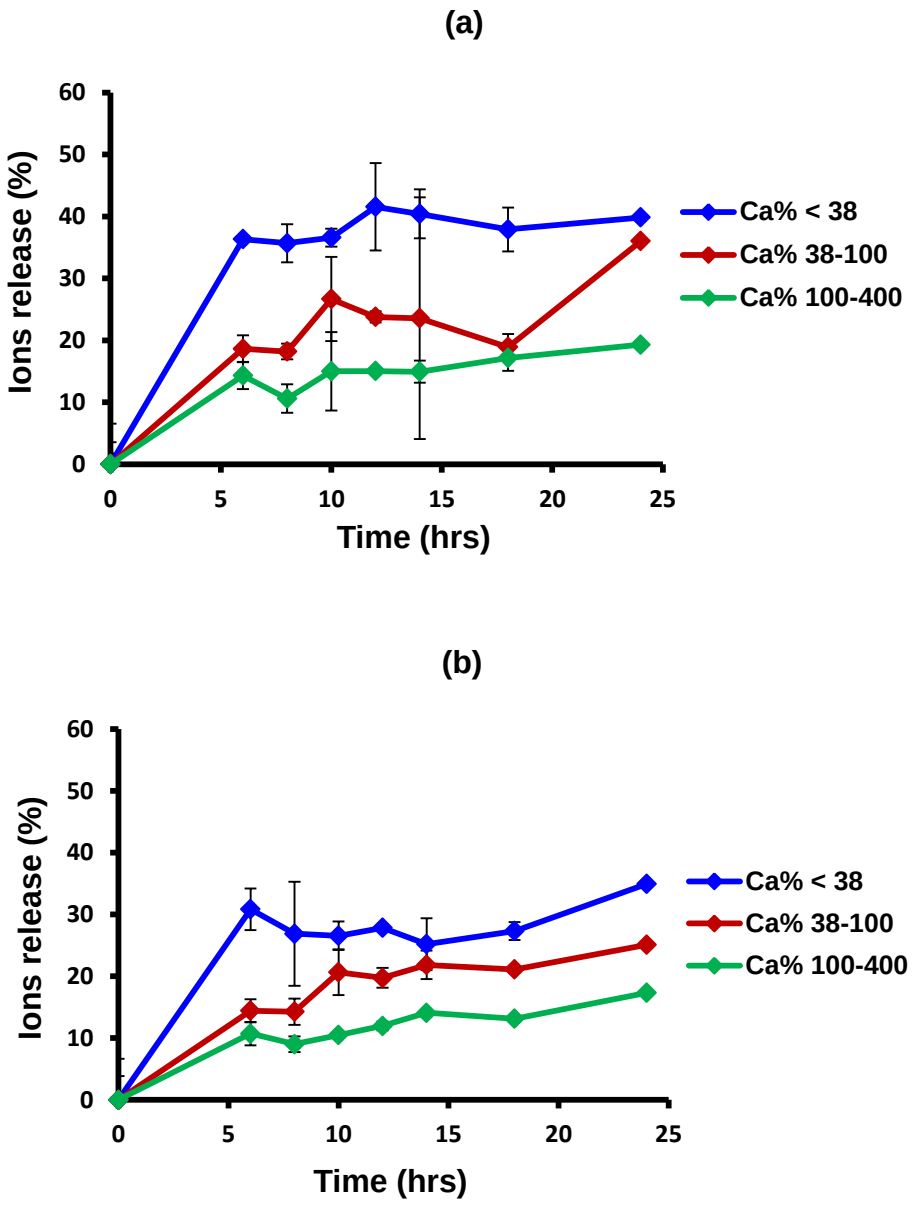

Figure 3.13 The percentage of the calcium ion concentration measured after the immersion of the glass powder (45S5 and G10) in SBF up to 24 hours. All the data were plotted as a function of time for three fractions of particles size (<38 µm, 38-100 µm and 100-400 µm), (a) 45S5 and (b) G10.

In order to understand the extent of the bioactive glass dissolution, the release of Ca^{2+} ion in SBF (Figure 3.13 (a) and (b)) is expressed as percentage dissolution. This percentage is calculated as a ratio between the Ca^{2+} ion release measured in

SBF and the maximum Ca^{2+} concentration, assuming that the glass is dissolved completely in SBF.

As expected, Figure 3.13 (a) and (b) revealed that the highest calcium ion release was associated with the fine particles size for both the 45S5 and the G10 due to the rapid glass dissolution rate associated with fine particles size. The calcium ion release of G10 glass <38 µm (Figure 3.13 b) dropped quickly after 6 hours treatment with SBF compared to the 45S5 <38 µm (Figure 3.13 a). This behavior might be attributed to much more apatite formed with G10, which consumed more calcium ions, whereas only a small amount of calcium ion was consumed to form apatite in 45S5. Therefore, the higher release of Ca^{2+} in SBF results in the pH increases more rapidly. The lower release of Ca^{2+} on immersion of the coarser particles in SBF reduces the rapid pH rise.

Overall, based on the above findings, it can be concluded that the large glass particles may slow down the release of Ca^{2+} and Na^{+} ions from the glass into the solution via the ion-exchange process. The lower release of Ca^{2+}/Na^{+} on immersion of the coarser particles in SBF reduces the rapid pH rise, thereby enabling earlier apatite formation. Whilst, the fine particle size generates a rapid pH rise due to faster ion release. The rapid pH rise suppresses the ion exchange process of glass dissolution, thus, slowing down any further glass dissolution and retarding apatite formation. Subsequently, the glass dissolution rate was the lowest for the largest particle size and a coarse particle size decreased a rapid pH rise & accelerated apatite formation.

4 Biodegradable Silicate/Phosphate Glass Mixtures (Development and Characterisation):

4.1 Introduction:

The high alkaline pH generated by PerioGlas® can facilitate the growth of periodontopathic bacteria such as *P.gingivalis*, which grows optimally at higher pH ≈ 8.3 (Takahashi and Schachtele, 1990). Furthermore, this high alkaline pH inhibits the apatite formation by suppressing the ion exchange process of bioactive glass dissolution (Bingel et al., 2015). The high pH also retards bone formation through the inhibition of osteoblast activity and suppression of osteogenic differentiation/proliferation in the local biological environment (Monfoulet et al., 2014). Therefore, the aim of this PhD project was to address the problem of PerioGlas® by mixing two degradable glasses, silicate (S-glass) and phosphate (P-glass). The phosphate glass as it degrades in physiological body fluid results in an acidic pH whilst the silicate bioactive glass results in an alkaline pH. The extreme pH rise generated by silicate glass can potentially be regulated by mixing the two glasses together to tailor the pH evolution and adjust it to the biological environment.

Strontium has been added to the phosphate glass since strontium upregulates osteoblasts (Gentleman et al., 2010) and is also bactericidal against some bacteria including *P. gingivalis* (Liu et al., 2016). It provides radio-opacity enabling the dissolution process to be followed clinically by X-rays.

4.2 Rationale of Silicate/Phosphate Glass Mixtures Design:

Table 4.1 Silicate and Phosphate glasses compositions in Mol% with NC of 2.11 for silicate glass.

Silicate glass composition (S-glass) in Mol%

SiO_2	CaO	Na_2O	Total	NC	Tg(°C)
51.5	25.5	23.1	100.0	2.1	538

Phosphate glass compositions (P-glass) in Mol%

P-glass	P_2O_5	SrO	K_2O	CaO	Tg(°C)
P1	55	30	15	0	367
P2	55	0	15	30	396
P3	55	10	15	20	387

The design strategy of glass mixtures used in this research is based on mixing one silicate glass (S-glass) composition with three compositions of phosphate glass (P-glass). Table 4.1 shows the compositions of silicate glass with network connectivity of 2.1 and all three phosphate glasses in mole percent. The silicate glass does not contain phosphate, potassium or strontium in its composition, thus these ions arise only from phosphate glass. Phosphate glass composition P1 contains phosphate, strontium and potassium without calcium, whilst phosphate glass P2 contains phosphate, potassium and calcium with no strontium. The design of phosphate glass P3 is composed of all these elements with various concentrations with both

calcium and strontium. In terms of the particle size, the silicate glass has a coarse particle size (100-400 μm), whereas all three phosphate glasses have a fine particle size (<38 μm). The phosphate glass will be dissolved first due to its fine particles followed by coarser silicate glass particles dissolution. Moreover, the large particles size of the silicate glass will reduce the silicate glass dissolution rate and decrease the rapid pH rise as previously discussed in Chapter 3, section 3.4.

Therefore, it is proposed in this mixture that phosphate glass (P-glass) can dissolve initially due to its smaller particles size producing an acidic pH, which inhibits the alkaline periodontal bacterial growth. Afterwards, this acidic pH catalyses the coarser silicate glass particle dissolution (Bingel et al., 2015), resulting in a smart pH modulation which should be favourable for new bone formation.

The schematic diagram below (Figure 4.1) below illustrates the essential strategy of novel silicate/phosphate glass mixtures:

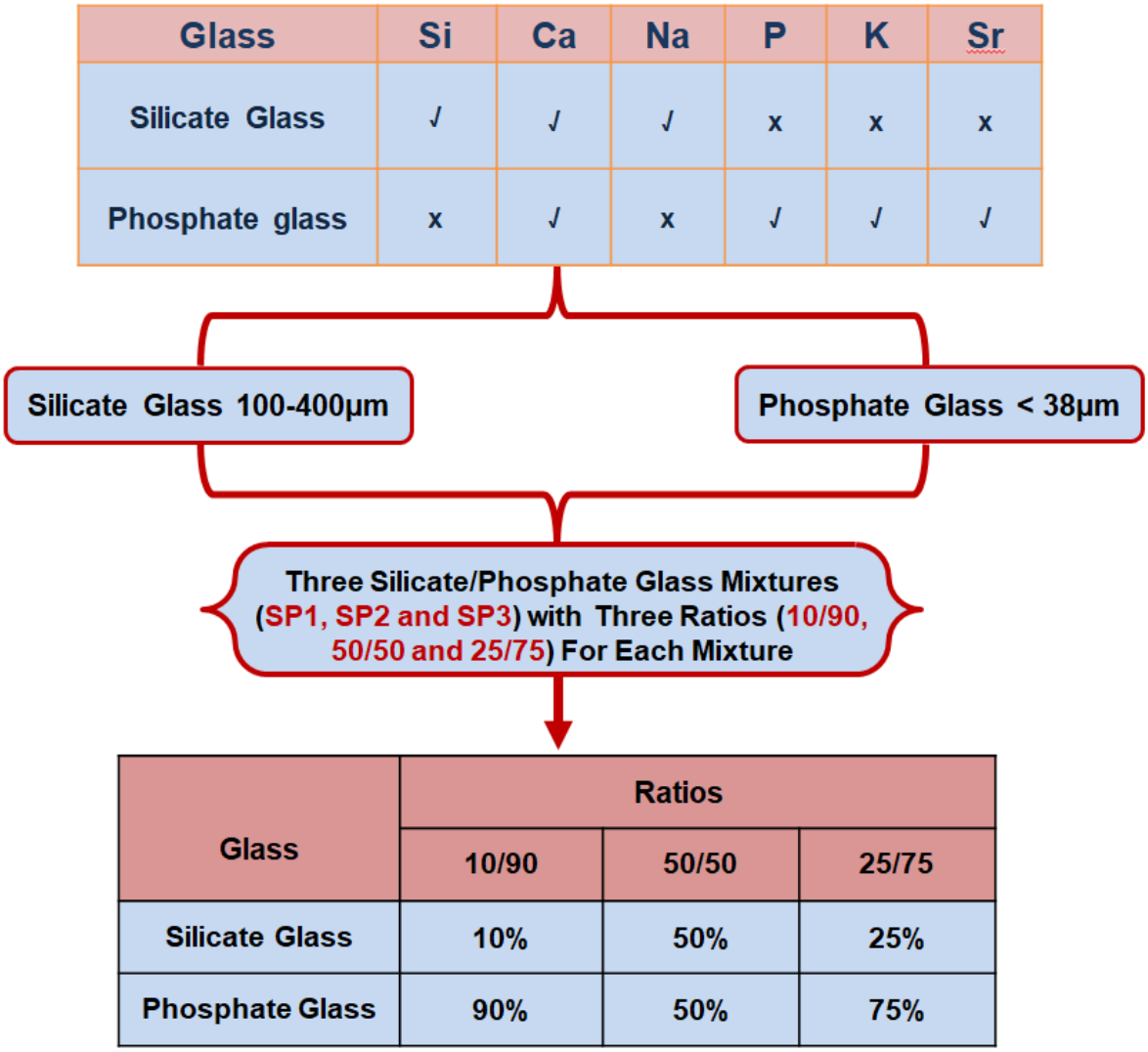

Figure 4.1 Schematic demonstration of the main strategy of the silicate/phosphate glass mixtures. The ratios given are by weight.

According to the schematic diagram shown above in Figure 4.1, three silicate/phosphate synthetic glass blends were developed, which have never been used previously but are thought to be the most promising. These mixtures are SP1, SP2 and SP3. Three mixtures were prepared with each of the phosphate glasses using the three ratios (10/90, 50/50 and 25/75), where 10% for silicate glass whilst

90% for phosphate glass, 50% for each glass and 25% for silicate glass whereas 75% for phosphate glass, all by weight. As a part of the concept design and in order to differentiate the stages of their dissolution in time, the silicate glass has a coarse particle size 100-400 μm and the phosphate glass has a small particle size <38 μm.

The dissolution experiments were performed in Tris buffer solution which does not contain any ions to interfere with the ion release analysis. During glass mixture dissolution, the ions of phosphate, strontium and potassium with mixture of SP1 emerge from P1 glass dissolution only; whilst silicate, calcium and sodium ions arise only from silicate glass dissolution. With respect to the SP2 mixture, the phosphate and potassium ions originate from P2 glass degradation only, whereas silicate and sodium ions arise only from silicate glass dissolution. In terms of SP3 mixture the phosphate, strontium and potassium ions emerge from P3 glass dissolution only, whereas silicate and sodium come only from silicate glass dissolution.

4.3 Characterisation of Untreated Individual Silicate and Phosphate Glasses (Results and Discussion):

4.3.1 X-ray Diffraction (XRD) Results:

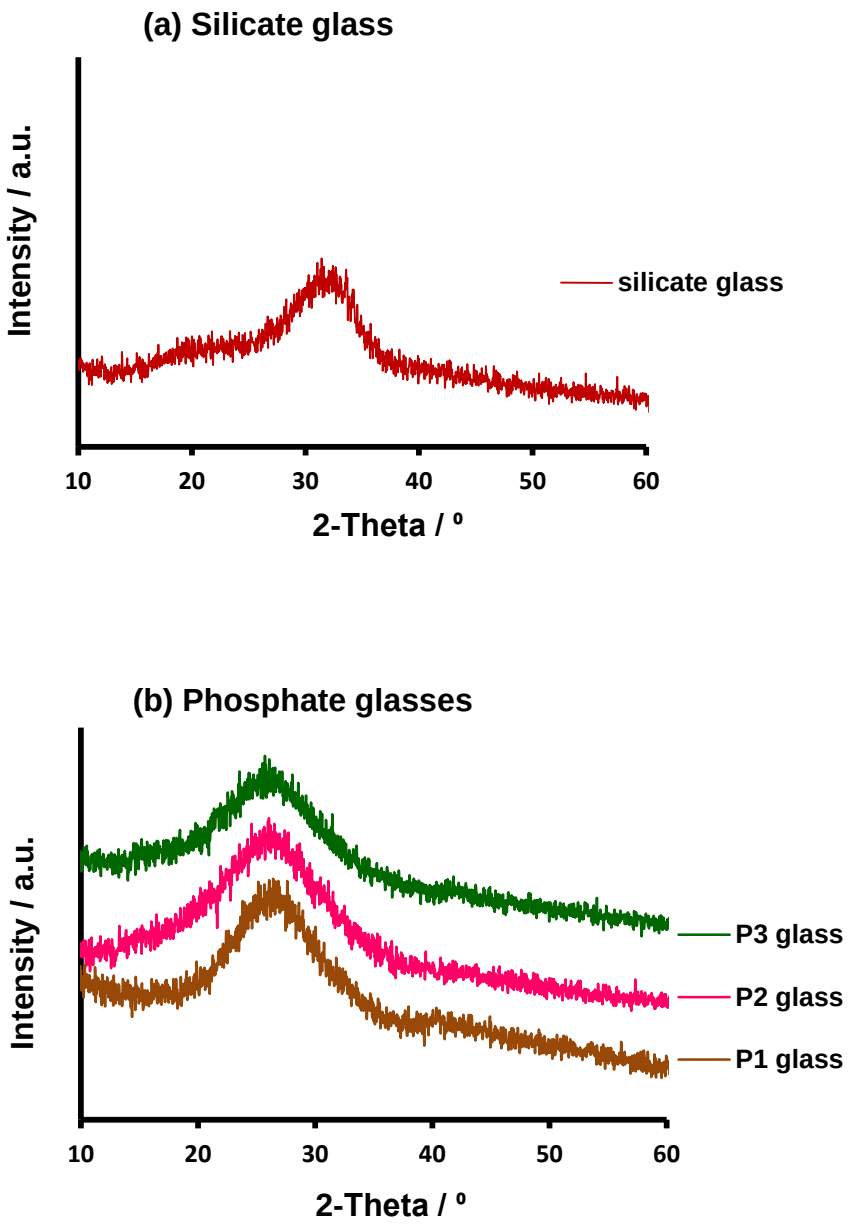

Figure 4.2 XRD patterns demonstrate that all unreacted glasses (a) silicate glass and (b) phosphate glasses P1, P2 and P3 were amorphous.

Figure 4.2 (a) and (b) shows that the silicate glass and all three phosphate glasses P1, P2 and P3 were amorphous by the absence of sharp Bragg peaks. All patterns

reveal broad halos, which was a characteristic feature of an amorphous system, indicating the absence of crystallinity of unreacted glasses.

4.3.2 Differential Scanning Calorimetry (DSC) Results:

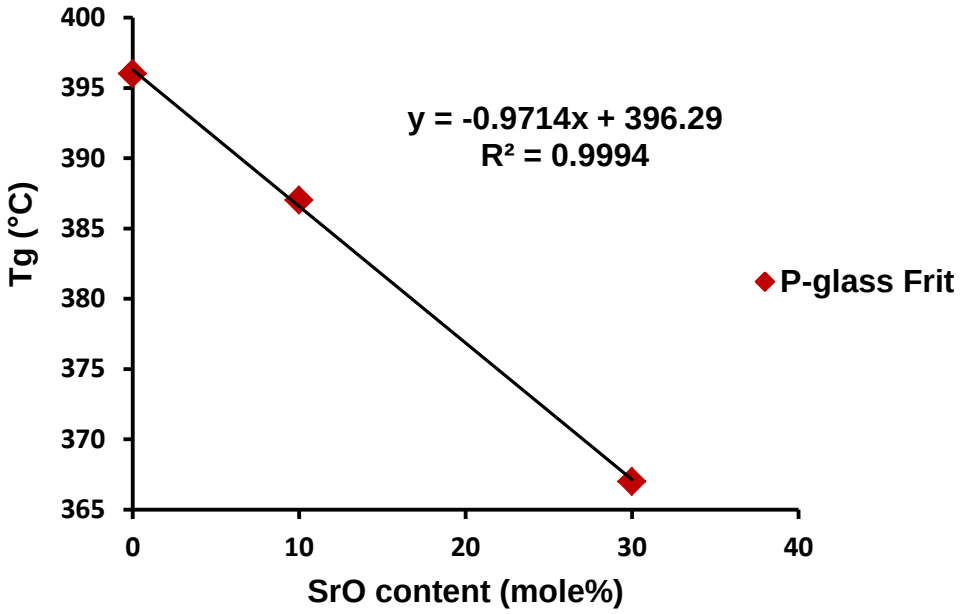

Figure 4.3 Showing the correlation between the glass transition temperature Tg (°C) as a function of the SrO content (mole %) in the prepared phosphate glasses.

Glass transition temperature values for all the glass are presented in Table 4.1. Figure 4.3 demonstrates the glass transition temperature against strontium content (mole %). It was clearly observed that there was a linear reduction with an increasing strontium content in the prepared phosphate glasses, with the correlation coefficient R^2 = 0.9994. A similar effect of strontium addition on glass transition of the silicate glasses (O'Donnell et al., 2010) can be typically explained by a slightly larger cationic size of strontium compared to calcium. This results in slight expansion of the glass network and reflects in reduction the glass transition temperature. Substitution of strontium for calcium in phosphate glasses is seen to result in a decrease in glass transition temperature.

4.3.3 Solid State ^{31}P MAS-NMR Analysis:

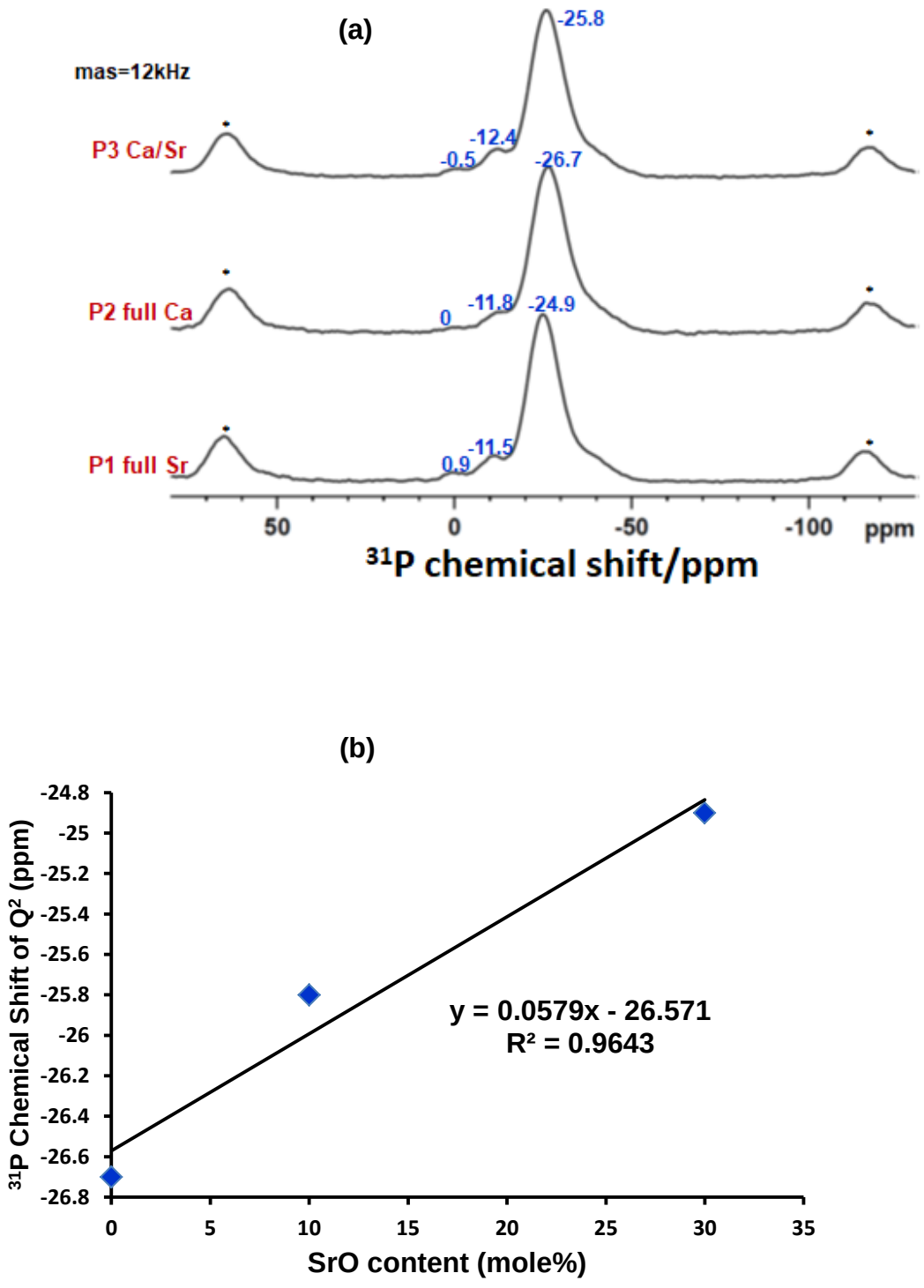

Figure 4.4 Showing (a) the ^{31}P MAS-NMR spectra of all untreated individual phosphate glasses before immersion in Tris buffer and (b) the linear correlation between the SrO content (mole%) and the ^{31}P chemical shift of Q^2 metaphosphate species. Asterisks show spinning side bands.

The atomic environment of phosphate in the prepared untreated phosphate glasses (P1, P2 and P3) was characterised by the ^{31}P MAS-NMR spectroscopy as demonstrated in Figure 4.4 (a). The dominant chemical shift from -24.9 ppm to -26.7 ppm can be assigned distinctly to the Q^2-metaphosphate species in the untreated glasses, whilst the chemical shift from -11.5 ppm to -12.4 ppm is assigned to the Q^1-phosphate species. The peaks of Q^1-phosphate species were in much smaller proportion compared to the dominant Q^2 species which was due to the constant phosphate ratio of 55 mole% in all three compositions. A small shoulder at ca -40 ppm on the right-hand side of the Q^2 signal corresponds to a minor fraction of the Q^3-phosphate species. This indicates that the structure of the glasses contains not just infinite chains or rings but these fragments can be also partly cross linked.

Figure 4.4 (b) illustrates the ^{31}P chemical shift of Q^2 metaphosphate species as a function of the strontium content. It was evident that the correlation between the ^{31}P chemical shift of Q^2 metaphosphate species and strontium content was linear with the coefficient of correlation $R^2 = 0.964$. This chemical shift linearity reveals that the substitution of calcium with strontium in Q^2-metaphosphate units occurs randomly and does not cause any significant change in the glass structure. The only sign of mixing cations was observed from the slight change in line width of the Q^2 signal. The line width is broad for the mixed cation glass composition P3 and becomes narrower in the spectra of the P2 and P1 glass.

4.3.4 pH Measurement Results:

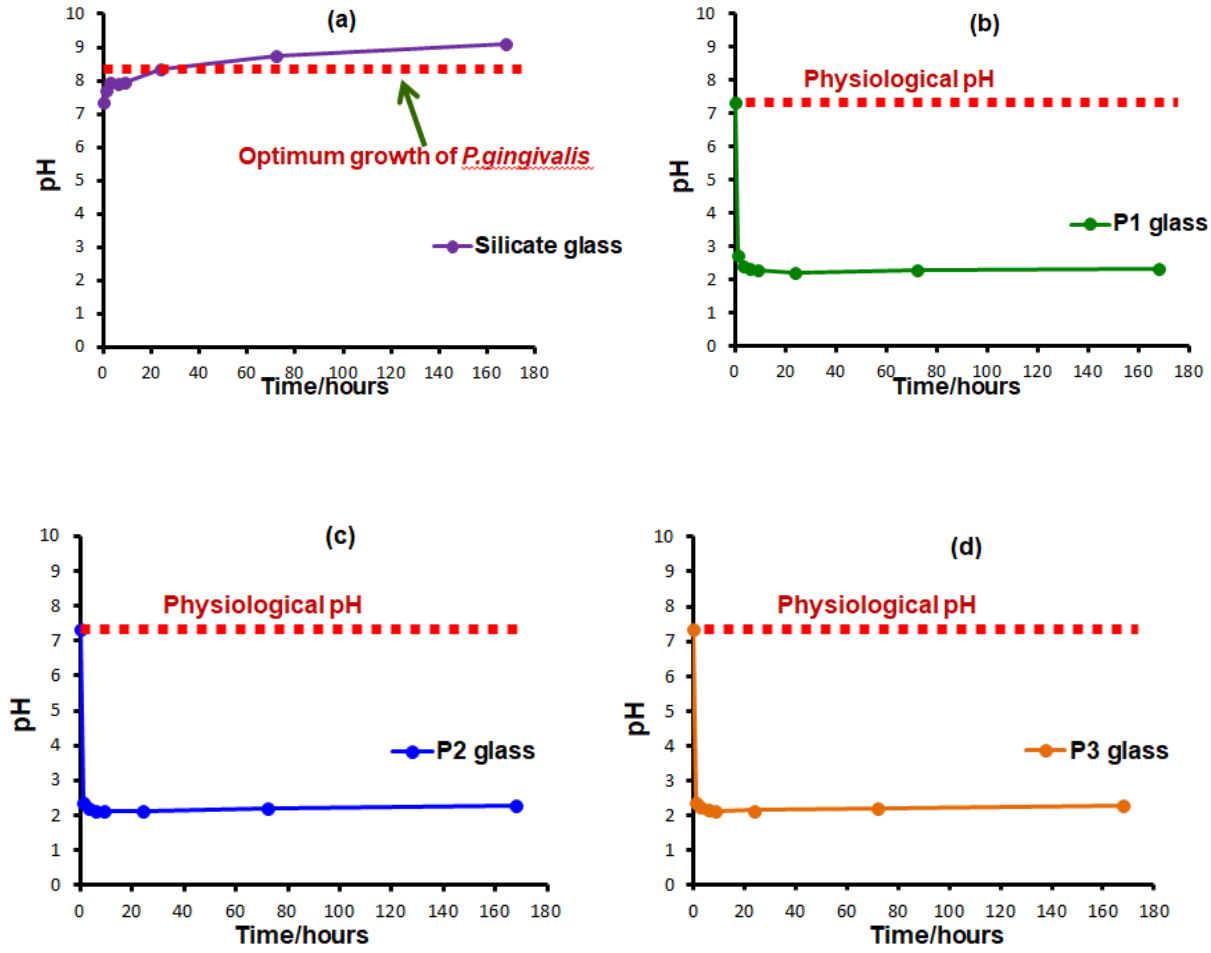

Figure 4.5 The pH behaviour in Tris buffer solution as a function of time for the four prepared glasses: (a) silicate glass; (b) P1 phosphate glass; (c) P2 phosphate glass and (d) P3 phosphate glass. Additional dashed lines in the Figures corresponds to the pH=8.3 (a), which is the optimal pH for growth of *P.gingivalis* and the pH=7.3 (b-d), which corresponds to the average physiological pH.

As can be observed in Figure 4.5 (a), the silicate glass dissolution in Tris buffer solution generated a dramatic increase in the pH measurements over the time periods of the experiment. The highest value of silicate glass pH (pH ≈ 9.12) was prominent after 168 hours of immersion time. This highly alkaline pH > 9 is the optimum pH for bacterial growth of the virulent *P.gingivalis* species (Takahashi and Schachtele, 1990), which is the main orchestrating bacteria in periodontal disease.

Figure 4.5 (b), (c) and (d) respectively revealed that all three phosphate glasses P1, P2 and P3 during their dissolution in Tris buffer showed a noticeable decrease in pH at the commencement of the experiment. Subsequently, the pH remained quite acidic and constant during the residual time of the experiment due to the capacity of the buffer solution to neutralise the sharp pH change in solution generated by further glass dissolution. This extremely acidic pH was far below the physiological pH range which is about 7.35 and this environment is also unfavourable for apatite formation.

The most noticeable drop in the solution pH of the phosphate glasses after 24 hours of immersion time was a pH of P2 (pH ≈ 2.11), followed by a pH of P3 (pH ≈ 2.13) and the least acidity was the pH of P1 (pH ≈ 2.23). Therefore, it appears that the addition of strontium results in a slight increase in pH of the individual phosphate glass dissolution. It is possible that a slightly higher alkalinity of strontium cation in solution compared to the calcium one has some effect on the pH values. Dissolution of the strontium containing phosphate glasses in SBF resulted in higher pH values than those that were obtained on dissolution of the calcium only containing phosphate glass as reported by Massera *et al*. (Massera et al., 2013).

4.4 Glass Mixtures Characterisation:

4.4.1 pH Measurement Results:

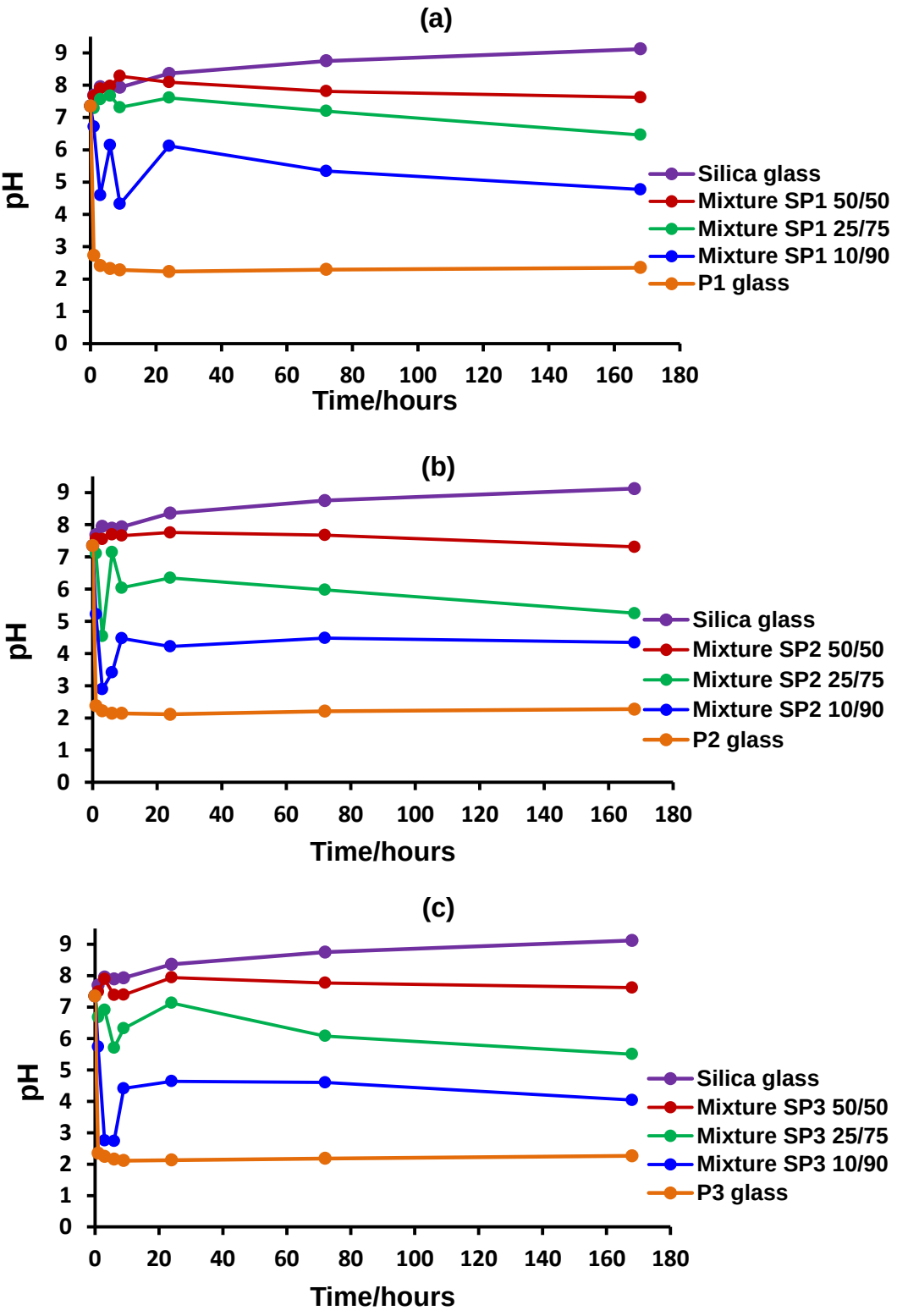

Figure 4.6 The pH behaviour in Tris buffer solution as a function of time of three different ratios for each glass mixture together with discrete silicate and phosphate glasses: (a) glass mixture SP1; (b) glass mixture SP2 and (c) glass mixture SP3.

Figure 4.6 (a), (b) and (c) demonstrated the pHs trend of all three glass mixtures SP1, SP2 and SP3 together alongside their three ratios respectively. The glass mixtures SP1, SP2 and SP3 with their three ratios (10/90, 50/50 and 25/75) exhibit smart modulation in pH behaviour in between the two undesirable extremes acidic and alkaline. It was clearly observed from Figure 4.6 (a), (b) and (c) that the initial pH drop can be manipulated by varying the ratios of glass mixtures 10/90, 50/50 and 25/75. The highest pH drop was with the ratio 10/90 where the phosphate ratio was 90%, whereas the less pH drop was observed with the ratio 25/75 followed by 50/50 which regulated the pH around the physiological range.

Therefore based on the experimental pH data of glass mixtures provided above, it should be taken into account how it would be possible to regulate this pH behaviour by varying the composition of these glass mixtures with their ratios.

4.5 Glass Mixtures Characterisation with the Ratio 10/90 (Results and Discussion):

4.5.1 Solid State ^{31}P MAS-NMR Results:

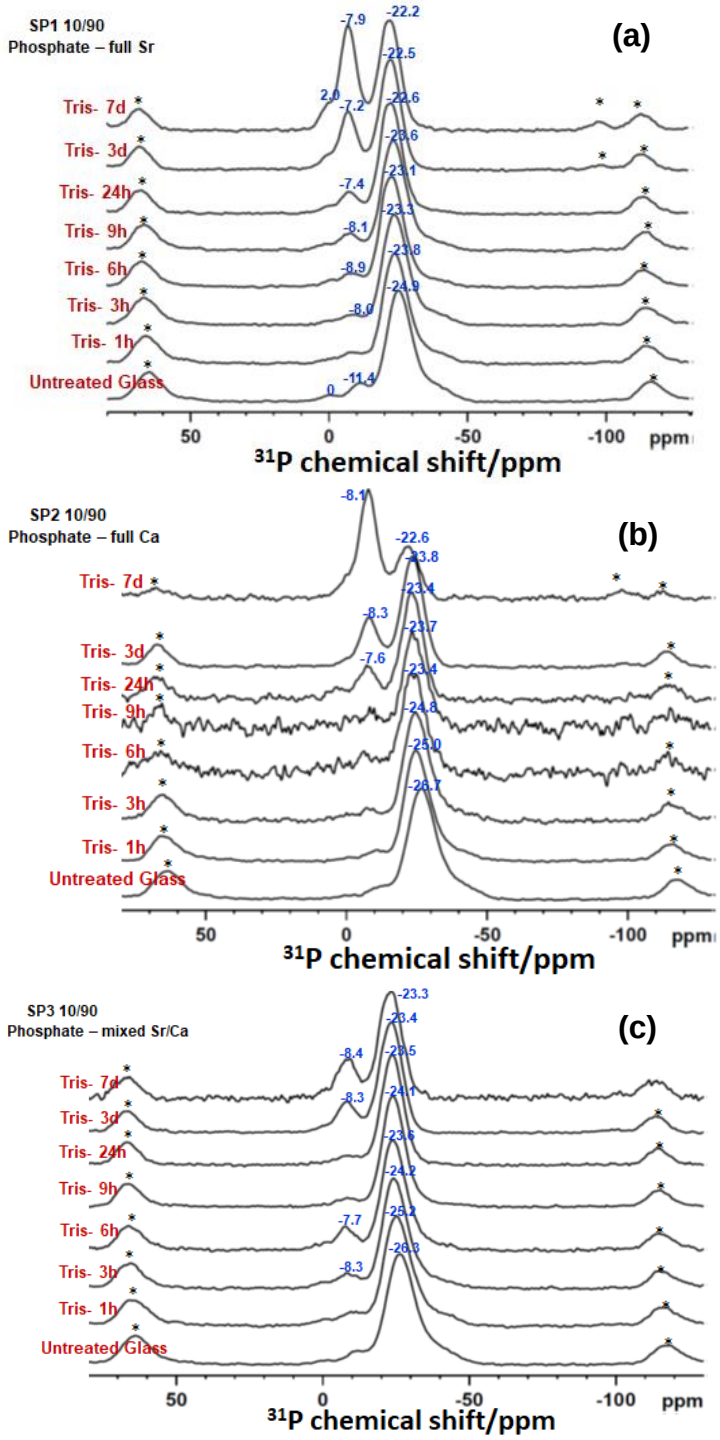

Figure 4.7 The ^{31}P MAS-NMR spectra (mas=22kHz) of studied glass mixtures with a 10/90 ratio before and after immersion in Tris buffer were plotted as a function of time for (a) SP1 mixture, (b) SP2 mixture and (c) SP3 mixture. Asterisks show spinning side bands.

Figure 4.7 (a), (b) and (c) illustrates the ^{31}P MAS-NMR spectra of the experimental glass mixtures with the 10/90 ratio of SP1, SP2 and SP3 respectively before and after immersion in Tris buffer solution up to 7 days. The signal from -24.9 ppm to -22.2 ppm in glass mixture SP1 corresponds with the chemical shift range of Q^2-metaphosphate species (Kirkpatrick and Brow, 1995, MacKenzie and Smith, 2002). A similar signal was identified in the two other glass mixtures, with a range of chemical shift signal from -26.7 ppm to -22.6 ppm in mixture SP2 and from -26.3 ppm to -23.3 ppm in mixture SP3.

Furthermore, the ^{31}P MAS-NMR spectra revealed another signal from -11.4 ppm to -7.2 ppm in glass mixture SP1, from -8.3 ppm to -7.6 ppm in mixture SP2 and from -8.4 ppm to -7.7 ppm in mixture SP3. This chemical shift range corresponds to the Q^1-phosphate species (Kirkpatrick and Brow, 1995, MacKenzie and Smith, 2002).

As a general trend, the appearance of Q^0-orthophosphate species can be only observed in very small amount with glass mixture SP1 10/90 at 3 days of immersion in Tris buffer at the peak position ≈ 2 ppm (Kirkpatrick and Brow, 1995, MacKenzie and Smith, 2002). In contrast, there was no visible or detectable presence of Q^0-orthophosphate species neither in glass mixture SP2 nor SP3.

The degradation of glass mixtures SP1, SP2 and SP3 was indicated by the transformation of phosphate in glass mixture from Q^2- species into Q^1-phosphate species. This degradation can be readily seen in Figure 4.7 (a), (b) and (c) for all glass mixtures SP1, SP2 and SP3 respectively; the amount of Q^2 decreases with time, whereas the amount of the Q^1 signal increases. The ^{31}P MAS-NMR spectra revealed that the fastest glass mixture degradation occurred with the ratio 10/90 was with SP2 (no strontium) followed by SP1 (no calcium), which was less degradable than SP2, whereas the slowest degradation was observed in SP3. This

could be seen from the comparison of the 7 days spectra between all three glass mixtures. The mixture SP3 have a dominant Q^2 signal in the 7 days spectrum, whereas the mixture SP2 showed dominant Q^1 signal in the spectrum, with the mixture SP1 showing significant both Q^1 and Q^2 signals. In the future work these spectra will be deconvoluted and integral intensities values will be obtained for more detailed comparison.

It is of interest to know that the emergence of Q^0-orthophosphate species in the glass mixture SP1 10/90 was likely to be as a result of precipitation of phosphate from the solution. Most probably this precipitation results from the hydrolysis of P—O—P bond of the Q^1-phosphate species to produce orthophosphate ions PO_4^{3-} as reported in the published literature (Gao et al., 2004) and (Bunker et al., 1984).

4.5.2 Fourier Transform Infrared Spectroscopy (FTIR) Results:

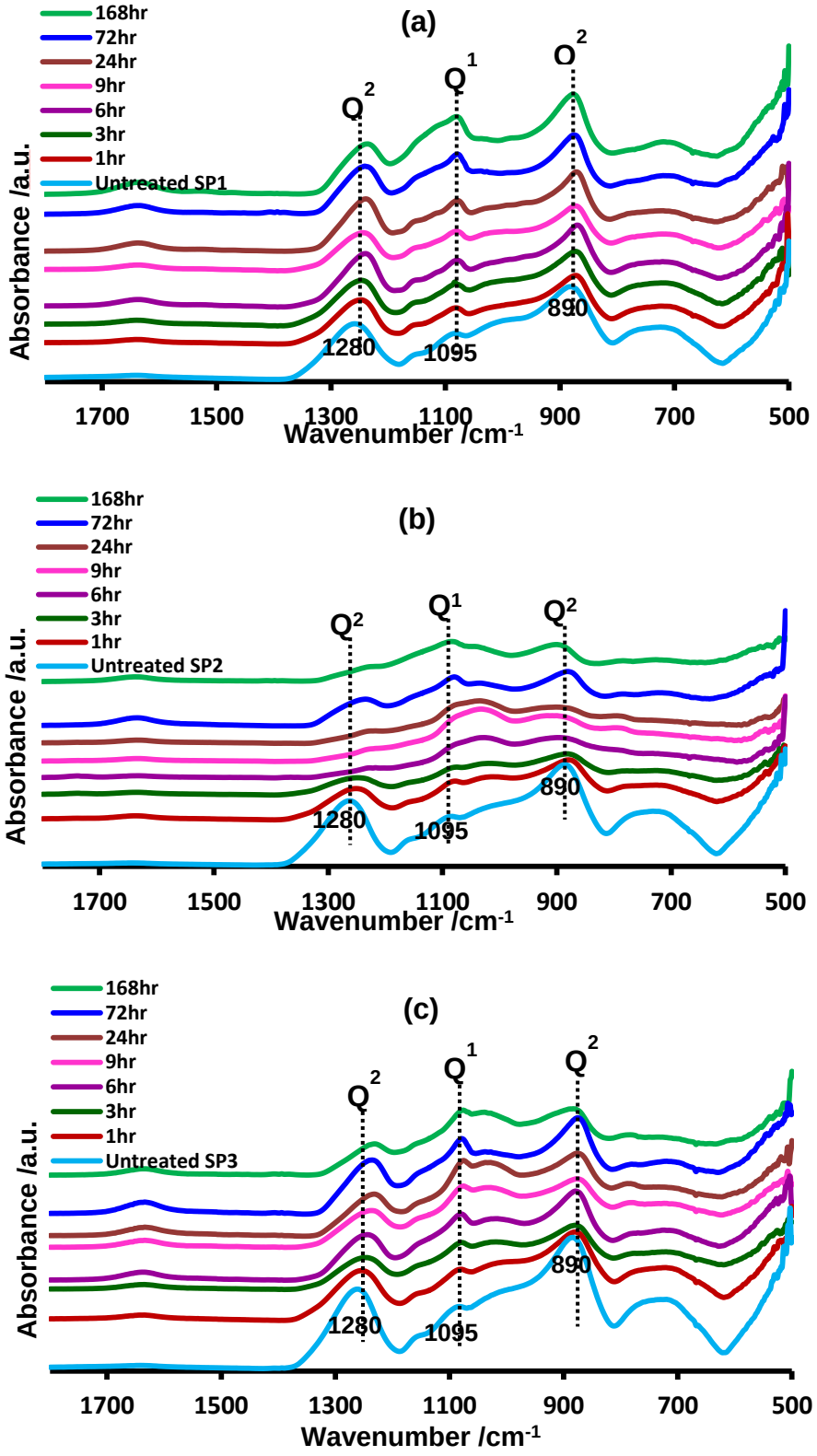

Figure 4.8 The FTIR spectra of studied glass mixtures with a 10/90 ratio before (untreated) and after immersion in Tris buffer for different time period indicated in hours plotted as a function of time for: (a) SP1 mixture, (b) SP2 mixture and (c) SP3 mixture.

Figure 4.8 revealed three main bands in the spectra. The two bands at 890 and 1280 cm^{-1} are assigned to the Q^2 metaphosphate stretching vibrational band (Moustafa and El-Egili, 1998, Ilieva et al., 2001, Patel et al., 2017). The band at approximately 1095 cm^{-1} is assigned to the Q^1-phosphate absorption band (Moustafa and El-Egili, 1998, Ilieva et al., 2001, Patel et al., 2017). It can be clearly observed that the fastest glass mixture degradation in Tris buffer solution with the ratio 10/90 is SP2 mixture (no strontium), indicating by: (i) the gradual disappearance of Q^2 metaphosphate vibrational band over the entire time of experiment and also (ii) the gradual emergence of Q^1-phosphate absorption band as a function of dissolution time.

Furthermore, FTIR did not show any significant difference in dissolution behaviour of glass mixtures SP1 10/90 and SP3 10/90 as given in Figure 4.8 (a) and (c) respectively. Even though the glass mixture SP3 after 7 days immersion in Tris buffer dissolved faster than SP1 as detected by decreasing the intensity of the Q^2 metaphosphate stretching bands compared to the equivalent bands of SP1 mixture after 7 days immersion in Tris buffer. However, both SP1 and SP3 10/90 mixtures in Figure 4.8 (a) and (c) respectively exhibited similar intensities in the appearance of the Q^1-phosphate absorption band over the immersion time points of the experiment. Thus, the FTIR spectra in Figure 4.8 (b) supported the results of the ^{31}P MAS-NMR spectra in Figure 4.7 (b), which were discussed in the previous section above.

4.5.3 pH Measurement Results:

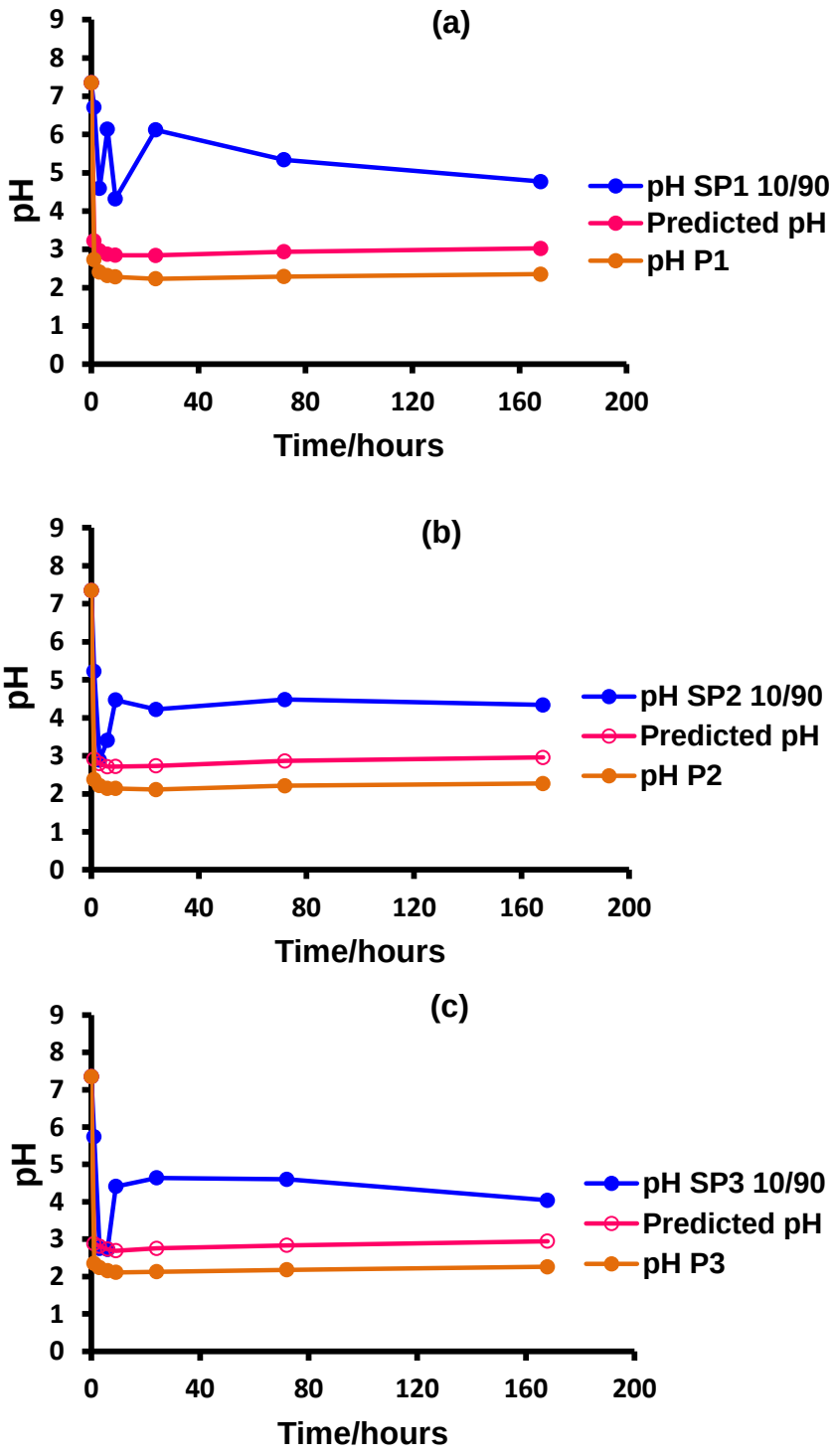

Figure 4.9 The pH behaviour in Tris buffer solution as a function of time of three experimental glass mixtures with a 10/90 ratio together with the expected pH value from each glass mixture based on the ratio 10/90 and pH value of each studied individual phosphate glass: (a) pH of SP1 & P1; (b) pH of SP2 & P2 and (c) pH of SP3 & P3. The data of predicted pH based on linear combination of the pH values for the individual glasses (S-glass and P-glass) taken in the proportions 10/90.

As a general trend, Figures 4.9 (a), (b) and (c) showed the pH behaviour of the studied glass mixtures SP1, SP2 and SP3 respectively with the ratio 10/90 after different time points of immersion in Tris buffer alongside their expected pH values. The latter was calculated from the pH measurements of the individual silicate and phosphate glasses P1, P2 and P3 in Tris buffer taking into account the ratio of the glasses.

The most noticeable drop in the solution pH of glass mixture at the beginning of the experiment was a pH of SP3 10/90 (pH ≈ 2.75) as shown in Figure 4.9 (c). Followed by the pH SP2 10/90 (pH ≈ 2.89) as in Figure 4.9 (b) and the least acidity was the pH of SP1 10/90 (pH ≈ 4.59).

Based on these pH results, it became clear that the acidity of phosphate glass can be regulated by mixing the phosphate glass with the silicate glass. Additionally, the pH behaviour of the silicate/phosphate glass mixture can be modulated accurately by varying the composition of these mixtures.

4.5.4 Ion Release Results:

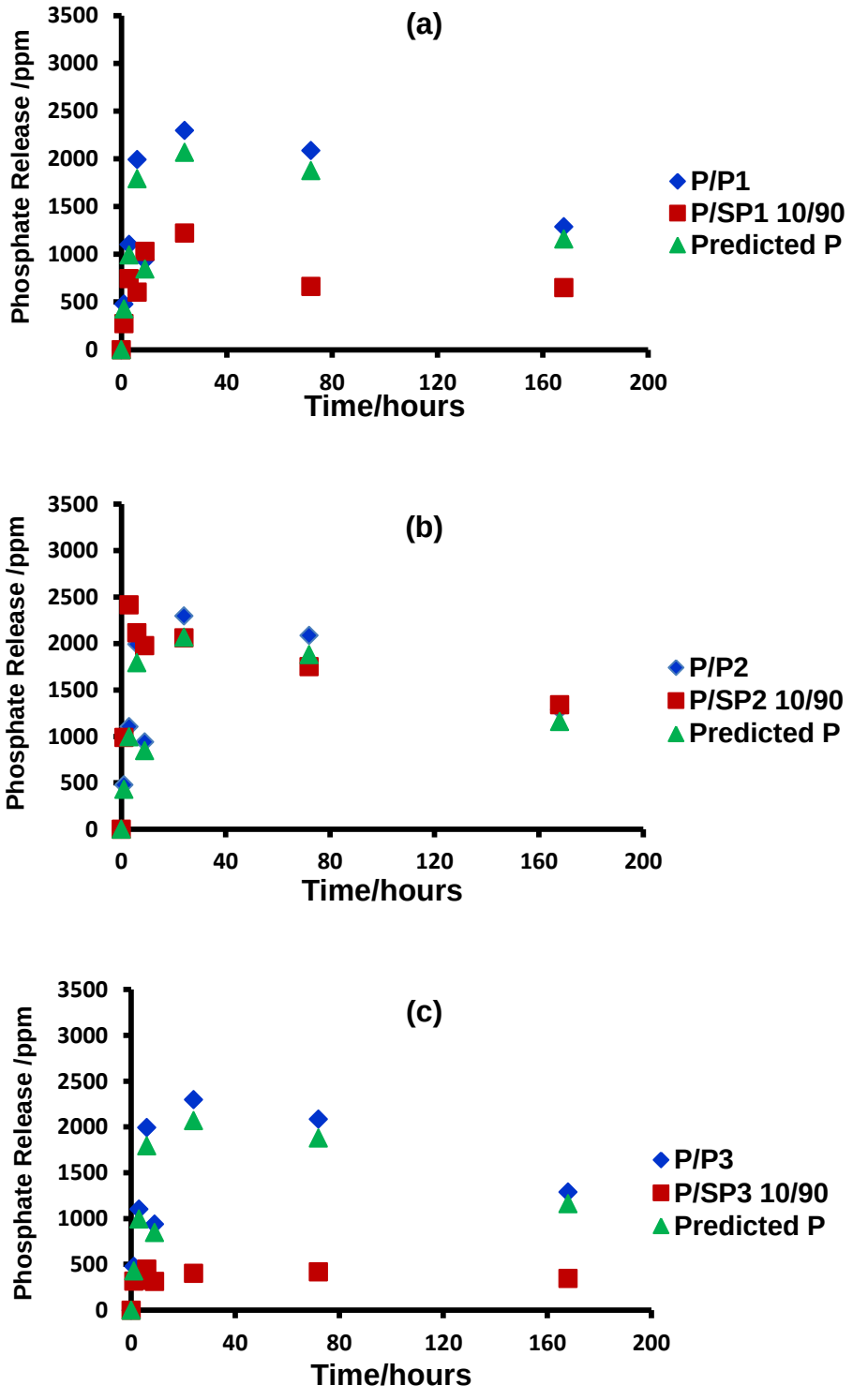

Figure 4.10 The phosphorus concentrations in ppm in Tris buffer solution plotted as a function of time for the experimental glass mixtures with a 10/90 ratio together. Predicted phosphorus release is estimated from the phosphorus release from each studied individual phosphate glass: (a) P from P1 & SP1; (b) P from P2 & SP2 and (c) P from P3 & SP3 reduced in the amount according to the ratio.

Figure 4.10 (a), (b) and (c) represents the phosphorus release after immersion in Tris buffer solution at different time points with respect to the 10/90 ratio for the three glass mixtures SP1, SP2 and SP3 respectively. Thereby, (a) represents the phosphorus originating from the individual phosphate glass (P1) in Tris buffer in addition to the phosphorus release in Tris of 10/90 SP1 mixture as well as the predicted phosphorus release from the P1 based on the 10/90 ratio. Likewise, (b) represents the phosphorus emerging from the individual phosphate glass (P2) in Tris buffer in addition to the phosphorus release in Tris of 10/90 SP2 mixture as well as the predicted phosphorus release from the P2 based on the 10/90 ratio. Thus, (c) represents the phosphorus release from the individual phosphate glass (P3) in Tris buffer in addition to the phosphorus release in Tris from 10/90 SP3 mixture as well as the predicted phosphorus release from the P3 based on the 10/90 ratio.

As can be observed from the Figure 4.10 (a), (b) and (c), the phosphorus release from the experimental data of SP2 followed closely the predicted patterns, whereas there was a massive deviation between the experimental phosphorus release from SP3 and the predicted ones. The intermediate deviation between the experimental phosphorus release and the predicted values were observed for the SP1.

Regardless of the fact that all three compositions contain the same amount of phosphate, the phosphorus release in Tris buffer (measured in ppm) was much higher in the glass mixture SP2. The relatively low phosphorus release was associated with the glass mixture SP1, whilst the least phosphorus release was from the glass mixture SP3.

These obtained phosphorus concentration data are in good agreement with the ^{31}P MAS-NMR spectra in Figure 4.7 (a), (b) and (c) as well as the FTIR results in Figure 4.8 (a), (b) and (c), where the fastest dissolution was observed in glass mixture SP2, the SP1 showed the lower rate of dissolution, whilst the slowest degradation

was seen in mixture is SP3. The faster dissolution seen in NMR spectra resulted in the highest concentration of phosphorus in solution (Figure 4.10 (b)).

The drop in the phosphorus concentration after 24 hours immersion as in Figure 4.10 (a) was in good consistency with the ^{31}P MAS-NMR spectra in Figure 4.7 (a). The reduction of the measured concentration of phosphorus in solution can be accounted to the uptake of phosphorus from solution and precipitation of the Q^0-orthophosphate species. The latter was detected in ^{31}P MAS-NMR spectrum of the glass mixture SP1 10/90 as the peak at the position ≈ 2 ppm at 3 days immersion in Tris buffer.

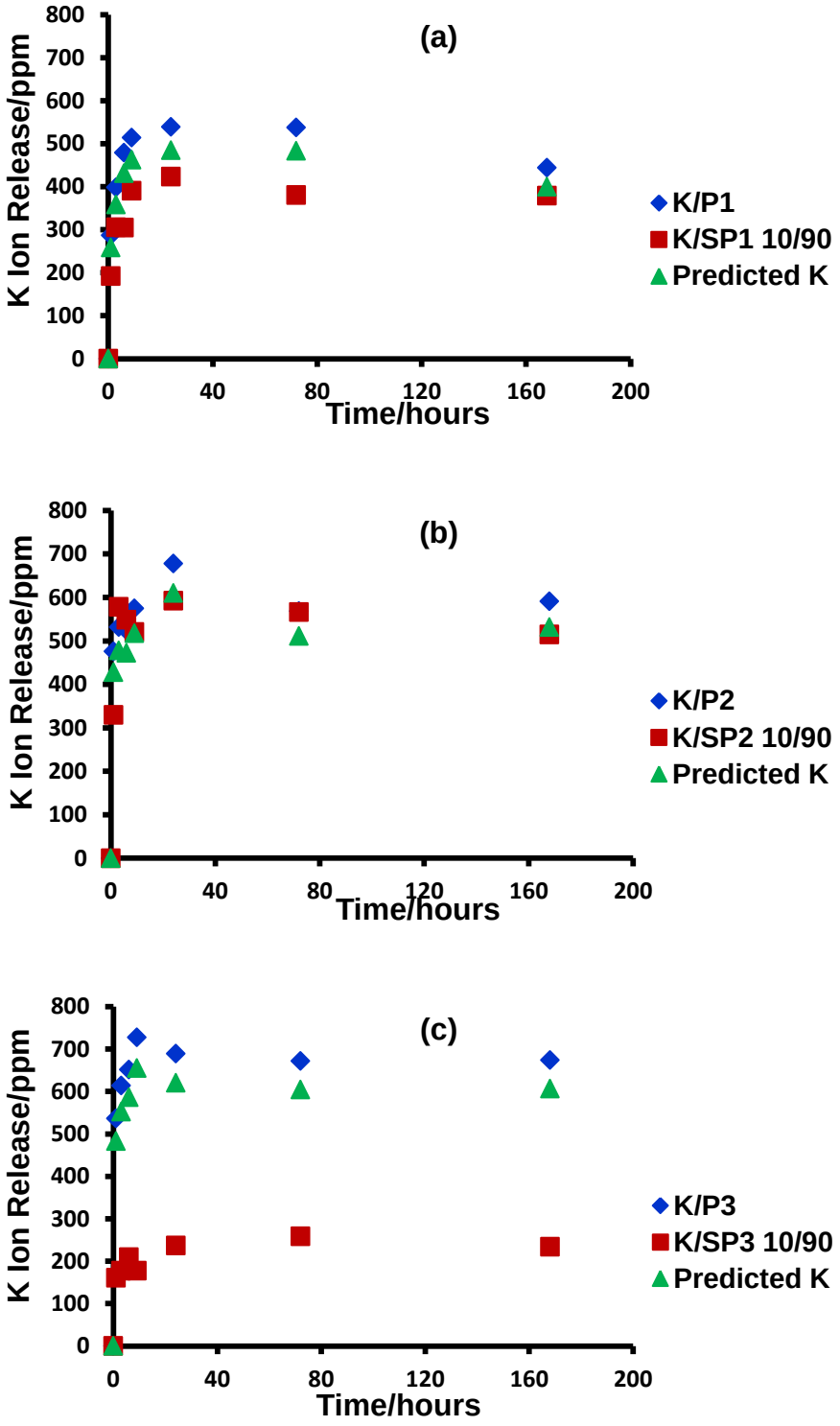

Figure 4.11 The potassium ion concentrations in ppm in Tris buffer solution plotted as a function of time for the experimental glass mixtures with a 10/90 ratio. Predicted potassium ion release is estimated from the potassium release from each studied individual phosphate glass: (a) K from P1 & SP1; (b) K from P2 & SP2 and (c) K from P3 & SP3 reduced in the amount according to the ratio 10/90.

Figure 4.11 (a), (b) and (c) exhibits the concentration of potassium ion measured in ppm as a function of dissolution time in Tris buffer solution for the three glass mixtures SP1, SP2 and SP3 respectively all with the 10/90 ratio.

Thereby, (a) demonstrates the potassium ion release from the individual phosphate glass (P1) after immersion in Tris buffer (blue diamonds), the release of potassium ion in Tris buffer of 10/90 SP1 mixture (red squares) as well as the predicted potassium ion release from the P1 depending on the 10/90 ratio (green triangles). Similarly and using the same markers, (b) illustrates the potassium ion release from the individual phosphate glass (P2) in Tris buffer, the potassium ion release in Tris immersion of 10/90 SP2 mixture as well as the predicted potassium ion release from the P2 based on the 10/90 ratio. Figure 4.11 (c) represents the potassium ion release from the individual phosphate glass (P3) in Tris buffer in addition to the potassium ion release in Tris of 10/90 SP3 mixture as well as the predicted potassium ion release from the P3 based on the 10/90 ratio.

From the Figure 4.11 (a), (b) and (c), the potassium ion release from the experimental patterns of SP1 and SP2 with the ratio 10/90 follows well the predicted behaviour, whereas there was a significant variation between the experimental potassium ion release from SP3 10/90 and the predicted ones. Thereby, the highest potassium ion release in Tris buffer was in conjunction with the glass mixtures SP1 and SP2 10/90, whilst the lowest potassium ion release emerged from the glass mixture SP3 10/90.

It is of interest to note that similarly to phosphorus release, the trend of potassium ion release data was also in good consistency with the ^{31}P MAS-NMR spectra in Figure 4.7 (a), (b) and (c) as well as the FTIR results in Figure 4.8 (a), (b) and (c). The fastest dissolution was observed in the SP2 10/90 and the less degradable was SP1 10/90, whilst the slowest dissolving mixture was SP3 10/90. The latter was in

agreement with the lowest potassium release from SP3 mixture. The lowest degradation rate leads to the lowest concentration species released from the glass.

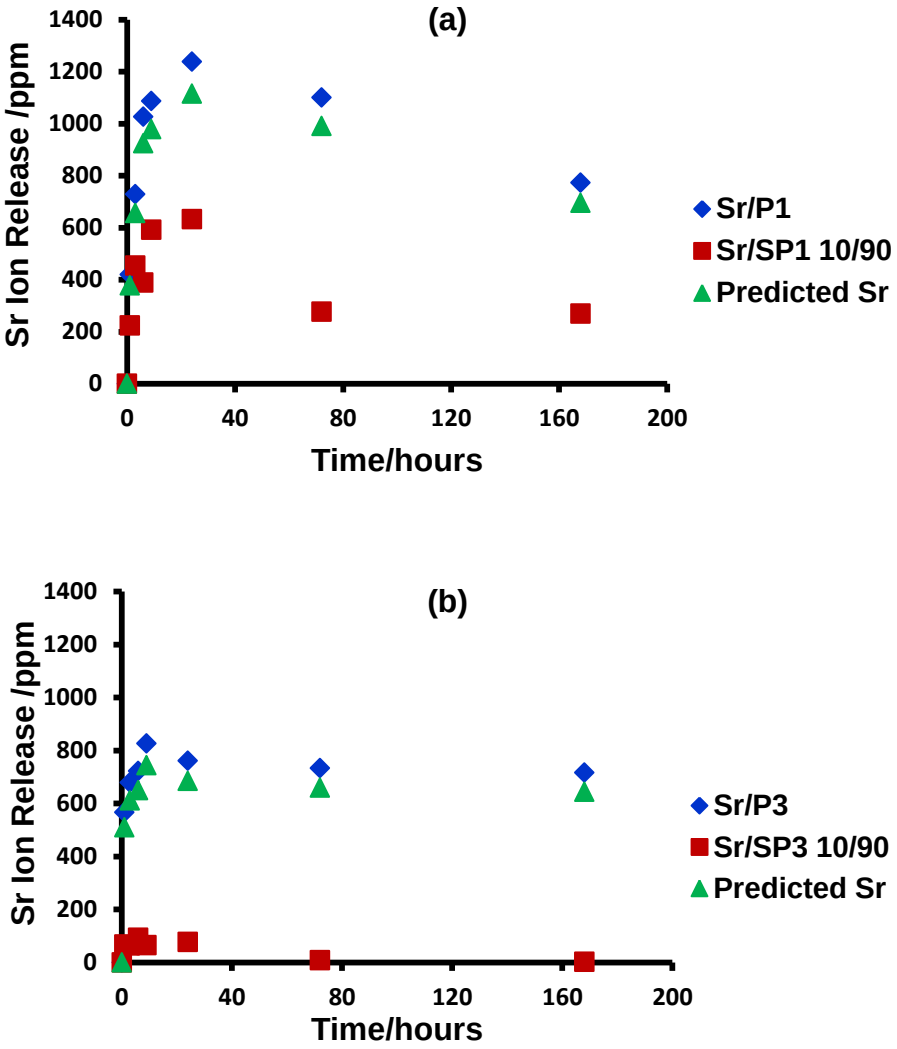

Figure 4.12 The strontium ion concentrations in ppm in Tris buffer solution plotted as a function of time for the experimental glass mixtures with a 10/90 ratio. Predicted strontium ion release is estimated from the strontium release from the individual phosphate glasses: (a) Sr from P1 & SP1; (b) Sr from P3 & SP3 reduced in the amount according to the ratio 10/90.

Figure 4.12 (a) and (b) exhibits the concentration of strontium ion measured in ppm as a function of dissolution time in Tris buffer solution for the glass mixtures SP1 and SP3 respectively with the 10/90 ratio.

As mentioned before, there was no strontium in SP2 therefore Figure 4.12 (a) displays the strontium ion release from the individual phosphate glass P1, the release of strontium ion from 10/90 SP1 mixture as well as the predicted strontium ion release from the P1 depending on the 10/90 ratio. Similarly, Figure 4.12 (b) illustrates the strontium ion release from the individual phosphate glass (P3), the strontium ion release from 10/90 SP3 mixture as well as the predicted strontium ion release from the P3 based on the 10/90 ratio.

From the Figure 4.12 (a) and (b), both patterns of strontium ion release from the experimental data of SP1 and SP3 with the ratio 10/90 do not closely follow the predicted strontium release, in particular the glass mixture SP3 shows the massive deviation between the experimental strontium ion release from SP3 10/90 and the predicted ones. Therefore, the maximal strontium ion release is from the glass mixture SP1, whereas the minimum strontium ion release is associated with the glass mixture SP3.

The profile of strontium ion release data and in particular the lowest concentration values seen in SP3 were in accordance with the ^{31}P MAS-NMR results in Figure 4.7 (a) and (c) as well as the FTIR results in Figure 4.8 (a) and (c), where the spectroscopy investigation indicated that the glass mixture SP3 10/90 was the slowest degradable glass mixture.

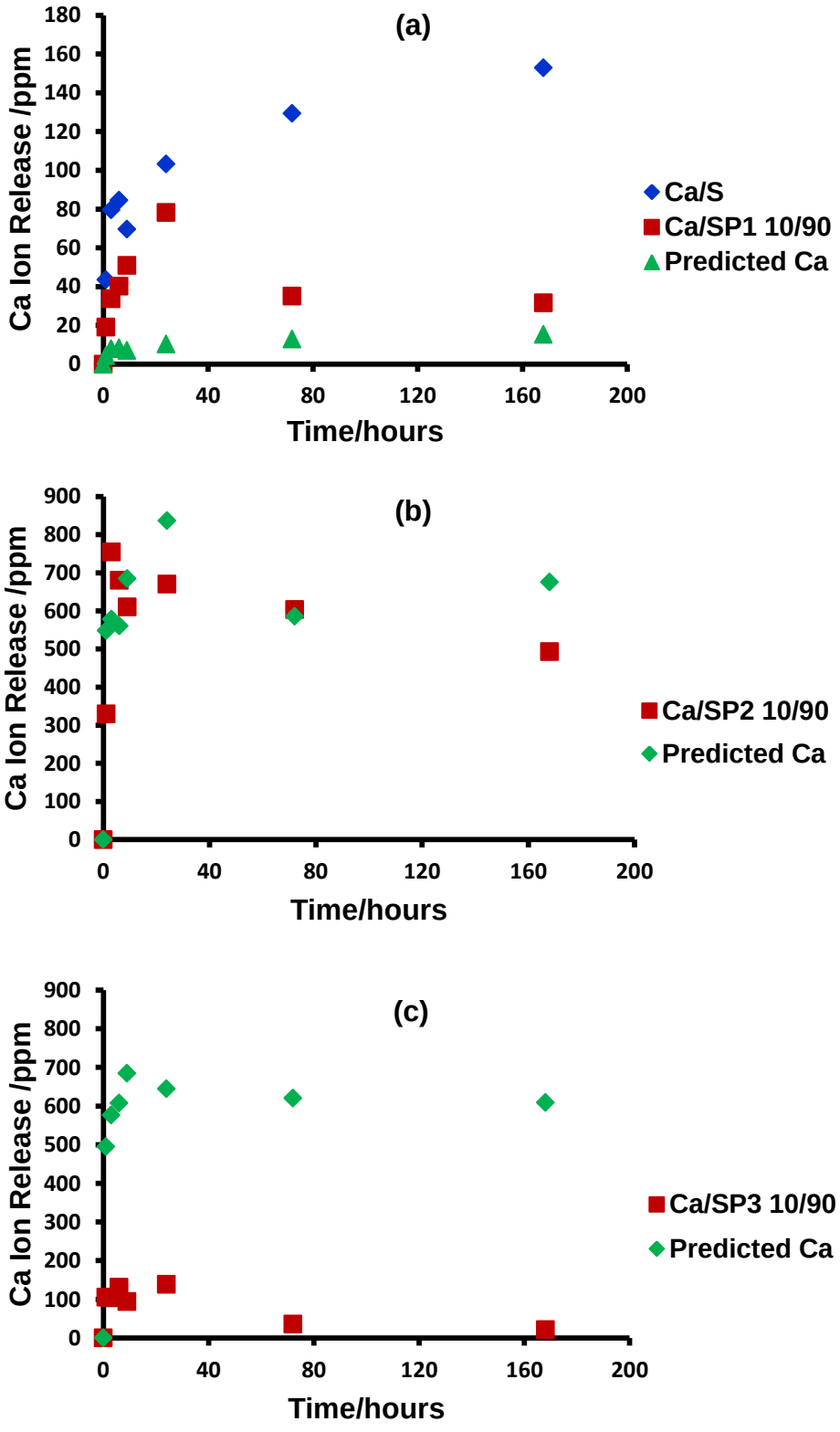

Figure 4.13 The calcium ion concentrations in ppm in Tris buffer solution plotted as a function of time for the experimental glass mixtures with a 10/90 ratio; together with the predicted calcium ion release based on the ratio 10/90 and calcium ion release from individual silicate glass: (a) Ca from S & SP1, (b) Ca from SP2 and (c) Ca from SP3.

It is important to realise that the calcium ion release in the glass mixture SP1 emerges totally from the silicate glass, whereas the release of calcium ion from the glass mixtures SP2 and SP3 arises from both the silicate and phosphate glasses as highlighted before in the rationale section 4.2.

Subsequently, Figure 4.13 (a), (b) and (c) exhibits the concentration of calcium ion measured in ppm as a function of dissolution time in Tris buffer solution for the three glass mixtures SP1, SP2 and SP3 respectively with the 10/90 ratio. Thereby, Figure 4.13 (a) demonstrates the calcium ion release from the individual silicate glass after immersion in Tris buffer, the release of calcium ion in Tris buffer of 10/90 SP1 mixture as well as the predicted calcium ion release from the silicate glass depending on the 10/90 ratio. Similarly, (b) illustrates the calcium ion release of 10/90 SP2 mixture in Tris immersion as well as the predicted calcium ion release 10% from silicate glass plus 90% from phosphate glass P2 based on the 10/90 ratio. Figure 4.13 (c) represents the calcium ion release in Tris from 10/90 SP3 mixture as well as the predicted calcium ion release 10% from silicate glass plus 90% from phosphate glass P3 based on the 10/90 ratio.

It is of interest to point out from the Figure 4.13 (a), (b) and (c), that the calcium ion release from the experimental data of SP2 10/90 roughly followed the predicted patterns, whereas there was a prominent difference between the experimental calcium ion release from both SP1 and SP3 of the ratio 10/90 and their predicted values.

Considering the absolute values of measured concentration, much higher calcium ion release in Tris buffer (measured in ppm) was observed in conjunction with the glass mixture SP2 10/90, followed by lower calcium ion release emerging from the glass mixture SP3 10/90, with the least calcium ion release arises from the glass mixture SP1 10/90.

The experimental calcium release behaviour of SP1 10/90 in Figure 4.13 (a) shows a particular interesting profile. The initial release profile closely follows the calcium release profile from the silicate glass regardless the fact that there was only 10% of the silicate glass in the mixture. The depletion in the calcium ion concentration after 24 hours of immersion in Tris buffer indicated that the consumption of calcium ion from solution which was consistent with the precipitation of the Q^0-orthophosphate species as detected by the ^{31}P MAS-NMR in Figure 4.7 (a).

Overall, the trend of the highest experimental calcium ion release from SP2 10/90 was in good agreement with the ^{31}P MAS-NMR spectra in Figure 4.7 (b) as well as the FTIR results in Figure 4.8 (b), where the highest dissolution rate was observed in SP2 10/90.

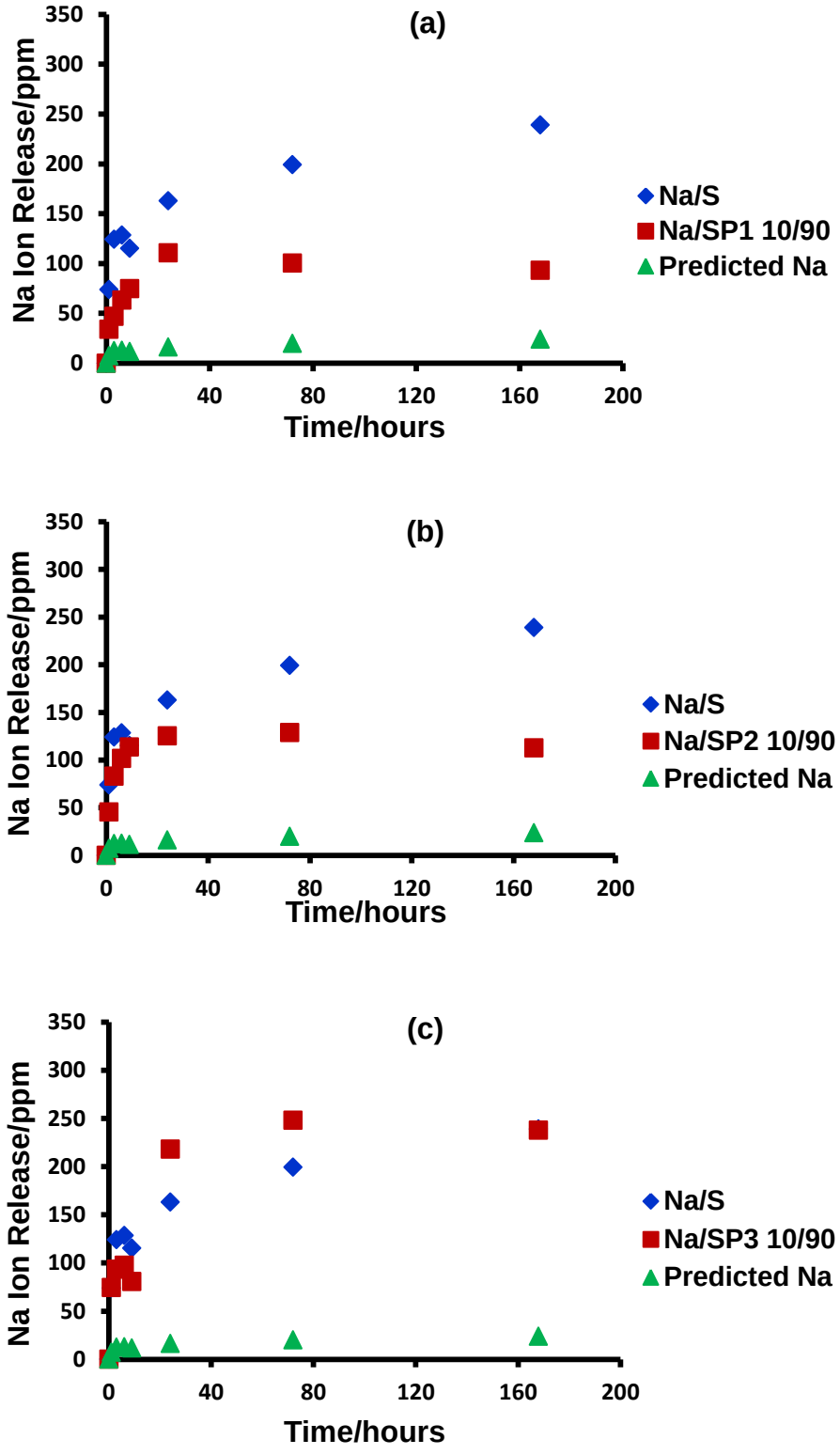

Figure 4.14 The sodium ion concentrations in ppm in Tris buffer solution plotted as a function of time for the experimental glass mixtures with a 10/90 ratio. The predicted sodium ion release from individual silicate glass based on the ratio 10/90 and sodium ion release from the studied individual silicate glass: (a) Na from S & SP1 and (b) Na from S & SP2 and (c) Na from S & SP3.

Another ion which emerges only from silicate glass is the sodium ion. Figure 4.14 (a), (b) and (c) exhibits the concentration of sodium ion measured in ppm as a function of dissolution time in Tris buffer solution for the three glass mixtures SP1, SP2 and SP3 respectively with the 10/90 ratio. Figure 4.14 (a) demonstrates the sodium ion release from the individual silicate glass after immersion in Tris buffer, the release of sodium ion in Tris buffer of 10/90 SP1 mixture as well as the predicted sodium ion release from silicate glass depending on the 10/90 ratio. Likewise, (b) illustrates the sodium ion release from the individual silicate glass in Tris buffer, the sodium ion release from 10/90 SP2 mixture in Tris immersion as well as the predicted sodium ion release from the silicate glass based on the 10/90 ratio. Figure 4.14 (c) represents the sodium ion release from the individual silicate glass in Tris buffer in addition to the sodium ion release in Tris of 10/90 SP3 mixture as well as the predicted sodium ion release from the silicate glass based on the 10/90 ratio.

It can be observed from the Figure 4.14 (a), (b) and (c), that all the patterns of sodium ion release from the experimental data of SP1, SP2 and SP3 with the ratio 10/90 do not follow the predicted sodium release and are much closer to the profile of the silicate glass on its own. The greatest amount of sodium ion release in Tris buffer is in conjunction with the glass mixture SP3 10/90, whilst the sodium ion release arising from both glass mixtures SP1 10/90 and SP2 10/90 is lower and quite similar to each other as a function of dissolution time.

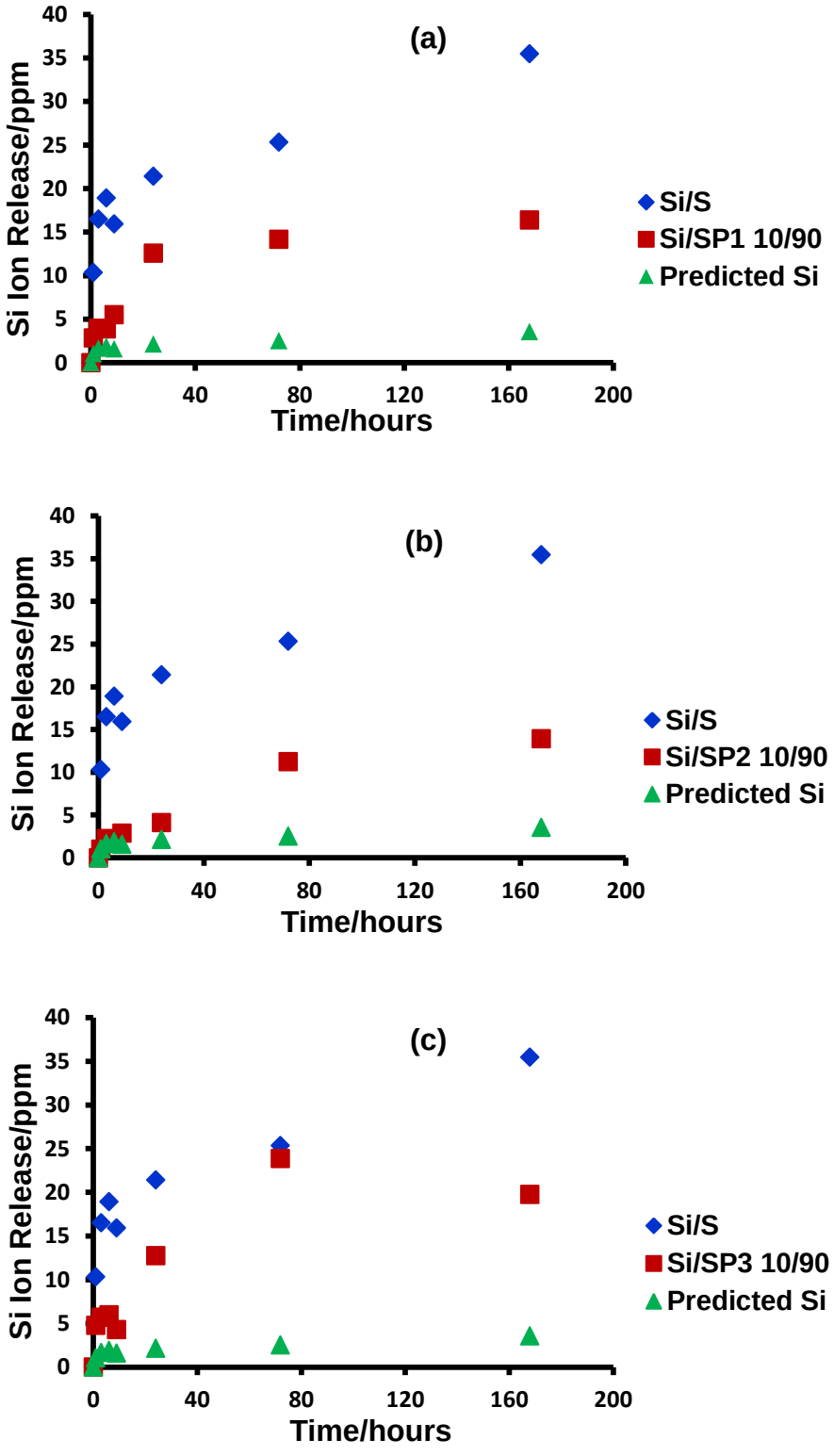

Figure 4.15 The silicon concentrations in ppm in Tris buffer solution plotted as a function of immersion time for the experimental glass mixtures with a 10/90 ratio together with the predicted silicate ion release from individual silicate glass based on the ratio 10/90 and silicate ion release from individual silicate glass: (a) Si from S & SP1 and (b) Si from S & SP2 and (c) Si from S & SP3.

Similar to sodium ion, silicon was another species that emerged only from the silicate glass as seen in Figure 4.15 (a), (b) and (c). Silicon species was plotted for each of three mixtures in comparison with release from silicate glass alone and predicted values based on 10/90 ratio in this Figure.

It can be observed from the Figure 4.15 (a), (b) and (c) that the experimental concentration of silicon measured in SP1, SP2 and SP3 mixtures with the ratio 10/90 are deviated distinctly from the predicted silicon release data. In particular the glass mixture SP3 where the deviation between the experimental silicon release from SP3 and the predicted ones is well-defined. Therefore, the greater amount of silicon release in Tris buffer is generated from the glass mixture SP3 10/90 as a function of dissolution time, followed by the lower amount of silicon release coming from the glass mixture SP1 10/90, and the least silicon release seen from the glass mixture SP2 10/90.

4.6 Glass Mixtures Characterisation with the Ratio 25/75 (Results and Discussion):

4.6.1 Solid State ^{31}P MAS-NMR Results:

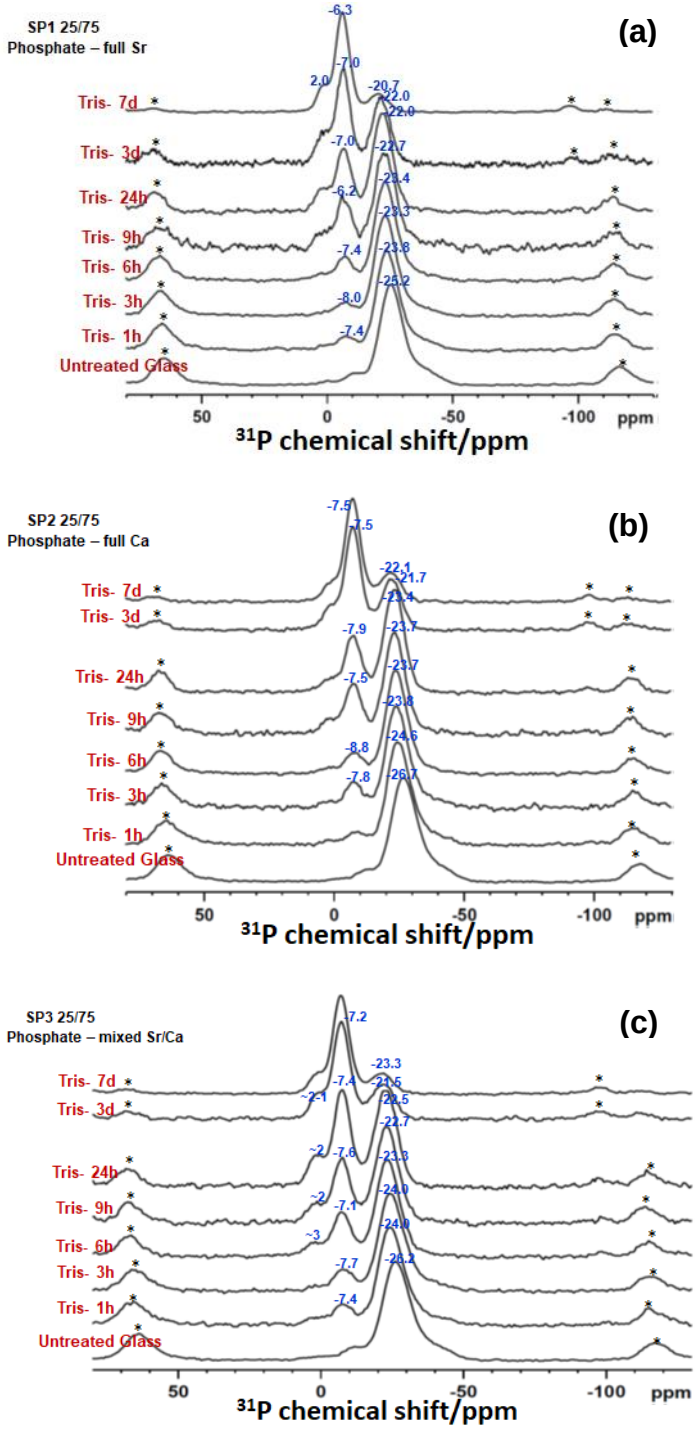

Figure 4.16 The ^{31}P MAS-NMR spectra (mas=22kHz) of studied glass mixtures with a 25/75 ratio before and after immersion in Tris buffer were plotted as a function of time for (a) SP1 mixture, (b) SP2 mixture and (c) SP3 mixture.

Figure 4.16 (a), (b) and (c) illustrates the ^{31}P MAS-NMR spectra of the experimental glass mixtures with the 25/75 ratio of SP1, SP2 and SP3 respectively before and after immersion in Tris buffer solution as a function of time up to 7 days. The chemical shift range from -25.2 ppm to -20.7 ppm in glass mixture SP1 was assigned to the Q^2-metaphosphate species. The signals from -26.7 ppm to -21.7 ppm in mixture SP2 and from -26.2 ppm to -21.5 ppm in mixture SP3 similarly were assigned to the Q^2-metaphosphate speciation (Kirkpatrick and Brow, 1995, MacKenzie and Smith, 2002).

The peaks observed in the ^{31}P MAS-NMR spectra were from -8.0 ppm to -6.2 ppm) in glass mixture SP1, from -8.8 ppm to -7.5 ppm in mixture SP2 and from -7.7 ppm to -7.1 ppm in mixture SP3. These signals were assigned to the chemical shift range of the Q^1-phosphate species (Kirkpatrick and Brow, 1995, MacKenzie and Smith, 2002).

In Figure 4.16 (a) and (b), the spectra of the glass mixtures SP1 and SP2 at early 9 hours of immersion in Tris buffer solution revealed a peak at the position of around 2 ppm. This corresponded to the emerging Q^0-orthophosphate species (Kirkpatrick and Brow, 1995, MacKenzie and Smith, 2002). Similarly, SP3 mixture revealed a small signal at 3 ppm at the early 6 hours immersion in Tris buffer as in Figure 4.16 (c), which also corresponded to precipitation of the Q^0-orthophosphate species.

As stated previously, the degradation of glass mixtures SP1 25/75, SP2 25/75 and SP3 25/75 was indicated by the transformation of phosphate in glass mixture from Q^2-metaphosphate species into Q^1-phosphate species. This degradation can be readily seen in Figure 4.16 (a), (b) and (c) for all glass mixtures SP1, SP2 and SP3 respectively. However, the ^{31}P MAS-NMR spectra in Figure 4.16 (a), (b) and (c) reveal that all three glass mixtures SP1, SP2 and SP3 with the ratio 25/75 have relatively similar behaviour of glass degradation rate in Tris buffer solution.

The most significant finding which was observed with the ratio 25/75 was the faster degradation rate of mixture SP1 compared to its degradation rate with the 10/90 ratio as demonstrated by the gradual conversion of the Q^2-metaphosphate species into the Q^1-pyrophosphate species.

Similar observation can be seen with the glass mixture SP3 25/75 indicated by rapid degradation of the Q^2-metaphosphate species and transformed into the Q^1-phosphate species which was more pronounced at the ratio 25/75 than the ratio 10/90. Thus, SP3 25/75 dissolved quickly in contrast to its dissolution with the ratio 10/90.

4.6.2 Fourier Transform Infrared Spectroscopy (FTIR) Results:

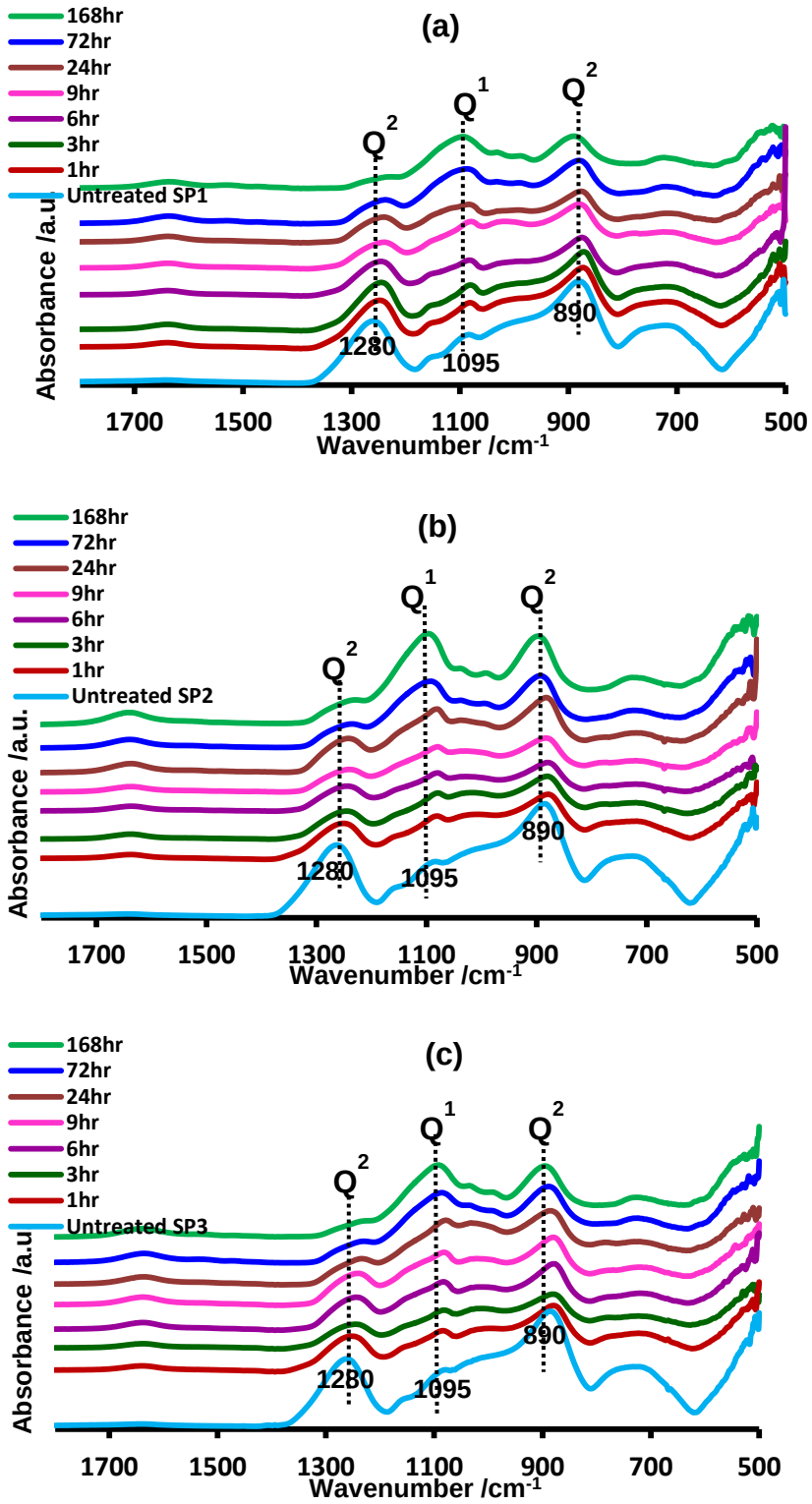

Figure 4.17 The FTIR spectra of studied glass mixtures with a 25/75 ratio before and after immersion in Tris buffer were plotted as a function of time for: (a) SP1 mixture, (b) SP2 mixture and (c) SP3 mixture.

The FTIR spectra in Figure 4.17 were similar to the spectra observed in the 10/90 mixture as described earlier. Similarly, three signals were identified in the spectrum of the glass mixture. The FTIR spectra showed a reduction of the band at approximately 1280 cm^{-1}, which was Q^2 metaphosphate vibrational frequency (Moustafa and El-Egili, 1998, Ilieva et al., 2001, Patel et al., 2017) with gradual emergence of the band at ≈ 1095 cm^{-1}, which was the Q^1 absorption band, (Moustafa and El-Egili, 1998, Ilieva et al., 2001, Patel et al., 2017).

Overall, the FTIR data revealed that the rate of glass mixtures degradation of SP1, SP2 and SP3 with the ratio 25/75 was to some extent similar to each other in Tris buffer solution.

The FTIR spectra in Figure 4.17 (a), (b) and (c) were consistent with the ^{31}P MAS-NMR spectra in Figure 4.16 (a), (b) and (c) respectively.

4.6.3 pH Measurement Results:

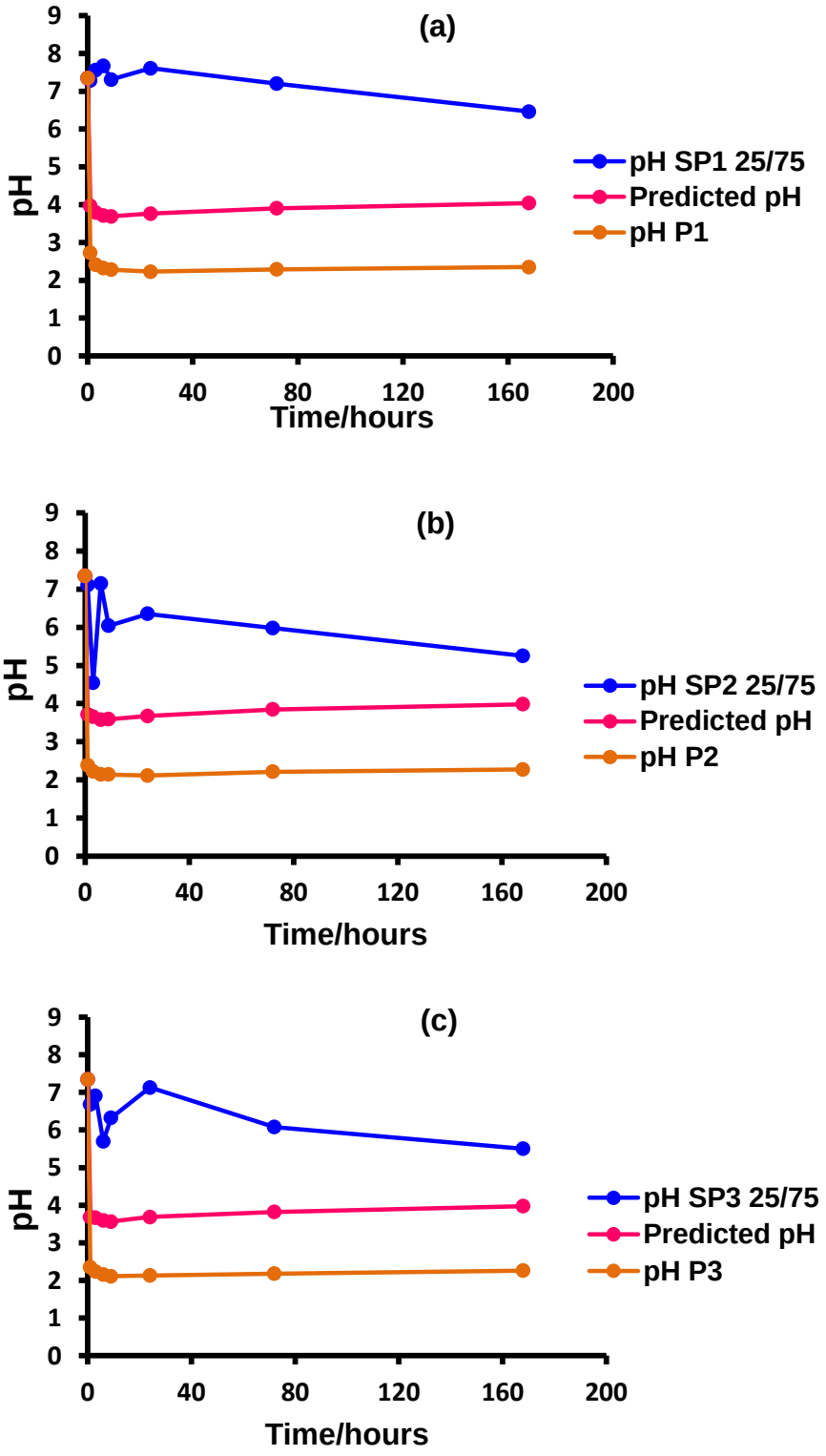

Figure 4.18 The pH behaviour in Tris buffer solution as a function of time of three experimental glass mixtures with a 25/75 ratio together with the predicted pH value from each glass mixture based on the ratio 25/75 and pH value of individual phosphate glass: (a) pH of SP1 & P1; (b) pH of SP2 & P2 and (c) pH of SP3 & P3.

Figure 4.18 (a), (b) and (c) respectively represents the pH change of the studied glass mixtures SP1, SP2 and SP3 with the specific ratio 25/75 as a function of immersion time in Tris buffer together with their expected pH values. The latter were calculated from pH measurements obtained by dissolving the individual phosphate glasses P1, P2 and P3 in Tris buffer solution applying this glass ratio.

The behaviour of pH change in solution shifted towards the relatively high acidity after the first 3 hours of glass mixture SP2 25/75 dissolution in Tris buffer (pH ≈ 4.54) as shown in Figure 4.18 (b). A neutral/slight acidity in solution within the same immersion time was from glass mixture SP3 25/75 where the solution pH was ≈ 6.91 as in Figure 4.18 (c). Moreover, the pH trend in solution shifted towards the neutral/slight alkalinity after 3 hours immersion of glass mixture SP1 25/75 as given in Figure 4.18 (a) where the pH was ≈ 7.56.

4.6.4 Ion Release Results:

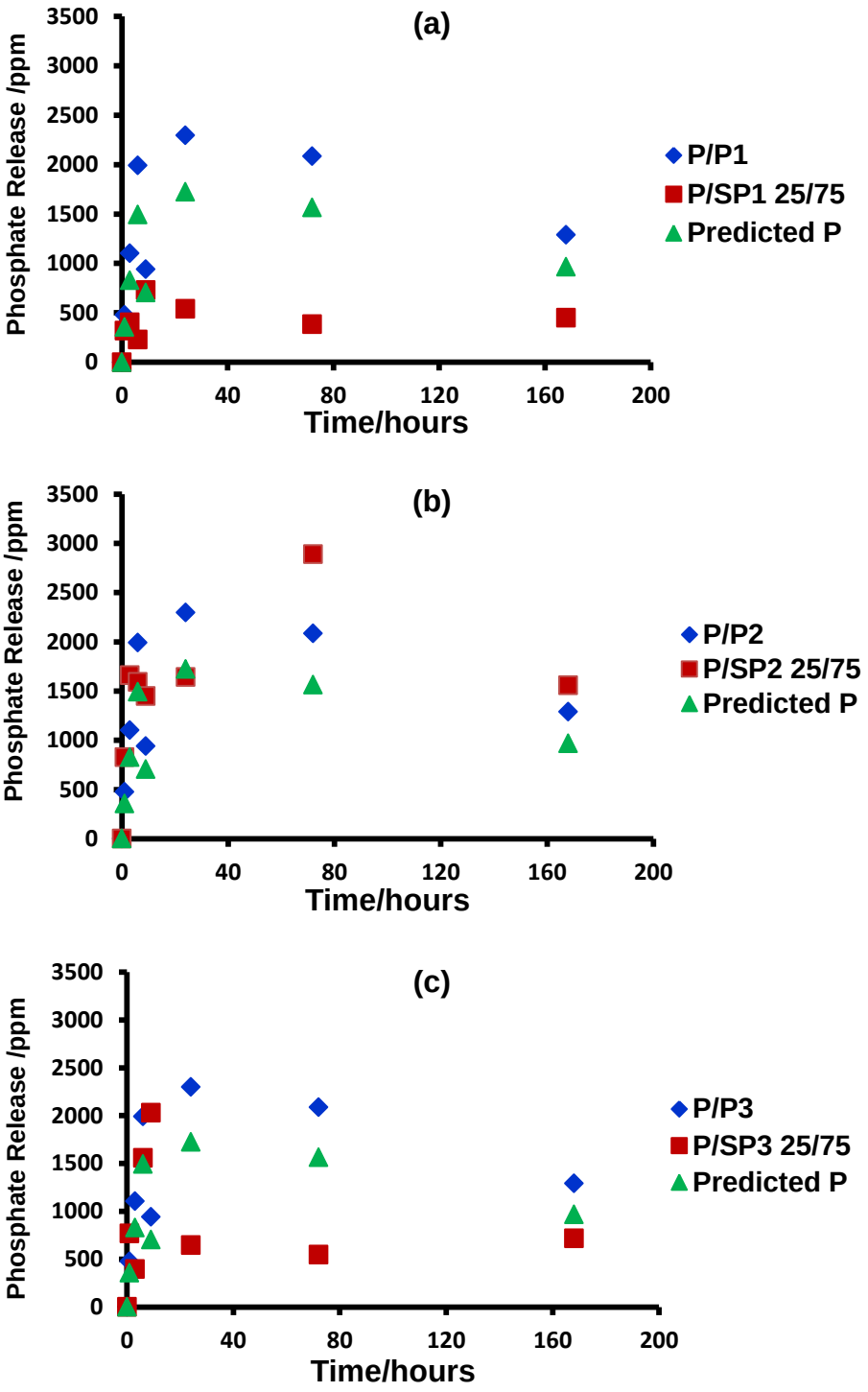

Figure 4.19 The phosphorus concentrations in ppm in Tris buffer solution plotted as a function of time for the experimental glass mixtures with a 25/75 ratio together with the predicted phosphorus release from each individual phosphate glass based on the ratio 25/75 and phosphorus release from each studied individual phosphate glass: (a) P from P1 & SP1; (b) P from P2 & SP2 and (c) P from P3 & SP3.

Figure 4.19 (a), (b) and (c) represents the release of phosphate ion in Tris buffer solution at different time points with respect to the 25/75 ratio for the three glass mixtures SP1, SP2 and SP3 respectively. Thereby, (a) represents the phosphorus coming from the individual phosphate glass (P1) in Tris buffer in addition to the phosphorus release in Tris of 25/75 SP1 mixture as well as the predicted phosphorus release from the P1 based on the 25/75 ratio. Likewise, (b) represents the phosphorus emerging from the individual phosphate glass (P2) in Tris buffer in addition to the phosphorus release in Tris of 25/75 SP2 mixture as well as the predicted phosphorus release from the P2 based on the 25/75 ratio. Thus, (c) represents the phosphorus release from the individual phosphate glass (P3) in Tris buffer in addition to the phosphorus release in Tris from 25/75 SP3 mixture as well as the predicted phosphorus release from the P3 based on the 25/75 ratio.

Generally, as can be observed from the Figure 4.19 (a), (b) and (c), the phosphorus release from the experimental data of SP2 25/75 follows closely the predicted patterns. The trend of the experimental phosphorus release from SP3 25/75 follows the pattern of the predicted values up to the initial 9 hours of immersion and afterwards it starts deviating strongly from the predicted phosphorus release. The experimental values of the phosphorus release from SP1 25/75 follow the predicted profile only up to 3 hours before the phosphorus concentration in solution significantly drops.

The highest level of phosphorus release in Tris buffer (measured in ppm) at the initial time points was observed in the glass mixture SP3 25/75. Followed by the lower phosphorus release associated with the glass mixture SP2 25/75, whilst the minimal phosphorus release was from the glass mixture SP1 25/75.

A dramatic drop in phosphorus concentration was seen in SP3 25/75 at 9 hours immersion results from precipitation of phosphate into the solid phase. The ^{31}P

MAS-NMR spectra in Figure 4.16 (c) reveal the emergence of a peak at around 3 ppm after 6 hours immersion in Tris. This peak corresponds to the Q^0-orthophosphate phosphate speciation. Then, and specifically beyond 24 hours of experimental time in Tris, the measured concentration of phosphorus in solution seems to plateau during the residual time of the experiment. Thus, the data of phosphorus release in Figure 4.19 was in good agreement with the ^{31}P MAS-NMR spectra in Figure 4.16.

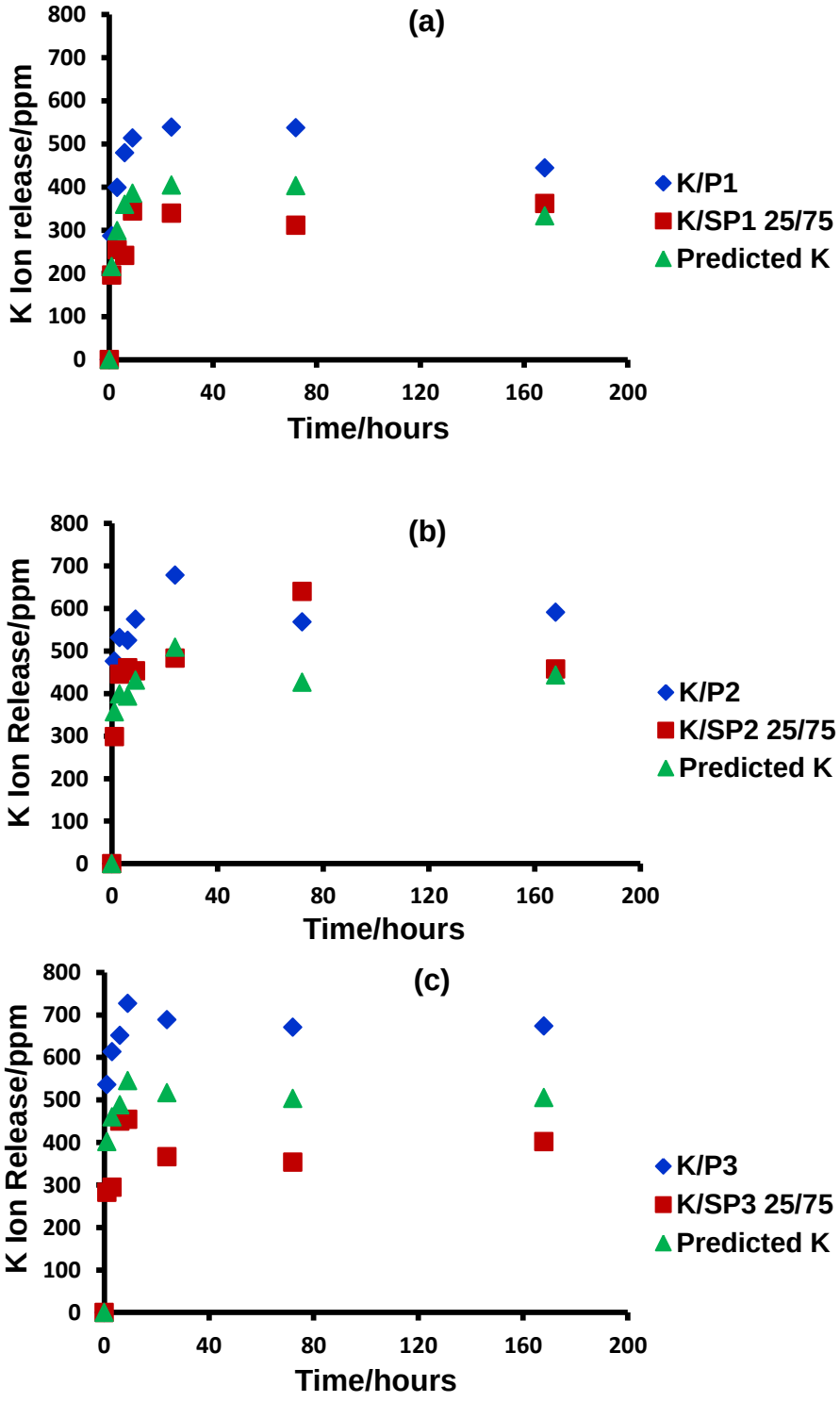

Figure 4.20 The potassium ion concentrations in ppm in Tris buffer solution plotted as a function of time for the experimental glass mixtures with a 25/75 ratio together with the predicted potassium ion release from each individual phosphate glass based on the ratio 25/75 and potassium ion release from each studied individual phosphate glass: (a) K from P1 & SP1; (b) K from P2 & SP2 and (c) K from P3 & SP3.

Figure 4.20 (a), (b) and (c) exhibits the concentration of potassium ion measured in ppm as a function of dissolution time in Tris buffer solution for the 25/75 ratio for the three glass mixtures SP1, SP2 and SP3 respectively. Thereby, (a) demonstrates the potassium ion release from the individual phosphate glass (P1) after immersion in Tris buffer, the release of potassium ion in Tris buffer of 25/75 SP1 mixture as well as the predicted potassium ion release from the P1 depending on the 25/75 ratio. Similarly, (b) illustrates the potassium ion release from the individual phosphate glass (P2) in Tris buffer, the potassium ion release in Tris immersion of 25/75 SP2 mixture as well as the predicted potassium ion release from the P2 based on the 25/75 ratio. Figure 4.20 (c) represents the potassium ion release from the individual phosphate glass (P3) in Tris buffer in addition to the potassium ion release in Tris of 25/75 SP3 mixture as well as the predicted potassium ion release from the P3 based on the 25/75 ratio.

It can be seen from the Figure 4.20 (a), (b) and (c), that the potassium ion release from the experimental patterns of SP1, SP2 and SP3 with the ratio 25/75 follows the predicted behaviour at the early immersion up to 9 hours. At a longer immersion period, there was a deviation between the experimental potassium ion release and the predicted release.

The highest potassium ion release in Tris buffer was observed in glass mixtures SP1 and SP2 10/90, whilst the lowest potassium ion release emerged from the glass mixture SP3 10/90.

The amount of potassium ion release in Tris buffer for all glass mixtures SP1, SP2 and SP3 with the ratio 25/75 appeared to be similar at the initial time points of the experiment up to 9 hours. Followed by a moderate deviation between the experimental potassium release and the predicted ones over the residual time of the experiment.

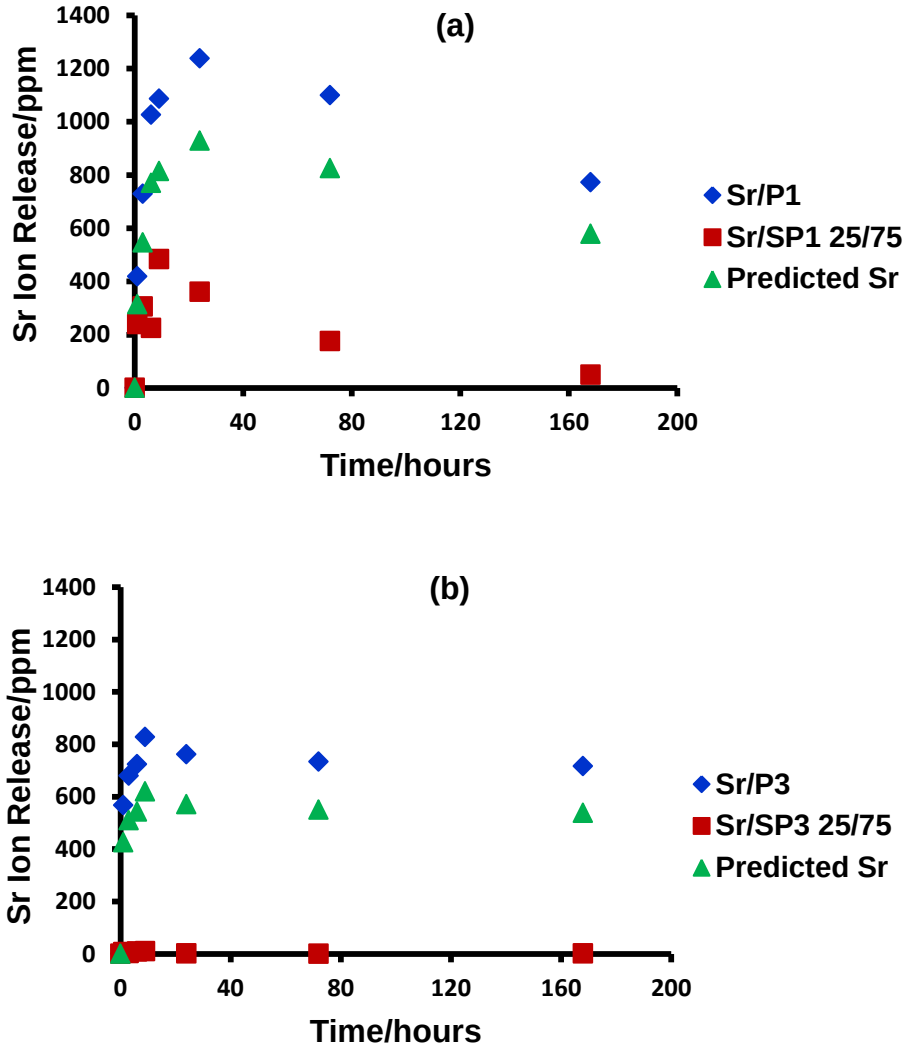

Figure 4.21 The strontium ion concentrations in ppm in Tris buffer solution plotted as a function of time for the experimental glass mixtures with a 25/75 ratio together with the predicted strontium ion release from each individual phosphate glass based on the ratio 25/75 and strontium ion release from each studied individual phosphate glass: (a) Sr from P1 & SP1 and (b) Sr from P3 & SP3.

As mentioned before, the glass mixture SP2 does not contain strontium in its composition, thus the Figure 4.21 (a) and (b) exhibits the concentration of strontium ion release measured in ppm as a function of dissolution time in Tris buffer solution regarding the 25/75 ratio for the glass mixtures SP1 and SP3 respectively.

Thus, Figure 4.21 (a) displays the strontium ion release from the individual phosphate glass P1 after immersion in Tris buffer, the release of strontium ion in Tris buffer of 25/75 SP1 mixture as well as the predicted strontium ion release from the P1 depending on the 25/75 ratio. Similarly, (b) illustrates the strontium ion release from the individual phosphate glass (P3) in Tris buffer, the strontium ion release in Tris immersion of 25/75 SP3 mixture as well as the predicted strontium ion release from the P3 based on the 25/75 ratio.

Figure 4.21 (a) and (b) revealed that both patterns of strontium ion release from the experimental data of SP1 and SP3 with the ratio 25/75 did not follow the predicted strontium release. The deviation between the experimental strontium ion release from SP3 25/75 and the predicted values was dramatic.

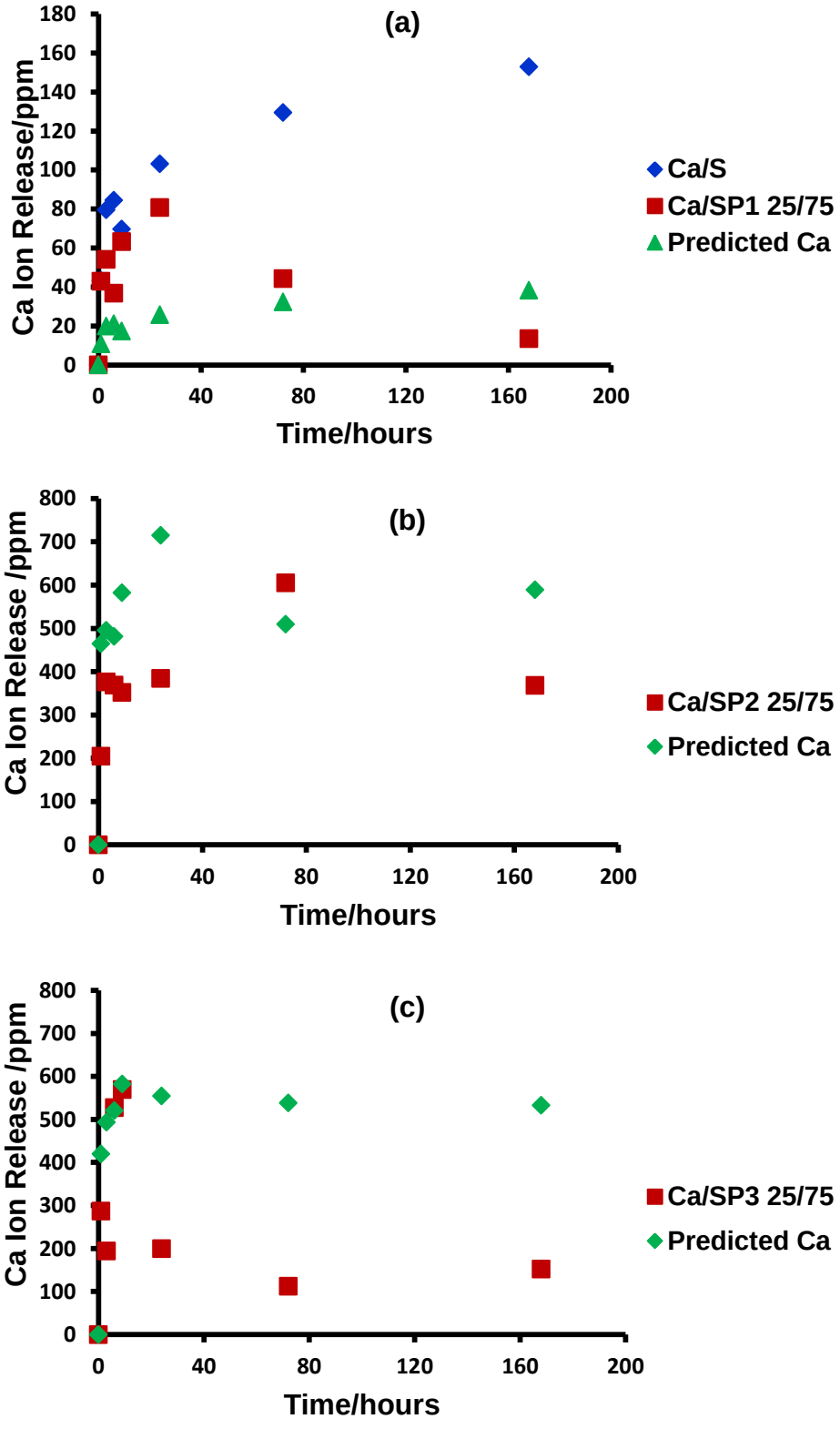

Figure 4.22 The calcium ion concentrations in ppm in Tris buffer solution plotted as a function of time for the experimental glass mixtures with a 25/75 ratio together with the predicted calcium ion release from individual silicate & phosphate glasses based on the ratio 25/75 and calcium ion release from individual silicate glass: (a) Ca from S & SP1, (b) Ca from SP2 and (c) Ca from SP3.

Figure 4.22 (a), (b) and (c) exhibits the concentration of calcium ion measured in ppm as a function of dissolution time in Tris buffer solution with respect to the 25/75 ratio for the three glass mixtures SP1, SP2 and SP3 respectively.

It is of interest to note from the Figure 4.22 (a), (b) and (c), that the calcium ion release from the experimental data of SP1, SP2 and SP3 with the ratio 25/75 does not follow the predicted patterns. In SP3 there was a prominent difference between the experimental calcium ion release and its predicted values. The concentration of calcium ion release of glass mixture SP3 25/75 in Tris buffer increased over the initial time points of experimental work up to 9 hours, then the concentration decreased sharply at the longer immersion time and tended to be plateaued during the residual time of the experiment. This drop in concentration indicated the consumption of calcium into a solid phase via the precipitation. Therefore, the Q^0-orthophosphate species was detected at the peak position ≈ 3 ppm in the sample at the early 6 hours immersion through the ^{31}P MAS-NMR spectra in Figure 4.16 (c).

The calcium concentration in SP1 follows closely the concentration of calcium found on immersion of silicate glass alone, thereby showing much higher concentration values at the initial stages of immersion up to 24 hours compared to the predicted one (Figure 4.22(a)). The calcium ion release from SP2 with the ratio 25/75 does not exhibit such dramatic increase or abrupt drop during the initial time of experiment.

The reduction in calcium ion concentration as in Figure 4.22 (a) and (c) was in good agreement with the ^{31}P MAS-NMR spectra in Figure 4.16 (a) and (c) respectively, where the Q^0-orthophosphate species appeared at the peak position ≈ 3 ppm at the early 6 hours immersion in Tris buffer. Thus, the depletion of the measured concentration of calcium ion in solution can be accounted to the uptake of calcium ion from solution following by its precipitation as orthophosphate.

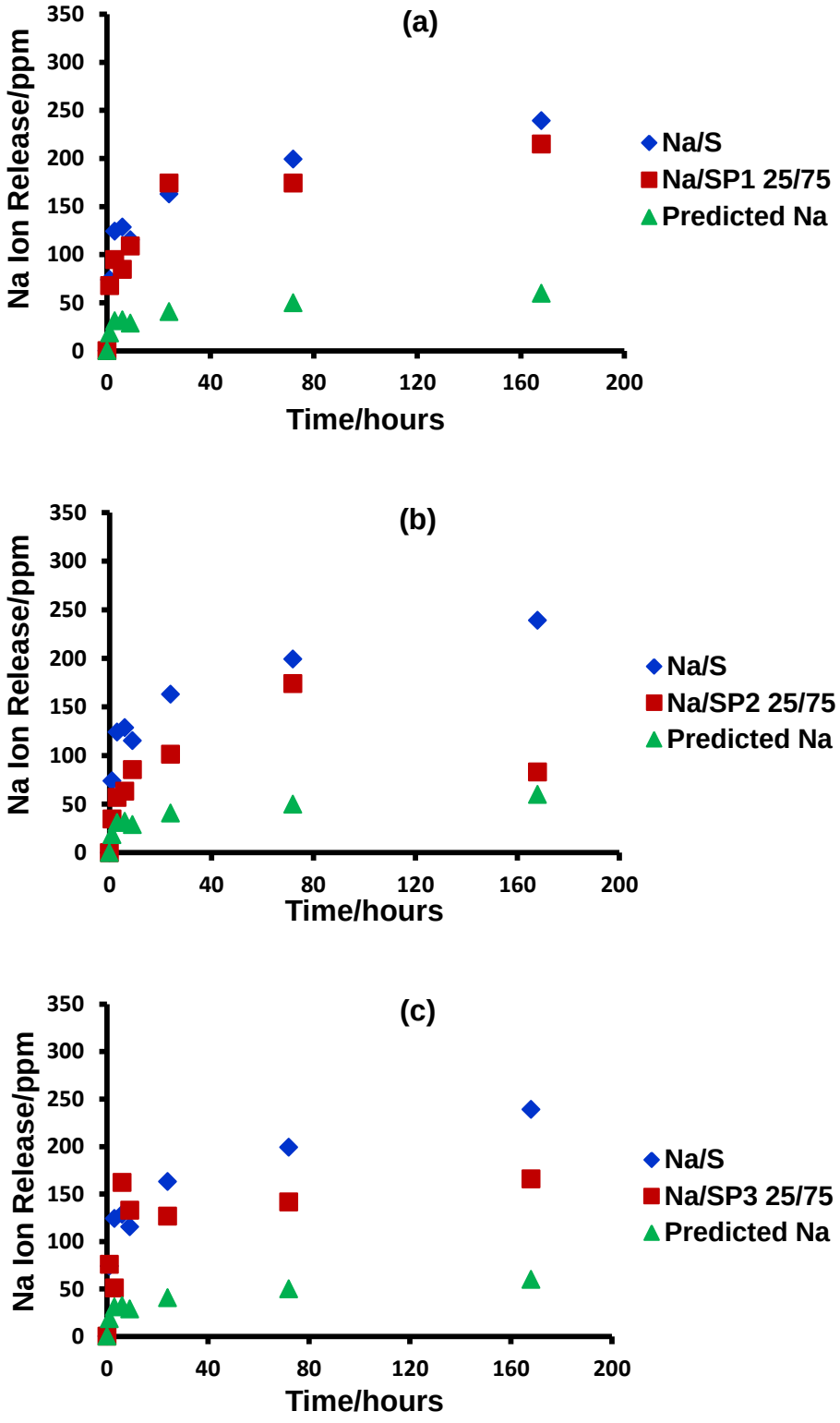

Figure 4.23 The sodium ion concentrations in ppm in Tris buffer solution plotted as a function of time for the experimental glass mixtures with a 25/75 ratio together with the predicted sodium ion release from individual silicate glass based on the ratio 25/75 and sodium ion release from studied individual silicate glass: (a) Na from S & SP1, (b) Na from S & SP2 and (c) Na from S & SP3.

Figure 4.23 (a), (b) and (c) presents the concentration of sodium ion measured in ppm as a function of dissolution time in Tris buffer solution regarding the 25/75 ratio for the three glass mixtures SP1, SP2 and SP3 respectively.

As can be seen from the Figure 4.23 (a), (b) and (c), that all the patterns of sodium ion release from the experimental data of SP1, SP2 and SP3 with the ratio 25/75 follow the release data measured on silicate glass immersion on its own rather than the predicted values for the mixtures.

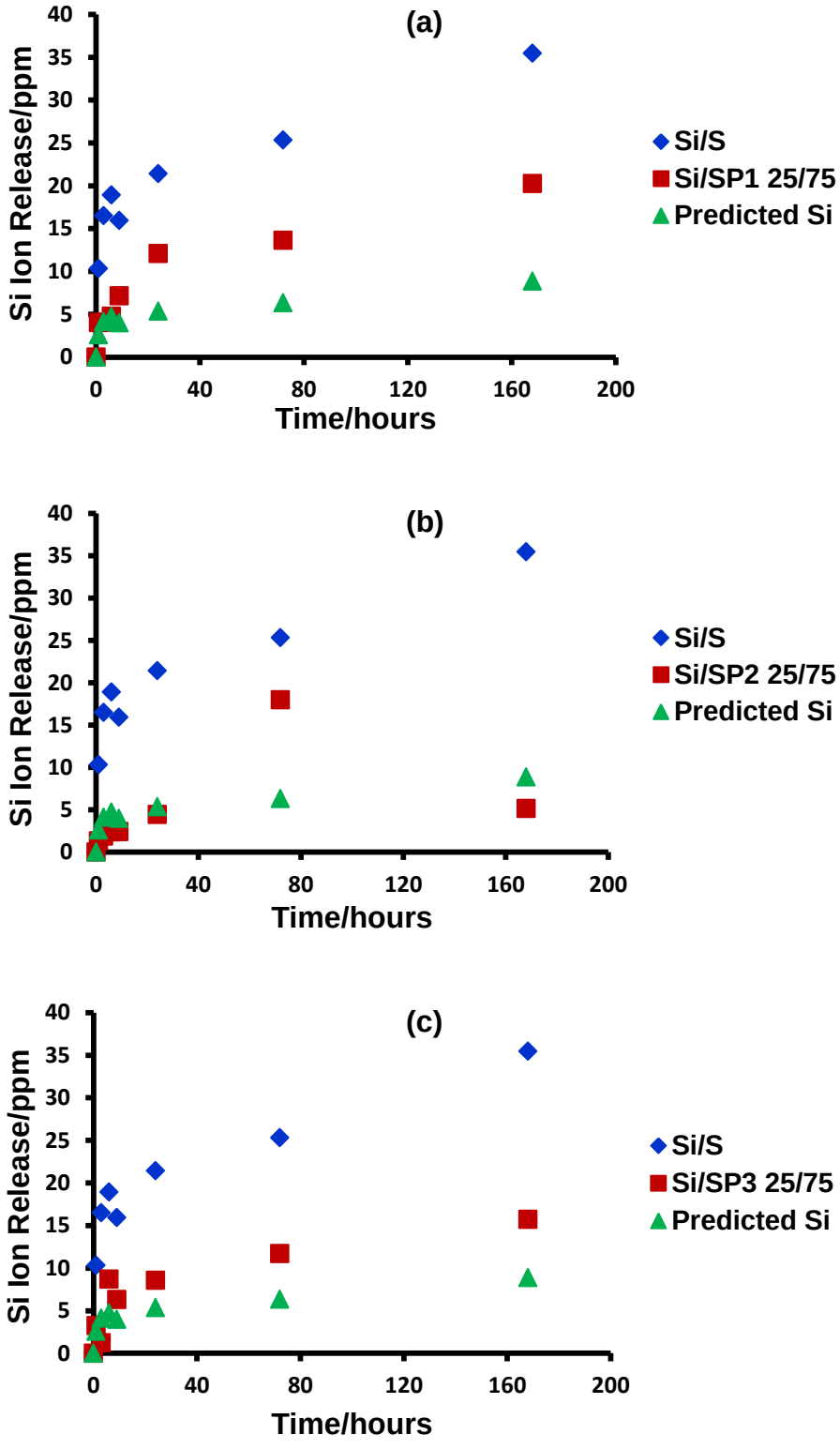

Figure 4.24 The silicon concentrations in ppm in Tris buffer solution plotted as a function of immersion time for the experimental glass mixtures with a 25/75 ratio together with the predicted silicon release from individual silicate glass based on the ratio 25/75 and silicon release from studied individual silicate glass: (a) Si from S & SP1, (b) Si from S & SP2 and (c) Si from S & SP3.

Figure 4.24 (a), (b) and (c) shows the concentration of silicon measured in ppm as a function of dissolution time in solution regarding the 25/75 ratio for the three glass mixtures SP1, SP2 and SP3 respectively.

The silicon concentration in solution of the SP2 mixture seems to be close to the predicted values. The other two mixtures show some deviations between the experimental and predicted values especially for the longer duration of immersion. The experimental values of concentration were higher than the predicted in SP3 and further above in SP1 mixture.

4.7 Glass Mixtures Characterisation with the Ratio 50/50 (Results and Discussion):

4.7.1 Solid State ^{31}P MAS-NMR Results:

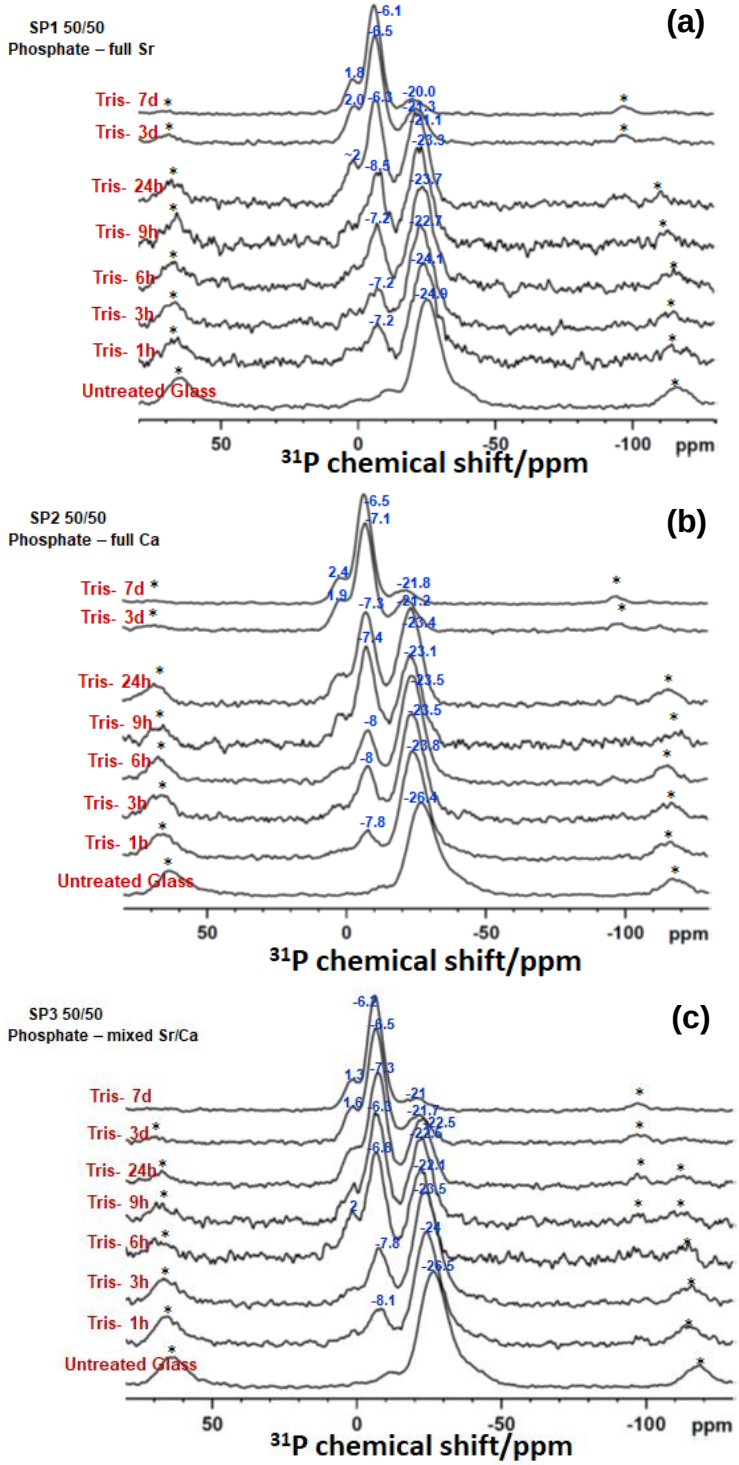

Figure 4.25 The ^{31}P MAS-NMR spectra (mas=22kHz) of studied glass mixtures with a 50/50 ratio before and after immersion in Tris buffer were plotted as a function of time for (a) SP1 mixture, (b) SP2 mixture and (c) SP3 mixture.

Figure 4.25 (a), (b) and (c) shows the ^{31}P MAS-NMR spectra of the experimental glass mixtures with the 50/50 ratio of SP1, SP2 and SP3 respectively before and after immersion in Tris buffer solution as a function of time up to 7 days. At the early immersion time, the dominant signal in the glass mixture SP1 50/50 spectra was at the position from -24.9 ppm to -20.0 ppm. This is the chemical shift range of Q^2-metaphosphate species (Kirkpatrick and Brow, 1995, MacKenzie and Smith, 2002). Similarly, the signal at the position from -26.4 ppm to -21.2 ppm in the mixture SP2 50/50 spectra and at the position from -26.5 ppm to -21 ppm in the mixture SP3 50/50 spectra corresponds to the Q^2-metaphosphate speciation.

In addition, ^{31}P MAS-NMR spectra show signal at the position from -8.5 ppm to -6.1 ppm in glass mixture SP1 50/50, from -8 ppm to -6.5 ppm in the SP2 50/50 mixture and from -8.1 ppm to -6.2 ppm in the SP3 50/50 mixture. All these are assigned to the Q^1-phosphate (Kirkpatrick and Brow, 1995, MacKenzie and Smith, 2002).

The minor ^{31}P signal at around 2ppm was detected in the spectra of all three glass mixtures. This is assigned to the Q^0-orthophosphate species (Kirkpatrick and Brow, 1995, MacKenzie and Smith, 2002), which are assumed resulting from precipitation from the solution phase. This species are seen in the spectra of the 24 hours sample of the SP1 50/50 and much earlier at 9 and 6 hours of the SP2 50/50 and SP3 50/50 mixtures.

4.7.2 Fourier Transform Infrared Spectroscopy (FTIR) Results:

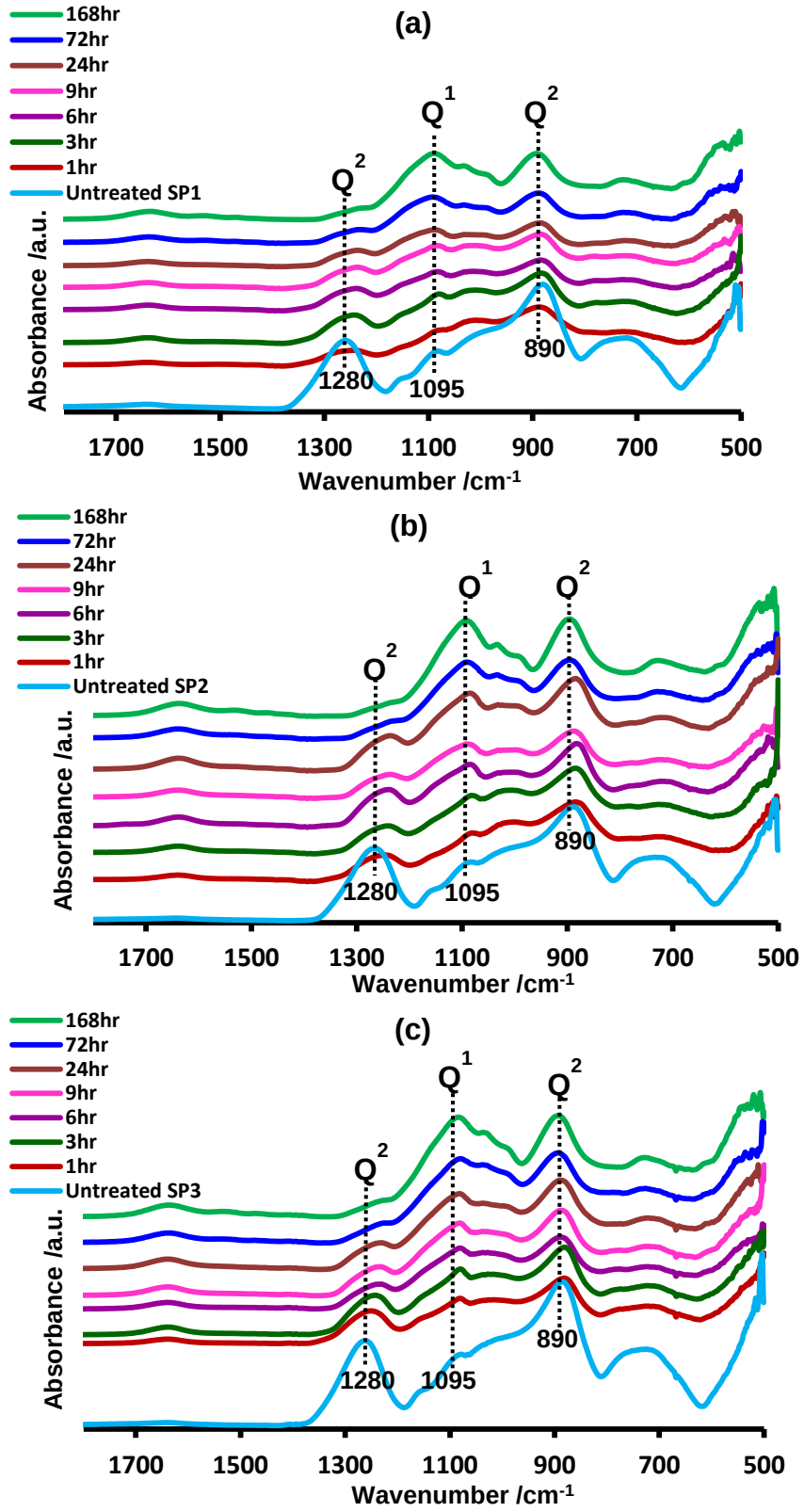

Figure 4.26 The FTIR spectra of studied glass mixtures with a 50/50 ratio before and after immersion in Tris buffer were plotted as a function of time for: (a) SP1 mixture, (b) SP2 mixture and (c) SP3 mixture.

Figure 4.26 shows the FTIR spectra of the three glass mixtures with the 50/50 ratio. Similar to the results on the 10/90 and 25/75 mixtures, three main bands were identified in the spectra. The band at approximately 1280 cm^{-1} is assigned to the Q^2-metaphosphate vibrational frequency (Moustafa and El-Egili, 1998, Ilieva et al., 2001, Patel et al., 2017). This feature gradually disappears with time. The absorption band at approximately 1095 cm^{-1} is assigned to the Q^1-pyrophosphate (Moustafa and El-Egili, 1998, Ilieva et al., 2001, Patel et al., 2017). This band emerges over the entire time of experiment. In other words, the phosphate in glass mixtures transforms gradually from Q^2 speciation to Q^1 speciation i.e. the Q^1 forms at the expense of Q^2 as a function of dissolution time. These FTIR results show that three 50/50 mixtures exhibit similar rate of degradation.

Thus, the FTIR spectra were consistent with the ^{31}P MAS-NMR spectra observations as described above.

4.7.3 pH Measurement Results:

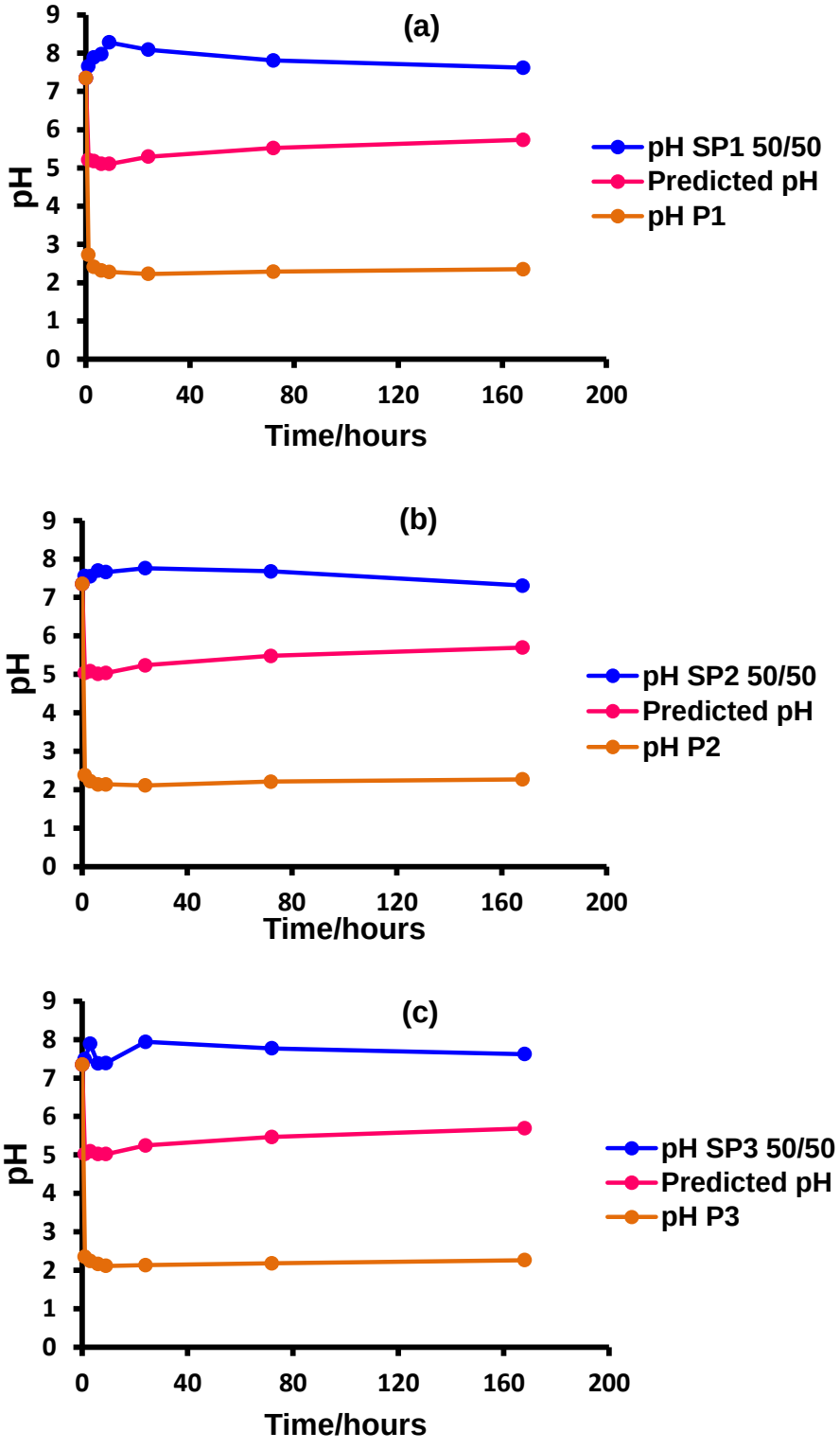

Figure 4.27 The pH behaviour in Tris buffer solution as a function of time of three experimental glass mixtures with a 50/50 ratio together with the predicted pH value from each glass mixture based on the ratio 50/50 and pH value of each studied individual phosphate glass: (a) pH of SP1 & P1; (b) pH of SP2 & P2 and (c) pH of SP3 & P3.

Figure 4.27 (a), (b) and (c) respectively demonstrates the pH change of the experimental glass mixtures SP1, SP2 and SP3 with the specific ratio 50/50 as a function of immersion time in Tris buffer together with their expected pH values which were calculated from the pH of the individual phosphate glasses P1, P2 and P3 in Tris buffer solution over the entire time of experiment.

As a general trend, the pH in solution appeared to remain around neutral and/or basic after immersion of all the glass mixtures SP1 50/50, SP2 50/50 and SP3 50/50 in Tris buffer as shown in Figure 4.27 (a), (b) and (c) respectively.

4.7.4 Ion Release Results:

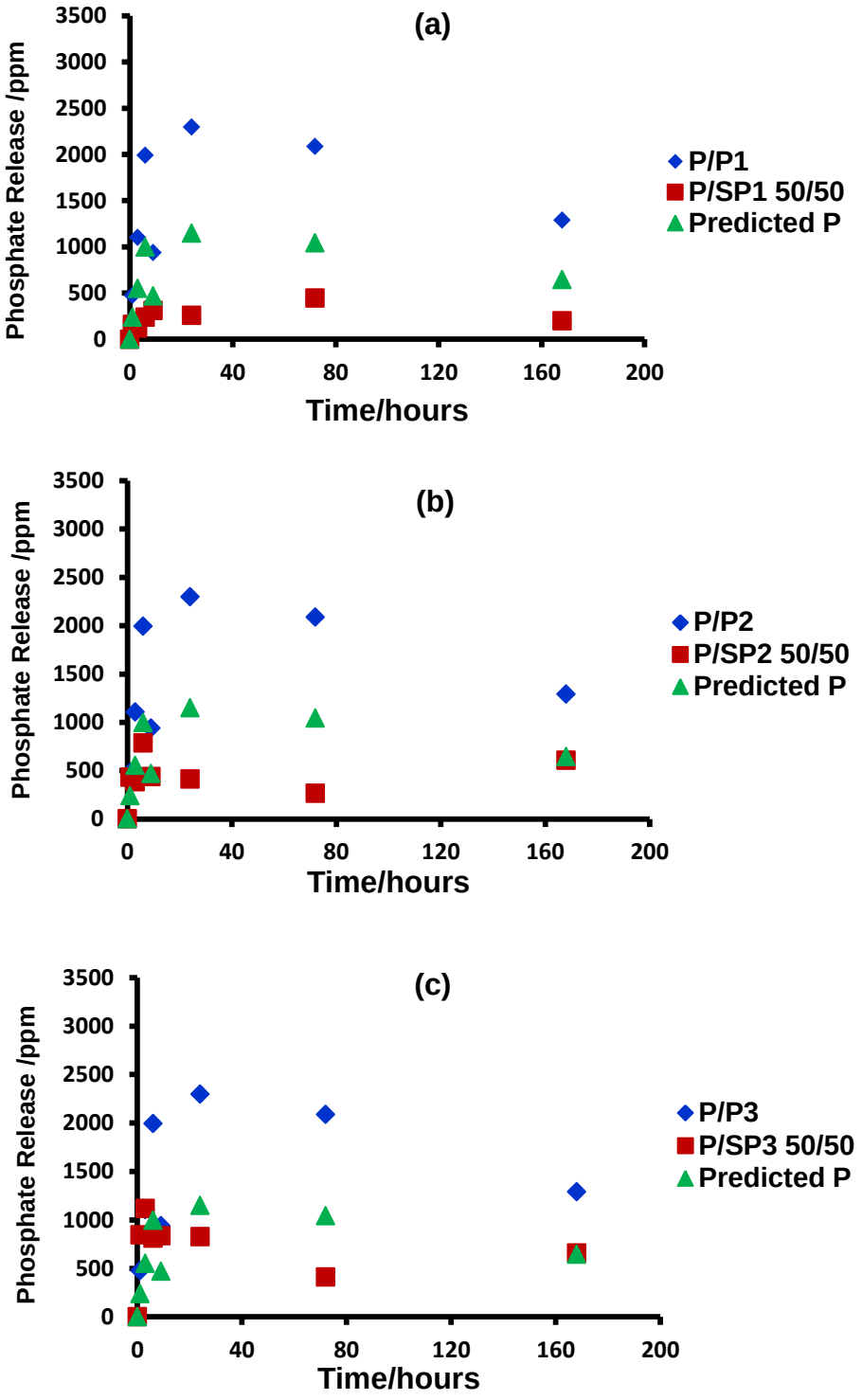

Figure 4.28 The phosphorus concentrations in ppm in Tris buffer solution plotted as a function of time for the experimental glass mixtures with a 50/50 ratio together with the predicted phosphorus release from each individual phosphate glass based on the ratio 50/50 and phosphorus release from each studied individual phosphate glass: (a) P from P1 & SP1; (b) P from P2 & SP2 and (c) P from P3 & SP3.

Figure 4.28 (a), (b) and (c) illustrates the concentration of phosphorus measured in ppm as a function of dissolution time in Tris buffer solution for the three glass mixtures SP1, SP2 and SP3 with 50/50 ratio respectively.

It can be seen from the Figure that the phosphorus release from the SP2 and SP3 50/50 follows the predicted data at initial time points up to 9 hours, then the experimental data starts deviating from the predicted values. In SP1 50/50 the experimentally obtained phosphorus release does not follow the predicted patterns and remains lower than the predicted values.

The observed deviations between the experimental phosphorus release and the predicted ones in all 50/50 mixtures was likely to be related to the precipitation of Q^0-orthophosphate species as demonstrated in Figure 4.25 (a), (b) and (c).

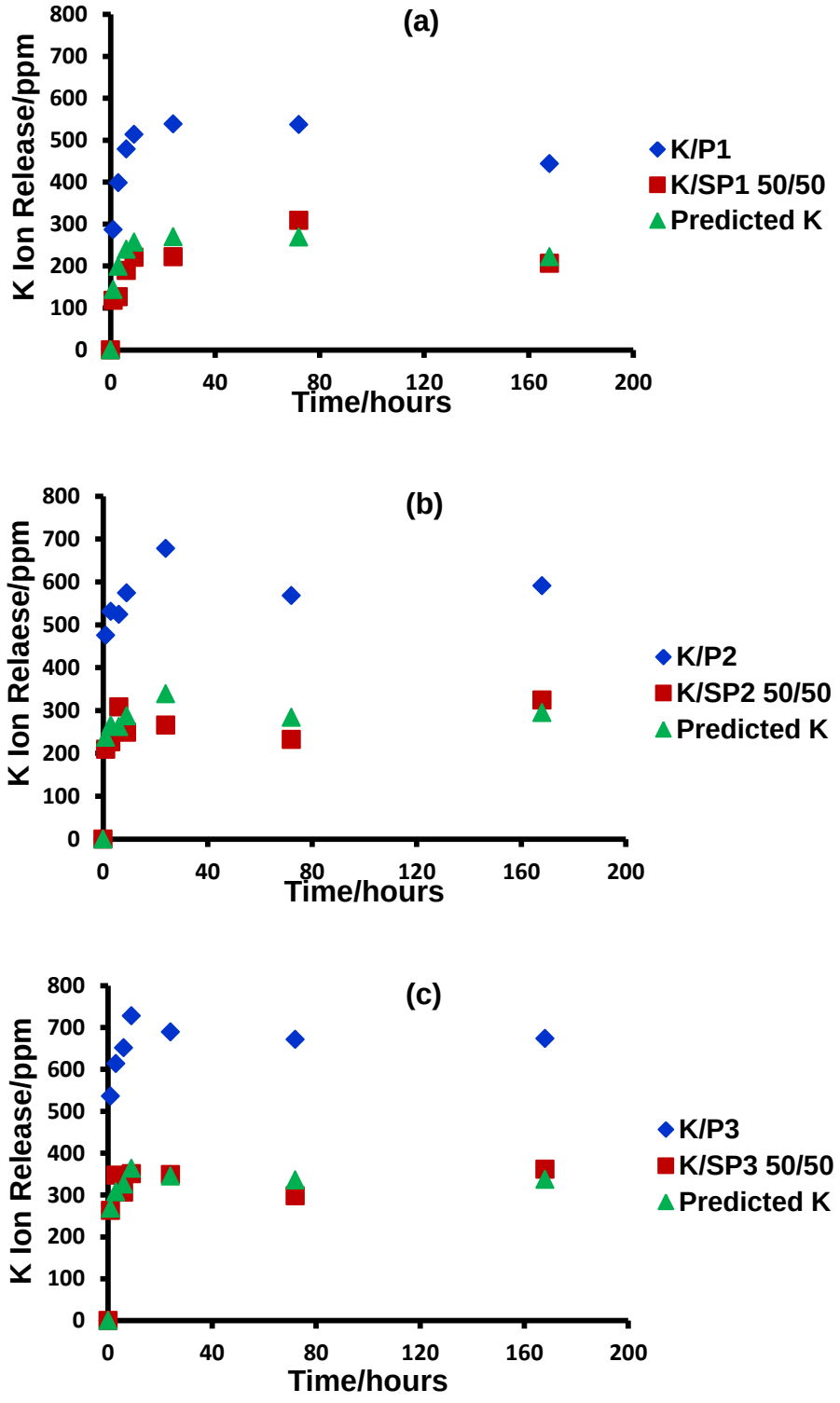

Figure 4.29 The potassium ion concentrations in ppm in Tris buffer solution plotted as a function of time for the experimental glass mixtures with a 50/50 ratio together with the predicted potassium ion release from each individual phosphate glass based on the ratio 50/50 and potassium ion release from each studied individual phosphate glass: (a) K from P1 & SP1; (b) K from P2 & SP2 and (c) K from P3 & SP3.

Figure 4.29 (a), (b) and (c) displays the level of potassium ion release measured in ppm as a function of dissolution time in Tris buffer solution for the three glass mixtures SP1, SP2 and SP3 all with the 50/50 ratio respectively.

The experimental concentration patterns show that the potassium ion release follows closely the predicted behaviour over the entire time of the experiment. The result for all three mixtures was very similar over the duration of the experiment.

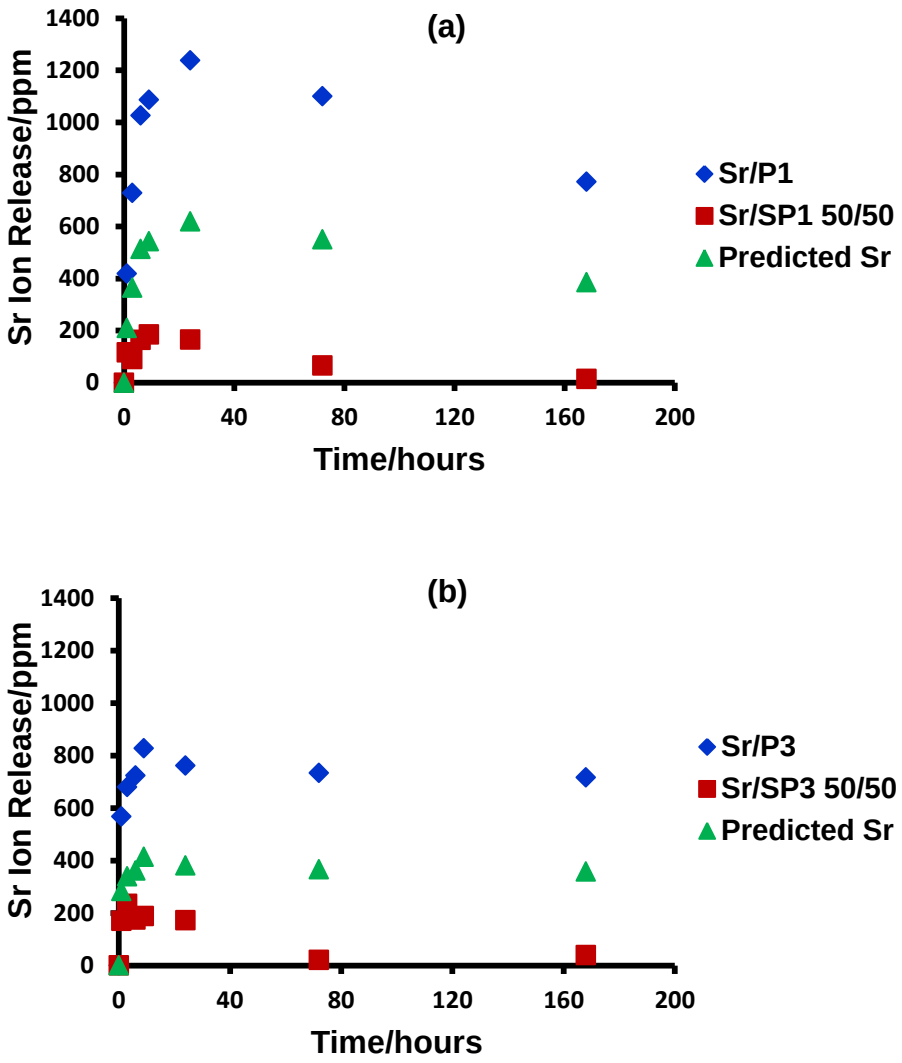

Figure 4.30 The strontium ion concentrations in ppm in Tris buffer solution plotted as a function of time for the experimental glass mixtures with a 50/50 ratio together with the predicted strontium ion release from each individual phosphate glass based on the ratio 50/50 and strontium ion release from each studied individual phosphate glass: (a) Sr from P1 & SP1 and (b) Sr from P3 & SP3.

Figure 4.30 (a) displays the strontium ion release from the individual phosphate glass P1 after immersion in Tris buffer, the release of strontium ion in Tris buffer of SP1 50/50 mixture as well as the predicted strontium ion release from the P1. Similarly, (b) illustrates the strontium ion release from the individual phosphate glass

(P3) in Tris buffer, the strontium ion release in Tris immersion of 50/50 SP3 mixture as well as the predicted strontium ion release from the P3.

As can be observed from Figure 4.30 (a) and (b) that the experimental data of strontium ion release from SP1 and SP3 with the ratio 50/50 did not follow the pattern of the predicted strontium released. The experimentally measured strontium concentrations remained lower and almost identical despite the fact that the P3 glass contained only 33% of the strontium of the P1 glass.

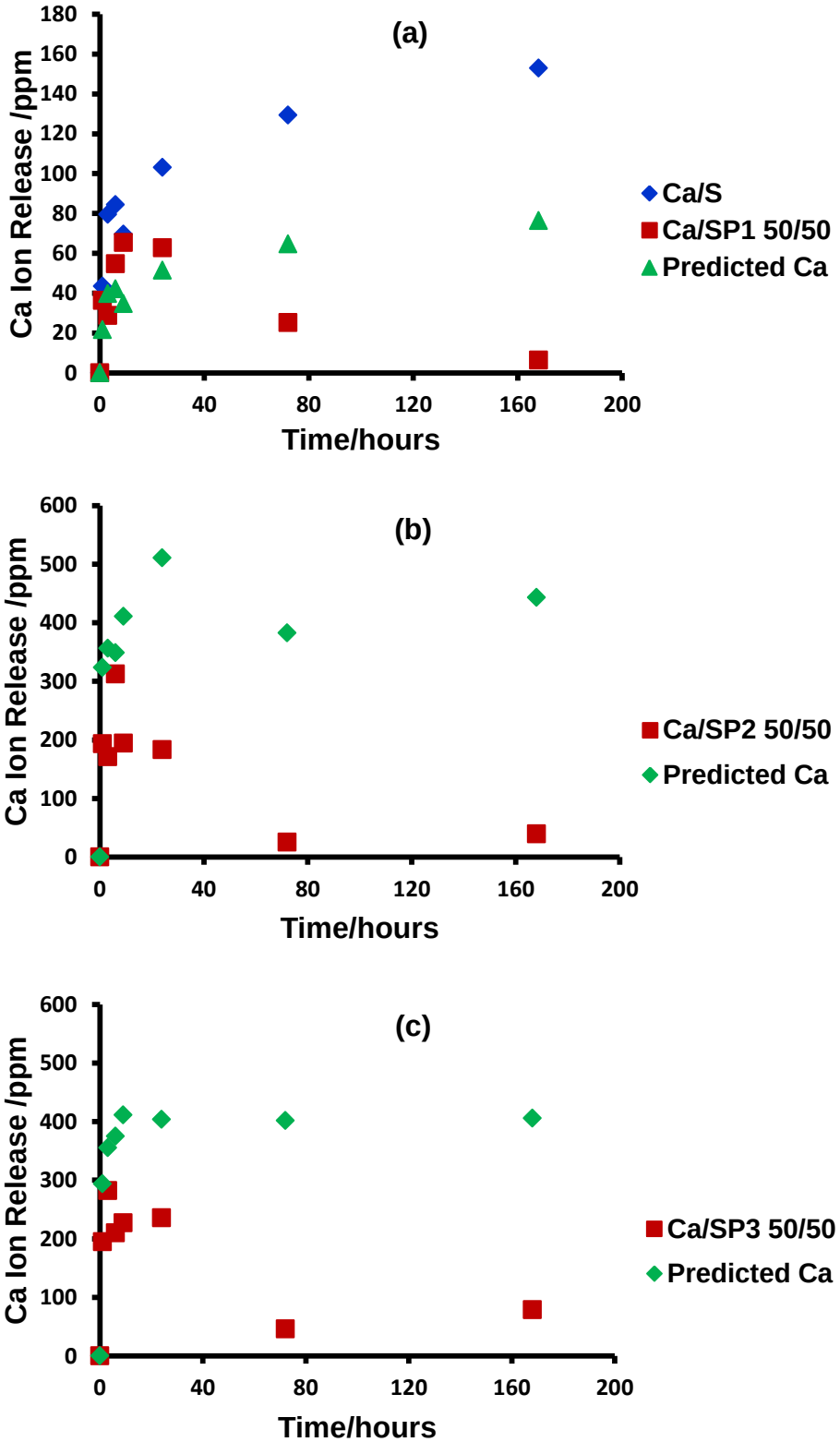

Figure 4.31 The calcium ion concentrations in ppm in Tris buffer solution plotted as a function of time for the experimental glass mixtures with a 50/50 ratio together with the predicted calcium ion release from individual silicate & phosphate glasses based on the ratio 50/50 and calcium ion release from individual silicate glass: (a) Ca from S & SP1, (b) Ca from SP2 and (c) Ca from SP3.

Figure 4.31 (a), (b) and (c) displays the concentration of calcium ion measured in ppm as a function of dissolution time in Tris buffer of the glass mixtures SP1, SP2 and SP3 with the 50/50 ratio respectively.

As demonstrated above in Figure 4.31 (a), (b) and (c), the highest concentration of calcium ion release was associated with glass mixtures SP2 and SP3, where the pattern of calcium ion release from both mixtures appeared to be very similar. Whereas, the lowest calcium concentration in solution was observed in the SP1. The experimental calcium release from SP1 50/50 follows the predicted pattern only up to 24 hours of the immersion duration then the experimental calcium concentration drops substantially compared to the predicted values. There was a prominent difference between the experimental calcium concentration in the SP2 and SP3 and their predicted values. The experimental were lower than the predicted values although the initial points of the SP2 and SP3 up to 9 hours had higher values where upon the concentration dropped. Afterwards, the calcium concentration tended to plateau during the residual time of the experiment.

This reduction in calcium ion concentration was in good agreement with the ^{31}P MAS-NMR spectra in Figure 4.25 (a), (b) and (c), where the depletion of the measured concentration of calcium ion in solution was due to the uptake of calcium ion from solution to precipitate the Q^0-orthophosphate species.

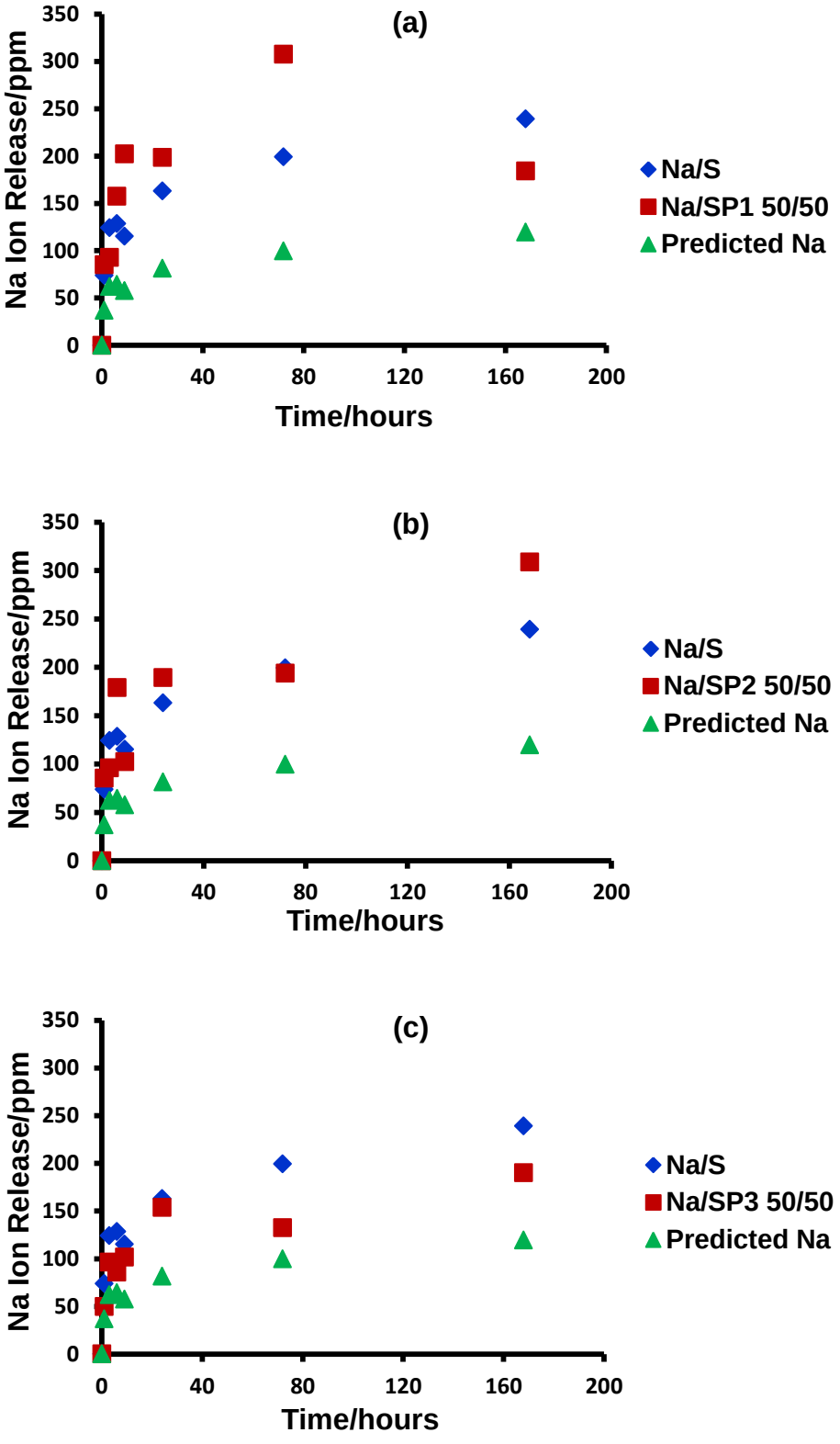

Figure 4.32 The sodium ion concentrations in ppm in Tris buffer solution plotted as a function of time for the experimental glass mixtures with a 50/50 ratio together with the predicted sodium ion release from individual silicate glass based on the ratio 50/50 and sodium ion release from studied individual silicate glass: (a) Na from S & SP1 and (b) Na from S & SP2 and (c) Na from S & SP3.

Figure 4.32 (a), (b) and (c) presents the concentration of sodium ion measured in ppm as a function of dissolution time in Tris buffer solution for the three glass mixtures SP1, SP2 and SP3 with the 50/50 ratio respectively.

As can be observed from the Figure 4.32 (a), (b) and (c), the patterns of experimental sodium release from all three glass mixtures SP1, SP2 and SP3 with the ratio 50/50 did not follow the predicted sodium release. The experimental concentration with the mixtures was higher and the values were closer to the values on silicate glass dissolution alone. There was little difference between the values for all three mixtures.

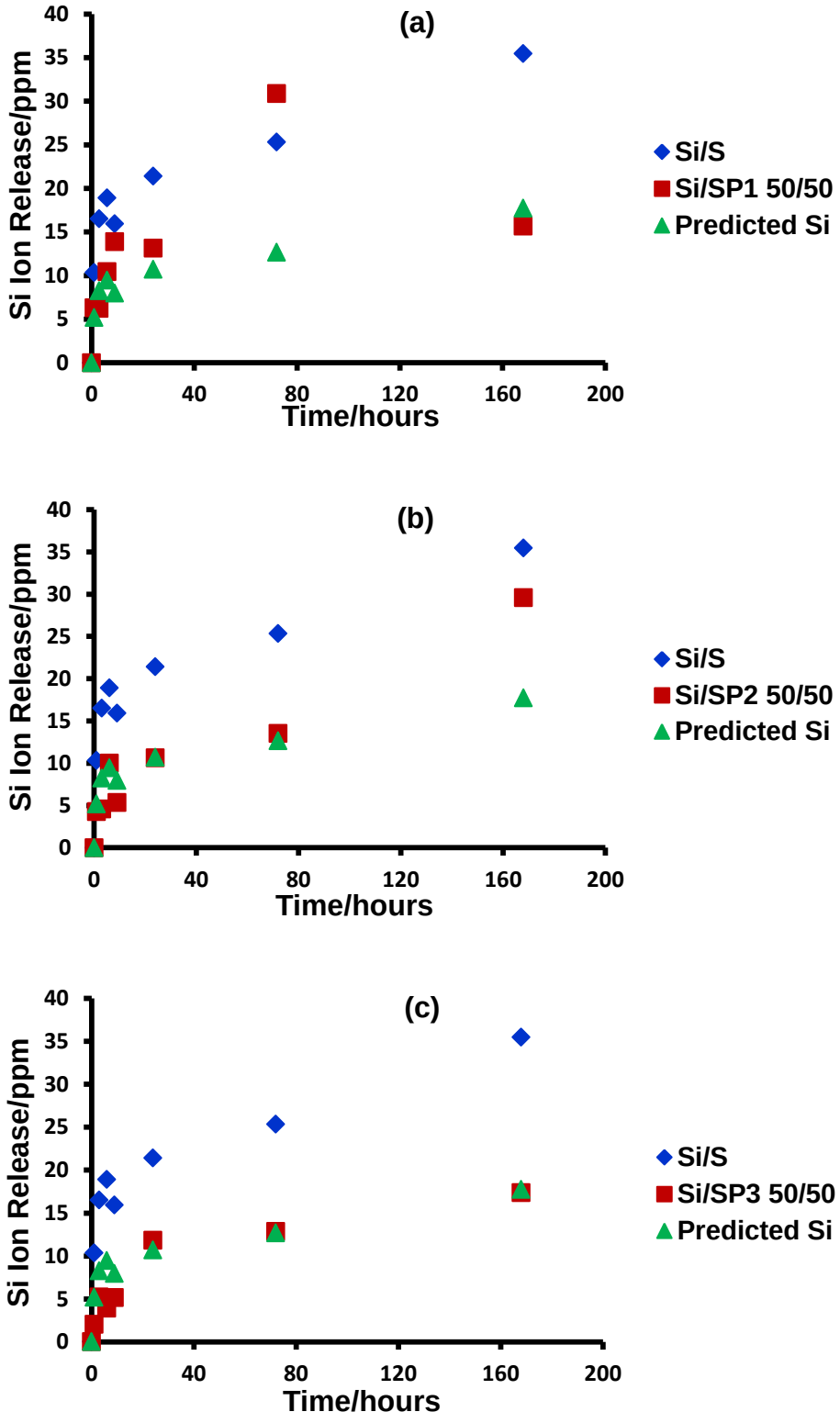

Figure 4.33 The silicon concentration in ppm in Tris buffer solution plotted as a function of immersion time for the experimental glass mixtures with a 50/50 ratio together with the predicted silicon release from individual silicate glass based on the ratio 50/50 and silicon release from studied individual silicate glass: (a) Si from S & SP1 and (b) Si from S & SP2 and (c) Si from S & SP3.

Figure 4.33 (a), (b) and (c) illustrates the concentration of silicon measured in ppm as a function of dissolution time in solution for the three glass mixtures SP1, SP2 and SP3 with the 50/50 ratio respectively.

As a general trend, it can be seen from the Figure 4.33 (a), (b) and (c) that the experimental values of the silicon concentration in three glass mixtures follows closely the predicted values without much difference between the mixtures.

4.8 Overall Discussion:

As an interesting comparison between the ratios 10/90 and 50/50 for all the glass mixtures SP1, SP2 and SP3, it can be concluded that all mixtures with the ratio 50/50 dissolve faster and quicker especially within the first 24 hours of immersion time than their equivalents with the ratio 10/90. The faster degradation of all glass mixtures with the ratio 50/50 than 10/90 was confirmed by the ^{31}P MAS-NMR spectroscopy as in Figure 4.7 (a), (b) and (c), as well as in Figure 4.25 (a), (b) and (c). In addition, this faster degradation was also confirmed by FTIR results as in Figure 4.8 (a), (b) and (c), as well as in Figure 4.26 (a), (b) and (c). Based on this, it can be concluded that the neutral and/or basic pH could be the key factor to accelerate the phosphate glass dissolution in the mixture. However, this conclusion is not in agreement with the published literature where it has been suggested that the phosphate glass dissolution was favoured by an acidic pH (Bunker et al., 1984, Gao et al., 2004, Ahmed et al., 2011).

The ^{31}P MAS-NMR both in Figure 4.16 (a), (b) and (c) and in Figure 4.25 (a), (b) and (c) reveal to some extent a similar glass degradation rate in the Tris buffer solution involving all glass mixtures SP1, SP2 and SP3 with respect to the ratio 25/75 and 50/50 respectively, despite the variation of appearance and intensity of the Q^0-orthophosphate species over the duration of the experiment.

No significant difference was detected through the ^{31}P MAS-NMR in the dissolution behaviour between mixture SP2 10/90 and mixture SP2 25/75, except for the earlier emergence of Q^1-phosphate species at 3 hours immersion time with the ratio 25/75 and later at 24 hours with the ratio 10/90.

It is worth mentioning that the SP3 glass contains two alkali earth cations calcium and strontium and might exhibit the mixed alkali earth effect. This could be revealed in the dissolution rate of the glass mixture and therefore should be taken into account. The experimental phosphorus and potassium follow their predicted patterns in the mixture SP2 10/90. In contrast, both experimental phosphorus and potassium deviate from their predicted values in the glass mixture SP3 10/90 (mixed alkali). The reason behind this ion release trend can be understood on the basis of the influence of the mixed alkali on the dissolution rate of the glass mixture. It is possible that this is attributed to the mixed alkali earth phenomenon reflecting the lowest glass degradation rate seen under acidic pH and highest degradation rate under slightly alkali condition of the 50/50 mixture.

There was a massive deviation between the experimental calcium ion release of SP1 10/90 and its predicted pattern, compared to the slight deviation between the experimental calcium ion release of SP1 50/50 and its predicted values. Taking into account that calcium ion in glass mixture SP1 emerges only from the silicate glass. The reason behind this variation could be attributed to the influence of acidic pH of SP1 10/90, which leads to the acceleration of the rate of silicate glass dissolution (Bingel et al., 2015) and subsequently producing much more ion release into the solution. This feature is advocated by the large percentage of calcium ion release from SP1 10/90 (acidic pH) within 24 hours immersion which is ≈ 30 % of calcium ion released into the solution as given in Table 4.2 compared to the small percentage of calcium ion release from SP1 50/50 (basic pH) within also 24 hours ≈ 5 % of calcium ion released into the solution. However, this reduction in the calcium concentration observed at later time points of immersion can be attributed to the Q^0 calcium phosphate species precipitation as observed in the ^{31}P MAS-NMR spectra.

Table 4.2 Percentage of calcium ion release from SP1 with both ratios 10/90 and 50/50 plotted as a function of time.

Time/hours	Ca% SP1 10/90	Ca% SP1 50:50
0	0	0
1	7	3
3	13	2
6	16	4
9	20	5
24	30	5
72	14	2
168	12	1

The higher level of sodium ion release in Tris buffer which was released from the glass mixture SP3 10/90 can be accounted to the higher acidic pH which was generated by glass mixture SP3 10/90 dissolution in Tris buffer (pH ≈ 2.75) as shown in Figure 4.9 (c). This could support the published observation that the higher acidic media, the higher accelerated silicate glass dissolution (Bingel et al., 2015). Therefore, it was expected to find such higher release of sodium ion in solution arising from the dissolution of the glass mixture SP3 10/90.

The amount of sodium ion release in solution was significantly correlated with the pH values because of the ion exchange process which in turn required a sodium ion to be replaced by a proton H^+ according to Hench's mechanism (Hench, 1991). Table 4.3 confirms that around 92% of sodium ion was released from SP3 10/90 into the solution due to the high acidic pH followed by 48% of sodium ion release from SP2 10/90 where the pH was little bit acidic (pH ≈ 2.89) and 37% of sodium ion release from SP1 10/90 (pH ≈ 4.59).

Table 4.3 Demonstrating the percentage of sodium ion release with 10/90 ratio from SP1, SP2 and SP3 at a corresponding immersion time. The sodium release values in percentage are calculated from the experimental values in ppm (plotted in 4.14) taken in relation to the total sodium content in silicate glass.

Time/hours	Na% SP1 10/90	Na% SP2 10/90	Na% SP3 10/90
0	0	0	0
1	13	17	28
3	18	31	35
6	24	38	36
9	28	42	30
24	41	47	81
72	37	48	93
168	35	42	89

It is clearly observed that the presence of both glasses had a certain effect on the dissolution of the other glass in the mixtures. Further studies will enable investigators to skilfully control the degradation level of both glasses in the mixture in order to achieve a desirable pH modulation and generate appropriate release of the therapeutic species stimulating bone formation.

To the best of our knowledge, this is the first systematic study undertaken on mixing phosphate and silicate glass. The only other published study on this glass mixture was completed by Novajra and his co-workers in 2015 (Novajra et al., 2015). The authors reported co-sintering of both the phosphate glass and silicate glass in order to produce three-dimensional porous scaffold. However, during the sintering process the two glasses silicate and phosphate were crystallised. In contrast, the two glasses which have been used in the present study did not sinter and crystallise. We have also designed mixture to be composed of the glass particles of different particle size. A large particle size 100-400 μm has been used for the

silicate glass and a fine one <38 μm for the phosphate glass as previously mentioned in the rationale of glass mixtures design (section 4.2) whereas Novajra and his group used fine particle size <32 μm for both glasses.

5 Novel Silicate/Phosphate Glass Mixtures Designed to Function Synergistically With Elevated ALP Enzyme Activity In Periodontal Bony Defects:

5.1 Introduction:

The biological marker ALP was used in periodontal research as an indicator for periodontal disease. It has been observed that the level of ALP in both saliva and gingival crevicular fluid (GCF) was directly proportional to the severity of periodontal disease (Bezerra Júnior et al., 2010). This enzyme is released from active osteoblast, salivary glands, polymorphonuclear leukocytes, and periodontal bacteria (Sanikop et al., 2012). Periodontopathic bacteria such as *P. gingivalis* and *P. intermedia* have been reported to have intense ALP activity (Shibata et al., 1994).

Chapter 4 demonstrated the breakdown of the Q^2 metaphosphate species in the phosphate glass to produce very small amount of the Q^0 orthophosphate species but with comparatively large amount of the Q^1 species. The Q^1 pyrophosphate species is well-known to inhibit bone mineralisation (Grover et al., 2013). Therefore, the application of glass mixtures in Chapter 4 is potentially undesirable for periodontal bone regeneration.

The question addressed in Chapter 5 is whether the elevated level of the ALP in GCF within periodontal bony defects can enzymatically hydrolyse the products of phosphate glass dissolution, e.g. the Q^1 phosphate species, to produce the Q^0 orthophosphate species, which are the mineral phase of natural bone, thereby to facilitate the apatite formation and ultimately bone formation.

Accordingly, the new concept in this Chapter is based on the creation of a unique smart material which functions in a synergistic way with the elevated ALP level within the periodontal bony defects. In order to achieve this objective, novel silicate

and phosphate glasses mixtures were developed to regulate the pH evolution in order to: (i) inhibit the alkaline periodontal bacterial growth of the virulent *P.gingivalis*, which is the main orchestrating bacteria in periodontal disease, (ii) create a neutral pH environment in the periodontal bony defects for osteoconductive bone regeneration and (iii) provide a controlled slightly acidic environment for the activity of ALP. The schematic diagram below (Figure 5.1) demonstrates the theoretical concept of the new glass mixtures degradation and the process of new bone formation by ALP enzyme activity:

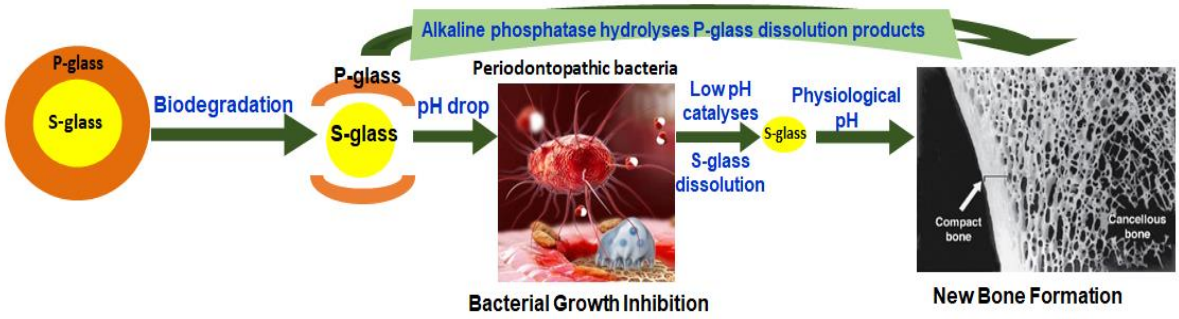

Figure 5.1 Schematic demonstration of the theoretical concept of the new glass mixtures degradation and the process of new bone formation by ALP activity.

5.2 Results and Discussion:

5.2.1 Solid State ^{31}P MAS-NMR Analysis:

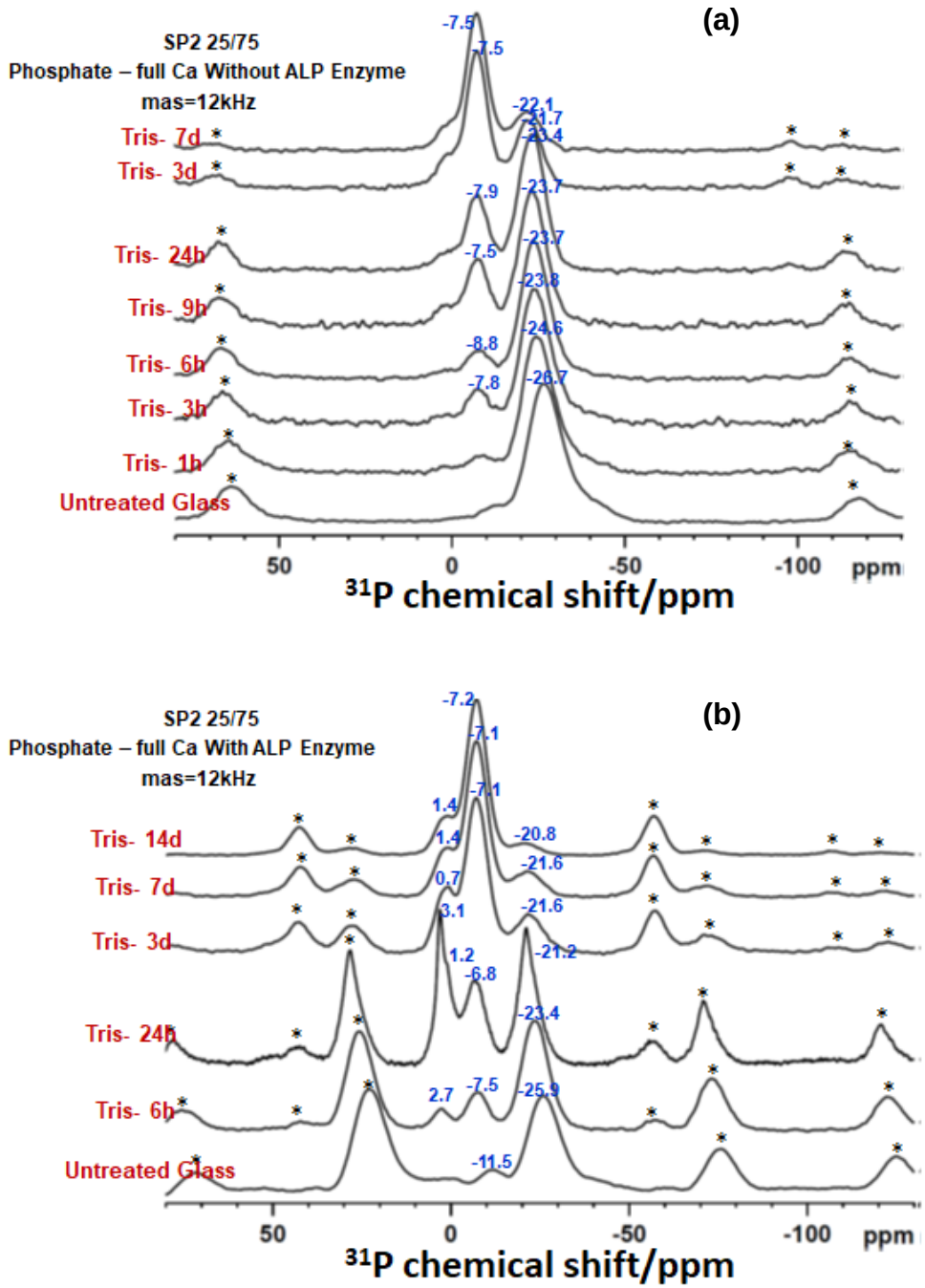

Figure 5.2 The ^{31}P MAS-NMR spectra of the studied glass mixture SP2 with a 25/75 ratio before (a) and after (b) treatment with the ALP enzyme plotted for the studied immersion time points. The numbers indicate the positions of the peaks in ppm. Asterisks show spinning side bands.

Figure 5.2 (a) and (b) illustrates the ^{31}P MAS-NMR spectra of the experimental glass mixture SP2 with the 25/75 ratio before and after treatment with the ALP respectively. The main signal at the early time point and in the untreated glass was observed at the position from -26.7 ppm to -20.8 ppm which corresponds to the chemical shift of the Q^2-metaphosphate species (Kirkpatrick and Brow, 1995, MacKenzie and Smith, 2002). As immersion progresses another signal becomes dominant in the spectra with the peak position between -11.5 ppm and -6.8 ppm. This corresponds to the Q^1-phosphate species (Kirkpatrick and Brow, 1995, MacKenzie and Smith, 2002). Another signal between 0 and 3 ppm was observed specifically in the spectra of the glasses immersed with ALP. This signal corresponds to the orthophosphate species (Kirkpatrick and Brow, 1995, MacKenzie and Smith, 2002). It was observed that the Q^0 signal appeared stronger in the spectra of the samples immersed with ALP rather than those immersed without the enzyme. The spectrum of the 24 hours sample with ALP showed the largest amount of the orthophosphate. Much sharper appearance of the signal indicated its high crystallinity compared to any other signal in the spectra.

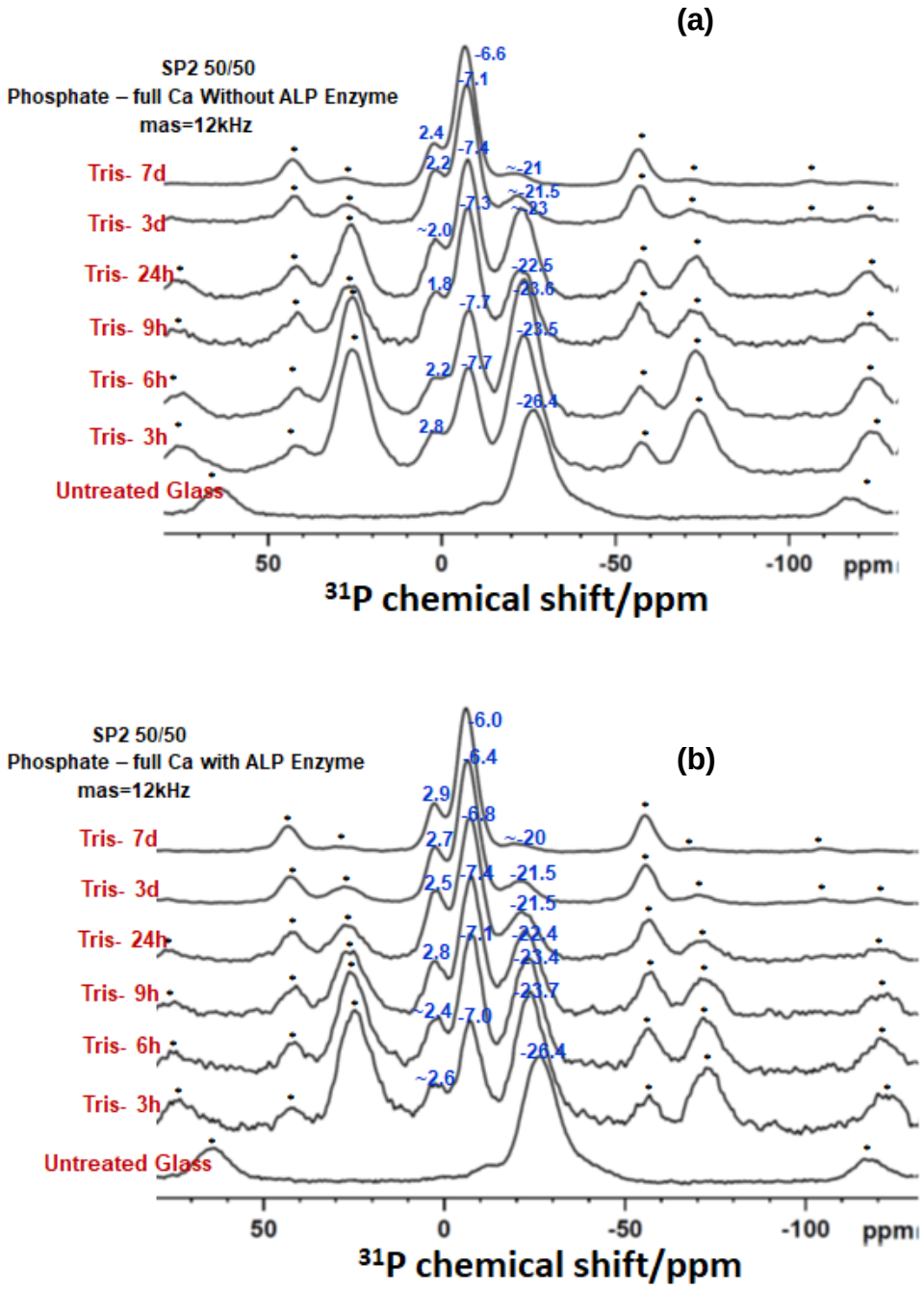

Figure 5.3 The ^{31}P MAS-NMR spectra of the studied glass mixture SP2 with a 50/50 ratio before (a) and after (b) treatment with the ALP enzyme plotted for the studied immersion time points. The numbers indicate positions of the peaks in ppm. Asterisks show spinning side bands; the spinning speed of 12 kHz was used for both (a) and (b).

Figure 5.3 (a) and (b) shows the ^{31}P MAS-NMR spectra of the solid material from the experimental glass mixture SP2 with the 50/50 ratio before and after ALP treatment as a function of time up to 7 days. The signal at the position between -

26.4 ppm to -20 ppm corresponds to the chemical shift of Q^2-metaphosphate species (Kirkpatrick and Brow, 1995, MacKenzie and Smith, 2002). The signal at the peak position between -7.7 and -6.0 ppm corresponds to the chemical shift of the Q^1-phosphate species (Kirkpatrick and Brow, 1995, MacKenzie and Smith, 2002). A minor signal around 2-3 ppm corresponds to the Q^0-orthophosphate species (Kirkpatrick and Brow, 1995, MacKenzie and Smith, 2002). It was observed in all the spectra but specifically it was the clearest in the 7 days of immersion ALP sample. Generally, the appearance of the Q^0 signal in the sample immersed with ALP was slightly sharper.

5.2.2 Solution State ^{31}P NMR Analysis:

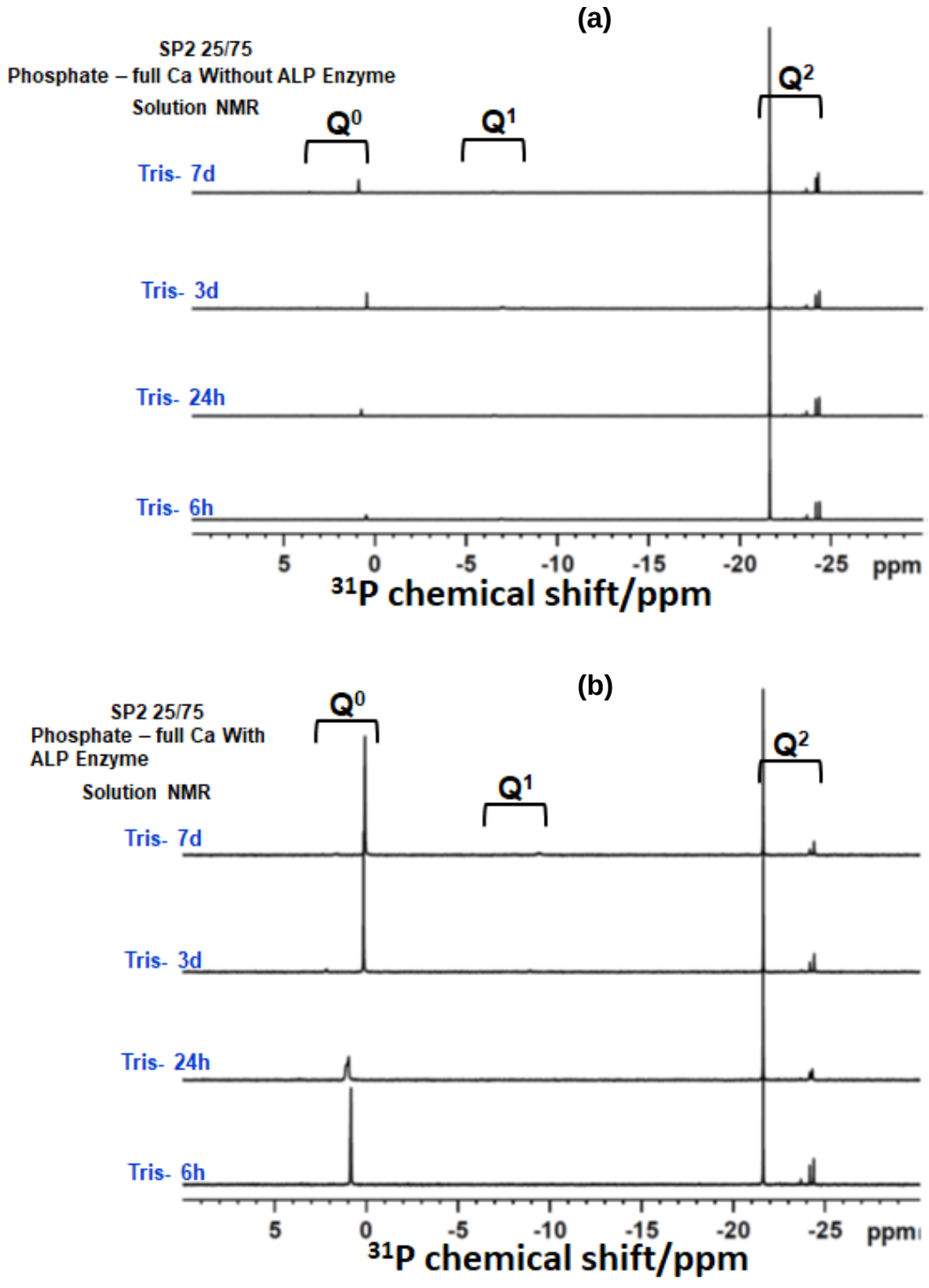

Figure 5.4 The ^{31}P Solution NMR spectra of the solution remained after immersion of the studied glass mixture SP2 with a 25/75 ratio (a) without ALP treatment and (b) with ALP treatment. Immersion time points are indicated next to the spectra.

Figure 5.4 (a) and (b) illustrates the ^{31}P solution NMR spectra of the solution remained after the immersion of the experimental glass mixtures SP2 with the ratio 25/75 without and with the ALP treatment plotted for the allocated time points respectively.

Three types of the signals were identified in the spectra. The signals with the chemical shift between -25.2 ppm and -21.7 ppm were assigned to the Q^2-metaphosphate species (Döhler et al., 2015). The signal between -9.8 ppm and -6.2 ppm was assigned to the Q^1-phosphate species (Döhler et al., 2015). Furthermore, the third signal with the position around 3ppm corresponds to the Q^0-orthophosphate species (Döhler et al., 2015).

Higher amounts of the Q^0-orthophosphate species were detected after treatment the glass mixture samples with ALP compared to the samples without ALP.

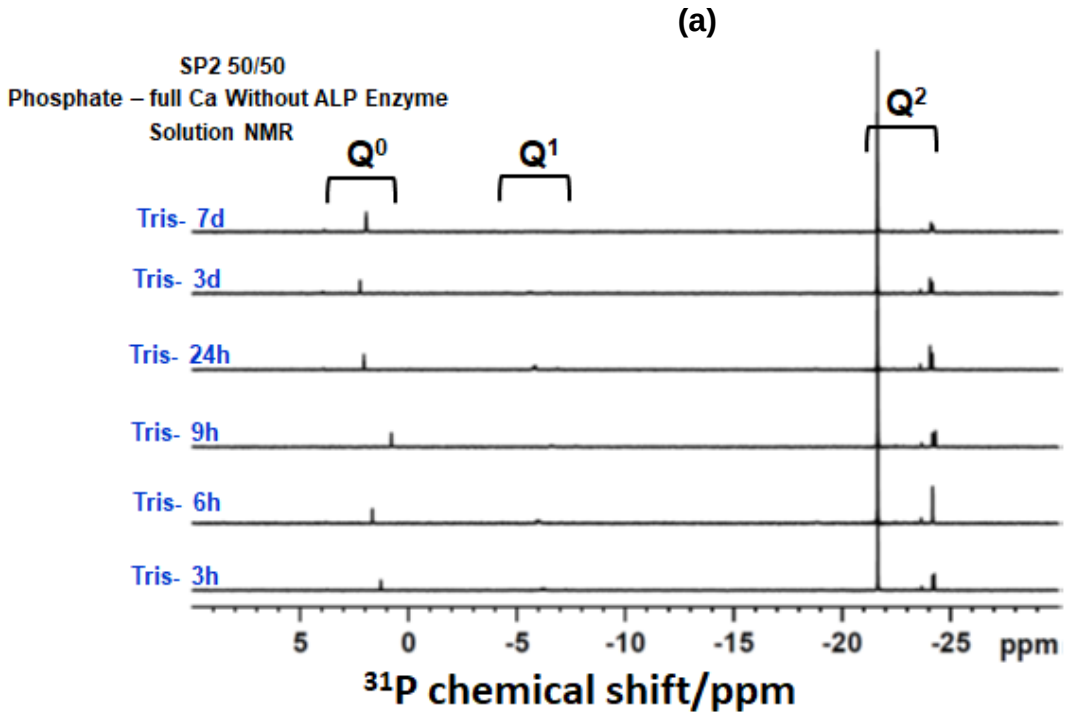

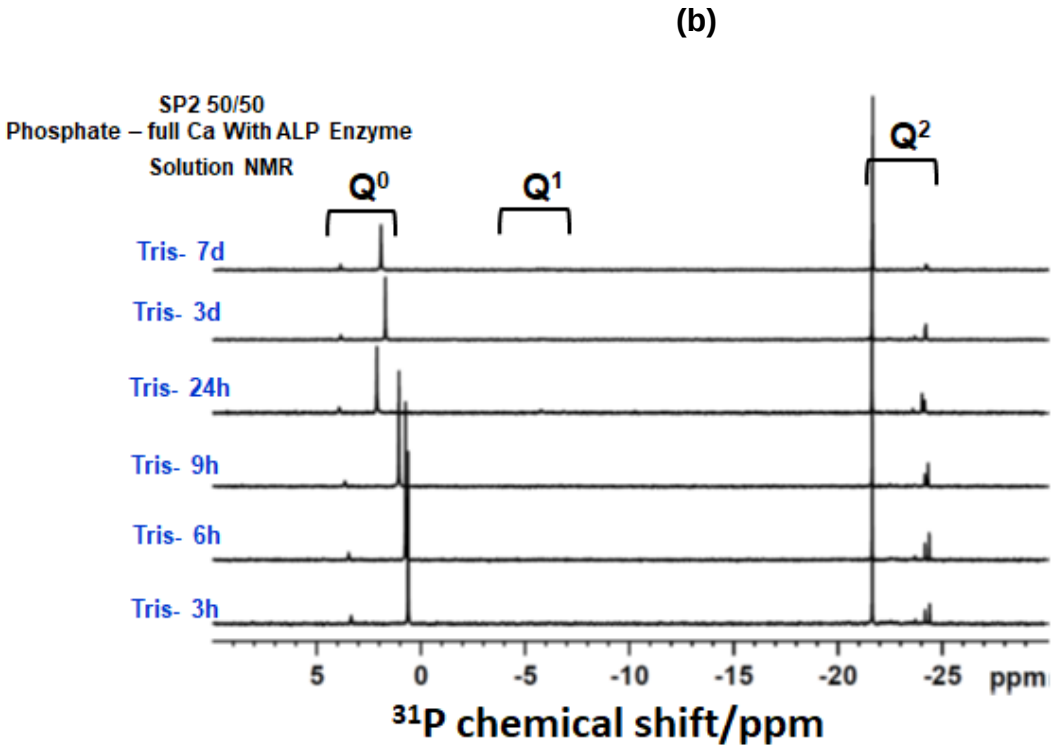

Figure 5.5 The ^{31}P Solution NMR spectra of the solution remained after immersion of the studied glass mixture SP2 with a 50/50 ratio (a) without ALP treatment and (b) with ALP treatment. Immersion time points are indicated next to the spectra.

Figure 5.5 (a) and (b) shows the ^{31}P solution NMR spectra of the experimental glass mixture SP2 with the 50/50 ratio with and without glass mixture treatment with the ALP respectively as a function of time up to 7 days. The chemical shift of the Q^2-metaphosphate species and the Q^1-phosphtate species in glass mixture SP2 50/50 appears similar to its equivalent in mixture SP2 25/75.

It can be observed according to the solution NMR spectra in Figure 5.5 (b) that higher amounts of the Q^0-orthophosphate species were produced after treatment SP2 50/50 with the ALP enzyme compared to the spectra with no enzyme.

5.2.3 The ^{31}P Solution NMR Integrals:

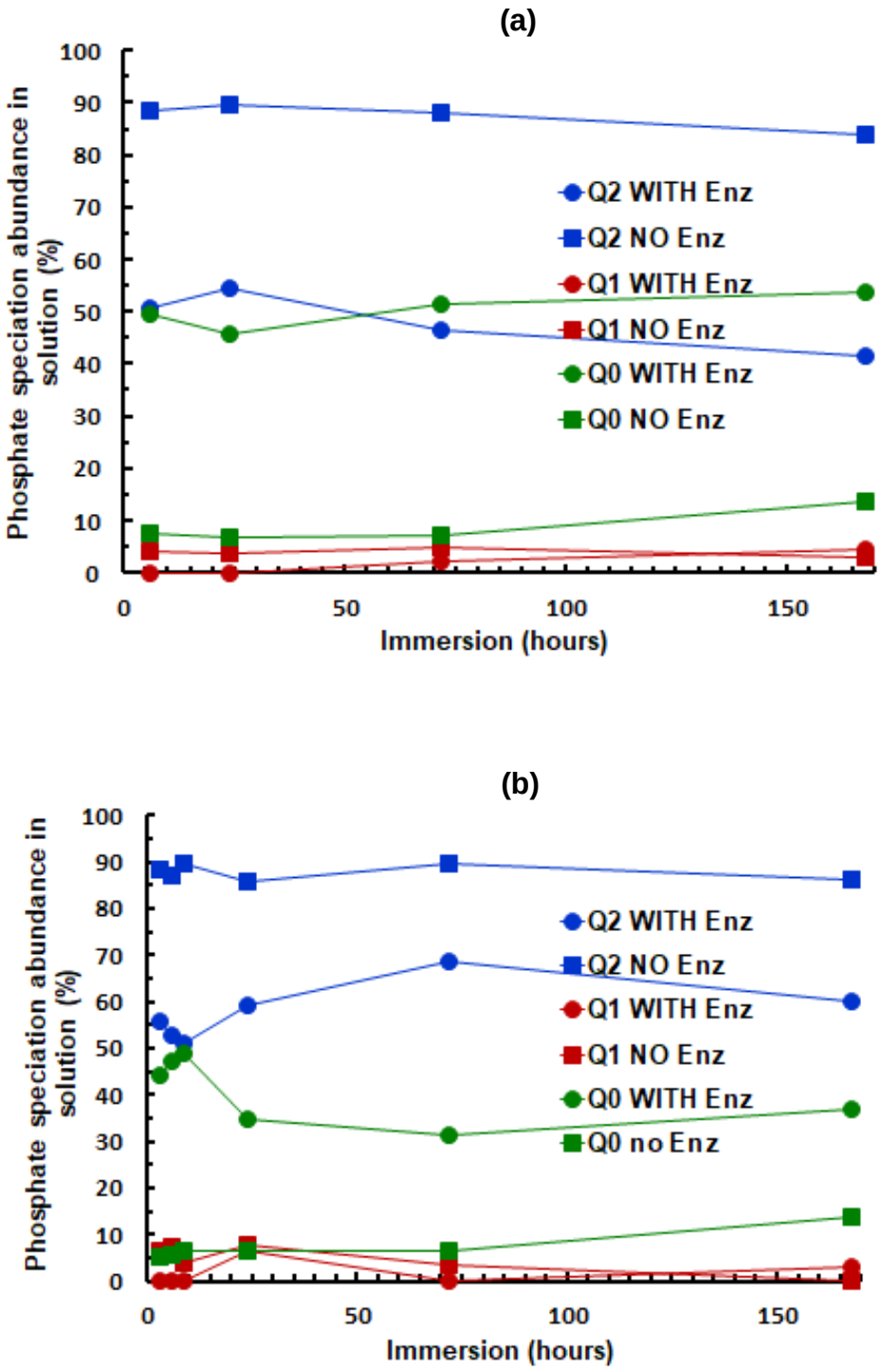

Figure 5.6 The integrals of three types of phosphate seen in the ^{31}P Solution NMR spectra of the studied glass mixture SP2 together with and without ALP treatment plotted as a function of time for (a) 25/75 ratio and (b) 50/50 ratio.

Figure 5.6 (a) and (b) shows the ^{31}P solution NMR integrals of the experimental glass mixture SP2 with the ratios 25/75 and 50/50 ratio with and without treatment with ALP as a function of time. With both glass mixture ratios without the enzyme treatment, the highest proportion of species released into the solution was Q^2-metaphosphate (≈ 90%). Followed by the Q^0-orthophosphate and the lowest proportion was the Q^1 species. This was in good agreement with the study of Ahmed *et al.* (Ahmed et al., 2005).

In the presence of the enzyme with both ratios, the proportion of the Q^2 species decreased and the proportion of the Q^0 species increased. There was also a reduction in the Q^1 species after enzyme treatment.

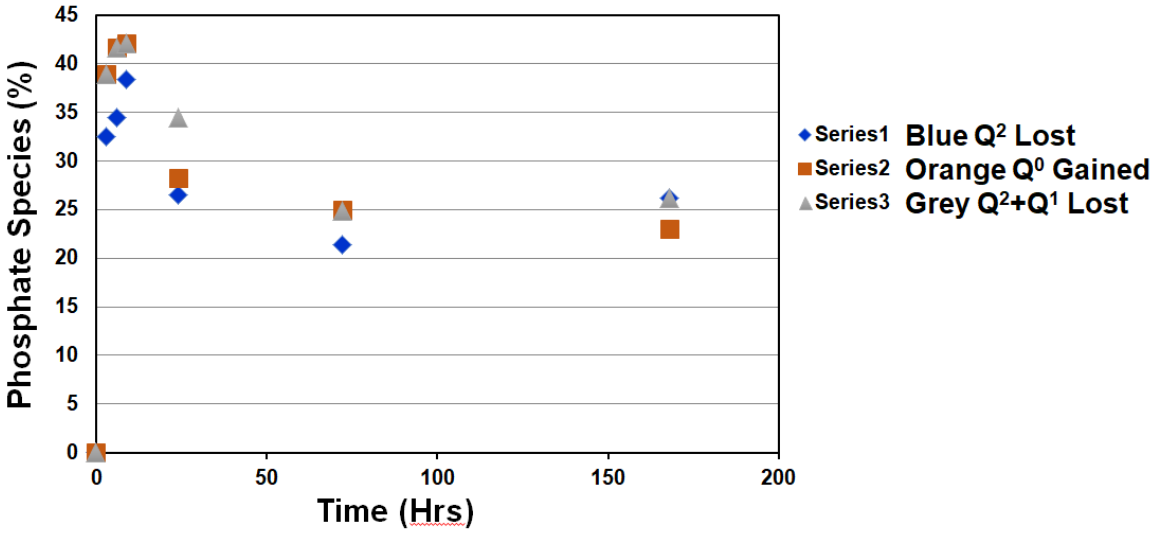

Figure 5.7 illustrating the Q species lost or gained after treatment glass mixture SP2 50/50 ratio with ALP as a function of time.

Figure 5.7 compares the evolution of the decrease in Q^2-metaphosphate species, with the increase in Q^0-orthophosphate species and also shows the decrease in both the Q^2- and Q^1-species together versus time. As can be observed from Figure 5.7, there were some differences between the proportion of the Q^2 species lost (the blue points) and the proportion of the Q^0 species gained (the orange points) as a function of time. In other words, the fraction of Q^2 species did not match exactly with the Q^0 species gained. However, there was a good match between the proportion of the (Q^2 + Q^1) lost (the grey points) and the proportion of the Q^0 gained.

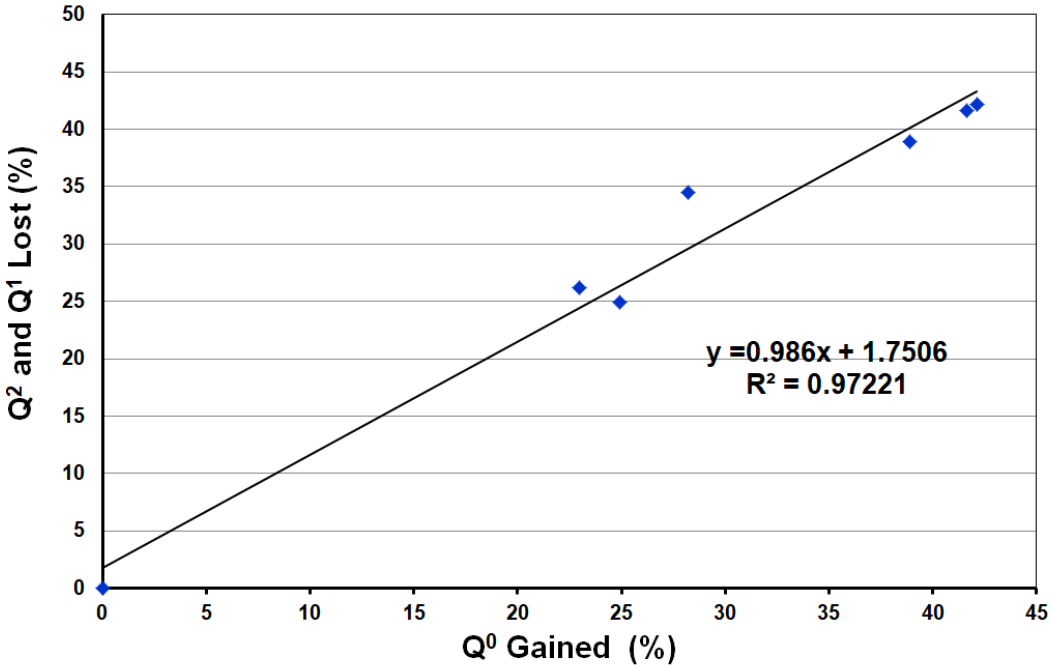

Figure 5.8 illustrating the correlation of Q^2 + Q^1 loss after ALP treatment versus the Q^0 gained.

Figures 5.8 and 5.9 demonstrate a direct correlation between the fractions as identified in Figure 5.7. Thus, Figure 5.8 demonstrates the correlation between the (Q^2 + Q^1) loss against the Q^0 gained. This correlation is linear (R^2 ≈ 0.97) and the slope is (0.986) which is close to (1.0). In other words, with the enzyme treatment the amount of (Q^2 + Q^1) loss was approximately equal to the amount of Q^0 gained.

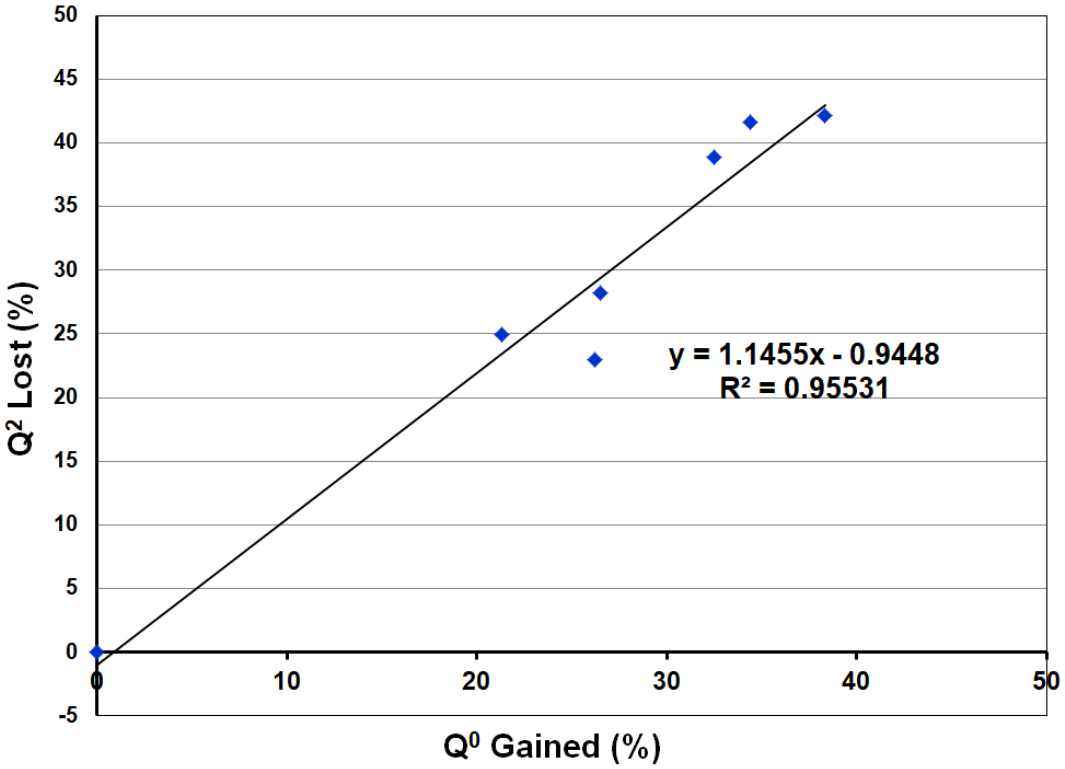

Figure 5.9 illustrating the correlation between the Q^2 lost after ALP treatment against the Q^0 gained.

Figure 5.9 exhibits the proportion of the Q^2 lost against the Q^0 gained. As seen the correlation is linear, with the correlation coefficient value 0.96.

5.2.4 pH Measurement Results:

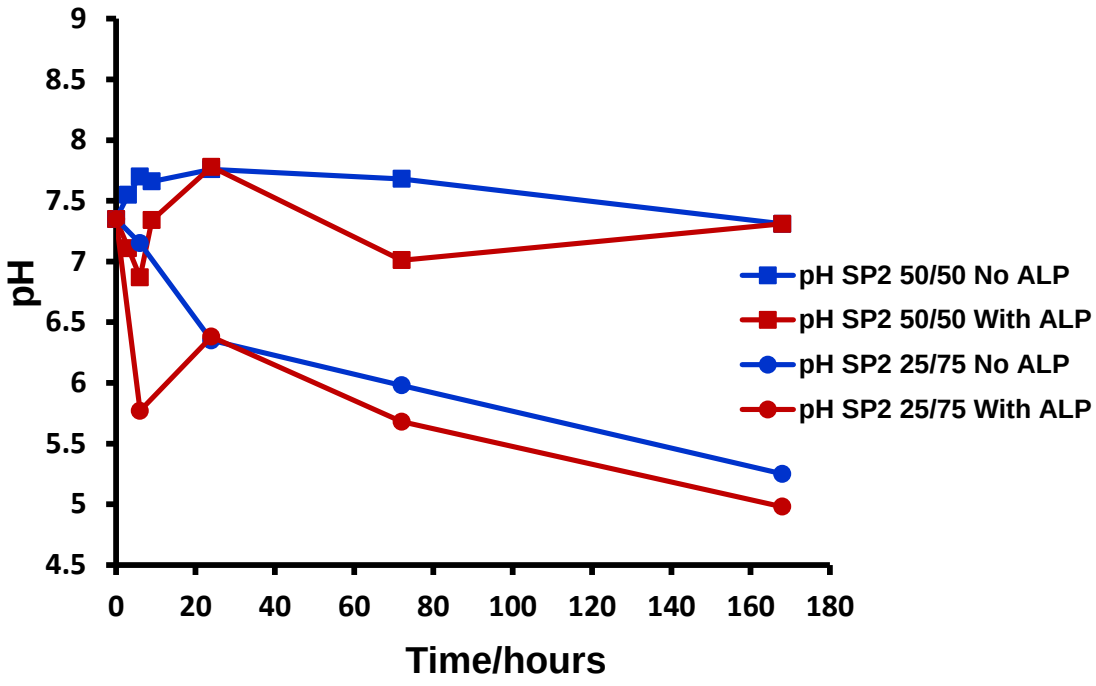

Figure 5.10 pH trend in solution plotted as a function of time for both ratios 25/75 and 50/50 of glass mixture SP2 with and without the ALP treatment.

Figure 5.10 shows the pH trend of the glass mixture SP2 with the ratios 25/75 and 50/50 against immersion time with and without ALP treatment. It was evident that the pH profile with the ALP appeared to be slightly more acidic for both ratios with the ALP.

5.3 Overall Discussion:

ALP is known for its biological role in cleaving the P-O-P linkages in phosphate containing compounds in solution. The results presented above reveal changes between three phosphate speciation(s) (Q^2-Q^1-Q^0) in solution which also resulted in significant changes between the speciation proportions in solid phase. The ^{31}P MAS-NMR spectra in Figures 5.2 and 5.3 show that in the presence of ALP, the Q^2-metaphosphate in the glass decreased much faster than when immersion without the ALP. This was noted particularly well in comparison with the spectra for 6 and 24 hours in Figures 5.2 and 5.3. Simultaneously, a clearly detectable decrease of the Q^2- and increase of the Q^0- species were observed in the solution in presence of the ALP. The 24 hour time point of the 25/75 mixture showed a particularly marked but consistent result. The solid-state ^{31}P NMR showed a significant fraction of Q^0 appearing in the spectra of the sample with the ALP. The Q^0 signals as well as the Q^2 have a characteristic sharp appearance, which was evident of the crystalline character of both species. The solution NMR of this sample presented an unusually low Q^0 fraction as seen from the Figure 5.4, which was consistent with a significant fraction of Q^0 crystallising out into the solid phase. However, this massive precipitation of Q^0 appeared only in one composition and this result requires further clarification.

The type of the Q^2 species in the phosphate glasses was largely metaphosphate where the proportion of phosphate to cations was equal. The proposed mode of phosphate glass dissolution in solutions has been previously reported in a study by Ahmed and his co-authors (Ahmed et al., 2005). In Ahmed's study, the amount of the released phosphate species into the solution upon phosphate glass degradation has been investigated using ion chromatography. Based on the chromatogram data, Ahmed and his co-workers stated that the phosphate species released into the

solution after phosphate glass dissolution can be identified as the following: (i) a high proportion of the Q^2-metaphosphate species which could be either linear chain or ring structure (unbranched) and the latter was suggested to be the predominant species in solution; followed by (ii) the Q^0-orthophosphate species (PO_4^{3-}); and (iii) a low proportion of the Q^1-pyrophosphate species (dimer $P_2O_7^{4-}$). This would suggest that the Q^1 observed from ^{31}P NMR both in solution and the solid state are largely from Q^1 end groups on Q^2 chains rather than from pyrophosphate.

The solution ^{31}P NMR spectra showed several signals corresponding to each phosphate speciation. For instance, the increase in the Q^0 speciation can be identified as due to a strong increase in the Q^0 signal at around 1-2 ppm in both mixtures in the presence of ALP. Whereas, another Q^0 signal at a higher chemical shift did not seem to change much and remained relatively small with time regardless of presence of the ALP. Several signals of the Q^2 metaphosphate speciation were also observed in the spectra. The decrease of the more negative signal at around -25 ppm appeared to be clearer. However, the stronger signal at around -22 ppm also decreased in intensity, although it was not clearly seen in the spectra plotted in Figure 5.4 and 5.5. The details of the phosphate speciation are not clear at the moment and particular signals of one speciation cannot be assigned yet. In a recent study by Döhler *et al*., the presence of both metaphosphate chains and rings were identified in solution containing dissolution products of the phosphate glasses in the ^{31}P solution state spectra (Döhler et al., 2015).

The presence of only a small fraction of Q^1-phosphate was observed in all solution NMR spectra (Figures 5.4 and 5.5). This low fraction of the Q^1 species indicates that this Q^1 is likely to be terminal to the Q^2-metaphosphate chains rather than the pyrophosphate dimer. Considering that every chain has two terminal Q^1 phosphorus atoms, the average length of the chain can be estimated. The average chain length

of the Q^2 species in the 50/50 mixture varies between 20 and 50, and is around 40 and 60 in the 25/75 mixture without the ALP. However, these values are only rough estimation as they do not take into account presence of the Q^2 ring fragments, which would have no terminal Q^1-phosphate species. Additionally, some of the time points have no detectable fraction of Q^1 even in the ALP-free samples (Figures 5.4 and 5.5).

In the presence of the ALP, the correlation between the decrease of the total Q^1 and Q^2 equated to the increase in Q^0 is established in the Figures 5.7 and 5.8. Most of the spectra of the samples with the ALP showed no detectable presence of Q^1. Assuming presence of both Q^2 chains and rings and this indicated that the amount of Q^2 chains substantially decreased in presence of the ALP.

Enzymatic degradation of the P-O-P bond by the ALP is well known for the Q^1 pyrophosphate species. Based on the findings presented above it is proposed that the ALP cleaves the Q^0 orthophosphate species from the terminal Q^1 phosphate group of the Q^2 metaphosphate linear chain. Therefore, the proportion of the Q^1 species in solution is the lowest as it is no longer available in the solution.

The pH results in Figure 5.10 supported the results of the ^{31}P solution NMR spectra in Figures 5.4 and 5.5 and also the results of the ^{31}P solution NMR integrals in Figure 5.6. The lower pH in presence of the ALP could be related to the ability of the ALP to hydrolyse the Q^2 metaphosphate chain and release more ionic phosphate products or groups such as the Q^0-orthophosphate species.

Accordingly, the proposed function of ALP is to hydrolyse the straight Q^2-metaphosphate chain by cleaving Q^1 terminal phosphate group to release Q^0 orthophosphate. The release of Q^0- orthophosphate species (PO_4^{3-}), results in

apatite mineral formation. Figure 5.11 below describes the hypothesized role of the ALP:

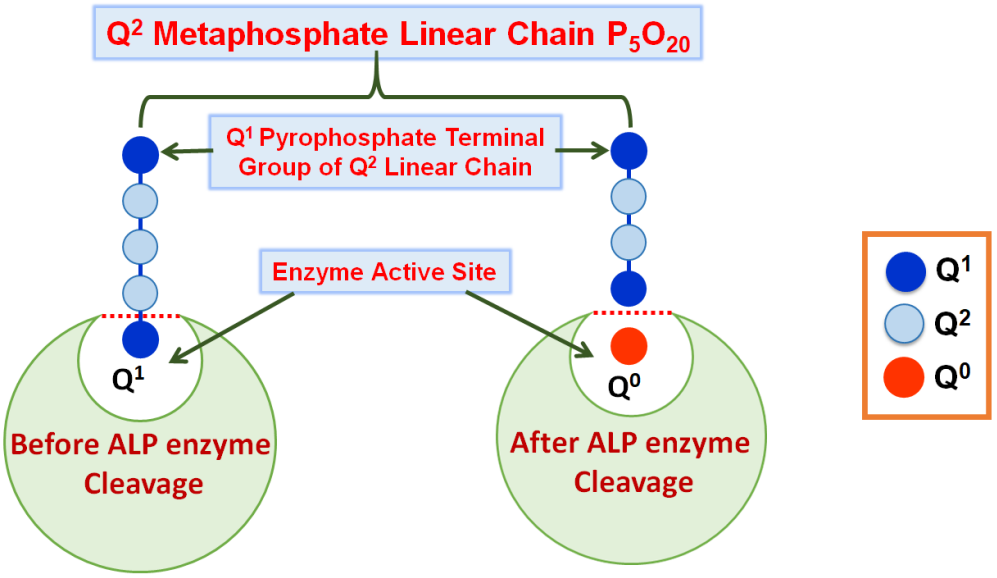

Figure 5.11 Schematic demonstration of the ALP enzyme activity in solution, describing the insertion of the Q^2 metaphosphate linear chain in the active site of the ALP enzyme and the Q^1 end group can be hydrolysed off to release Q^0 orthophosphate species.

There were two slightly contradicting observations reported in the published literature. Lorenz and Schröder reported that the ALP cleaved the Q^0-orthophosphate species from the Q^2-metaphosphate species (Lorenz and Schröder, 2001). Grover *et al*., however demonstrated that Q^0 formed from the Q^1-pyrophosphate species in presence of the ALP (Grover et al., 2013). Our findings presented in this Chapter did not contradict either of the reports. Moreover, the results presented here delivered specific details explaining how the two contradictive observations from the literature can be part of the same mechanism of phosphate chain degradation. Our findings revealed that the terminal Q^1 species belonging to the Q^2 metaphosphate chains was hydrolysed by the ALP and converted into a Q^0 species.

It is important to point out that the Q^2-metaphosphate unit still exists predominantly in the solution NMR spectra after treatment glass mixture with ALP. This could be attributed to the Q^2 ring structure generated by the dissolution of phosphate glass into the solution, which may not be hydrolysed by ALP function.

In this study the phosphate glass of the glass mixtures was designed to work with the biological environment in the periodontal bony defect that is elevated with ALP (Sanikop et al., 2012).

6 Conclusions and Suggestions for Future Work:

6.1 Conclusions:

6.1.1 Silicate Glass:

- The silicate glass Bioglass®45S5 (PerioGlas®) generates a rapid pH rise (pH > 8) during glass dissolution in physiological solutions. This higher alkaline pH can retard further glass dissolution in body fluids and subsequently inhibit the apatite formation.
- The inhibition of apatite precipitation found with PerioGlas® is attributed to the suppression of the ion exchange process during glass dissolution.
- The particle size of the bioactive glass powder is an essential factor for both the pH rise and apatite formation in buffer solutions, which may override any difference in the glass composition. Subsequently, the glass bioactivity is dominated by particles size.

6.1.2 Silicate/Phosphate Glass Mixtures:

- The high alkaline pH produced by the silicate glass can be regulated by using a silicate/phosphate glass mixture with fine PS for phosphate glass and large PS for silicate glasses. This PS selection was designed to reduce the high pH initially in order to inhibit the alkaline bacterial growth of *P.gingivalis.* Subsequently, this pH gradually rises to stimulate new bone regeneration.
- The trend of glass mixtures pH could be programmed by changing the ratio of S-glass to P-glass in mixture.
- Upon glass mixture degradation in buffer solution, the Q^2 metaphosphate species of phosphate glass transforms into small amount of Q^0

orthophosphate species and large amount of Q^1 species as detected by solid state NMR spectroscopy.

- The degree of conversion of the Q^2 metaphosphate into the Q^1 species and Q^0 orthophosphate during the glass mixture dissolution is controlled by the composition of glass mixture.
- The Q^1 pyrophosphate species produced on degradation of the phosphate glass is known as an inhibitor of apatite precipitation and bone formation.

6.1.3 Silicate/Phosphate Glass Mixtures with ALP:

- ALP is known to be elevated in periodontal bony defects delivers Q^0 orthophosphate from the Q^1 end group of the Q^2 metaphosphate linear chains. The released Q^0-orthophosphate ions are essential for apatite crystal formation.
- There is no biomaterial used in periodontal treatment that would take into account the presence of elevated levels of ALP in periodontal bony defects.
- The newly developed silicate/phosphate glass mixtures have a capacity to degrade in presence of ALP. Therefore, this new glass mixture can potentially adapt to the severity of periodontal disease.

6.2 Suggestions for Future Work:

- The current three ratios of P-glass to S-glass in the glass mixtures studied were 10/90, 25/75 and 50/50 by weight. It would be advantageous to study more ratios of P-glass to S-glass, such as 90/10, 75/25 and 60/40 and investigate the influence on the pH changes, ion release data and glass degradation. In addition the FTIR and NMR spectra could also be investigated.

- The particle size of the glass mixtures used in this study was a small particle size for P-glass and coarse for S-glass, which is beneficial in periodontal application. It would be worth considering as further studies to change the particle size for both P-glass and S-glass. For example, P-glass has large particle size and S-glass has small ones, both glasses have fine or both have large. This change in particle size range may alter the pH behaviour, the rate of glass mixtures degradation and ion release data; therefore, the FTIR and NMR spectra could be different. The pH profile could be different in terms of large particle size for P-glass and fine for S-glass. It would be predicted that the pH trend may illustrate dramatic increase in pH values at the beginning of the experiment due to the S-glass dissolution, and then follow by reduction in pH measurements owing to the dissolution of P-glass. This initial pH behaviour emerges from S-glass dissolution could be valuable in bone graft researches to inhibit the growth of bacteria found in this area such as *Staphylococcus aureus.* Neutral pH might be obtained if both glasses have fine particle size or both have large.
- As demonstrated before in Chapter 5, the Q^2-metaphosphate unit is still prominent in the solution NMR spectra after treatment of the glass mixture with ALP. It has been suggested that this can be related to the presence of the Q^2 rings in phosphate glass structure which when released are not readily hydrolysed by ALP. This ring phosphate has only Q^2 groups and does not contain Q^1 end groups in its structure. Therefore, it could be perhaps too large to enter the active site of the enzyme and may not be enzymatically hydrolysed by ALP readily. Accordingly, the future work should investigate whether ALP can cleave the cyclic Q^2 phosphates or not. This could be studied by using cyclic trimetaphosphate and hexametaphosphate

with ALP and then compare the results with the control data (without ALP) under the same circumstances using ^{31}P solution state NMR spectroscopy.

- Further work should include the co-sintering of the phosphate glass with the silicate glass in order to form three-dimensional amorphous porous scaffolds which can be used in regenerative bone grafts applications. The sintering process should fuse the two glasses (silicate with phosphate) without crystallisation occurring. The fundamental key of amorphous sintering can be achieved by expanding the sintering window which is defined as the temperature difference between the glass transition temperature and the onset of the crystallisation temperature. Therefore, in order to fuse the particles of the two glasses without crystallising, the sintering temperature must be above their glass transition temperature and below their onset of crystallisation temperature.
- Using SEM-EDX analysis would be beneficial after immersion test to qualify and quantify the apatite formation on the surface of the glass mixture particles.
- Cytotoxicity and bactericidal studies of the newly developed glass mixtures on *P. gingivalis* and other periodontal pathogens should be investigated in the future work.
- Futuristic animal studies of the newly developed glass mixtures should also be investigated in order to translate this novel technology into the clinical trials.

7 References:

ABOELSAAD, N. S., SOORY, M., GADALLA, L. M., RAGAB, L. I., DUNNE, S., ZALATA, K. R. & LOUCA, C. 2009. Effect of soft laser and bioactive glass on bone regeneration in the treatment of infra-bony defects (a clinical study). *Lasers in medical science,* 24**,** 387-395.

AHMED, A., ALI, A., MAHMOUD, D. A. & EL - FIQI, A. 2011. Preparation and characterization of antibacterial P2O5–CaO–Na2O–Ag2O glasses. *Journal of Biomedical Materials Research Part A,* 98**,** 132-142.

AHMED, I., LEWIS, M., NAZHAT, S. & KNOWLES, J. 2005. Quantification of anion and cation release from a range of ternary phosphate-based glasses with fixed 45 mol% P2O5. *Journal of biomaterials applications,* 20**,** 65-80.

AHSAN, M. R., UDDIN, M. A. & MORTUZA, M. G. 2005. Infrared study of the effect of P 2 O 5 in the structure of lead silicate glasses. *Indian Journal of Pure and Applied Physics*.

ALI, S., FAROOQ, I. & IQBAL, K. 2014. A review of the effect of various ions on the properties and the clinical applications of novel bioactive glasses in medicine and dentistry. *The Saudi dental journal,* 26**,** 1-5.

ALOMAR, J., LEBERT, A. & MONTEL, M.-C. 2008. Effect of temperature and pH on growth of Staphylococcus aureus in co-culture with Lactococcus garvieae. *Current microbiology,* 56**,** 408-412.

ARMITAGE, G. C. 2004. The complete periodontal examination. *Periodontology 2000,* 34**,** 22-33.

ASHMAN, A. 1992. The use of synthetic bone materials in dentistry. *Compendium (Newtown, Pa.),* 13**,** 1020, 1022, 1024-6, passim.

BEZERRA JÚNIOR, A. A., PALLOS, D., CORTELLI, J. R. & SARACENI, C. H. C. 2010. Evaluation of organic and inorganic compounds in the saliva of patients with chronic periodontal disease. *Revista odonto ciência,* 25**,** 234-238.

BICKEL, M. & CIMASONI, G. 1985. The pH of human crevicular fluid measured by a new microanalytical technique. *Journal of periodontal research,* 20**,** 35-40.

BINGEL, L., GROH, D., KARPUKHINA, N. & BRAUER, D. S. 2015. Influence of dissolution medium pH on ion release and apatite formation of Bioglass® 45S5. *Materials Letters,* 143**,** 279-282.

BISSWANGER, H. 2014. Enzyme assays. *Perspectives in Science,* 1**,** 41-55.

BISSWANGER, H. 2017. *Enzyme kinetics: principles and methods*, John Wiley & Sons.

BITAR, M., KNOWLES, J., LEWIS, M. & SALIH, V. 2005. Soluble phosphate glass fibres for repair of bone-ligament interface. *Journal of Materials Science: Materials in Medicine,* 16**,** 1131-1136.

BITAR, M., SALIH, V., MUDERA, V., KNOWLES, J. C. & LEWIS, M. P. 2004. Soluble phosphate glasses: in vitro studies using human cells of hard and soft tissue origin. *Biomaterials,* 25**,** 2283-2292.

BOHNER, M. & LEMAITRE, J. 2009. Can bioactivity be tested in vitro with SBF solution? *Biomaterials,* 30**,** 2175-2179.

BONNELYE, E., CHABADEL, A., SALTEL, F. & JURDIC, P. 2008. Dual effect of strontium ranelate: stimulation of osteoblast differentiation and inhibition of osteoclast formation and resorption in vitro. *Bone,* 42**,** 129-138.

BRAUER, D. S., KARPUKHINA, N., KEDIA, G., BHAT, A., LAW, R. V., RADECKA, I. & HILL, R. G. 2012. Bactericidal strontium-releasing injectable bone cements based on bioactive glasses. *Journal of The Royal Society Interface***,** rsif20120647.

BRAUER, D. S., KARPUKHINA, N., O'DONNELL, M. D., LAW, R. V. & HILL, R. G. 2010. Fluoride-containing bioactive glasses: effect of glass design and structure on degradation, pH and apatite formation in simulated body fluid. *Acta Biomaterialia,* 6**,** 3275-3282.

BRAUER, D. S., KARPUKHINA, N., SEAH, D., LAW, R. V. & HILL, R. G. Fluoride-containing bioactive glasses. Advanced Materials Research, 2008. Trans Tech Publ, 297-302.

BROW, R. K. 2000. the structure of simple phosphate glasses. *Journal of Non-Crystalline Solids,* 263**,** 1-28.

BUNKER, B., ARNOLD, G. & WILDER, J. A. 1984. Phosphate glass dissolution in aqueous solutions. *Journal of Non-Crystalline Solids,* 64**,** 291-316.

CARTA, D., KNOWLES, J. C., SMITH, M. E. & NEWPORT, R. J. 2007. Synthesis and structural characterization of P2O5–CaO–Na2O sol–gel materials. *Journal of Non-Crystalline Solids,* 353**,** 1141-1149.

CHACKO, N. L., ABRAHAM, S., RAO, H. S., SRIDHAR, N., MOON, N. & BARDE, D. H. 2014. A clinical and radiographic evaluation of periodontal regenerative potential of PerioGlas®: a synthetic, resorbable material in treating periodontal infrabony defects. *Journal of international oral health,* 6**,** 20.

CHO, Y.-D., SEOL, Y.-J., LEE, Y.-M., RHYU, I.-C., RYOO, H.-M. & KU, Y. 2017. An overview of biomaterials in periodontology and implant dentistry. *Advances in Materials Science and Engineering,* 2017.

CHOU, L., AL-BAZIE, S., COTTRELL, D., GIODANO, R. & NATHASON, D. Atomic and Molecular Mechanisms Underlying the Osteogenic Effects of Bioglass [R] Materials. BIOCERAMICS-CONFERENCE-, 1998. 265-268.

COSTANTINO, P. D. & FRIEDMAN, C. D. 1994. Synthetic bone graft substitutes. *Otolaryngologic Clinics of North America,* 27**,** 1037-1074.

CULLITY, B. D. & WEYMOUTH, J. W. 1957. Elements of X-ray Diffraction. *American Journal of Physics,* 2**5,** 394-395.

CYPHER, T. J. & GROSSMAN, J. P. 1996. Biological principles of bone graft healing. *The Journal of foot and ankle surgery,* 35**,** 413-417.

DALTABAN, Ö., SAYGUN, I., BAL, B., BALOŞ, K. & SERDAR, M. 2006. Gingival crevicular fluid alkaline phosphatase levels in postmenopausal women: effects of phase I periodontal treatment. *Journal of periodontology,* 77**,** 67-72.

DÖHLER, F., MANDLULE, A., VAN WÜLLEN, L., FRIEDRICH, M. & BRAUER, D. S. 2015. 31 P NMR characterisation of phosphate fragments during dissolution of calcium sodium phosphate glasses. *Journal of Materials Chemistry B,* 3**,** 1125-1134.

DOYLE, W. M. 1992. Principles and applications of Fourier transform infrared (FTIR) process analysis. *Process control and quality,* 2**,** 11-41.

DRAGO, L., VASSENA, C., FENU, S., DE VECCHI, E., SIGNORI, V., DE FRANCESCO, R. & ROMANÒ, C. L. 2014. In vitro antibiofilm activity of bioactive glass S53P4. *Future microbiology,* 9**,** 593-601.

DRAGO, L., VECCHI, E. D., BORTOLIN, M., TOSCANO, M., MATTINA, R. & ROMANÒ, C. L. 2015. Antimicrobial activity and resistance selection of different bioglass S53P4 formulations against multidrug resistant strains. *Future microbiology,* 10**,** 1293-1299.

DUMITRESCU, A. L. 2011. Bone grafts and bone graft substitutes in periodontal therapy. *Chemicals in surgical Periodontal therapy***,** 73-144.

EDÉN, M. 2011. The split network analysis for exploring composition–structure correlations in multi-component glasses: I. Rationalizing bioactivity-composition trends of bioglasses. *Journal of Non-Crystalline Solids,* 357**,** 1595-1602.

ELGAYAR, I. 2004. *The influence of alkali metal content and network connectivity on bioactive glasses.* University of London.

ELGAYAR, I., ALIEV, A., BOCCACCINI, A. & HILL, R. 2005. Structural analysis of bioactive glasses. *Journal of Non-Crystalline Solids,* 351**,** 173-183.

FETNER, A., HARTIGAN, M. & LOW, S. 1994. Periodontal repair using PerioGlas in nonhuman primates: clinical and histologic observations. *Compendium (Newtown, Pa.),* 15**,** 932, 935-8; quiz 939.

FLYNN, A., JONES, D., MAN, E., SHIPMAN, S. & TUNG, S. 2002. The effects of pH on Type VII-NA Bovine Intestinal Mucosal Alkaline Phosphatase Activity. *Journal of Experimental Microbiology and Immunology (JEMI) Vol,* 2**,** 50-56.

FREDHOLM, Y. C., KARPUKHINA, N., BRAUER, D. S., JONES, J. R., LAW, R. V. & HILL, R. G. 2012. Influence of strontium for calcium substitution in bioactive glasses on degradation, ion release and apatite formation. *Journal of The Royal Society Interface,* 9**,** 880-889.

GAO, H., TAN, T. & WANG, D. 2004. Dissolution mechanism and release kinetics of phosphate controlled release glasses in aqueous medium. *Journal of controlled release,* 96**,** 29-36.

GARRETT, S., LOOS, B., CHAMBERLAIN, D. & EGELBERG, J. 1988. Treatment of intraosseous periodontal defects with a combined adjunctive therapy of citric acid conditioning, bone grafting, and placement of collagenous membranes. *Journal of clinical periodontology,* 15**,** 383-389.

GENTLEMAN, E., FREDHOLM, Y. C., JELL, G., LOTFIBAKHSHAIESH, N., O'DONNELL, M. D., HILL, R. G. & STEVENS, M. M. 2010. The effects of strontium-substituted bioactive glasses on osteoblasts and osteoclasts in vitro. *Biomaterials,* 31**,** 3949-3956.

GROENEVELD, M., BOS, T., EVERTS, V. & BEERTSEN, W. 1996. Cell - bound and extracellular matrix - associated alkaline phosphatase activity in rat periodontal ligament. *Journal of periodontal research,* 31**,** 73-79.

GROVER, L. M., WRIGHT, A. J., GBURECK, U., BOLARINWA, A., SONG, J., LIU, Y., FARRAR, D. F., HOWLING, G., ROSE, J. & BARRALET, J. E. 2013. The effect of amorphous pyrophosphate on calcium phosphate cement resorption and bone generation. *Biomaterials,* 34**,** 6631-6637.

HAFFAJEE, A. D. & SOCRANSKY, S. S. 1994. Microbial etiological agents of destructive periodontal diseases. *Periodontology 2000,* 5**,** 78-111.

HAJISHENGALLIS, G., DARVEAU, R. P. & CURTIS, M. A. 2012. The keystone-pathogen hypothesis. *Nature Reviews Microbiology,* 10**,** 717.

HENCH, L. & ETHRIDGE, E. 1982. Biomaterials: An Interfactial Approach. Academic Press.

HENCH, L. L. 1991. Bioceramics: from concept to clinic. *Journal of the american ceramic society,* 74**,** 1487-1510.

HENCH, L. L., SPLINTER, R. J., ALLEN, W. & GREENLEE, T. 1971. Bonding mechanisms at the interface of ceramic prosthetic materials. *Journal of Biomedical Materials Research Part A,* 5**,** 117-141.

HILL, R. 1996. An alternative view of the degradation of bioglass. *Journal of Materials Science Letters,* 15**,** 1122-1125.

HILL, R. G. & BRAUER, D. S. 2011. Predicting the bioactivity of glasses using the network connectivity or split network models. *Journal of Non-Crystalline Solids,* 357**,** 3884-3887.

ILIEVA, D., JIVOV, B., BOGACHEV, G., PETKOV, C., PENKOV, I. & DIMITRIEV, Y. 2001. Infrared and Raman spectra of Ga2O3–P2O5 glasses. *Journal of non-crystalline solids,* 283**,** 195-202.

JONES, J. R. 2015. Reprint of: Review of bioactive glass: From Hench to hybrids. *Acta biomaterialia,* 23**,** S53-S82.

JONES, J. R., SEPULVEDA, P. & HENCH, L. L. 2001. Dose - dependent behavior of bioactive glass dissolution. *Journal of Biomedical Materials Research Part A,* 58**,** 720-726.

KIRKPATRICK, R. J. & BROW, R. K. 1995. Nuclear magnetic resonance investigation of the structures of phosphate and phosphate-containing glasses: a review. *Solid state nuclear magnetic resonance,* 5**,** 9-21.

KOKUBO, T., KUSHITANI, H., SAKKA, S., KITSUGI, T. & YAMAMURO, T. 1990. Solutions able to reproduce in vivo surface - structure changes in bioactive glass - ceramic A - W3. *Journal of Biomedical Materials Research Part A,* 24**,** 721-734.

KOKUBO, T. & TAKADAMA, H. 2006. How useful is SBF in predicting in vivo bone bioactivity? *Biomaterials,* 27**,** 2907-2915.

KURZ, L. T., GARFIN, S. R. & BOOTH JR, R. E. 1989. Harvesting autogenous iliac bone grafts. A review of complications and techniques. *Spine,* 14**,** 1324-1331.

LAKHKAR, N., ABOU NEEL, E. A., SALIH, V. & KNOWLES, J. C. 2011. Titanium and strontium-doped phosphate glasses as vehicles for strontium ion delivery to cells. *Journal of biomaterials applications,* 25**,** 877-893.

LAKHKAR, N. J., PARK, J.-H., MORDAN, N. J., SALIH, V., WALL, I. B., KIM, H.-W., KING, S. P., HANNA, J. V., MARTIN, R. A. & ADDISON, O. 2012. Titanium phosphate glass microspheres for bone tissue engineering. *Acta biomaterialia,* 8**,** 4181-4190.

LEE, H. K., HWANG, S. J. & KANG, W. H. Preparation of K2O-CaO-P2O5 eco-glass fertilizers and effect in crops. Materials Science Forum, 2005. Trans Tech Publ, 407-410.

LEGEROS, R. Z. 1993. Biodegradation and bioresorption of calcium phosphate ceramics. *Clinical materials,* 14**,** 65-88.

LI, R., CLARK, A. & HENCH, L. 1991. An investigation of bioactive glass powders by sol - gel processing. *Journal of Applied Biomaterials,* 2**,** 231-239.

LIU, J., RAWLINSON, S. C., HILL, R. G. & FORTUNE, F. 2016. Strontium-substituted bioactive glasses in vitro osteogenic and antibacterial effects. *Dental Materials,* 32**,** 412-422.

LIU, Q., CHEN, X. & LI, X. 1996. The hydrolysis of Na2OÁCaOÁ2P2O5 bioglass. *J Wuhan Univ Technol,* 18**,** 26-29.

LOCKYER, M., HOLLAND, D. & DUPREE, R. 1995. NMR investigation of the structure of some bioactive and related glasses. *Journal of Non-Crystalline Solids,* 188**,** 207-219.

LORENZ, B. & SCHRÖDER, H. C. 2001. Mammalian intestinal alkaline phosphatase acts as highly active exopolyphosphatase. *Biochimica et Biophysica Acta (BBA)-Protein Structure and Molecular Enzymology,* 1547**,** 254-261.

LOVELACE, T. B., MELLONIG, J. T., MEFFERT, R. M., JONES, A. A., NUMMIKOSKI, P. V. & COCHRAN, D. L. 1998. Clinical evaluation of bioactive glass in the treatment of periodontal osseous defects in humans. *Journal of periodontology,* 69**,** 1027-1035.

MACKENZIE, K. J. & SMITH, M. E. 2002. *Multinuclear solid-state nuclear magnetic resonance of inorganic materials*, Elsevier.

MAÇON, A. L., KIM, T. B., VALLIANT, E. M., GOETSCHIUS, K., BROW, R. K., DAY, D. E., HOPPE, A., BOCCACCINI, A. R., KIM, I. Y. & OHTSUKI, C. 2015. A unified in vitro evaluation for apatite-forming ability of bioactive glasses and their variants. *Journal of Materials Science: Materials in Medicine,* 26**,** 115.

MARIE, P., AMMANN, P., BOIVIN, G. & REY, C. 2001. Mechanisms of action and therapeutic potential of strontium in bone. *Calcified tissue international,* 69**,** 121-129.

MARTIN, R. A., YUE, S., HANNA, J. V., LEE, P., NEWPORT, R. J., SMITH, M. E. & JONES, J. R. 2012. Characterizing the hierarchical structures of bioactive sol–gel silicate glass and hybrid scaffolds for bone regeneration. *Phil. Trans. R. Soc. A,* 370**,** 1422-1443.

MASSERA, J., PETIT, L., CARDINAL, T., VIDEAU, J.-J., HUPA, M. & HUPA, L. 2013. Thermal properties and surface reactivity in simulated body fluid of new strontium ion-containing phosphate glasses. *Journal of Materials Science: Materials in Medicine,* 24**,** 1407-1416.

MATHEW, R., TURDEAN-IONESCU, C., STEVENSSON, B., IZQUIERDO-BARBA, I., GARCÍA, A., ARCOS, D., VALLET-REGÍ, M. & EDÉN, M. 2013. Direct probing of the phosphate-ion distribution in bioactive silicate glasses by solid-state NMR: evidence for transitions between random/clustered scenarios. *Chemistry of Materials,* 25**,** 1877-1885.

MCDERMID, A. S., MCKEE, A. S. & MARSH, P. D. 1988. Effect of environmental pH on enzyme activity and growth of Bacteroides gingivalis W50. *Infection and immunity,* 56**,** 1096-1100.

MCMILLAN, P. 1979. Non-Metallic Solids. *Glass-ceramics, 2nd Edition, Academic Press, London*.

MENGEL, R., SOFFNER, M. & FLORES-DE-JACOBY, L. 2003. Bioabsorbable membrane and bioactive glass in the treatment of intrabony defects in patients with generalized aggressive periodontitis: results of a 12-month clinical and radiological study. *Journal of periodontology,* 74**,** 899-908.

MNEIMNE, M., HILL, R. G., BUSHBY, A. J. & BRAUER, D. S. 2011. High phosphate content significantly increases apatite formation of fluoride-containing bioactive glasses. *Acta Biomaterialia,* 7**,** 1827-1834.

MNEIMNE, M. A. 2014. *Development of Bioactive Glasses for Dental Treatments* The Degree of Doctor of Philosophy Barts and The London, School of Medicine and Dentistry.

MONFOULET, L.-E., BECQUART, P., MARCHAT, D., VANDAMME, K., BOURGUIGNON, M., PACARD, E., VIATEAU, V., PETITE, H. & LOGEART-AVRAMOGLOU, D. 2014. The pH in the microenvironment of human mesenchymal stem cells is a critical factor for optimal osteogenesis in tissue-engineered constructs. *Tissue Engineering Part A,* 20**,** 1827-1840.

MOORE, W. R., GRAVES, S. E. & BAIN, G. I. 2001. Synthetic bone graft substitutes. *ANZ journal of surgery,* 71**,** 354-361.

MOUSTAFA, Y. & EL-EGILI, K. 1998. Infrared spectra of sodium phosphate glasses. *Journal of non-crystalline solids,* 240**,** 144-153.

MYSEN, B. O., RYERSON, F. J. & VIRGO, D. 1981. The structural role of phosphorus in silicate melts. *American Mineralogist,* 66**,** 106-117.

NAKAYAMA, K. 2015. Porphyromonas gingivalis and related bacteria: from colonial pigmentation to the type IX secretion system and gliding motility. *Journal of periodontal research,* 50**,** 1-8.

NEEL, E. A. A., PICKUP, D. M., VALAPPIL, S. P., NEWPORT, R. J. & KNOWLES, J. C. 2009. Bioactive functional materials: a perspective on phosphate-based glasses. *Journal of Materials Chemistry,* 19**,** 690-701.

NEWMAN, M. G., TAKEI, H., KLOKKEVOLD, P. R. & CARRANZA, F. A. 2011. *Carranza's clinical periodontology*, Elsevier health sciences.

NOVAJRA, G., PERDIKA, P., PISANO, R., MIOLA, M., BARI, A., JONES, J., DETSCH, R., BOCCACCINI, A. & VITALE-BROVARONE, C. 2015. Structure optimisation and biological evaluation of bone scaffolds prepared by co-sintering of silicate and phosphate glasses. *Advances in Applied Ceramics,* 114**,** S48-S55.

O'DONNELL, M., CANDARLIOGLU, P., MILLER, C., GENTLEMAN, E. & STEVENS, M. 2010. Materials characterisation and cytotoxic assessment of strontium-substituted bioactive glasses for bone regeneration. *Journal of Materials Chemistry,* 20**,** 8934-8941.

O'DONNELL, M., FREDHOLM, Y., DE ROUFFIGNAC, A. & HILL, R. 2008a. Structural analysis of a series of strontium-substituted apatites. *Acta Biomaterialia,* 4**,** 1455-1464.

O'DONNELL, M., WATTS, S., HILL, R. & LAW, R. 2009. The effect of phosphate content on the bioactivity of soda-lime-phosphosilicate glasses. *Journal of Materials Science: Materials in Medicine,* 20**,** 1611-1618.

O'DONNELL, M., WATTS, S., LAW, R. & HILL, R. 2008b. Effect of P 2 O 5 content in two series of soda lime phosphosilicate glasses on structure and properties–Part I: NMR. *Journal of Non-Crystalline Solids,* 354**,** 3554-3560.

O'DONNELL, M., WATTS, S., LAW, R. & HILL, R. 2008c. Effect of P 2 O 5 content in two series of soda lime phosphosilicate glasses on structure and properties–Part II: Physical properties. *Journal of Non-Crystalline Solids,* 354**,** 3561-3566.

OGUNSALU, C. 2011. Bone substitutes and validation. *Implant Dentistry-The Most Promising Discipline of Dentistry.* InTech.

PATEL, U., MOSS, R., HOSSAIN, K. M. Z., KENNEDY, A. R., BARNEY, E., AHMED, I. & HANNON, A. 2017. Structural and physico-chemical analysis of calcium/strontium substituted, near-invert phosphate based glasses for biomedical applications. *Acta biomaterialia,* 60**,** 109-127.

PAUL, A. 1989. *Chemistry of glasses*, Springer Science & Business Media.

PAZZAGLIA, U. E., GABBI, C., LOCARDI, B., DI NUCCI, A., ZATTI, G. & CHERUBINO, P. 1989. Study of the osteoconductive properties of bioactive glass fibers. *Journal of Biomedical Materials Research Part A,* 23**,** 1289-1297.

PEDONE, A., CHARPENTIER, T., MALAVASI, G. & MENZIANI, M. C. 2010. New insights into the atomic structure of 45S5 bioglass by means of solid-state NMR spectroscopy and accurate first-principles simulations. *Chemistry of Materials,* 22**,** 5644-5652.

PHILLIPS, J. C. & THORPE, M. 1985. Constraint theory, vector percolation and glass formation. *Solid State Communications,* 53**,** 699-702.

PUDIDOTDK. 2009. *Structure of liquids and glasses* [Online]. Wikipedia. Available: https://en.wikipedia.org/wiki/Structure_of_liquids_and_glasses [Accessed 22/05/2018 2018].

SALIH, V., PATEL, A. & KNOWLES, J. 2007. Zinc-containing phosphate-based glasses for tissue engineering. *Biomedical Materials,* 2**,** 11.

SANIKOP, S., PATIL, S. & AGRAWAL, P. 2012. Gingival crevicular fluid alkaline phosphatase as a potential diagnostic marker of periodontal disease. *Journal of Indian Society of Periodontology,* 16**,** 513.

SATYANARAYANA, K., ANURADHA, B., SRIKANTH, G., CHANDRA, P., ANUPAMA, T. & DURGA, P. 2012. Clinical evaluation of intrabony defects in localized aggressive periodontitis patients with and without bioglass-an in-vivo study. *Kathmandu Univ Med J,* 37**,** 11-5.

SCHEPERS, E., BARBIER, L. & DUCHEYNE, P. 1998. Implant placement enhanced by bioactive glass particles of narrow size range. *International Journal of Oral & Maxillofacial Implants,* 13.

SHEIKH, Z., ABDALLAH, M., HAMDAN, N., JAVAID, M. A. & KHURSHIDD, Z. 2014. Barrier Membranes for Periodontal Guided Tissue Regeneration Applications. *Handbook of Oral Biomaterials; Pan Stanford Publishing: Singapore,* 6**,** 605-636.

SHIBATA, Y., YAMASHITA, Y., MIYAZAKI, H., UENO, S. & TAKEHARA, T. 1994. Effective method for discriminating between oral bacterial and human alkaline phosphatase activity. *Molecular Oral Microbiology,* 9**,** 35-39.

SHIMIZU, Y., SUGAWARA, H., FURUSAWA, T., MIZUNUMA, K., INADA, K. & YAMASHITA, S. 1997. Bone remodeling with resorbable bioactive glass and hydroxyapatite. *Implant dentistry,* 6**,** 269-274.

SINGH, R., CHANDRASHEKAR, K., MISHRA, R. & TRIPATHI, V. D. Perioglas® And Prf As Graft Materials in The Treatment of Intrabony Defects in Chronic Generalized Periodontitis: A Clinical And Radiological Evaluation.

SOCRANSKY, S. S. & HAFFAJEE, A. D. 1997. The nature of periodontal diseases. *Annals of periodontology,* 2**,** 3-10.

SOHRABI, K., SARAIYA, V., LAAGE, T. A., HARRIS, M., BLIEDEN, M. & KARIMBUX, N. 2012. An Evaluation of Bioactive Glass in the Treatment of Periodontal Defects: A Meta - Analysis of Randomized Controlled Clinical Trials. *Journal of periodontology,* 83**,** 453-464.

SUÁREZ-LÓPEZ DEL AMO, F., MONJE, A., PADIAL-MOLINA, M., TANG, Z. & WANG, H.-L. 2015. Biologic agents for periodontal regeneration and implant site development. *BioMed research international,* 2015.

TABA, M., KINNEY, J., KIM, A. S. & GIANNOBILE, W. V. 2005. Diagnostic biomarkers for oral and periodontal diseases. *Dental Clinics,* 49**,** 551-571.

TAKAHASHI, N. & SCHACHTELE, C. 1990. Effect of pH on the growth and proteolytic activity of Porphyromonas gingivalis and Bacteroides intermedius. *Journal of dental research,* 69**,** 1266-1269.

THORPE, M. F. 1983. Continuous deformations in random networks. *Journal of Non-Crystalline Solids,* 57**,** 355-370.

TILOCCA, A. Structural models of bioactive glasses from molecular dynamics simulations. Proceedings of the Royal Society of London A: Mathematical, Physical and Engineering Sciences, 2009. The Royal Society, 1003-1027.

TILOCCA, A. & CORMACK, A. N. 2007. Structural effects of phosphorus inclusion in bioactive silicate glasses. *The Journal of Physical Chemistry B,* 111**,** 14256-14264.

TONETTI, M. S., PINI-PRATO, G. & CORTELLINI, P. 1993. Periodontal regeneration of human intrabony defects. IV. Determinants of healing response. *Journal of periodontology,* 64**,** 934-940.

TONETTI, M. S., PRATO, G. P. & CORTELLINI, P. 1996. Factors affecting the healing response of intrabony defects following guided tissue regeneration and access flap surgery. *Journal of Clinical Periodontology,* 23**,** 548-556.

TURNBULL, D. 1969. Under what conditions can a glass be formed? *Contemporary physics,* 10**,** 473-488.

WADHAWAN, A., GOWDA, T. M. & MEHTA, D. S. 2012. Gore-tex® versus resolut adapt® GTR membranes with perioglas® in periodontal regeneration. *Contemporary clinical dentistry,* 3**,** 406.

WALLACE, K., HILL, R., PEMBROKE, J., BROWN, C. & HATTON, P. 1999. Influence of sodium oxide content on bioactive glass properties. *Journal of Materials Science: Materials in Medicine,* 10**,** 697-701.

WALSH, W., MORBERG, P., YU, Y., YANG, J. L., HAGGARD, W., SHEATH, P., SVEHLA, M. & BRUCE, W. 2003. Response of a calcium sulfate bone graft substitute in a confined cancellous defect. *Clinical Orthopaedics and Related Research®,* 406**,** 228-236.

WHITNEY. 2018. *We use state-of-the-art technologies to build you a foundation for long-term oral health* [Online]. Available: http://www.thesmilesurgeon.com/ [Accessed 22/05/2018 2018].

WILSON, J., CLARK, A., DOUEK, E., KRIEGER, J., SMITH, W. K. & ZAMET, J. S. Clinical applications of bioglass implants. Bioceramics: Proceedings of the 7th International Symposium on Ceramics in Medicine, 1994. Elsevier, 415-422.

WILSON, J., LOW, S., FETNER, A. & HENCH, L. 1987. Bioactive materials for periodontal treatment: a comparative study. *Biomaterials and clinical applications,* 5**,** 223-228.

WILSON, J. & LOW, S. B. 1992. Bioactive ceramics for periodontal treatment: comparative studies in the Patus monkey. *Journal of Applied Biomaterials,* 3**,** 123-129.

WILSON, J. & NOLLETTI, D. 1990. Bonding of soft tissues to bioglass. *Handbook of bioactive ceramics,* 1**,** 283-302.

WILSON, J., PIGOTT, G., SCHOEN, F. & HENCH, L. 1981. Toxicology and biocompatibility of bioglasses. *Journal of Biomedical Materials Research Part A,* 15**,** 805-817.

YANG, L., PEREZ-AMODIO, S., BARRÈRE-DE GROOT, F. Y., EVERTS, V., VAN BLITTERSWIJK, C. A. & HABIBOVIC, P. 2010. The effects of inorganic additives to calcium phosphate on in vitro behavior of osteoblasts and osteoclasts. *Biomaterials,* 31**,** 2976-2989.

ZACHARIASEN, W. H. 1932. The atomic arrangement in glass. *Journal of the American Chemical Society,* 54**,** 3841-3851.

ZARZYCKI, J. 1991. *Glasses and the vitreous state*, Cambridge University Press.

ZHANG, Y., WEI, L., WU, C. & MIRON, R. J. 2014. Periodontal regeneration using strontium-loaded mesoporous bioactive glass scaffolds in osteoporotic rats. *PLoS One,* 9**,** e104527.

8 Appendices:

1) Conferences Presentations:

July 2018	**International Association for Dental Research (IADR)** London, England Title: **Novel Strontium/High Phosphate Containing Bioactive Glass for Periodontal Treatment**.
August 2017	**Annual Congress of the Scandinavian Society of Periodontology (ScSP)** **Young Researcher Award Competition** Mariehamn, Åland Islands, Finland Title: **Novel Biodegradable Silicate/Phosphate Glass Mixtures for The Treatment of Periodontal Infra Bony Defects.** **Awarded Travel Grant from the ScSP for the Best Abstract for Oral Presentation in the Young Researcher Award Competition.**
March 2017	**International Association for Dental Research (IADR)** San Francisco, USA Title: **pH Conditions Significantly Influence Glass Bioactivity of Perioglas®.**
June 2016	**International Association for Dental Research (IADR)** Seoul, Republic of Korea Title: **Effect of Particle Size and Glass Composition on Bioactive Glasses.** **Awarded Student Travel Grant from Armourers & Brasiers' Gauntlet Trust**
October 2015	**William Harvey Day** Barts and The London School of Medicine and Dentistry, London Title: **Regeneration of Periodontal Tissues with Strontium Substituted Bioactive Glasses.**
September 2015	**British Society of Dental Research Annual Conference (BSODR)** Cardiff, UK Title: **Treatment of Periodontal Pocket with Novel Bioactive Glass Containing Strontium.**

2) Supplementary Results:

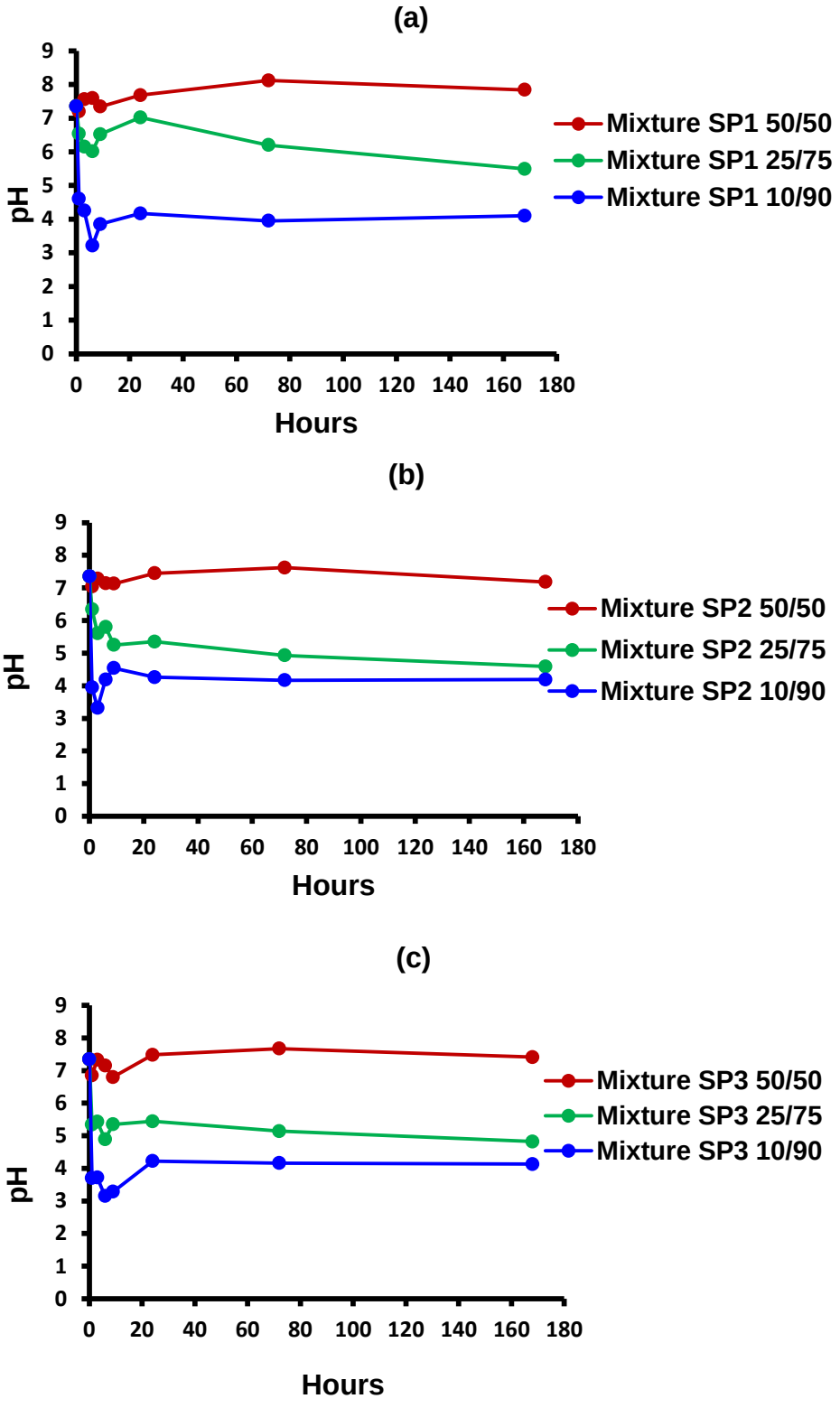

The pH behaviour in SBF solution as a function of time of three different ratios for each glass mixture (a) glass mixture SP1, (b) glass mixture SP2 and (c) glass mixture SP3.

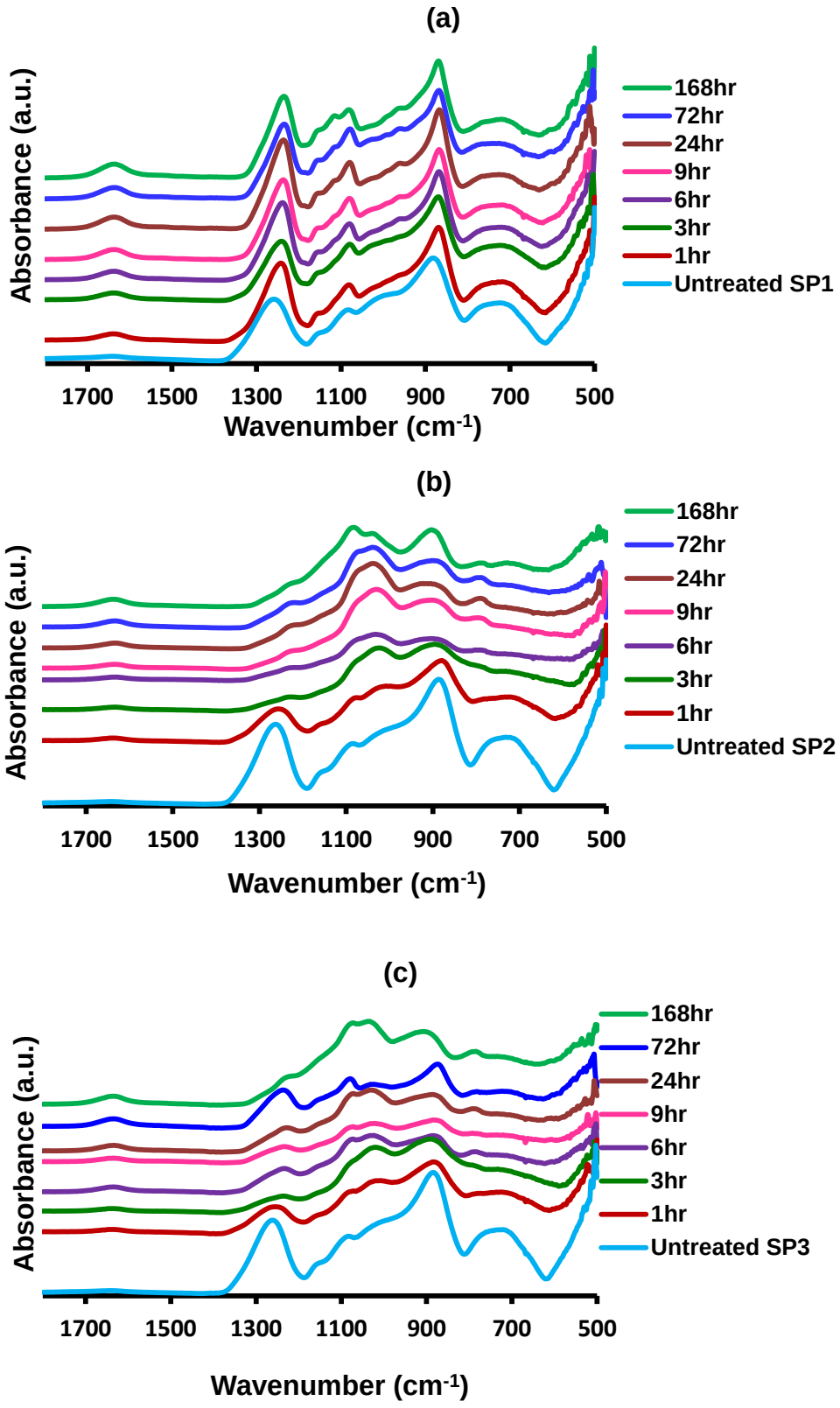

The FTIR spectra of studied glass mixtures with a 10/90 ratio before (untreated) and after immersion in SBF for different time period indicated in hours plotted as a function of time for: (a) SP1 mixture, (b) SP2 mixture and (c) SP3 mixture.

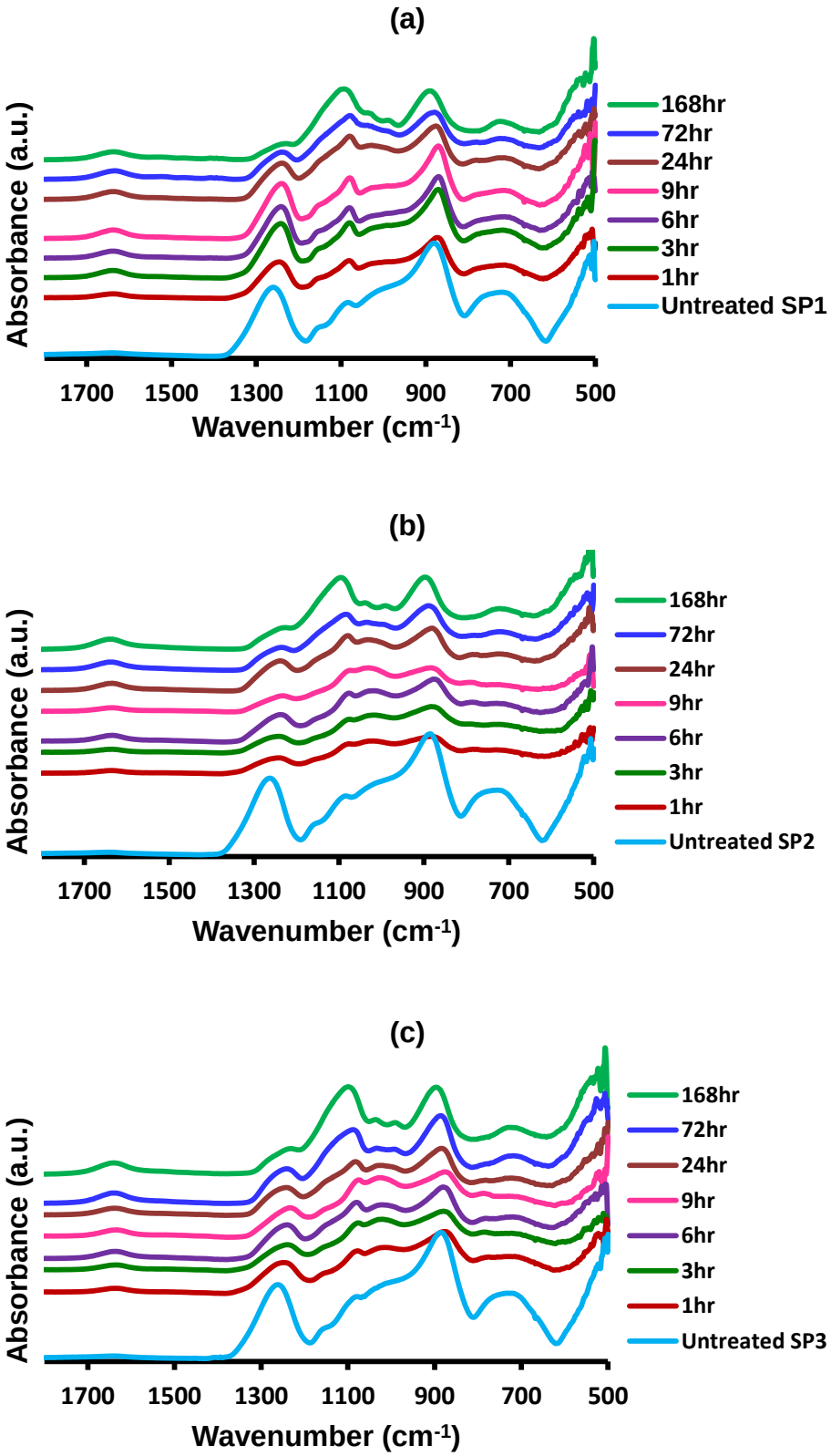

The FTIR spectra of studied glass mixtures with a 25/75 ratio before and after immersion in SBF were plotted as a function of time for: (a) SP1 mixture, (b) SP2 mixture and (c) SP3 mixture.

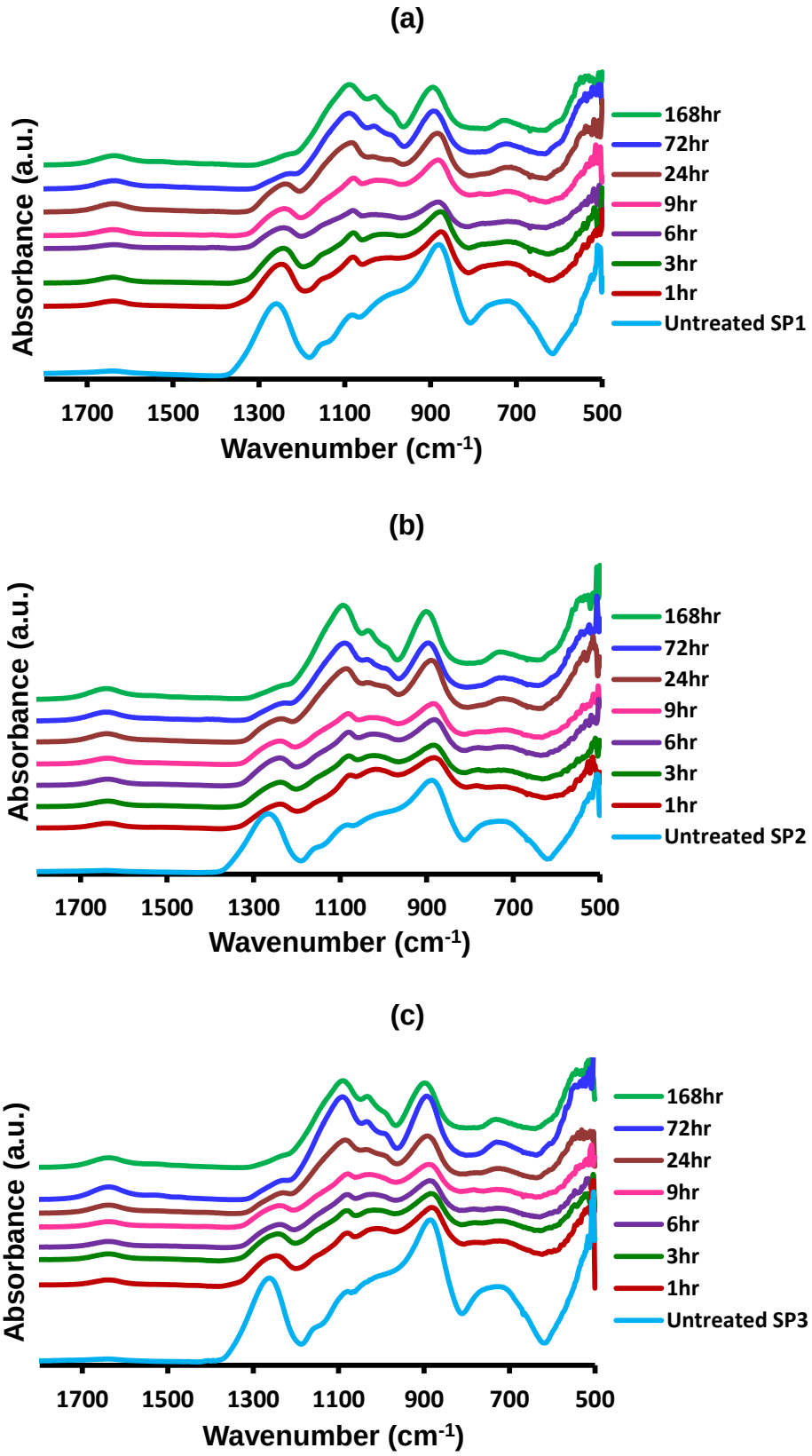

The FTIR spectra of studied glass mixtures with a 50/50 ratio before and after immersion in Tris buffer were plotted as a function of time for: (a) SP1 mixture, (b) SP2 mixture and (c) SP3 mixture.

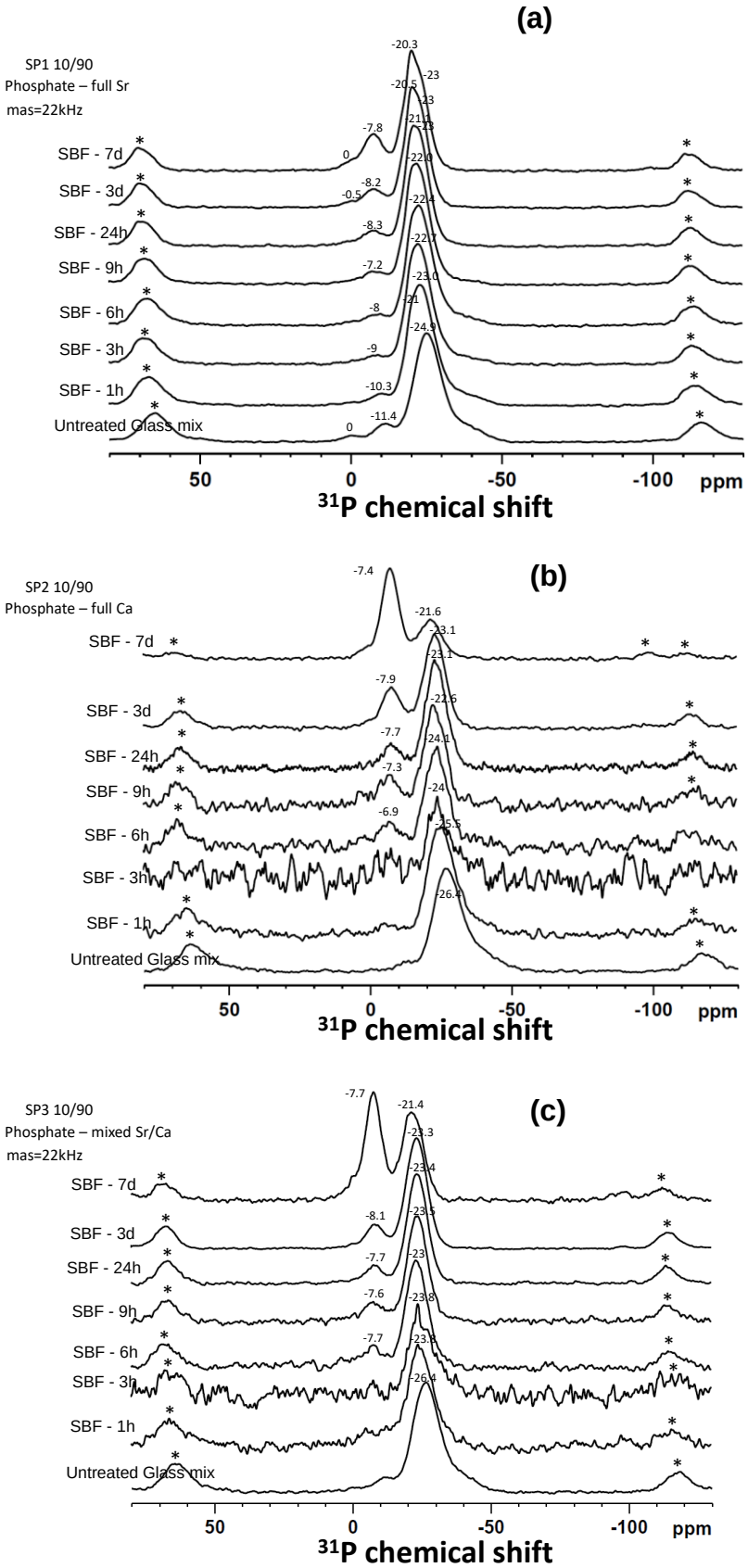

The ^{31}P MAS-NMR spectra (mas=22kHz) of studied glass mixtures with a 10/90 ratio before and after immersion in SBF plotted as a function of time for (a) SP1 mixture, (b) SP2 mixture and (c) SP3 mixture. Asterisks show spinning side bands.

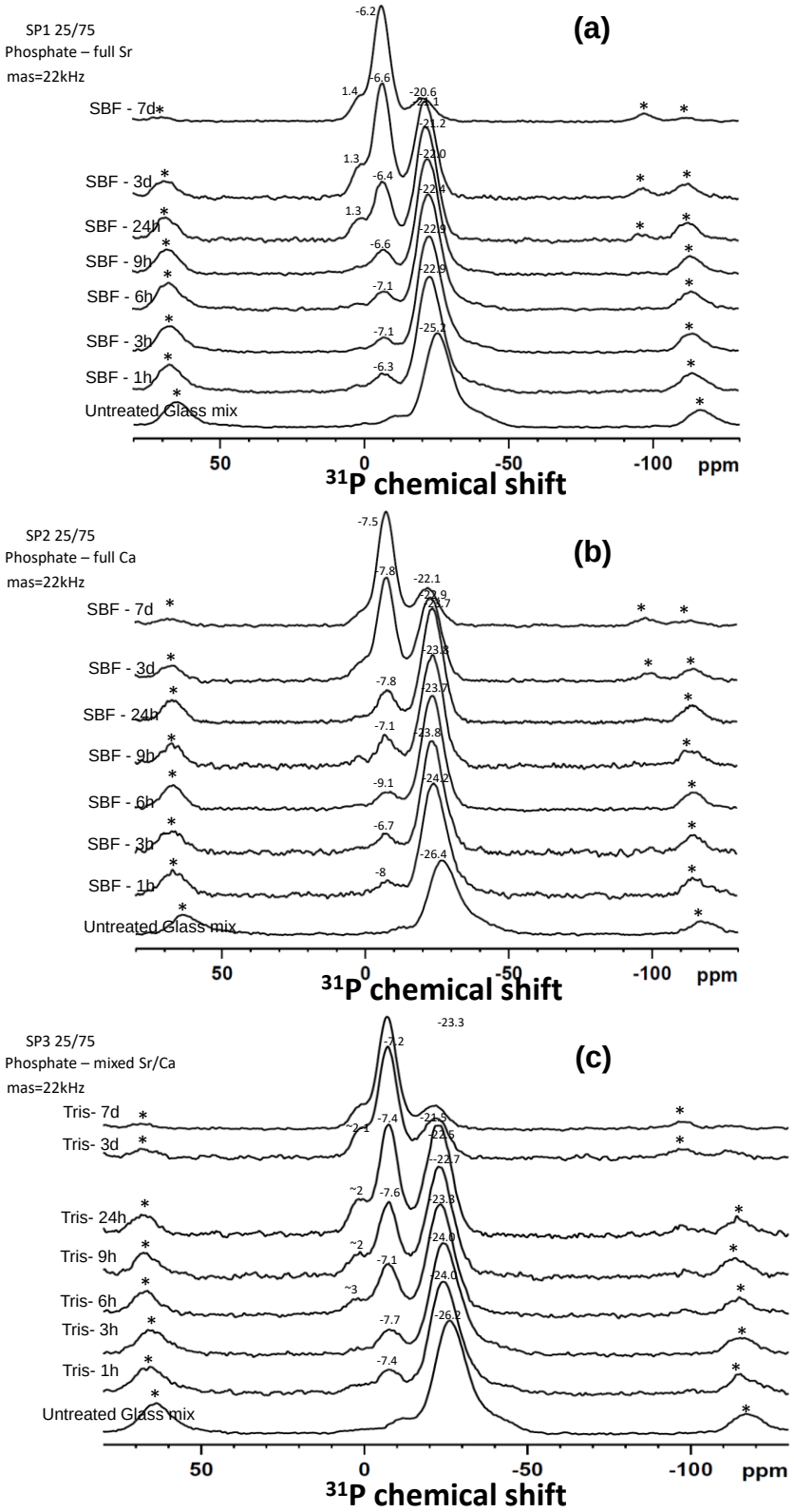

The ^{31}P MAS-NMR spectra (mas=22kHz) of studied glass mixtures with a 25/75 ratio before and after immersion in SBF plotted as a function of time for (a) SP1 mixture, (b) SP2 mixture and (c) SP3 mixture.

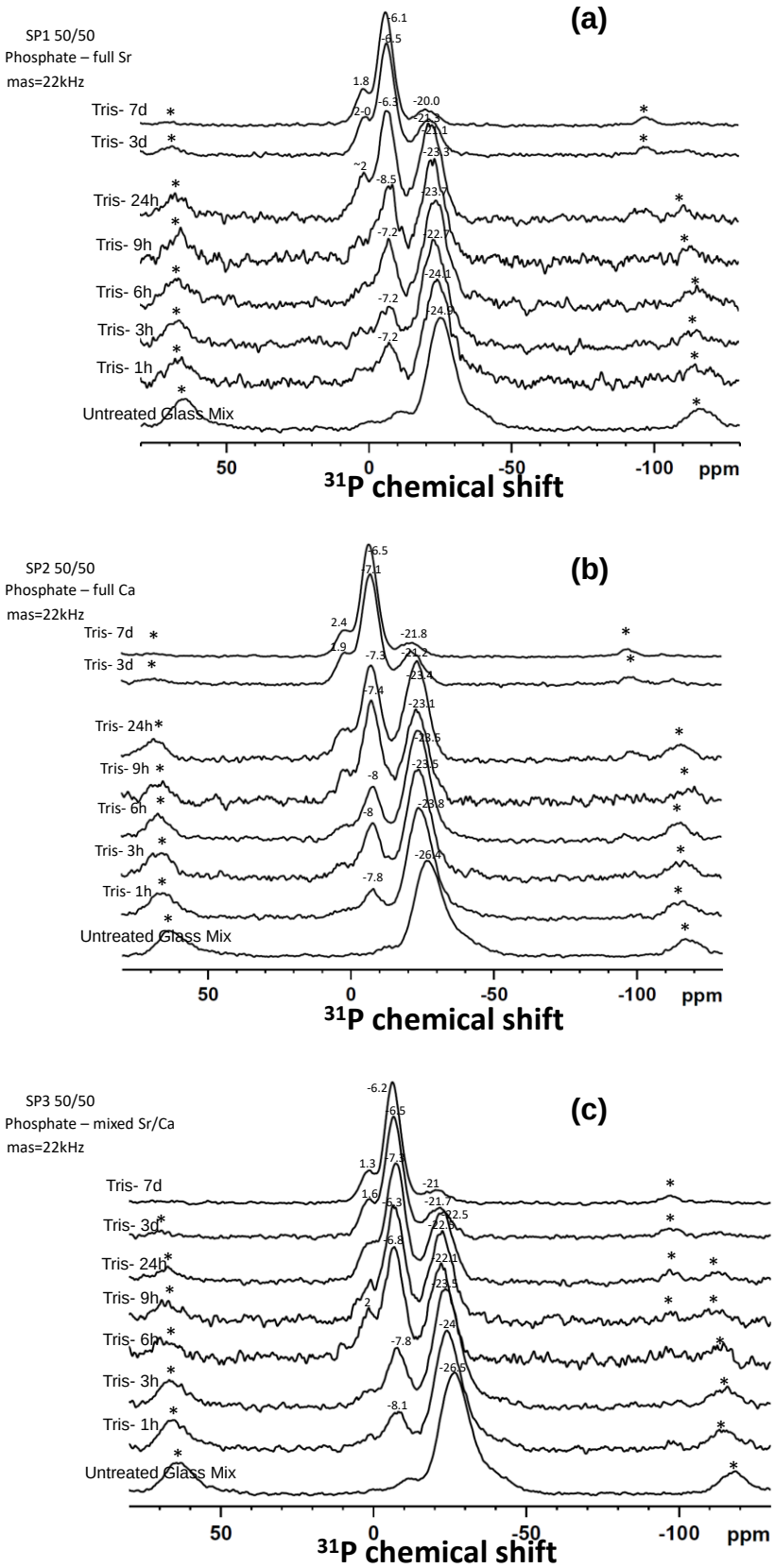

The ^{31}P MAS-NMR spectra (mas=22kHz) of studied glass mixtures with a 50/50 ratio before and after immersion in SBF plotted as a function of time for (a) SP1 mixture, (b) SP2 mixture and (c) SP3 mixture.